UNIVERSITY OF LIVERPOOL

ANALYSIS OF THE CYTOKINE-INDUCED SIGNALLING DYNAMICS OF STAT3 AND NF-κB

Thesis submitted in accordance with the requirement of the University of Liverpool for the degree of Doctor of Philosophy

Stephanie Claire Baldwin

January 2015

Declaration

This thesis is the result of my own work, unless otherwise stated. It is based upon the results from experimental work performed as a PhD student between October 2010 and January 2015 in the Institute of Integrative Biology within the University of Liverpool.

Neither this thesis or any part of it has been submitted in support of an application for another degree or qualification at this or any other University or other institute of learning.

Stephanie Baldwin

January 2015

Acknowledgements

It has been one heck of a journey and there are many people to thank. First of all, I want to thank my supervisors, Dr Violaine Sée and Professor Mike White. Thank you for taking me on and for all the interesting conversations and fantastic opportunities you have provided. I would also like to thank my collaborators, Dr Núria Domedel-Puig, Dr Elena Abad and Professor Jordi Garcia-Ojalvo, at the Universitat Pompeu Fabra, Barcelona. It's been an absolute delight working with you.

I would like to thank all those I've worked alongside with in the lab during my Ph.D. Dr Dave Spiller, for being an all-round great guy and god of the microscopes, your experience and knowledge has been invaluable. To all the former lab members who have moved on to pastures new, it was good working with you. I particularly want to thank Raheela Awais, Sheila Ryan and Antony Adamson for helping me with the BACs, and Louise Ashall for teaching me qPCR. Lloyd Bridges, thanks for our modelling discussions and Ulfert Rand, thanks for informing me of the JAK-STAT 2012 Conference – it was so inspiring to meet the leaders of the field. To the current post-docs, thanks for your continued support and assistance. There are too many to name, but again particular thanks are due. Polly Downton, you're a star, thanks for your help with the Fluidigm project, my cloning, and for reading my drafts. Anne McNamara, Claire Harper and Connie Lam, thanks for your company in tissue culture and all your pep talks. Boyd and Baggers, a.k.a. James Boyd and James Bagnall, and also Dr Pawel Paszek, it's been fun arguing science with you and I will never, ever, forget the canoeing trip in the Highlands! I must also thank Kate Goodheart and Lorraine Schmidt - you are the unsung heroines of the group. Kate, for keeping us all organised and Loz, for helping with all things lab-based. And of course, how could I forget my fellow Ph.D. students in the White, Jackson and Paszek groups? I've thoroughly enjoyed working with you. For those of you still in the thick of it, good luck, I believe in you. Special thanks go to Drs. Karen Dunn, Nisha Patel and Jane Pulman. You are some of the best friends a girl could wish for and I am so proud of you for making it through to the end of your doctorates!

Now to express my deepest gratitude to my amazing family and friends. Mum, Dad, Simon and Ian, I love you all. To my best friend in all the world, Ellie, where would I be without you? Here's to many more years of friendship, wine and countryside holidays. To my support network, Tina, Dee, and Adela, and my fellow bloggers, Keelie Chaisson, Elodie Glass and Kasey Weird, thank you for your many words of encouragement. Finally, Arthur, my rock in the storm, I love you so much, I couldn't have finished this Ph.D. without you. I can't wait to see what the next chapter brings.

Abstract

The transcription factors STAT3 and NF-κB play key roles in inflammation, immunity and cell fate. In the liver, they are responsible for transcribing hundreds of genes in response to combinations of IL-6, TNFα and IL-1β, and so together co-ordinate the acute phase response to infection. Dysregulated STAT3 and NF-κB signalling leads to chronic inflammation and is implicated in the development of many cancers. A variety of highly context-dependent intercellular and intracellular mechanisms have been discovered which facilitate both positive and negative cross-talk between STAT3 and NF-κB. Whilst the long-term signalling dynamics of NF-κB have been characterised in single cells, and were found to be oscillatory, imaging studies on STAT3 have focused upon the short-term mechanisms of nuclear transport rather than the long-term dynamics. STAT3 has been shown to oscillate in a population of synchronised cells so it is possible that STAT3 will exhibit oscillatory spatio-temporal signalling dynamics in response to cytokine stimulation.

The primary aim of this thesis was to characterise the long-term signalling dynamics of STAT3 in response to IL-6, using fluorescent fusion protein reporters for STAT3 and its inhibitor SOCS3, in conjunction with live single cell fluorescence microscopy. Towards these aims, STAT3 and SOCS3 fluorescent fusion proteins were constructed. The responses of a candidate cell line to IL-6 and TNFα were investigated, and then the fluorescent reporters were characterised in that cell line. The N-terminal tagged EGFP-STAT3 reporter was found to be the most accurate reporter of IL-6 signalling. The EGFP-STAT3 was then used to investigate the single cell spatio-temporal dynamics of STAT3 in response to differently timed lengths of IL-6 stimulation. STAT3 was found to oscillate with a period of approximately 90 min in response to continuous IL-6 stimulation, but only underwent a transient nuclear translocation in response to a 30 min IL-6 pulse. Furthermore, the patterns of gene expression were characterised for the timed IL-6 treatments. The quantified single cell dynamics were used to constrain an existing generic model of STAT:SOCS signalling; the model was able to capture the observed single cell dynamics using a minimal ordinary differential equation approach.

The secondary aim of the thesis was to study cross-talk between STAT3 and NF-κB using live cell microscopy techniques. The effects of co-stimulation of NF-κB and STAT3 were investigated using combinations of TNFα and IL-6 stimuli. Combinations of single or dual transfections, and single or dual stimulation were performed as controls in order to tease apart the effects of co-expression and co-stimulation. The importance of the timing of cytokine stimulation was also investigated. Finally, the effects of IL-1β upon IL-6 induction of STAT3 were investigated, as this was shown elsewhere to inhibit STAT3 signalling and so was expected to produce interesting spatio-temporal signalling effects. This preliminary study revealed distinct subpopulations of cells with different p65 and STAT3 response patterns. The STAT3 response was knocked down or significantly delayed in many cells but a small subset exhibited atypical oscillatory dynamics. Interestingly, the p65 dynamics were also significantly perturbed by IL-6 and IL-1β co-stimulation, indicating that there are cross-talk events occurring in both directions. Consequently these studies represent a very important area for future investigation.

Table of Contents

List of Abbreviations

Abbreviations used as per SI unit conventions with the following additions:

A2M	Alpha-2-macroglobulin
APR	Acute Phase Response
APRF	Acute Phase Response Factor
APS	Ammonium Persulphate
ARD	Ankyrin Repeat Domain
ATP	Adenosine Tri-Phosphate
BAC	Bacterial Artificial Chromosome
BSA	Bovine Serum Albumin
CBM	Cytokine-binding module
CBP	CREB-binding Protein
CDK5	Cyclin-dependent kinase 5
cDNA	Complementary DNA
CDS	Coding sequence
CFP	Cyan Fluorescent Protein
CIS	Cytokine-inducible SH2 domain containing protein
CMV	Cytomegalovirus
CNTF	Ciliary Neurotrophic Factor
Cp	Crossing point
Cq	Quantification cycle
Ct	Cycle threshold
CT-1	Cardiotrophin-1
DBD	DNA-binding domain
DMSO	Dimethylsulphoxide
DNA	Deoxyribonucelaic Acid
dsRedXP	*Discosoma* sp. Red Express fluorescent protein
D-STAT	*Drosophila*-STAT
Dd-STAT	*Dictyostelium* STAT
E. coli	*Escherichia coli*
EDTA	Ethylenediaminetetraacetic acid
EGF	Epidermal Growth Factor
EGFP	Enhanced Green Fluorescent Protein
E/MEM	Eagle's / Minimum Essential Media
EPO	Erythropoietin
ESS	Extended SH2 sequence

FERM	4.1, Ezrin, Radixin and Moesin domain
FGG	Gamma Fibrinogen
FNIII	Fibronectin Type III domain
GalK	Galactokinase K gene
GAPDH	Glyceraldehyde-3-phosphate dehydrogenase
GAS	Gamma activated sequence
GFP	Green Fluorescent Protein
GH	Growth Hormone
gp130	glycoprotein-130
HepG2	Human Hepatoma G2
IFN	Interferon
IKK	Inhibitor-KappaB Kinase
IL	Interleukin
IL-1β	Interleukin-1 Beta
IL-6	Interleukin-6
IL6R	IL-6 Receptor
IRC	Inter-Run Calibration
IκB	Inhibitory Kappa B protein
IκBα	Inhibitor Kappa B Alpha
IκBε	Inhibitor Kappa B Epsilon
JAK	Janus Kinase
KIR	Kinase Inhibitory Region
LB	Luria Bertani
LIF	Leukaemia Inhibitory Factor
LucF	Firefly Luciferase vector
MAPK	Mitogen Activated Protein Kinase
MEF	Mouse embryonic fibroblasts
$MgCl_2$	Magnesium Chloride
mRNA	messenger Ribonucleic Acid
mTOR	mammalian Target Of Rapamycin
NES	Nuclear Export Signal
NF-κB	Nuclear Factor – KappaB
NK	Natural Killer cells
NLS	Nuclear Localisation Signal
NPC	Nuclear Pore Complex
N-PTP	Nuclear – Protein Tyrosine Phosphatase

N/T	Nuclear/Total Fluorescence
ODE	ordinary differential equation
OSM	Oncostatin-M
PEST	'Proline, glutamic acid, serine, threonine' motif
PIAS	Protein Inhibitors of Activated STATs
PGSI	Phosphatidylglycerophosphate synthase I gene
POLR2A	Polymerase (RNA) II (DNA directed) polypeptide A
ppSOCS3	SOCS3 proximal promoter
ppSOCS3-EGFP	ppSOCS3-SOCS3-EGFP expression vector
P-STAT	Phosphorylated-STAT
PTP	Protein Tyrosine Phosphatase
PTRF	Polymerase I and Transcription Release Factor gene
qPCR	Quantitative Polymerase Chain Reaction
RDH	Rel Homology Domain
ROI	Region of Interest
RTK	Receptor Tyrosine Kinase
SAA1	Serum Amyloid A 1
SDS	Sodium Dodecyl Sulphate
SEM	Standard Error of the Mean
SK-N-AS	Human S-Type Neuroblastoma
SH2	Src-Homology-2 domain
SHP1/2	SH2-domain-containing tyrosine phosphatases- 1 and -2
SOCS	Suppressor Of Cytokine Signalling
STAT	Signal Transducer and Activator of Transcription
SUMO	Small Ubiquitin-related Modifiers
SW102	*E. coli* strain developed by Warming et al, (2005)
TAD	Trans-Activation Domain
TBS	Tris Buffered Saline
TEMED	Tetramethylethylenediamine
TF	Transcription Factor
TNFα	Tumour Necrosis Factor alpha
Tris-PO3	Tris Phosphate
U-STAT	Unphosphorylated-STAT
UTR	Untranslated Region
YFP	Yellow Fluorescent Protein

List of Figures

Chapter 6

List of Tables

Chapter 1
Introduction to JAK-STAT and NF-κB

1.1 Dynamic Intracellular Signalling and Systems Biology

Cellular communication and monitoring of the local environment is essential to cell survival and proper functioning of the organism (Jordan et al, 2000). It is vitally important for the immune system, as without sufficient environmental surveillance and effective response co-ordination, infections may quickly become established. Conversely, an excessive immune response may endanger the organism in the short-term, through events like asthma attacks, allergic reactions and anaphylaxis, and in the long-term, through the development of chronic inflammation and auto-immune disorders, such as Rheumatoid Arthritis, asthma and Crohn's Disease (Pernis & Rothman, 2002; Mihara et al, 2012). Cell signalling pathways monitor different aspects of the cell's environment and use Transcription Factors (TFs), including the Signal Transducer and Activator of Transcription (STAT) and Nuclear Factor-kappaB (NF-κB) protein families, to convey instructions from the cell membrane to the nucleus to regulate gene expression and determine biological outcomes (Ghosh et al, 1998; Imada & Leonard, 2000).

The multiplicity of signals to be monitored presents the cell with the difficult task of performing the most appropriate response to the signals it detects (Jordan et al, 2000). Consequently signalling pathways are not discrete entities, rather they form complex integrated networks, able to influence each other through events commonly referred to as 'cross-talk' (Klipp & Liebermeister, 2006). Cross-talk may be positive or negative and may influence the timing of particular events (Kholodenko, 2006). Direct protein-protein interactions, whether at the cell membrane or on gene promoters, provide points of contact, as do post-translational modifications of signalling proteins, such as phosphorylation, acetylation, ubiquitination and sumoylation by other intermediaries (Bruce Alberts, 2002). In addition, signalling networks possess a variety of positive and negative feedback and feed-forward loops to modulate signal duration and intensity (Kholodenko, 2006). They may require the induction of specific proteins, such as the Suppressors of Cytokine Signalling (SOCS) that down-regulate STAT signalling (Krebs & Hilton, 2001), or the

Inhibitory-kappaB (IκB) proteins which inhibit NF-κB signalling (Karin & Ben-Neriah, 2000). These feedback loops may be inducible or modifiable by more than one pathway and so may facilitate cross-talk between those signalling pathways (Kholodenko, 2006).

The vast number of possible points and modes of interaction within and between signalling pathways makes studying cross-talk a challenge at the molecular level using reductionist techniques. However the molecular signals may generate signalling dynamics at the bulk-protein level in single cells, as a result of the fundamental properties of the network. These emergent network dynamics may be observed as spatial and/or temporal events across cellular compartments, such as the cytoplasm and nucleus (Kholodenko, 2006; Mullassery et al, 2008). Often these dynamics cannot be observed by traditional population-based biochemical methods since intercellular variation may be masked in the population average. Fortunately developments in time-lapse, confocal fluorescence microscopy provide a means to investigate signalling dynamics within single cells over long periods (Ankers et al, 2008; Mullassery et al, 2008). Systems biology, by combining single cell data with mathematical modelling and iterative testing of hypotheses, has proved to be a fruitful investigative approach towards understanding the complex dynamics of the signalling network (Kitano, 2002).

1.2 JAK-STAT Signalling

1.2.1 Introduction to JAK-STAT Signalling

1.2.1.1 Discovery of JAK-STATs

JAK-STAT (Janus Kinase-Signal Transducers and Activators of Transcription) signalling was first discovered in the late 1980s in various contexts throughout the immune system, as a pathway responsible for processing cytokine signals, particularly the Interferons, and for mediating the Acute Phase Response to infection. Eventually it was realised these transcription factors had numerous roles throughout the immune system, in both innate and adaptive immunity, and formed a family of related proteins that became known as STATs (Aaronson & Horvath, 2002; Levy & Lee, 2002).

1.2.1.2 The JAK and STAT Family Members and Their Roles

There are seven mammalian STAT proteins: STAT1, STAT2, STAT3, STAT4, STAT5A, STAT5B and STAT6, and analogues exist in the distantly-related *Drosophila* (D-STAT) and *Dictyostelium* (Dd-STAT) organisms (Hibi & Hirano, 1998). In addition there are four Janus Kinase (JAK) proteins: JAK1, JAK2, JAK3 and TYK2, which constitutively associate with cytokine receptors. JAKs directly activate the STATs through tyrosine phosphorylation in response to cytokine signalling and in doing so, enable STATs to translocate to the nucleus and initiate gene transcription (Hibi & Hirano, 1998; Heinrich et al, 2003).

STAT1 was the first to be discovered. It forms homodimers and heterodimers with STAT2, which are essential for mediating Interferon (IFN) signals (Platanias, 2005), promoting inflammation and antagonising proliferation. STAT2 specifically is pivotal to the response to Type I IFNs (Schindler et al, 2007). STAT4 has a quite limited role amongst the STATs. It is involved in polarising naïve $CD4^+$ lymphocytes in to Th1 cells in response to Interleukin (IL)-4, whilst in response to IL-12, STAT4 is necessary for Natural Killer (NK) cell activation (Kisseleva et al, 2002). STAT5A and B are pleiotropic transcription factors that mediate a large number of signals from the IL-2- and IL-3-type cytokine families. They also mediate hormone signals, such as Prolactin, Growth Hormone (GH) and Erythropoietin (EPO) (Gouilleux et al, 1994; Levy & Lee, 2002). STAT6 transduces IL-4 and IL-13 signals. Similar to STAT4, STAT6 is involved in polarising $CD4^+$ lymphocytes, but turns them into Th2 cells (Kaplan et al, 1996). STAT6 is also necessary for mast cell activation in the allergic response and B cell isotype switching (Schindler et al, 2007). Finally there is STAT3, the most pleiotropic of all the STATs and the only one that results in embryonic lethality when knocked out in mice (Takeda et al, 1997).

1.2.1.3 Biological Importance of STAT3 and the Acute Phase Response

STAT3 was initially identified as the Acute Phase Response Factor (APRF) responsible for orchestrating the acute phase response (APR) to infection and injury (Moshage, 1997). The acute phase response is a systemic inflammatory response, featuring fever, oedema, considerable metabolic changes and the biosynthesis of a variety of plasma proteins, whose purpose is to eliminate

pathogens and aid healing afterwards (Moshage, 1997). The liver is the primary site of the APR, responding via the JAK-STAT and NF-κB networks to the cytokines Tumour Necrosis Factor-α (TNFα), IL-1β and IL-6 which are produced by tissue macrophages and liver-specific macrophages (Kupffer cells). In addition to its roles in the APR where STAT3 transduces IL-6 signalling, STAT3 is also responsible for another 18 related cytokines from the IL-6 and IL-10 sub-families, as well as several growth factors, all of which have different but partially over-lapping functions (Schindler et al, 2007).

The lethality of complete STAT3 knock-out in mice revealed the key involvement of STAT3 in early embryogenesis but also presented difficulties for understanding its function in adults. Conditional, tissue-specific knock-outs were generated using the Cre-*loxP* system and these studies identified roles in the skin and thymus, mammary development, the nervous system, T cells and the myeloid lineage (macrophages and neutrophils), and re-iterated its role in the acute phase response (Kisseleva et al, 2002; Levy & Lee, 2002). The phenotypes ranged from severely compromised wound healing in the skin, loss of thymocytes and hypersensitivity to stress in adult mice, to susceptibility to endotoxic shock due to STAT3-deficient macrophages (Levy & Lee, 2002). Additionally, absence of STAT3 in the liver lead to a significantly impaired APR and increased mortality, which rose even further if NF-κB was also knocked out in the liver, thus highlighting the importance of STAT3 and NF-κB cross-talk (Quinton et al, 2012).

1.2.1.4 Summary of JAK-STAT Signalling Pathway

The key events of the JAK-STAT signalling pathway are summarised in Fig. 1.1. JAK-STAT signalling is initiated by the binding of a cytokine to its cognate cytokine receptor. Receptor association and concomitant conformational re-arrangement increases JAK activity, enabling them to trans-phosphorylate each other (Kisseleva et al, 2002). This increases their catalytic activity further so they can phosphorylate the receptor (Hibi & Hirano, 1998). Pre-formed, unphosphorylated STAT dimers (U-STATs) bind to the newly phosphorylated receptor and are phosphorylated by the JAKs (Braunstein et al, 2003; Sehgal, 2008). This triggers a re-arrangement of the STAT dimer, increasing its DNA-

binding affinity, and causing phosphorylated STATs (P-STATs) to accumulate in the nucleus where they can induce transcription of their target genes (Braunstein et al, 2003; Kretzschmar et al, 2004; Mao et al, 2005). The accumulation of STATs in the nucleus represents a bulk redistribution of STATs between the nuclear and cytoplasmic compartments. This phenomenon has been visualised using fluorescence microscopy though only short time-lapse experiments have been performed (Pranada et al, 2004). Phospho-STATs transcribe their target genes, with each STAT dimer transcribing a specific set of target genes (Alvarez & Frank, 2004; Hebenstreit et al, 2006). Interestingly, U-STAT1 and U-STAT3 (Unphosphorylated-STAT1/3) are known to transcribe a limited set of genes, sometimes in concert with other transcription factor families, such as NF-κB (Yang et al, 2005; Yang & Stark, 2008).

Inactivation of STAT signalling occurs through several processes, each acting at different points in the pathway. There are the constitutive processes of dephosphorylation within the nucleus, performed by Protein Inhibitors of Activated STATs (PIAS) and Nuclear-Protein Tyrosine Phosphatases (N-PTPs), whose actions together facilitate export of STATs from the nucleus (Heinrich et al, 2003). There are also constitutive and inducible processes utilising SH2 (Src-Homology-2) domain proteins that deactivate phosphorylated receptor complexes and their associated JAKs, preventing subsequent rounds of STAT activation (Heinrich et al, 2003). Certain constitutive events involve SH2 proteins such as SHP1 and SHP2 (SH2-domain-containing tyrosine phosphatase), whereas inducible inhibition of STATs involve the family of Suppressors Of Cytokine Signalling (SOCS) proteins. Four of the eight SOCS proteins, CIS (cytokine-inducible SH2 domain containing protein), SOCS1, SOCS2, and SOCS3, are of particular interest as they act by specifically inhibiting phosphorylated receptors (Heinrich et al, 2003). Since these four SOCS are induced by activated STATs, they form delayed negative feedback loops that down-regulate JAK-STAT signalling after a certain period of time (Wormald et al, 2006). Theoretically, this could prime the JAK-STAT-SOCS system for dynamic spatio-temporal signalling. Whilst considerable attention has been applied to the short-term signalling dynamics of nuclear import and export (Pranada et al, 2004; Herrmann et al, 2007; Meyer et al, 2007; Chen & Reich,

2010; Vogt et al, 2011) and the mid-term dynamics at the population level (Yoshiura et al., 2007), long-term analysis at the single cell level has not been attempted. This represents an important gap in our understanding of JAK-STAT signalling and it is one of the issues this thesis seeks to address.

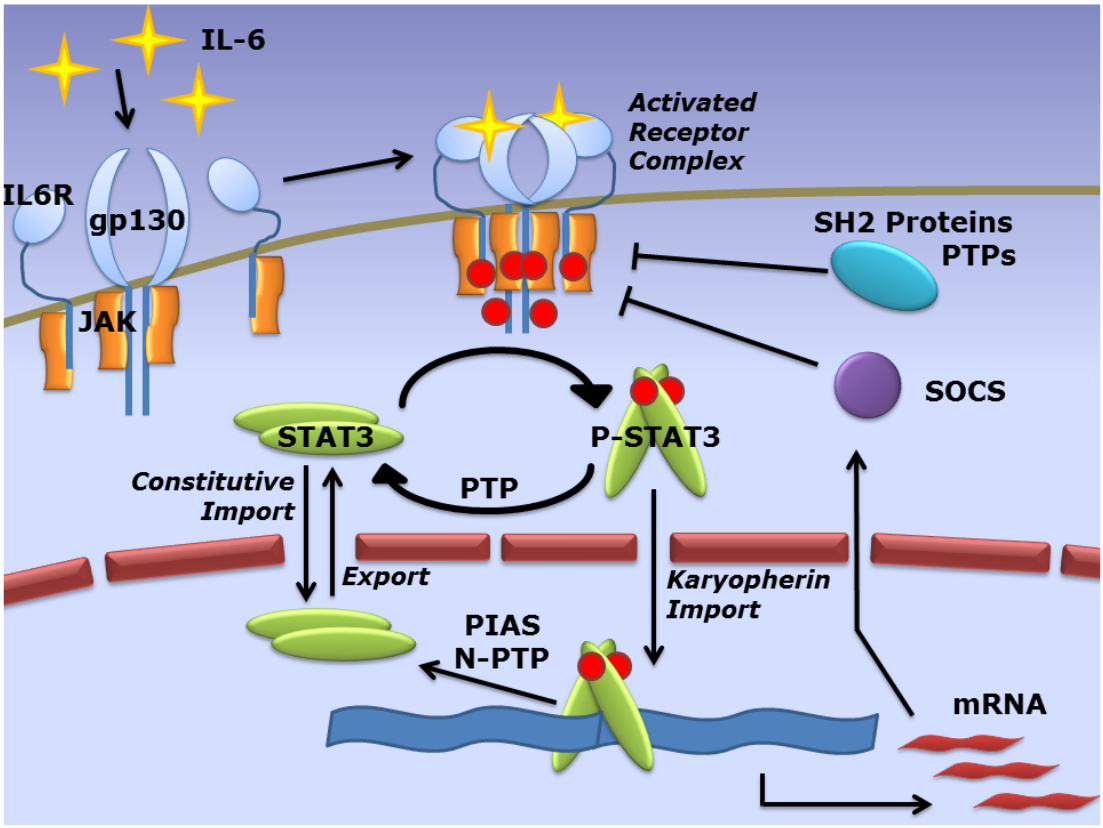

Figure 1.1: The JAK-STAT Pathway, for IL-6 and STAT3.
Application of IL-6 (yellow stars) triggers the activation of IL-6 Receptor complex, 2 IL-6, 2 IL6R (IL-6 Receptor), 2 gp130 (glycoprotein-130), leading to JAK and gp130 tail phosphorylation (red circles). Unphosphorylated STAT3 antiparallel dimers are phosphorylated by the JAKs and assume the parallel conformation (P-STAT3, with red circles). P-STAT3 accumulates in the nucleus and binds to DNA (blue ribbon) where it transcribes target genes. Nuclear P-STAT3 is dephosphorylated by Protein Inhibitors of Activated STATs (PIAS) and Nuclear-Protein-Tyrosine Phosphatases (N-PTP) and then STAT3 is exported back to the cytoplasm. PTPs also dephosphorylate cytoplasmic P-STATs. SH2-adaptor proteins and PTPs dephosphorylate the receptor and target it for lysosomal degradation. SOCS proteins, produced from STAT-induced mRNAs, also directly inhibit the JAKs and prevent the subsequent re-phosphorylation of STAT dimers.

1.2.2 Cytokine Receptors

1.2.2.1 Cytokine Receptor Classes

Cytokines form a large, diverse family of intercellular mediators which includes hormones, interleukins and growth factors, with roles in many aspects of immunoregulation, embryogenesis, growth and regeneration (Heinrich et al, 1998). They signal via cytokine receptors, transmembrane proteins formed from multiple subunits, which are divided into Type I and Type II Receptors. Type I receptors mediate a wide variety of cytokines and hormones whilst interferons, IL-10- and IL-20-type cytokines signal exclusively via Type II receptors (Gadina et al, 2001). Type I receptors are further classified according to the protein subunits used. They typically consist of two long transmembrane signal transduction subunits and, in many cases, also a short transmembrane cytokine-specific subunit (Heinrich et al, 2003). The signal transduction subunits are γc, βc, and gp130, and there are a number of homodimeric receptors for specific hormones and growth factors, e.g. Prolactin and EPO (Hibi & Hirano, 1998). Different combinations of signal transduction units and short cytokine-specific receptors provide cytokine specificity and signal fidelity which, when coupled with cell type-limited expression of the cytokine-specific receptors, explains the diverse outcomes of cytokine signalling (Kisseleva et al, 2002).

1.2.2.2 IL-6 Family of Cytokines and their Cognate Receptors

The IL-6-type cytokines are a structurally related family which signal through gp130 in combination with a number of different receptors. The family shares a four α-helix bundle structure (Boulton et al, 1994) and consists of the IL-6, IL-10, IL-12, LIF (Leukaemia Inhibitory Factor), CT-1 (cardiotrophin-1), CNTF (ciliary neurotrophic factor) and OSM (oncostatin-M) cytokines (Heinrich et al., 2003). The majority signal via a gp130:LIF-Receptor heterodimer, some also utilising the short CNTF-Receptor, whilst OSM can signal via both gp130:LIF-R and gp130:OSM-Receptor. IL-6 and IL-11 are unique in that they use a gp130 homodimer paired with the IL-6 Receptor (IL-6R) and IL-11R respectively (Taga et al, 1989; Murakami et al, 1993; Heinrich et al, 2003).

Complete structures of the receptor components are not available, however good progress has been made with the structure of the extracellular portions of the receptors. IL-6R consists of three ectodomains, one Ig-like and a cytokine-binding module (CBM) consisting of two fibronectin type III (FNIII) domains, whereas gp130 has six: one Ig-like, one CBM and three additional membrane-proximal FNIII domains (Heinrich et al, 1998; Matadeen et al, 2007). The final components of the receptor complex are the Janus Kinase (JAK) proteins which provide the catalytic activity that enables down-stream signal transduction (Yeh & Pellegrini, 1999).

1.2.2.3 Janus Kinases

Janus Kinases (JAKs) catalyse tyrosine phosphorylation for the Type I receptors which lack a catalytic domain in their cytoplasmic regions. There are four JAKs: JAK1, JAK2, JAK3 and TYK2 (Gadina et al, 2001), and JAK1 and JAK2 are necessary for IL-6 signalling via gp130 (Guschin et al, 1995). Each receptor type is constitutively pre-associated with one or two specific JAKs in a non-reversible manner; receptor-bound JAKs do not exchange with cytosolic JAKs (Giese et al, 2003). The JAKs themselves are large tyrosine kinases, between 120-140 kDa in size, and work in pairs to phosphorylate each other and the receptor to initiate STAT signalling (Yeh & Pellegrini, 1999).

JAKs have four domains: the kinase domain, the pseudokinase domain, an atypical Src homology 2 (SH2) domain and a divergent FERM (4.1, ezrin, radixin and moesin) domain (Fig. 1.2) (Haan et al, 2006). The kinase domain catalyses the phosphorylation of the target tyrosine residue, whereas the pseudokinase domain lacks key catalytic residues and instead auto-inhibits JAK kinase activity (Yeh & Pellegrini, 1999; Lupardus et al, 2014). The atypical SH2 and FERM domains are responsible for the constitutive binding of JAKs to the signal transduction proteins because they recognise and bind specific residues and hydrophobic regions of the cytoplasmic tail (Haan et al, 2006; Wallweber et al, 2014).

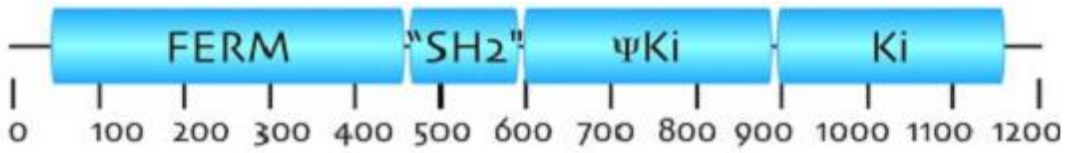

Figure 1.2: JAK structure. Listing the FERM, SH2, pseudo-kinase (ΨKi) and kinase (Ki) domain with illustrative amino acid numbers, reproduced from (Schindler et al, 2007).

1.2.2.4 IL-6 Receptor Expression Dynamics

IL-6R and gp130 are expressed very differently throughout the body. IL-6R is limited to specific cell types, for example hepatocytes and the haematopoietic lineage, whereas gp130 is ubiquitously expressed by nearly all cell types (Heinrich et al, 2003). In addition, IL-6R is expressed at very low levels, between 500 and 2000 receptors per cell (Zohlnhofer et al, 1992), although it can be up-regulated by other signalling pathways, e.g. glucocorticoids (Snyers et al, 1990; Schooltink et al, 1992).

Receptor levels at the cell membrane were shown to be stable over time in the absence of IL-6 signalling, due to the balance of *de novo* protein synthesis and constitutive endocytosis and subsequent degradation. Maturation and surface expression of newly synthesized IL-6R takes 45 min, and 60 min for gp130 (Gerhartz et al, 1994). Once at the cell membrane, gp130 has a half-life of about 15 min, and the protein half-life is approximately 2-3 h (Thiel et al, 1998). IL-6 stimulation does not affect gp130 internalisation but does change its degradation from proteasomal to lysosomal (Tanaka et al, 2008). Its internalisation rate can be altered by other cytokines, such as IL-1β (Radtke et al, 2010), providing a potential means for cross-talk between different signalling networks. IL-6R has a surface expression half-life of approx. 7 h in unstimulated HepG2 cells but only 15-30 min in IL-6 stimulated cells, when its protein half-life decreases to approximately 2 h (Zohlnhofer et al, 1992).

1.2.3 Structure and Function of STATs

1.2.3.1 Structure of the STATs

The STATs range from 750 to 900 amino acids in size, with a molecular weight of between 84 and 92 kDa, and share six structurally and functionally conserved domains. The first five domains are highly conserved while the sixth is less well conserved and contributes to protein specificity (Kisseleva et al, 2002). The domains, in order from N- to C-termini are: i) the N-terminal domain, ii) the coiled-coil domain, iii) the linker domain, iv) the DNA-binding domain, v) the SH2 domain and vi) the C-terminal Trans-Activation Domain (TAD), the most divergent of the domains (Chen et al, 1998; Schindler et al, 2007) (Fig. 1.3A). Each domain has its own set of functions, while some functions are spread across several domains e.g. sequences for nuclear transport. Various partial structures of STATs have been published, both DNA-bound and free, from crystal and solution-based studies. A 'core fragment' of human STAT1, consisting of the coiled-coil domain, DNA-binding domain, linker and SH2 domains, bound to DNA was solved in 1998 (Chen et al, 1998) and a few months later a similar 'core fragment' of murine STAT3β was also solved (Becker et al, 1998). In addition, structures for the unphosphorylated dimers of murine STAT5A (Neculai et al, 2005) and human STAT1 (Mao et al, 2005) have been solved. Coupled with work on the STAT4 N-terminal domain (Vinkemeier et al, 1998; Chen et al, 2003), a composite structure can be produced for the phosphorylated (Fig. 1.3B) and unphosphorylated STAT dimer structures (Fig. 1.3C and D).

1.2.3.2 Domain Functions

The N-terminal domain is necessary for the formation of unphosphorylated STAT1 and STAT3 homodimers, and also for nucleocytoplasmic shuttling of phosphorylated STAT3 dimers (Pranada et al, 2004; Mao et al, 2005; Vogt et al, 2011). The coiled-coil region is essential for recruitment to the cytokine receptor and is necessary for dimer formation, nuclear import and DNA binding (Zhang et al, 2000). The DNA-binding domain (DBD) binds directly to a specific promoter sequence with a core motif of $TTCN_{2-4}GAA$, with each STAT displaying different specificities for the N_{2-4} variants (Ehret et al, 2000). The linker domain

joins the DNA-binding domain and the SH2 domain together and interacts specifically with both domains (Chen et al, 1998). The SH2 domain recognises specific phospho-tyrosine residues on the cytokine receptor and the conserved tyrosine residue on the STAT monomer, which is Y705 in STAT3 and Y701 in STAT1. It is therefore essential for phosphorylated STAT dimerisation (Haan et al, 1999).

The conserved tyrosine residue is situated next to the SH2 domain to prevent self-activation. The transactivation domain varies greatly between different STATs whilst STAT1 and STAT3 also have TAD alternative splice variants (Ning et al, 2003; Ng et al, 2012). The TAD contains numerous STAT-specific conserved serine phosphorylation sites and facilitates interactions with other transcription factors, such as p300, CBP (CREB-binding Protein) and Histone Acetyletransferases (Schindler et al, 2007).

1.2.3.3 STAT3 mRNA and Protein Expression

STAT3 is constitutively expressed in most tissues and can also be specifically up-regulated by IL-6 signalling in some cell types (Ichiba et al, 1998). STAT3 mRNA was detected at increasing concentrations 1 h after addition of IL-6 to HepG2 cells, plateaued out after 3 h of continuous IL-6 signalling and could still be detected at 6 h. An extended time-course performed in M1 macrophages found STAT3 mRNA was sustained for up to 48 h of continuous IL-6 treatment (Ichiba et al, 1998). The half-life of STAT3 proteins was determined through a cycloheximide chase in COS-7 cells. The STAT3α isoform (full-length C-terminal domain) had a half-life of 8.5 h whereas the half-life of the truncated C-terminal isoform, STAT3β, was only 4.5 h (Siewert et al, 1999). Meanwhile STAT1 was found to be expressed at 1 x 10^5 molecules per cell in the HeLa cell line (Wenta et al, 2008), and it is assumed that STAT3 is expressed at a similar level.

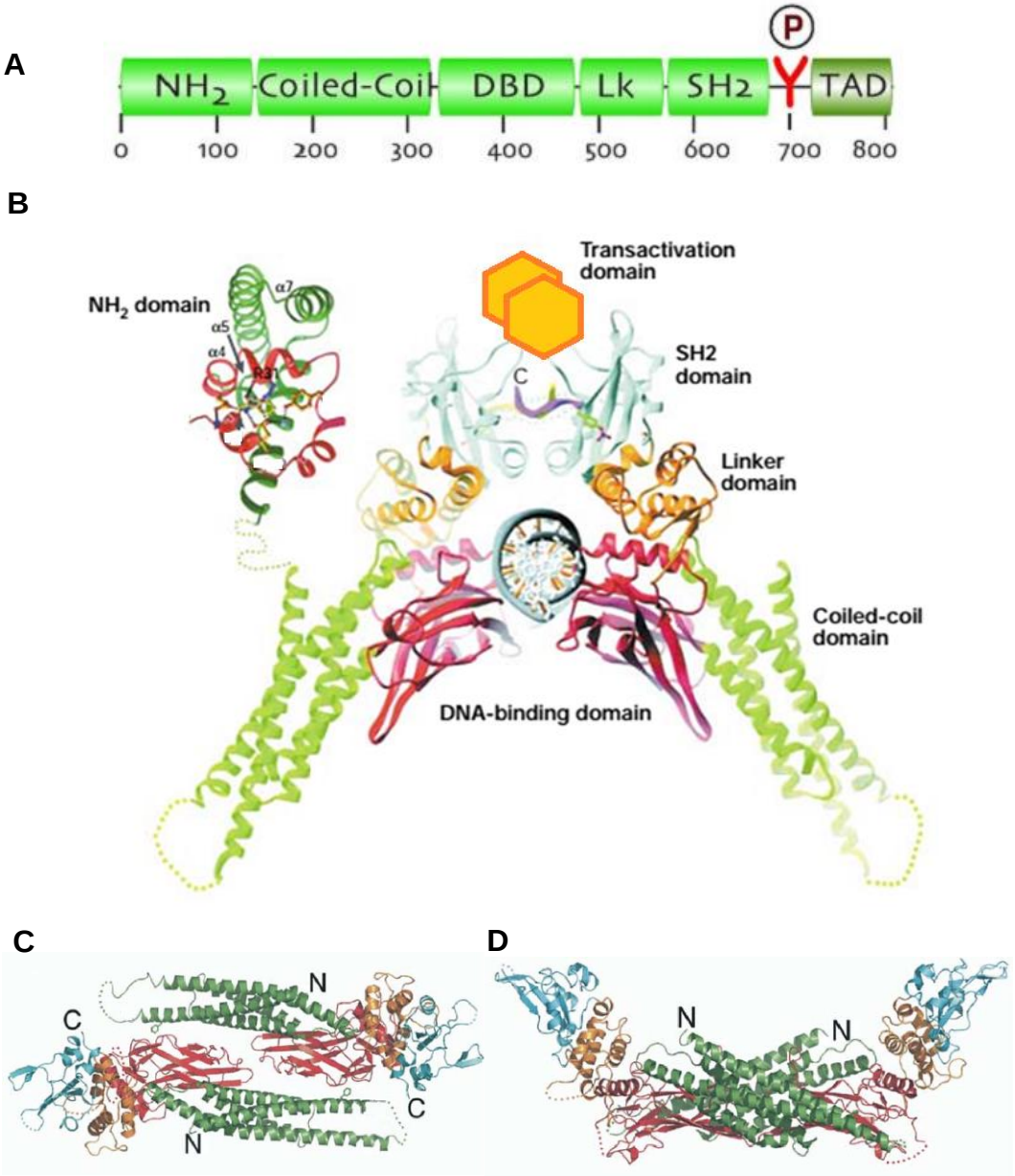

Figure 1.3: Structure of STAT dimers. A Generic domain structure of STATs with illustrative amino acid numbers, indicating location of conserved phospho-tyrosine residue (red Y). **B** Structure of human STAT1 'core fragment' (Chen et al, 1998) modified to include STAT4 N-terminal domain (Vinkemeier et al, 1998; Chen et al, 2003) and indicate the location of the C-terminal TAD (Levy & Darnell, 2002). **C** Bird's-eye view and **D** side-on view of unphosphorylated STAT1 homodimer (reproduced from Mao et al, 2005).

1.2.3.4 STATs in the Un-Stimulated Cell

In the unstimulated cell, STATs exist as dimers (Haan et al, 2000; Braunstein et al, 2003; Kretzschmar et al, 2004; Schröder et al, 2004). These non-phosphorylated dimers have been shown to adopt an 'anti-parallel' conformation (Fig. 1.3C and D), whereby the C-termini are at opposite ends of the homodimer (Mao et al, 2005). Two interfaces, one between the coiled-coil domain and DNA-binding domain, and one between N-terminal domains, were identified as stabilising the anti-parallel dimer (Mao et al, 2005).

The non-phosphorylated dimers are not restricted to the cytoplasm but instead shuttle constitutively between the nucleus and cytoplasm, despite being predominantly located in the cytoplasm (Meyer et al, 2002; Vinkemeier, 2004). The STAT subcellular distributions are maintained by the balance of nuclear import and export mechanisms, which vary between STATs. Consequently different STATs have different nucleocytoplasmic equilibria, that also differ between cell lines. For example, STAT1 exhibits a predominantly cytoplasmic distribution whereas in some cell types, e.g. HepG2, STAT3 is evenly distributed between the cytoplasm and the nucleus (Meyer et al, 2002).

1.2.4 Early JAK-STAT Signalling Events

1.2.4.1 Activating the gp130:IL-6Rα Receptor Complex

Cytokine stimulation triggers the formation of the receptor complex within the cell membrane. In the case of IL-6, the IL-6 receptor complex forms in a specific order within minutes of IL-6 binding. First IL-6 binds to IL-6R prior to associating with pre-formed gp130 homodimers. A second IL-6:IL-6R dimer joins, completing the hexameric structure of 2IL-6:2IL-6R:2gp130 (Bravo et al, 1998; Boulanger et al, 2003; Schroers et al, 2005; Tenhumberg et al, 2006). Since the structure of the extracellular region has been solved in detail (Fig. 1.4), there is a good understanding of the sequence of induced conformational changes that lead to the trans-activation of the gp130-associated JAKs (Boulanger et al, 2003; Xu et al, 2010).

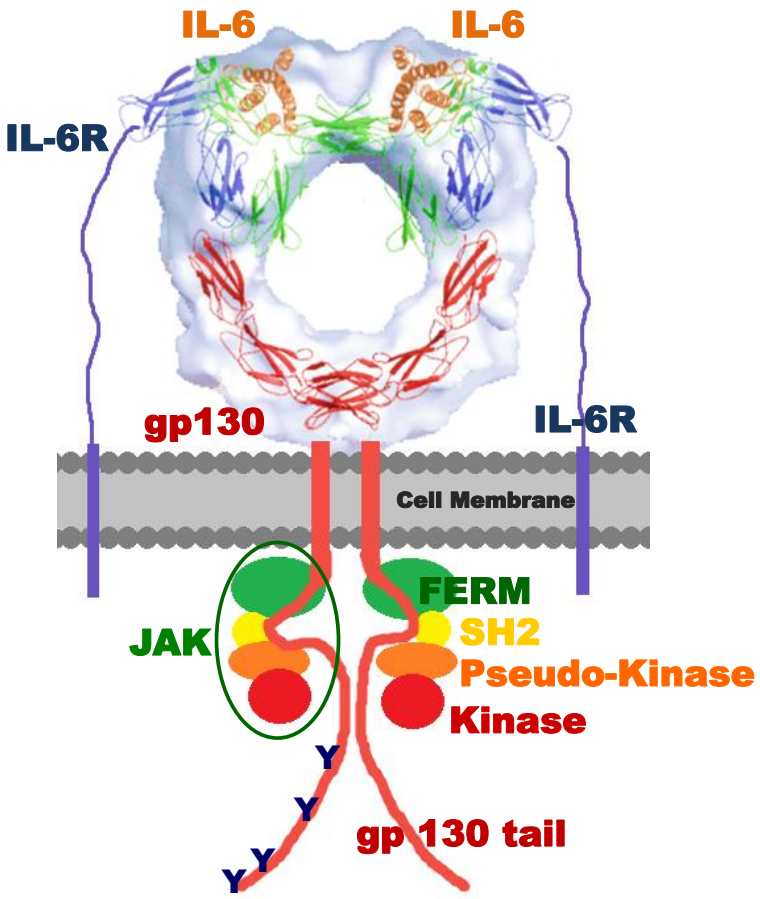

Figure 1.4: Cartoon of the activated IL-6 complex. The IL-6 receptor complex consists of 2 x gp130, 2 x IL-6R, 2 x IL-6 and 2 x JAK. JAK: FERM, SH2, pseudokinase and kinase domains labelled. Y = phospho-tyrosine residue. Based on the structure published (Matadeen et al, 2007) and the model figure in Heinrich, et al (Heinrich et al, 2003).

The conformational changes of the gp130 receptor that lead to activation of the associated JAKs may involve: a shift from an extended to compressed form for gp130, a rotation around the vertical axis of symmetry of the complex and a "flapping" movement of the IL-6-bound domains (Matadeen et al, 2007). Together these movements could result in the repositioning of the rigid transmembrane α-helices of gp130 relative to each other, bringing the JAKs into closer proximity and affecting the interface between the JAKs and the gp130 tail to increase JAK activity (Haan et al, 2002; Matadeen et al, 2007; Wallweber et al, 2014). The increased activity due to conformation rearrangement enables the JAKs to phosphorylate each other. This increases their catalytic ability further and enables their phosphorylation of specific gp130 tyrosine residues in YXXQ

motifs, specifically Y^{767}, Y^{814}, Y^{905} and Y^{915} in IL-6 signalling (Heinrich et al, 2003). In turn, the phosphorylated gp130 tyrosines provide binding sites for STAT3 dimers, leading to the next step in the JAK-STAT signalling pathway: JAK phosphorylation of STAT dimers. These signal transduction events are swift; JAK and gp130 phosphorylation are detectable within 2 min of IL-6 stimulation and STAT3 phosphorylation occurs within 5 min (Wang & Fuller, 1994).

1.2.4.2 Signalling Beacon Hypothesis

The IL-6-induced activation of the receptor complex on its own is insufficient for downstream STAT3 activation and transcriptional activity; endosome trafficking is needed for maximal STAT3 activity. Disruption of both clathrin-mediated receptor internalisation and early endosome signalling inhibits STAT3-dependent transcription (Bild et al, 2002). Clathrin-coated vesicles become early endosomes which present activated IL-6 receptors to the cytoplasm and act as 'beacons of STAT3 activation' (German et al, 2011). STAT3 dimers rapidly cycle on and off the signalling endosomes where they are tyrosine phosphorylated at Y705 (Shah et al, 2006). The signalling process is terminated by the maturation of early endosomes into late endosomes and subsequently into lysosomes where the IL-6, IL-6R and gp130 are finally degraded; the entire process takes 2-3 h in total (Graeve et al, 1996; Tanaka et al, 2008).

1.2.4.3 STAT Phosphorylation and Dimer Conformation Switching

Tyrosine phosphorylation of the STAT dimers by the activated JAKs located on the signalling endosomes happens rapidly. It is generally described as rendering STATs transcriptionally active, even though there is now evidence that the non-phosphorylated STAT dimers, especially STAT1 and STAT3, have specific transcriptional and non-transcriptional roles within the cell (Yang et al, 2005; Yang & Stark, 2008; Stark & Darnell, 2012). It is more accurate to say that tyrosine phosphorylation stabilises a "parallel" dimer conformation that has a high DNA-binding affinity. In this parallel configuration, the C-termini are located at the same end of the dimer and the dimer is stabilised by the SH2-phospho-tyrosine interactions between the monomers (Fig. 1.3B) (Mao et al, 2005; Zhong et al, 2005). As well as increasing the DNA-binding affinity, the

configuration change alters the modes of nuclear import and prevents nuclear export, thereby perturbing the nucleocytoplasmic shuttling equilibrium and resulting in the accumulation of phosphorylated STATs within the nucleus (Vinkemeier, 2004).

STATs are also phosphorylated on conserved serine residues located in the transactivation domain, for example Ser727 in STAT3 (Decker & Kovarik, 2000). MAP (Mitogen Activated Protein) Kinases, induced by other cytokine signalling in addition to IL-6, and other kinases, such as CDK5 (cyclin-dependent kinase 5) and the mTOR (mammalian target of rapamycin) kinase, are responsible for serine phosphorylation (Decker & Kovarik, 2000; Wakahara et al, 2012). The MAP kinases are recruited by SH2 adaptor proteins and Erk1/2, JNK and p38 are among the MAPKs recruited to the IL-6 activated receptor complex located on the early signalling endosomes (Hibi & Hirano, 1998). Serine phosphorylation has roles in transcription co-factor recruitment and in regulating tyrosine phosphorylation and therefore STAT transcriptional activity (Schuringa et al, 2001; Wakahara et al, 2012).

1.2.5 Getting the STAT Signal to the Nucleus

1.2.5.1 Nuclear Import of STATs

STAT1, STAT3, STAT5 and STAT6 constitutively shuttle between the nucleus and cytoplasm and accumulate upon tyrosine phosphorylation whereas STAT2 and STAT4 require tyrosine-phosphorylation to translocate into the nucleus (Reich, 2013). As such, nuclear trafficking is highly complex and varies between STATs (Vinkemeier, 2004). Thus despite considerable efforts, the precise mechanisms of STAT nuclear trafficking are still rather unclear (Reich, 2013).

STAT proteins are too large to enter or exit the nucleus by diffusing through the Nuclear Pore Complex (NPC), instead they must either interact directly with nucleoporins, the protein components of the NPC, or indirectly via karyopherins, the chaperone trafficking proteins for the NPC consisting of the importins and exportins (Komeili & O'Shea, 2001). Direct interaction with the NPC in carrier-free transport is rare; most proteins rely on carrier-dependent

transport by the karyopherins. To interact with either system, the protein must possess Nuclear Localisation Signals (NLS) and Nuclear Export Signals (NES), weakly conserved amino acid sequences on the surface of the protein (Vinkemeier, 2004). A number of NLS and NES have been identified for each STAT, some conserved between STATs and others not (Kisseleva et al, 2002; Pranada et al, 2004; Vinkemeier, 2004). The different combinations of NLS and NES maintain the finely balanced equilibrium that result in the observed nucleocytoplasmic distributions of STATs 1, 3, 5 and 6.

Unphosphorylated STAT1 and STAT3 use carrier-free transport to enter and exit the nucleus (Marg et al, 2004; Vogt et al, 2011) but it is unclear whether other STATs also use this mechanism. In addition, STAT1 enters the nucleus using the karyopherins importin-α1:importin-β, whilst STAT3 uses importin-α3:importin-β (reviewed Reich, 2013). Meanwhile nuclear export of U-STATs requires but does not entirely depend on CRM-1/exportin-1; inhibiting CRM-1 with Leptomycin-B leads to the slow nuclear accumulation of STAT3 and STAT1 because carrier-dependent nuclear export has been blocked (Bhattacharya & Schindler, 2003; Marg et al, 2004; Vinkemeier, 2004).

1.2.5.2 Live Cell Imaging of STAT Nuclear Accumulation

The nuclear accumulation of STATs has been visualised through live cell imaging experiments using fluorescent protein-tagged STATs. STAT1 was shown to accumulate in the nucleus and the nuclear localisation was sustained for 24 h after IFN-γ stimulation (Fig. 1.5) (Köster & Hauser, 1999). STAT3 accumulation in the nucleus was imaged at 5 minute intervals for 1 h in HepG2 cells stimulated with 20 ng/ml IL-6 for the duration of the experiment (Fig. 1.6) (Pranada et al, 2004). The maximum nuclear intensity was observed between 30 and 40 min post-IL-6 stimulation. STAT6 was similarly shown to accumulate in the nucleus over a 1 h period after IL-4 signalling, and in this instance both N- and C-terminal GFP tags were considered (Nelson et al, 2002). The N-terminal tag translocated into the nucleus faster and was more transcriptionally active and this raises questions about how best to tag STATs with fluorescent proteins.

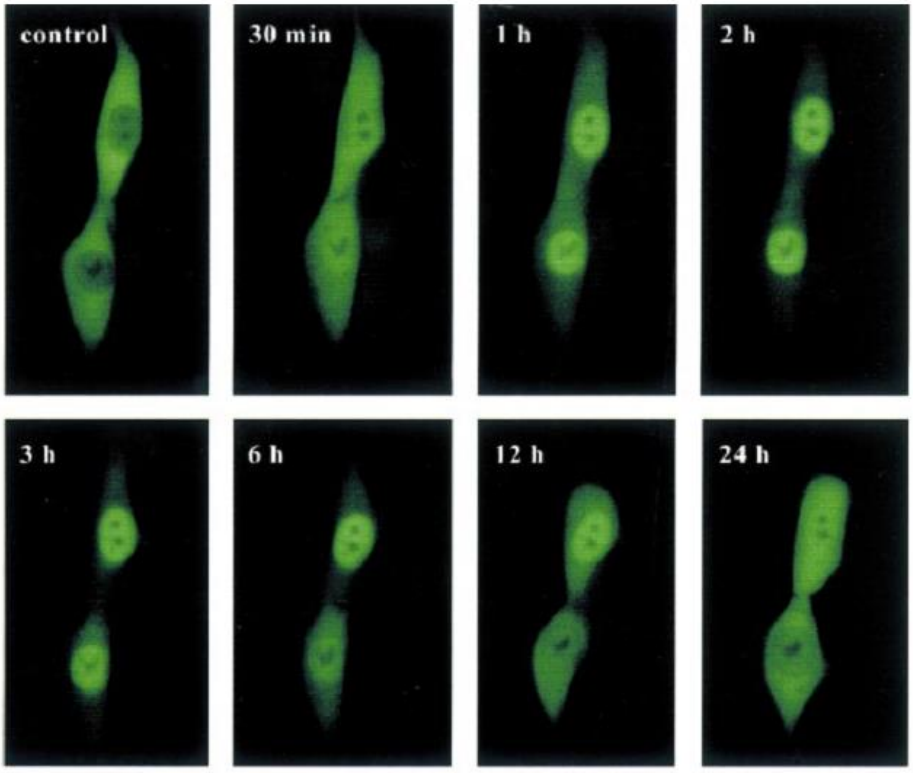

Figure 1.5: STAT1 time-dependent accumulation in the nucleus. STAT1-GFP in stably-transfected C243 cells, stimulated with IFN-γ. Reproduced from Köster and Hauser (1999).

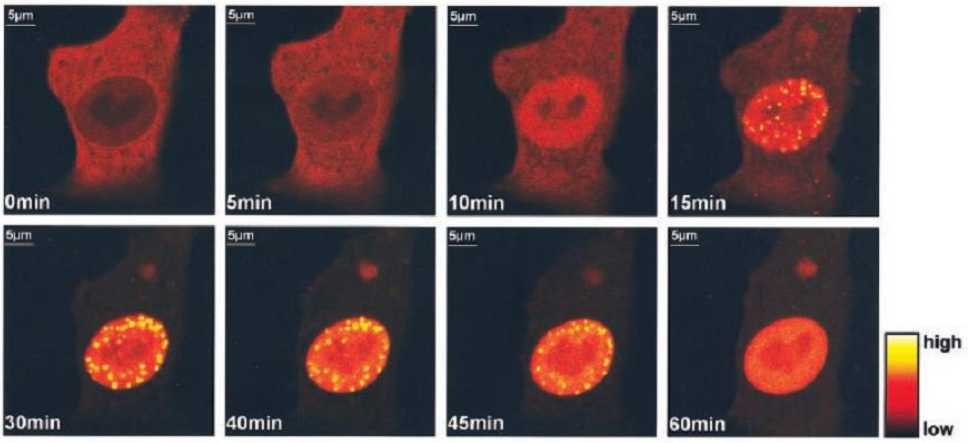

Figure 1.6: Live cell fluorescence imaging of STAT3 nuclear accumulation. STAT3-CFP-YFP transfected into HepG2 cells and stimulated with 20 ng/ml IL-6. Artificially coloured heat map of fluorescence intensity. Reproduced from Pranada et al, (2004) .

1.2.5.3 STAT DNA Binding and Gene Transcription

Tyrosine phosphorylated STATs bind DNA with much higher affinity that non-phosphorylated STATs and this is thought to be what traps them in the nucleus, leading to nuclear accumulation (Pranada et al, 2004; Wenta et al, 2008). As phospho-STATs accumulate in the nucleus they specifically bind γ-activated sequences (GAS), palindromic motifs of $TTCN_{2-5}GAA$, so called because they were first discovered through gamma-Interferon signalling (Decker et al, 1997).

STAT3 initiates transcription of a host of genes in the co-ordination of the Acute Phase Response in response to IL-6 signalling (Moshage, 1997). Genes responsive to IL-6 typically have a consensus GAS sequence within their promoter region. The products of these genes include critical effectors of the innate immune response, such as the complement system, and also the proteins and enzymes needed for the repair response, such as fibrinogen which is necessary for blood clotting (Bode et al, 2012a). Other STAT3-responsive genes are regulated in a more complex fashion and rely on non-consensus STAT3 response elements. For example, Serum Amyloid A is strongly induced in response to IL-6 in conjunction with NF-κB stimuli (Bode et al, 2012a). In this instance, STAT3 binds to a site 3' of the NF-κB response element, after forming a heteromeric complex with p65 and p300, a transcriptional co-activator (Hagihara et al, 2005). Several other APR genes are also co-operatively induced by STAT3 and NF-κB whereas other genes are up-regulated by STAT3 but down-regulated by NF-κB, highlighting the complexity of the transcriptional outcomes of STAT3 and NF-κB cross-talk.

An additional important set of genes induced by STAT signalling are for the SOCS proteins. The SOCS proteins form negative feedback loops for STAT signalling and are essential for the proper regulation of JAK-STAT signalling and STAT-induced gene transcription.

1.2.6 Turning Off JAK-STAT Signalling

1.2.6.1 Deactivation and Nuclear Export

Phosphorylated STATs must be dephosphorylated before they can be exported from the nucleus; inhibition of protein-tyrosine phosphatases (PTPs) prevents nuclear export (Meyer et al, 2003). Several different PTPs which

dephosphorylate STATs in the nucleus have been identified, including SHP2 (SH2-domain-containing tyrosine phosphatase), PIAS3 (protein inhibitor of activated STAT3) and TC45/TC-PTP (T cell-PTP) (Yamamoto et al, 2002; Wakahara et al, 2012). Phosphorylation of a conserved serine residue, Ser727 in STAT3, regulates TC45 phosphatase activity (Wakahara et al, 2012). The rate of STAT dephosphorylation is partially regulated by STAT DNA binding, with the rate of dephosphorylation being proportional to the DNA off-rate (Meyer et al, 2003). It is hypothesized that the parallel dimer, once unbound from DNA, spontaneously switches to the anti-parallel configuration, facilitating dephosphorylation of phospho-tyrosine-STAT dimers by nuclear PTPs. Loss of the phospho-tyrosine:SH2 interaction further destabilises the parallel dimer conformation, promoting the antiparallel STAT dimer configuration (Zhong et al, 2005). The dephosphorylated antiparallel STAT dimers are finally exported by the mechanisms that govern nuclear export in unstimulated cells, namely CRM-1 mediated export and constitutive STAT carrier-free export, and the export rate after stimulation is unchanged from before stimulation (Cimica et al, 2011).

1.2.6.2 Constitutive Inhibitors of STAT Signalling

The protein tyrosine phosphatases essential for STAT dephosphorylation are constitutive inhibitors of cytokine signalling and do not require *de novo* protein synthesis. Although previously discussed in the context of nuclear dephosphorylation, PTPs are also active in the cytoplasm and have other roles besides inhibiting cytokine signalling. The cytoplasmic PTPs include SHP1, SHP2, TC-PTP, PTP-Receptor, CD45 and PTP1B (Heinrich et al, 2003; Wakahara et al, 2012). SHP2 is particularly interesting because in addition to dephosphorylating STATs, it also dephosphorylates gp130 and the associated JAKs. In doing so it prevents the phosphorylation of additional STATs and contributes to turning cytokine signalling off at the source (Schmitz et al, 2000; Lehmann et al, 2003).

PIAS3 is part of a family that includes PIAS1, PIAS2 and PIAS4 (Yagil et al, 2010). Although PIAS1 and PIAS3 were discovered in the context of inhibiting STAT1 and STAT3 respectively (Chung et al, 1997), inhibiting STATs is by far

from their only role. The PIAS family has since been found to regulate upwards of 60 proteins, mostly transcription factors including NF-κB and SMADs, and they positively up-regulate some and down-regulate many others (Yagil et al, 2010). PIAS proteins have several different mechanisms for regulating target proteins. They possess a SUMO-E3-ligase domain and are also able to bind to chromatin at scaffold attachment sites, often near gene enhancers. They also have a domain that inhibits STATs and another that activates nuclear receptors (Yagil et al, 2010). Unfortunately the precise details of how exactly PIAS proteins regulate their many targets, including STAT3, are unclear.

1.2.7 SOCS Proteins and Inducible Negative Feedback

1.2.7.1 The SOCS Family

The SOCS family was first discovered as inhibitors of cytokine signalling, induced by STATs. CIS (cytokine-inducible SH2-domain containing protein) was discovered in 1995 (Yoshimura et al, 1995) while SOCS1 was discovered by three groups simultaneously, each using different techniques (Endo et al, 1997; Naka et al, 1997; Starr et al, 1997). SOCS2 and SOCS3 were identified at the same time (Starr et al, 1997). Four additional SOCS, SOCS4, SOCS5, SOCS6 and SOCS7, were subsequently identified on the basis of conserved DNA sequences (Hilton et al, 1998). The roles of CIS, SOCS1-3 and their mechanisms of signalling inhibition are now reasonably well understood. SOCS1-3 and CIS are virtually undetectable in most cell types but are rapidly induced by STATs in response to cytokine signalling. They inhibit the activity of the cytokine receptor type that induced their expression by targeting the activated receptors for proteasomal degradation and, in the case of SOCS1 and SOCS3, by also directly preventing JAK kinase activity (Linossi et al, 2013). In doing so, SOCS1-3 and CIS form classical negative feedback loops. For example, IL-6 induces STAT3 activation, which induces SOCS3 expression, which in turn inhibits the active IL-6 receptor complex.

Conversely the *in vivo* functions of SOCS4-7 are far less clear. They are constitutively expressed at high levels in many cell types, and seem to be predominantly involved in down-regulating Receptor Tyrosine Kinase (RTK) signalling pathways, including insulin, growth hormone and epidermal growth

factor (EGF), through proteasomal degradation of the receptors (Croker et al, 2008a; Babon et al, 2014).

1.2.7.2 Biological Roles of SOCS

CIS and SOCS2, which share 45% sequence homology, act in a similar fashion and have some overlap in the cytokine signals they inhibit. CIS and SOCS2 both inhibit cytokines that signal via STAT5 including leptin (Lavens et al, 2006), prolactin (Dif et al, 2001; Endo et al, 2003), and Growth Hormone (GH) (Ram & Waxman, 2000; Greenhalgh et al, 2005; Vesterlund et al, 2011) whilst CIS also inhibits EPO (Verdier et al, 1998) and IL-2 signalling (Aman et al, 1999). SOCS4 and SOCS5 are both inhibitors of EGF (Kario et al, 2005) and SOCS4 may have a role in ovarian folliculogenesis (Sutherland et al, 2012). SOCS6 and SOCS7 down-regulate RKTs, such as KIT (Bayle et al, 2004) and the Insulin Receptor (Kabir et al, 2014). They appear to inhibit MAPK signalling from the RTKs, including ERK1/2, p38 and AKT (Kabir et al, 2014). SOCS6 can be found in the nucleus as well as the cytoplasm and has also been reported to regulate STAT3 protein levels (Hwang et al, 2007). SOCS1 and SOCS3 are the most potent of the SOCS and each specifically regulates one particular class of cytokines. SOCS1 inhibits Type I and Type II Interferons which signal to STAT1 via the γC-receptor (reviewed Linossi et al, 2013) whereas SOCS3 inhibits IL-6-type cytokines that signal via gp130 to STAT3 (Croker et al, 2003; Babon et al, 2014).

1.2.7.3 Domain Organisation of SOCS Proteins

The eight related proteins all possess an SH2 domain and an extended SH2 domain (ESS) for binding phospho-tyrosine residues, and a domain called the 'SOCS box', approximately 40 amino acids long, that functions as a recruiter for an E3 ligase complex (Kile et al, 2002; Kershaw et al, 2014). The SOCS proteins are divided into two groups according to the length of their N-terminal region; CIS, SOCS1-3 have short N-terminal regions whereas SOCS4-7 have extended N-terminal regions (Linossi et al, 2013). Different pairs of SOCS proteins also have additional shared features. For example, SOCS1 and SOCS3 have a Kinase Inhibitory Region (KIR) which is essential for the direct inhibition of their JAK targets (Sasaki et al, 1999). SOCS3 and CIS both have a PEST (proline, glutamic acid, serine and threonine) sequence which reduces their stability *in vivo* (Babon et al, 2005). SOCS4 and SOCS5 meanwhile share a conserved region

within their extended N-terminal regions, whose function is unclear (Feng et al, 2012). Fig 1.7 illustrates the domain structures of the different SOCS proteins (Linossi et al, 2013).

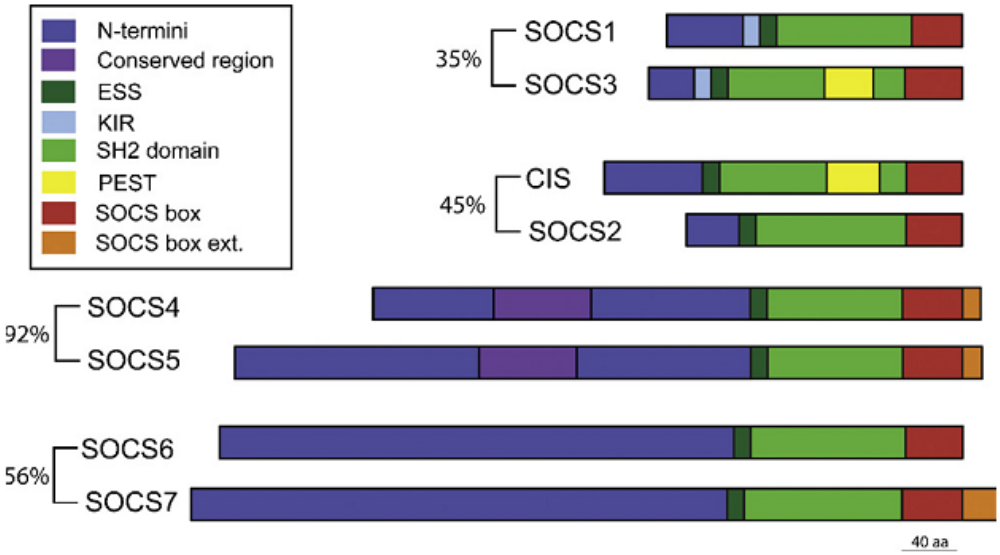

Figure 1.7: SOCS proteins' domain architecture. Each contains a C-terminal SOCS Box motif, the SH2 domain, extended SH2 domain (ESS) and a variable N-terminal region. SOCS1 and SOCS3 also contain the kinase inhibitory region (KIR), while SOCS3 and CIS have a PEST domain. Domains colour-coded, and SOCS paired by sequence homology (%). Reproduced from Linossi et al, (2013).

1.2.7.4 Mechanisms of Inhibition

SOCS proteins bind to their targets using their ESS and SH2 domains, which together recognise specific phospho-tyrosine residues on the JAKs and associated signalling receptors e.g. γC-Receptor or gp130 (Linossi et al, 2013). Some SOCS bind phospho-tyrosines on the JAKs but SOCS3 preferentially binds to the phospho-tyrosines of the gp130 cytoplasmic tail (Nicholson et al, 2000). It has been shown that SOCS3 preferentially binds simultaneously to gp130 and either JAK1, JAK2 or TYK2, using two independent interaction faces to do so. This three-way complex of JAK, gp130 and SOCS3 explains the high binding avidity of SOCS3 (Kershaw et al, 2013). It is hypothesised that at least SOCS1 will also use this mechanism (reviewed Linossi et al, 2013).

Once bound to their targets, all SOCS proteins function as E3 ligase recruiters, targeting the receptors for proteasomal degradation. The SOCS box forms an active E3 ligase complex with Cullin-5 and Elongins-B/C which ubiquitinates the target on Lys48 (Bullock et al, 2006; Kershaw et al, 2014). This leads to the down-regulation of activated receptor complexes through proteasomal degradation, and so to the cessation of cytokine signalling.

Of particular interest is the additional mechanism of inhibition used by SOCS1 and SOCS3. These SOCS proteins both possess a kinase inhibitory region. This is a small, unstructured, 12 amino acid motif located N-terminally of the ESS and SH2 domains (Babon et al, 2005; Babon et al, 2006). It was originally hypothesized that the KIR acted as a pseudo-substrate for activated JAKs, based on the KIR's similarity to the JAK activation loop (Sasaki et al, 1999). However, recent work revealed that the KIR binds alongside the JAK activation loop and so blocks substrate, e.g. STAT3, access to the active site (Kershaw et al, 2013). By blocking the JAK kinase domain and decreasing its catalytic activity, as well as increasing the receptor degradation rate, SOCS1 and SOCS3 reduce the rate of STAT1 and STAT3 phosphorylation, thereby inhibiting STAT transcriptional activity and cytokine signalling, and shaping the immune response appropriately (Croker et al, 2008b; Linossi et al, 2013).

1.2.7.5 Regulation of SOCS3 Expression

The expression of inducible SOCS proteins is tightly regulated to prevent uncontrolled immune responses. SOCS3 is rapidly induced by IL-6-activated STAT3, appearing within 15 min of IL-6 stimulation and peaking around at 1 h (Siewert et al, 1999; Yoshiura et al, 2007). In addition to intrinsic proteasomal degradation, the half-life of SOC3 protein varies in a cell-line dependent manner and can also be altered by additional signalling events, thus facilitating cross-talk between STATs and other signalling pathways. The protein half-life of SOCS3 varies between 20 min and as much as 4 h, depending on the cell-line and additional post-translational modifications (Siewert et al, 1999; Sasaki et al, 2003). SOCS3 can be phosphorylated on two tyrosines, Tyr^{204} and Tyr^{221}, within the SOCS box by Src kinases or RTKs, active as a result of other cytokine signals. These phosphorylation events destabilise the interaction between SOCS3 and

elongin-C, facilitating SOCS3 degradation by the proteasome (Haan et al, 2003; Sommer et al, 2005). In turn, SOCS3 protein levels decrease and the SOCS3 inhibition of STAT3 activation is reduced, with important implications for cross-talk between signalling pathways (Sommer et al, 2005).

SOCS3 mRNA is another point of cross-talk between STAT3 and other signalling networks. Not only does SOCS3 mRNA half-life vary by cell type, but it can be increased by other signalling pathways. In NIH-3T3 (mouse embryo fibroblast) cells, the half-life of SOCS3 mRNA is 22 $\pm$ 5 min and in RAW 264.7 macrophages it is 17 $\pm$ 3 min but in primary human bone-derived macrophages it is 49 $\pm$ 4 min (Ehlting et al, 2007). These half-lives increase by approximately 20 min in response to TNFα signalling through the p38/MAPK stress-response pathway, which stabilises the SOCS3 mRNA in a mechanism involving a destabilising A/U-rich element in its 3' UTR (untranslated region) (Ehlting et al, 2007). By increasing the mRNA half-life and thus the quantity of SOCS3 protein in the cell, the other cytokine signal, in this case TNFα, strengthens the inhibition of STAT3 and influences the overall immune response to IL-6.

1.2.8 STAT3 and SOCS3 as an Oscillating System

The induction of SOCS3 by IL-6-activated phospho-STAT3 forms a negative feedback loop that regulates phospho-STAT3 signalling within the cell, through the SOCS3 inhibition of JAK kinase activity at the IL-6 receptor (Fig. 1.8) (Yoshiura et al, 2007). Temporal delays between the key steps of the pathway, i.e. STAT3 translocation to the nucleus, SOCS3 gene transcription and SOCS3 protein expression, fulfil the basic requirements for oscillatory dynamics to arise within a signalling system.

Indeed, phospho-STAT3 and SOCS3 mRNA and protein were shown to interdependently oscillate in a population of serum-synchronised presomitic mesoderm cells (C3H10T½), in the context of the somite segmentation clock in the embryo (Yoshiura et al, 2007). Phospho-STAT3 (P-STAT3) had an oscillatory period of 2 h, as did SOCS3 protein, however the SOCS3 protein oscillations were an hour behind those of P-STAT3 (Fig. 1.9). In addition, there was a 1 h delay between SOCS3 mRNA translation and protein expression. SOCS3 siRNA knockdown abolished P-STAT3 oscillations, resulting in sustained

P-STAT3 whereas expression of a dominant-negative STAT3 abolished SOCS3 oscillations (Fig. 1. 9) (Yoshiura et al, 2007). This demonstrated the interdependence of the STAT3-SOCS3 oscillations.

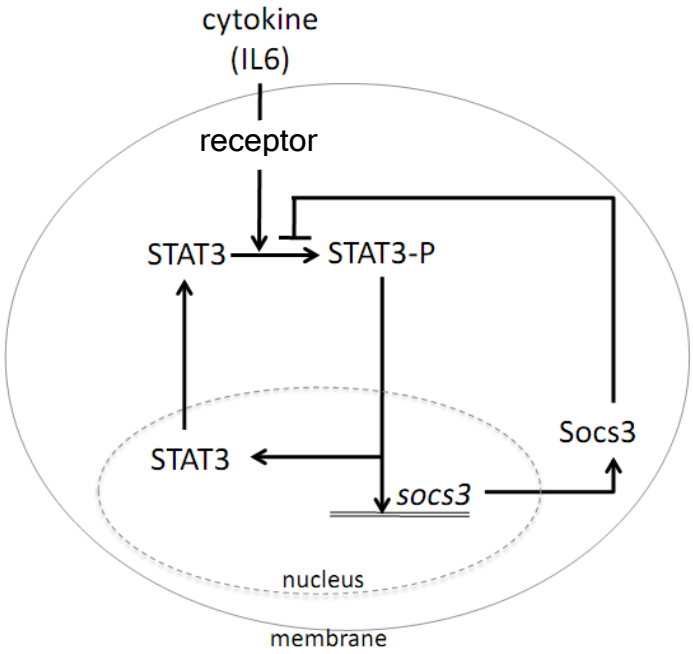

Figure 1.8: Schematic representation of STAT3-SOCS3 signalling, illustrating the SOCS3 negative feedback loop. Components include the IL-6-activated Receptor, unphosphorylated STAT3, phosphorylated STAT3 (P-STAT3), SOCS3 mRNA (*socs3*) and SOC3 protein (Socs3), compartmentalised into the cytoplasm and nucleus. Figure provided by N. Domedel-Puig.

In addition to the oscillations seen in serum-synchronised cells, biphasic kinetics were observed in the phosphorylation of STAT3 and SOCS3 mRNA levels in primary bone-marrow derived macrophages continuously stimulated with IL-6 (Wormald et al, 2006). The kinetics were dependent on SOCS3 as SOCS3-/- macrophages exhibited sustained STAT3 phosphorylation without biphasic kinetics. Furthermore, SOCS3 desensitised cells pre-treated with a 15 min pulse of IL-6 to a subsequent 15 min IL-6 pulse in a time-dependent manner, according to the rest period between pulses (Wormald et al, 2006). Elsewhere, biphasic kinetics at the population level have been indicative of oscillations within single cells being masked by intercellular heterogeneity (Ashall et al, 2009), suggesting that P-STAT3 also oscillates at the single cell level.

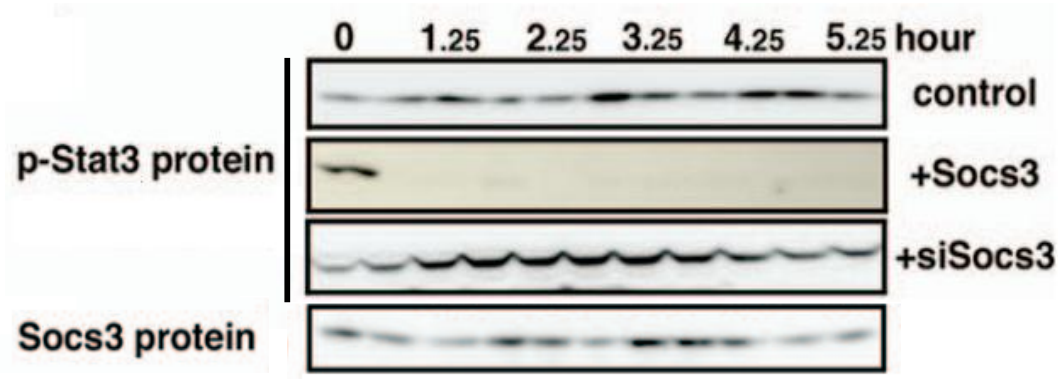

Figure 1.9: Oscillations in P-STAT3 and SOCS protein. Obtained from serum-stimulated C3H10T1/2 cells. Includes STAT3 control, expression with dominant SOCS3 (+SOCS3), and siRNA knock-down of SOCS3 (+siSOCS3). Blots reproduced from Yoshiura et al, 2007.

Together these two studies strongly suggest that P-STAT3 and SOCS3 mRNA and protein will oscillate in single cells in response to continuous IL-6 stimulation. Unfortunately it is not generally possible to study phosphorylation states using live cell fluorescence microscopy. However, since STAT3 undergoes a net nuclear translocation in response to IL-6 (Fig. 1.6) (Pranada et al, 2004), it may be possible to use bulk STAT3 translocation dynamics as a proxy for the phosphorylation state of STAT3 in long-term live cell fluorescence microscopy experiments. It may also be possible to observe SOCS3 mRNA and protein oscillations with the appropriate luciferase and fluorescent protein tagged reporter constructs.

1.3 NF-κB Signalling

1.3.1 Biological Context of NF-κB Signalling

The NF-κB (Nuclear Factor-kappaB) family of transcription factors has many roles throughout the immune system, and also in the cell cycle, proliferation, differentiation, and apoptosis (Gerondakis et al, 2006). Similar to the STATs, dysregulated NF-κB signalling is implicated in a host of diseases, including asthma, arthritis, heart disease, chronic inflammatory diseases and many cancers, and thus NF-κB is a prime target for medical intervention (Hayden & Ghosh, 2008). A wide variety of signals are transduced by NF-κB, including cytokines such as the TNFα, IL-1β, bacterial products e.g. lipopolysaccharide (LPS), and B and T cell mitogens. NF-κB also responds to genotoxic stress e.g. UV radiation, and to oxidative stress (Hayden & Ghosh, 2008). Consequently NF-κB is a major regulator of transcription and controls of upwards of 300 genes (Hoffmann & Baltimore, 2006).

1.3.2 Overview of NF-κB Signalling

As with the JAK-STAT system, NF-κB signalling is considerably complex therefore this section provides a brief overview of the canonical NF-κB pathway (Fig. 1.10). In unstimulated cells, NF-κB dimers are predominantly localised to the cytoplasm by Inhibitor of KappaB (IκB) proteins (Hayden & Ghosh, 2008). Activation of the NF-κB network by specific signals culminates in the activation of IKK, the Inhibitory-KappaB Kinase complex (Karin, 2008). This three component kinase phosphorylates IκB proteins, which targets them for ubiquitination and subsequent degradation, releasing NF-κB in the process (Karin, 1999). Unbound NF-κB dimers translocate to the nucleus where they bind to κB DNA sequences and initiate transcription. The nuclear translocation is short-lived and has been extensively imaged using fluorescence microscopy (Nelson et al, 2002; Nelson et al, 2004; Ashall et al, 2009). One gene activated by NF-κB is IκBα. Consequently, IκBα accumulates in the cytoplasm and translocates to the nucleus where it disrupts NF-κB:DNA binding, binds to NF-κB and exports it from the nucleus, thus halting transcription (Arenzana-

Seisdedos et al, 1997). In this way IκBα forms a classical negative feedback loop and is the primary negative regulator of NF-κB activity (Perkins, 2006). Other NF-κB regulated feedback genes include IκBε and A20, which have different roles within the NF-κB network.

1.3.3 NF-κB Proteins

Five homologous proteins comprise the NF-κB family (Bonizzi & Karin, 2004). They were first discovered as a nuclear factor bound to Kappa Light Chain promoters in B cells (Sen & Baltimore, 1986). The family members are RelA (p65), RelB, cRel, and NF-κB1(p105/p50) and NF-κB2 (p100/p52) (Chen & Greene, 2004). They form a variety of homo- and heterodimers, which each have different transcriptional roles (Perkins et al, 1992; Hayden & Ghosh, 2008).

NF-κBs all have an N-terminal RHD (Rel Homology Domain), an ~300 amino acid sequence responsible for DNA binding, interaction with IκBs, dimerisation, and nuclear localisation (Gilmore, 1999). In addition, p65, RelB and cRel contain a non-homologous C-terminal transactivation domain (TAD) which allows them to activate transcription by recruiting transcriptional co-factors and the basal transcription machinery to the promoter (O'Shea & Perkins, 2008). NF-κB1 and NF-κB2 do not contain a TAD and instead contain ARDs (Ankyrin Repeat Domains), a feature shared with the IκBs. Therefore NF-κB1 and NF-κB2 are considered to be inhibitory proteins (Rice et al, 1992). The C-terminal domains of NF-κB1 and NF-κB2 can be cleaved off at a specific site, either through proteolysis or arrested translation, resulting in p50 and p52 respectively (Moorthy et al, 2006). P50 and p52 are however able to form transcriptionally active heterodimers with p65, RelB and cRel (Siebenlist et al, 1994). The predominant dimer, p65:p50, is representative of the canonical signalling pathway, and is found in virtually all cell types for the regulation of inflammatory and immune responses (Siebenlist et al, 1994). The alternative pathway uses a RelB:p52 dimer to regulate lymphoid organogenesis, B cell survival and maturation, and dendritic cell activation (Sun, 2011).

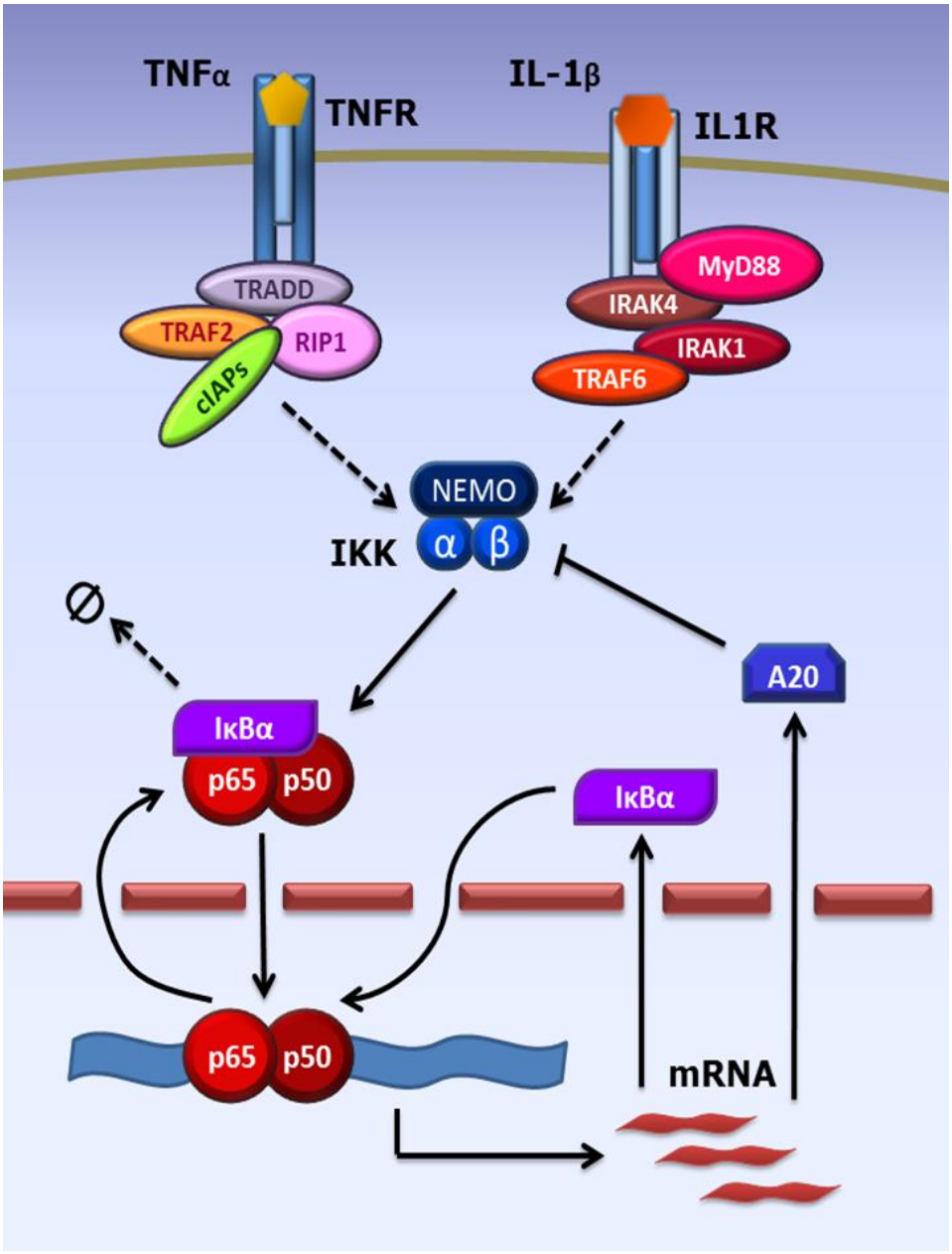

Figure 1.10: Overview of the Classical NF-κB Signalling pathway

TNFα and IL-1β bind to their respective receptors (TNFR and IL1R), triggering receptor activation. Mediator proteins including TRADDs, TRAFs and IRAKs lead to the activation of the IKK complex (NEMO, IKKα and IKKβ) through phosphorylation events. IKK then phosphorylates IκBs (here, IκBα), marking them for lysine ubiquitination. Ubiquitinated-IκBs are targeted to the proteasome for degradation, releasing NF-κB dimers (here p65 and p50) from inhibition. NF-κB dimers translocate to the nucleus *en mass* where they induce gene transcription. The genes transcribed include the inducible IκBs (IκBα, β, ε), and also the inhibitor A20. A20 inhibits IKK activity using a variety of mechanisms. Newly synthesized IκBα translocates to the nucleus where it binds NF-κB dimers and shifts their localisation equilibrium to the cytoplasm, resetting the system.

1.3.4 IKK Complex

The IKK complex is the focal point of the many signalling cascades that result in NF-κB activation (Hacker & Karin, 2006). It consists of three proteins, IKKα, IKKβ and NEMO (NF-κB Essential Modifier, also known as IKKγ), in 1:1:1 arrangement. IKKα and IKKβ phosphorylate NF-κB-bound IκB proteins whilst NEMO regulates the activity of IKKα and IKKβ (Rothwarf et al, 1998). IKKα and IKKβ possess an N-terminal serine kinase domain for phosphorylating targets, a leucine zipper and a helix-loop-helix domain to mediate protein:protein interactions and a NEMO-binding domain (NBD) (Zandi et al, 1997). Phosphorylation of the IKKα/β activation loops activates the kinase domain and enables phosphorylation of IκB targets (Hacker & Karin, 2006). Progressive auto-phosphorylation of IKK causes a conformational change that decreases kinase activity and makes the IKK more susceptible to phosphatases for complete deactivation (Hacker & Karin, 2006).

1.3.5 IκB Proteins

IκBs are a major regulatory mechanism for NF-κB signalling. They function in a number of different ways, notably by sequestering NF-κB in the cytoplasm, disrupting DNA binding, and facilitating nuclear export (Hayden & Ghosh, 2008). Certain IκBs may also have additional functions. Eight IκBs have been described so far, comprising two groups: classical and nuclear. All possess multiple ARDs, which facilitate binding to the NF-κB RHD (Siebenlist et al, 1994). Other common features include a C-terminal PEST sequence (important for destabilising the IκB), NLS and NES motifs, and Death Domains for interacting with particular receptors. The classical IκBs, IκBα, IκBβ, IκBε, and IκBγ (a splice variant of NF-κB1) and NF-κB2, all bind to NF-κB dimers and cause them to be retained in the cytoplasm. The nuclear IκBs, Bcl-3, IκBζ and IκBδ, are located in the nucleus where they are able to modulate NF-κB transcriptional activity (Hayden & Ghosh, 2008). The IκBs preferentially bind different NF-κB dimers, with IκBα and IκBε binding most strongly to the p65:p50 NF-κB heterodimer of the classical pathway.

It is important to note that 'cytoplasmic sequestration' of NF-κB by classical IκBs is an oversimplification. As with STATs, NF-κB dimers constitutively shuttle between the nucleus and cytoplasm but are localised predominantly in the cytoplasm of resting cells. This is because IκB binding obscures the NLS motif of NF-κB, allowing the exposed NF-κB NES to drive nuclear export (Turpin et al, 1999). IκB binding also interferes with DNA binding and in conjunction with cytoplasmic localisation, renders NF-κB transcriptionally inactive (Tergaonkar et al, 2005). NF-κB is only released from IκB inhibition once IKK-phosphorylated IκBs are recognised and poly-ubiquitinated on specific lysine residues by an ubiquitin ligase complex; this results in proteasomal degradation of ubiquitinated IκBs, thus releasing NF-κB and triggering its net nuclear translocation (Karin & Ben-Neriah, 2000; Perkins, 2006).

1.3.6 Regulation of NF- κB Transcriptional Activity

NF-κB transcriptional activity is regulated through a number of different mechanisms, including nuclear import, post-translational modifications and recruitment of co-activators and co-repressors of transcription (Hayden & Ghosh, 2008). Nuclear import is primarily regulated by interactions with the IκBs, however nuclear localisation is insufficient for NF-κB activity. Post-translational modifications e.g. phosphorylation and acetylation, further regulate NF-κB activity by determining which transcriptional co-activators and co-repressors interact with NF-κB (Perkins, 2006). Finally, ubiquitination by SOCS1 and other E3 ligases targets p65/NF-κB for proteasomal degradation (Ryo et al, 2003) and contributes to the deactivation of NF-κB signalling.

Other regulatory feedbacks exist besides the IκBs and post-transcriptional modifications. One is A20, a zinc-finger protein with de-ubiquitinating and ubiquitin ligase domains, which is rapidly induced by TNFα stimulation of NF-κB. Various inhibitory mechanisms have been proposed for A20 which predominantly act on events between receptor activation and IκB degradation, including blocking IKK phosphorylation and targeting key signalling components for proteasomal and lysosomal degradation (Verstrepen et al, 2010).

1.3.7 Dynamics of Classical NF- κB Signalling

As stated above, the classical NF-κB signalling pathway uses p65:p50 heterodimers. These dimers are retained in the cytoplasm by IκBα, IκBβ and IκBε. IκBα is strongly and rapidly induced by NF-κB signalling, forms a classical negative feedback loop, and is therefore particularly important to the regulation of the p65:p50 dimer. IκBα is rapidly degraded as a result of phosphorylation and ubiquitination, allowing p65:p50 to translocate into the nucleus (Turpin et al, 1999). NF-κB dimers reside in the nucleus until IκBα re-accumulates, at which point IκBα-mediated nuclear export takes over and returns NF-κB to the cytoplasm (Hayden & Ghosh, 2008) (Fig. 1.11). IκBβ is a weaker inhibitor of p65:p50 than IκBα but can compensate for its loss in genetic knock outs whilst IκBε preferentially inhibits p65 homodimers and therefore may regulate a specific subset of genes (Whiteside et al, 1997). These processes, from IKK activation to IκB expression, take time to occur but the delay between initiation of IκBα transcription and the accumulation of expressed IκBα protein represents a significant temporal delay. This delay, in conjunction with the negative feedback of IκBα inhibition of NF-κB transcriptional activity, primes the NF-κB signalling system for oscillatory dynamics.

Early biochemical studies of bulk cell populations on NF-κB signalling identified the stimulus-induced transient translocation of NF-κB to the nucleus as a biphasic response, caused by the degradation and resynthesis of IκBs (Baeuerle & Baltimore, 1988; Hoffmann et al, 2002). Subsequently, live cell imaging studies in the HeLa and the neuroblastoma SK-N-AS cell lines (Figure 1.12) (Nelson et al, 2004; Ashall et al, 2009) determined that in fact NF-κB exhibited oscillatory nucleocytoplasmic translocation dynamics that persisted for >20 hours.

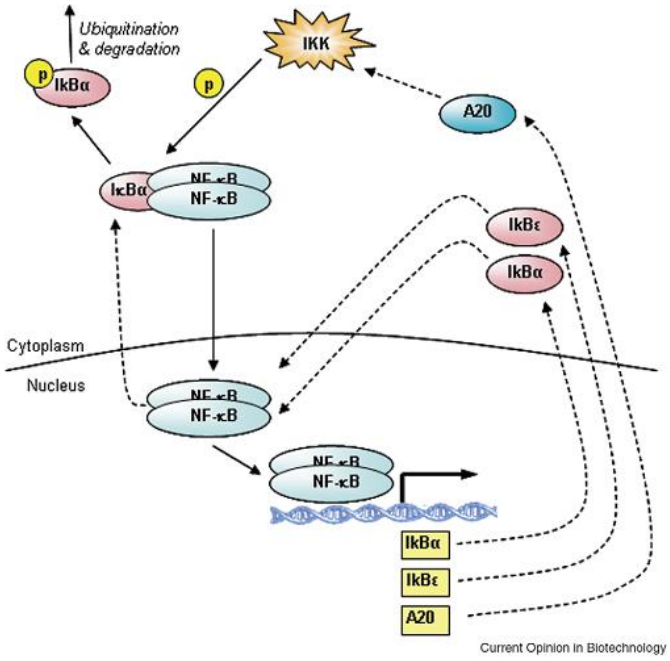

Figure 1.11: Representation of core components from the classical NF-κB pathway, modelled in Ashall et al, (2009). Reproduced from (Ankers et al, 2008).

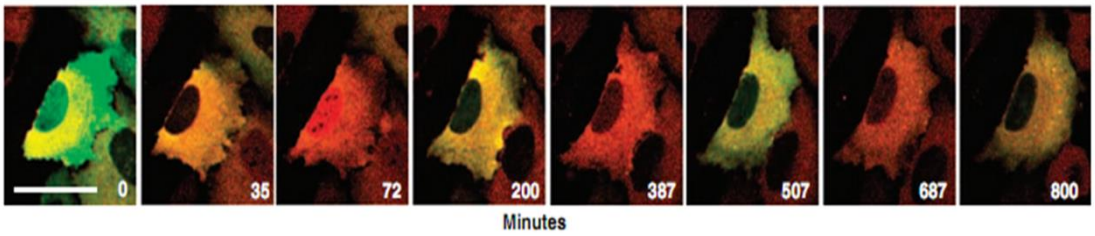

Figure 1.12: HeLa cell displaying oscillatory NF-κB nuclear translocations and IκBα degradation and resynthesis (Nelson et al, 2004).
Confocal microscopy time course of a single HeLa cell expressing p65-dsRed-Express (Red) under the control of a consensus κB promoter and IκBα-EGFP (green) under the control of a control κB promoter. The cell was treated with 10 ng/ml TNFα at time zero. Loss of green signal indicates degradation of IκBα. Net nucleocytoplasmic translocation of p65 is particularly clear at 72 min. Scale bar represents 50 μm.

The first p65 nuclear translocation was highly synchronised across the population but subsequent translocations, which decreased in amplitude over time, were heterogeneous between cells. The mean oscillatory period was 100 min. Because the oscillations were heterogeneous, the dynamics could be masked by population averaging, which would explain why oscillations were not seen in population-based studies. More recently, it was suggested that intercellular heterogeneity may contribute to a robustly maintained tissue level

response to cytokine signalling, which in this instance is driven by the 45 min delay in IκBε transcription relative to IκBα (Kearns et al, 2006; Paszek et al, 2010). Further studies have also found oscillations in mouse embryonic fibroblasts (MEFs) from NF-κB transgenic mice (Sung et al, 2009) and from a stable lentiviral transduced 3T3 cell line (Tay et al, 2010). Additionally, imaging IκBα using a κB promoter driven EGFP-tagged IκBα resulted in IκBα levels oscillating out-of-phase with NF-κB nucleocytoplasmic oscillations (Nelson et al, 2004).

A single 5 min TNFα pulse caused a single synchronous NF-κB nuclear translocation in over 97% of cells with no following cycles of activation (Nelson et al, 2004). Repeat pulses of TNFα were able to trigger additional rounds of activation, indicating that the system was still responsive. Pulses at 60 and 100 min intervals resulted in synchronous but weaker translocations whereas a 200 min interval was able to trigger a full strength translocation, indicating that the system has a re-set period (Ashall et al, 2009). Since translocations were responsive to the period of stimulation, this suggested that the oscillation frequency may be functionally important. The strength of the TNFα dose is also important to the NF-κB response. Reducing TNFα from the saturating 10 ng/ml dose was found to reduce the percentage of responding cells but not the translocation amplitude in cells that responded (Turner et al, 2010).

To investigate the importance of oscillation frequency, gene expression patterns in response to differently timed TNFα pulses were investigated (Ashall et al, 2009). NF-κB regulated genes have been classified into early, middle and late responders, depending on how quickly they are induced by TNFα (Tian et al, 2005), and it was found that certain genes from these groups exhibited different transcriptional profiles in response to the different pulsing regimes (Ashall et al, 2009). This strongly suggests that oscillation frequency is important for differential transcription, and suggests that pulsatile stimulation may be more important in driving immune responses of cells and tissues than continuous exposure to cytokines.

1.3.8 Modelling NF-κB Dynamics

The complexity of the NF-κB signalling network and the dynamic responses of the system makes an intuitive understanding difficult, making NF-κB a prime candidate for mathematical modelling. Numerous mathematical models have been developed over the years, initially aimed at understanding how IκBs retained NF-κB in the cytoplasm of unstimulated cells (Carlotti et al, 2000) and the biphasic population response (Hoffmann et al, 2002). With the advent of fluorescent single cell microscopy, quantitative time-resolved data became available which was ideal for constraining models of NF-κB signalling (Nelson et al, 2004). This early model had a core motif of NF-κB retained in the cytoplasm by IκBα, which was degraded upon TNFα activation of the IKK. NF-κB translocation to the nucleus led to IκBα synthesis which pulled NF-κB out of the nucleus and returning it to the starting state. Later, an IKK module was introduced with three states for IKK activity and A20 feedback onto IKK activation was also incorporated (Ashall et al, 2009). IκBε transcription with the 45 min delay was also included. The IκBα and IκBε components formed a dual delayed negative feedback motif (Alon, 2007). This model predicted that IκBε feedback would be responsible for the intercellular heterogeneity of NF-κB oscillations (Ashall et al, 2009).

The prediction regarding IκBε feedback was investigated using both experimental and theoretical approaches (Paszek et al, 2010). This analysis indicated that the delayed IκBε feedback was optimised for maximum heterogeneity, and was supported by experimental data which found that IκBε$^{-/-}$ MEFs had more synchronous oscillations. Additionally, the study found that IκBε contributed to maintenance of oscillations. (Paszek et al, 2010).

There remain many aspects of the NF-κB pathway that modelling is attempting to address, such as the role of different IκBs, IKK activity, and other feedbacks e.g. A20; a variety of modelling approaches are being applied. Many different models have been produced by both theoretical and biological groups and both single cell data and population data, obtained from a variety of cell lines in response to different stimuli, continue to be crucial in their development (for detailed reviews, see Basak et al, 2012; Williams et al, 2014).

1.4 STAT and NF-κB Cross-Talk

The NF-κB and STAT networks are instrumental to the regulation of immune system functions and may affect each other considerably towards this end. The two networks together have been shown to link inflammation to cancer development, and may be co-opted by different cancers to avoid the immune system and to promote their own survival (for reviews see Bollrath & Greten, 2009; Grivennikov & Karin, 2010; He & Karin, 2011; Fan et al, 2013; Hoesel & Schmid, 2013). Numerous interaction mechanisms have been proposed for STATs and NF-κB, including autocrine and paracrine events through secretion of cytokines, as well as intracellular mechanisms involving feedback loops, other signalling pathways and direct interactions between STAT and NF-κB family members.

Intercellular cross-talk through secretion of IL-6 is well documented in a variety of cellular contexts: it helps cancer cells escape TNFα-triggered apoptosis (Li et al, 2012), is involved in graft rejection (Lee et al, 2012), and auto-immunity (Ogura et al, 2008). IL-6 can also modulate LPS (lipopolysaccharide) - TLR4 inflammation via STAT3 signalling (Greenhill et al, 2011).

Mechanisms for intracellular cross-talk are more complex and context-dependent, as different effects predominate depending on cell line and cytokine stimulus. Modulation of SOCS feedback has been found in a number of contexts, using both SOCS1 and SOCS3. The earliest example is of LPS and TNFα co-operatively inducing SOCS3 expression in macrophages, thereby inhibiting IL-6 signalling via STAT3 (Bode et al, 1999). This was found to occur via TLR4 activation of p38/MAPK, leading to the stabilisation of SOCS3 mRNA (Bode et al, 2001; Ehlting et al, 2007; Bode et al, 2012b). By stabilising SOCS3 mRNA, LPS/TNFα signalling is able to inhibit STAT3 activation. This mechanism was also found for IL-1β in macrophages (Yang et al, 2004). Similarly, the influenza virus inhibits the antiviral IFN response by using NF-κB to drive SOCS3 expression, thereby inhibiting STAT1 and STAT3 (Pauli et al, 2008). MAPK/p38 was also found to inhibit IL-6 signalling via a SOCS3-independent mechanism, for LPS, TNFα and IL-1β (Bode et al, 2003; Yang et al, 2004; Albrecht et al, 2007; Kiu et al, 2007). This was subsequently found to be facilitated by

phosphorylation of the gp130 receptor, via SHP2 and MK2, leading to increased internalisation and proteasomal degradation of activated receptor complexes (Bode et al, 2003; Radtke et al, 2010).

Conversely, SOCS1 and SOCS3 have been shown to down-regulate NF-κB signalling (Park et al, 2003; Albanesi et al, 2007), and a possible mechanism for this is the destabilisation of NF-κB in the nucleus via SOCS-mediated ubiquitination (Strebovsky et al, 2011). Yet another effect using feedback loops requires A20, a negative NF-κB feedback known to inhibit IKK activation. A20 was in fact shown to decrease SOCS3 expression and thereby increase IL-6-STAT3 signalling (da Silva et al, 2013).

In addition to the indirect cross-talk via modulation of feedback loops, there is some evidence for direct interaction of specific NF-κB and STAT species. Most of this evidence is for direct interactions on the promoters of specific genes (Bode et al, 2012a), where STAT3 and NF-κB co-operate for the maximal transcription, e.g. for Serum Amyloid A (Hagihara et al, 2005) alpha-2-macroglobulin (Uskokovic et al, 2007), and hepcidin (Sow et al, 2009). However there are two examples of direct interaction between p65 and STAT3, for both the phosphorylated and unphosphorylated forms of STAT3, Lee et al., (2009) and Yang et al., (2007) respectively. Phospho-STAT3 was shown to maintain p65 activity in the nucleus through the hyper-acetylation of p65 by p300, whereby P-STAT3 facilitated the interaction between p300 and p65 (Lee et al, 2009). Unphosphorylated-STAT3 meanwhile was shown to bind to NF-κB, outcompeting IκBα for p65 dimers, consequently forcing p65/NF-κB translocation to the nucleus via a STAT3 NLS (Yang et al, 2007). This effect was only seen after prolonged IL-6 signalling, which causes U-STAT3 dimers to accumulate in the cell. The nuclear U-STAT3:p65 complexes initiate transcription of a specific subset of genes, that has only limited overlap with IL-6-STAT3 or TNFα-p65 target genes, thereby altering late gene expression profiles in response to co-activation of STAT3 and NF-κB (Yang et al, 2007).

In light of these different and opposing mechanisms for cross-talk between STAT3 and NF-κB, it would be unsurprising if the signalling dynamics of the two networks were perturbed by co-stimulation protocols. Given that many of these

mechanisms are indirect, the results of the interplay between them might be quite subtle, but may also be non-intuitive, with surprising consequences for their respective dynamics. It may be possible to visualise these effects without a detailed understanding of which processes are at work in any given situation, and as such, the single cell fluorescence microscopy techniques may be highly informative.

1.5 Thesis Aims

The studies presented in this chapter provide evidence to suggest that STAT3 may be capable of oscillatory nucleocytoplasmic dynamics in single cells. Therefore the first aim of this thesis is to image IL-6-induced STAT3 dynamics in single cells using fluorescent fusion protein reporters for STAT3 and its inhibitor SOCS3. If STAT3 oscillatory dynamics are confirmed in single cells, this data will be used to refine an existing mathematical modelling of the pathway that predicts single cell oscillations (Domedel-Puig, unpublished), with the intention of generating new testable hypotheses about the nature of IL-6-induced STAT3 signalling. The second aim of this thesis is to investigate cross-talk between STAT3 and NF-κB, a system with known oscillatory dynamics, through a consideration of their respective dynamics in response to combinations of different stimuli. This thesis will also attempt to correlate any dynamic outputs to gene expression patterns, as changes in signalling dynamics have been shown to be biologically important elsewhere.

Chapter 2
Materials and Methods

2.1 Materials

Suppliers for specific reagents are stated in the text. All other general chemicals and reagents were from Sigma-Aldrich, (Gillingham, UK) or Invitrogen (Paisley, UK). Sigma supplied the antibiotics tetracycline, kanamycin, chloramphenicol and ampicillin. Zeocin™ was supplied by Invitrogen.

2.2 Fluorescent Fusion and Luciferase Reporter Plasmids

The Invitrogen Gateway® System was used to construct the fluorophore fusion expression plasmids necessary to study the STAT3-SOCS3 dynamics, as it provides a flexible method for changing the fluorescent protein cassette. Both N- and C-terminal tagged STAT3 fusions with Enhanced Green Fluorescent Protein (EGFP) were made, as well as SOCS3 tagged with EGFP at the C-terminus. The fusions were expressed under the control of the viral CMV promoter.

The process can be summarised in three steps (Fig. 2.1, adapted from Dr J. Bagnall). After amplification of the protein coding sequence with primers to add specific *Att*B recombination sites at the ends, two successive recombination steps using BP and LR Clonase™ enzymes (Invitrogen) are performed, using two antibiotic selection markers. The coding sequence cassette is integrated into the pDONR vector in a BP Recombinase mediated reaction, producing the entry vector. The entry vector is then recombined by LR Recombinase with a specific destination vector containing the fluorophore gene and features required for propagation in mammalian cells to generate the expression vector. In the first selection step the target coding sequence replaces the *ccd*B gene which is lethal to *E. coli* (*Escherichia coli*) DH5α. The second recombination process results in four different vectors, but only the expression vector will have the correct antibiotic resistance marker and lack the *ccd*B gene. Consequently only colonies carrying the completed expression vector survive the final selection step.

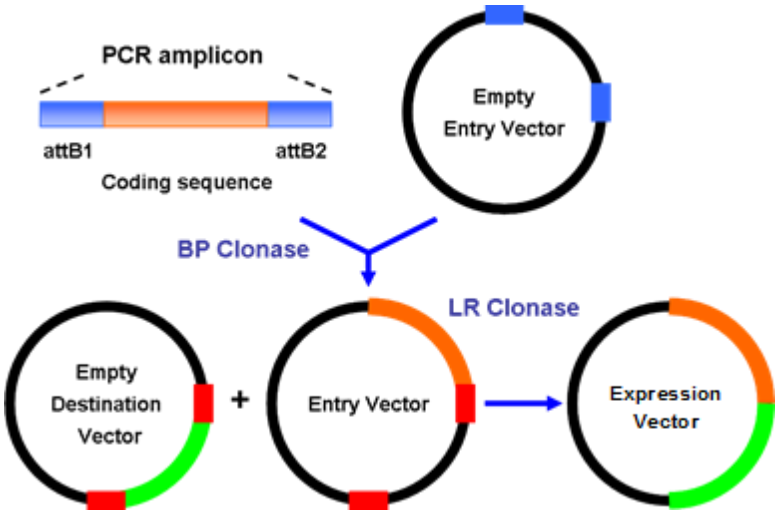

Figure 2.1: Schematic representation of the Gateway® Invitrogen homologous recombination cloning strategy, employed to generate plasmids encoding fluorescent tagged proteins. Orange indicates coding sequence of interest and green denotes fluorescent protein coding sequence. The recombination sites are shown in blue and red.

2.2.1 Amplicon Production

*Att*B flanking primers (Table 2.1) for amplifying STAT3 and SOCS3 coding sequences were designed manually with and without a Stop codon. Primers were checked using the PCR Primer Stats tool of the Sequence Manipulation Suite (P, 2000). The cassettes were amplified from cDNA extracted from HepG2 cells stimulated for 4 h with 20 ng/ml IL-6, using KOD Polymerase (Novagen, Merck, Nottingham, UK) as per the kit instructions. To check whether amplification was successful 5 µl samples were run with 5x Loading Buffer (Bioline, London, UK) on a 1% Agarose/TAE gel with 12% v/v SYBR Safe Dye (Invitrogen) for 75 min at 100 V (SYBR Safe was used throughout to visualise DNA bands). The gel was visualised on a Gel Doc™ XR+ machine (BioRad, UK). Successful reactions were combined and purified using the QIAquick PCR purification kit, as per the manufacturer's instructions (Qiagen, Manchester, UK). DNA concentration and purity were measured using the NanoDrop ND-1000 spectrophotometer (LabTech, East Sussex, UK).

Amplicon	Forward Primer	Reverse Primer
STAT3-Stop	GGGGACAAGTTTGTACAAA AAAGCAGGCTCAATGGCCCA ATGGAATCAG	GGGGACCACTTTGTACAAGA AAGCTGGGTATCACATGGGG GAGGTAGC
STAT3-Non-Stop	GGGGACAAGTTTGTACAAA AAAGCAGGCTCAATGGCCCA ATGGAATCAG	GGGGACCACTTTGTACAAGA AAGCTGGGTACATGGGGGA GGTAGCGCA
SOCS3-Stop	GGGGACAAGTTTGTACAAA AAAGCAGGCTATGGTCACCC ACAGCAAGTT	GGGGACCACTTTGTACAAGA AAGCTGGGTCTAAAGCGGGG CATCGTAC
SOCS3-Non-Stop	GGGGACAAGTTTGTACAAA AAAGCAGGCTCGCTGGCTCC GTGCGCC	GGGGACCACTTTGTACAAGA AAGCTGGGTAAGCGGGGCAT CGTACTGG

Table 2.1: Primers used to generate Stop and Non-Stop amplicons of STAT3 and SOCS3. Underlined sequences are for the start and end of those genes.

2.1.1 Gateway® Cloning of STAT3 and SOCS3 Expression Vectors

The *att*B amplicons were combined with the pDONR™-Zeo vector (Invitrogen) to make the Entry Vectors using the BP Clonase™ II Kit, as per the manufacturer's instructions. 1 µl reaction mix was used to transform 50 µl of competent DH5α cells via heat-shock. The DNA was incubated with the cells on ice for 30 min, then the cells were transferred to a 42°C water bath for exactly 45 sec, before being put back on ice for 2 min. The cells were rescued in 1 ml S.O.C. media (Invitrogen), and incubated for 30 min at 37°C with shaking, then plated out on low salt Luria Bertani (LB) agar plates with 60 µg/ml Zeocin. Plates were incubated over night at 37°C. (LB broth and agar used throughout supplied by Merck, UK).

Colonies containing Entry Vectors were analysed by colony PCR. A pipette tip touched to a colony was rinsed in 5 µl Milli-Q water to lyse the cells, and 10 colonies per Entry vector were selected. The 5 µl bacterial lysates were used in place of plasmid DNA in the KOD Polymerase kit and results were analysed via agarose gel electrophoresis as above. Successful transformants were amplified

by mini-prep using the QIAprep Mini-Prep Kit as per the manufacturer's instructions (Qiagen).

The second stage of the Gateway® System entails mixing 250 ng/ml Entry vector with 250 ng/ml of the appropriate Destination vector using the LR Clonase™ II kit as per the instructions. As before, 1 µl reaction mix was transformed into competent DH5α cells following the heat-shock protocol. The resulting expression vectors were selected by using LB agar plates with 50 µg/ml kanamycin. Formation of 100's of colonies indicated a successful reaction, and so a number of colonies were mini-prepped for the expression vector as above. To ensure the plasmids were correct, samples subjected to a simple restriction digest and were sent for in-house sequencing, according to their directions. Sequencing primers, listed in Table 2.2, were designed using Primer3 (v0.4.0) (Koressaar T, 2007; Untergasser et al, 2012).

Name	Primer Sequence
CMV Fwd	CAACGGGACTTTCCAAAATGTC
DsRedXP Fwd	ACTCCAAGCTGGACATCACC
DsRedXP Rvs	AAGCGCATGAACTCCTTGAT
EGFP Fwd	CGACAACCACTACCTGAGCA
EGFP Rvs	GAACTTCAGGGTCAGCTTGC
STAT3 400 nt Fwd	CAGGATGTCCGGAAGAGAG
STAT3 1000 nt Fwd	CAGGTTGCTGGTCAAATTC
Destination Vec Rvs	CAAGTTAACAACAACAATTGCATTC

Table 2.2: Primers used for DNA sequencing of finalised Expression Vectors.

2.1.2 Primer Design for SOCS3 proximal promoter Cassettes

A 1.1 kb region of the SOCS3 proximal promoter (*ppSOCS3*) was identified using the USCS Genome Browser (Kent et al, 2002), starting 770 bp upstream of the transcription start site, continuing to include the SOCS3 exon 1 and multiple transcription factor binding sites. This region was chosen as it had been used in a commercially available *Renilla* Luciferase reporter (SOCS3 sequence product ID S720285, available in the vector backbone pLightSwitch_Prom; ID S790005),

produced by SwitchGear Genomics (www.switchgeargenomics.com; first accessed 2012).

This proximal promoter region was to be amplified for ligation into the Firefly Luciferase vector pGL4.12 (luc2CP) (Promega) and to replace the CMV promoter in the SOCS3-EGFP expression vector. Two pairs of restriction enzymes were chosen that would not cut anywhere inside the *ppSOCS3* sequence nor anywhere in the target vector apart from the insertion site. The pGL4.12 vector had a multiple cloning site, making enzyme selection straightforward. The CMV promoter in the SOCS3-EGFP expression plasmid had to be precisely cut out, limiting the choice of restriction enzymes. Consideration was also given to how compatible the optimal enzyme buffers were. The plasmid maps and promoter sequences were examined in Vector NTI (Invitrogen Life Sciences) and the software used to select two non-complementary restriction enzymes according to the conditions above.

Amplification primers (Table 2.3) were designed manually to introduce the correct restriction sites at the 5' and 3' ends of *ppSOCS3* for the selected enzyme pairs, and were checked using PCR Primer Stats.

Final Vector	Amplicon	Forward Primer	Reverse Primer
*pp*SOCS3-EGFP	*Afl*II-*ppSOCS3*-*Nhe*I	GTAAACATGTAGTGCATGAAAGCGT	GTGAGCTAGCCTTCCTACCTGGTCC
ppSOCS3-LucF	*Kpn*I-*ppSOCS3*-*Nhe*I	AGGAGGTACCAAGCGTTTTCATAGGG	GTGAGCTAGCCTTCCTACCTGGTCC

Table 2.3: Primers used to amplify the SOCS3 proximal promoter for cloning into the SOCS3-EGFP expression vector and the pGL4.12 (luc2CP) Firefly Luciferase vector (LucF).

2.1.3 *Socs3* proximal promoter-SOCS3-EGFP Vector

The SOCS3 proximal promoter was amplified from the SOCS3 BAC (Section 2.3.2) using the *pp*SOCS3-EGFP primers and the KOD PCR kit. Optimisation of the reaction was required; Dimethylsulphoxide (DMSO, Sigma-Aldritch, UK) was added to a final concentration of 5% v/v due to the 74% CG content of the promoter sequence. The optimum annealing temperature was experimentally determined as 59ºC by running a temperature gradient PCR (data not shown). A

sample of the amplicon was sent for sequencing to confirm the PCR. A double restriction digest of the amplicon was performed with *Nhe*I and *Afl*II in Buffer 2 (New England Biolabs, Herts, UK), in a 50 µl reaction at 37ºC for four hours. The products were cleaned using the QIAquick PCR fragment cleaning kit. The DNA concentration was measured using the NanoDrop, and stored at -20ºC until the ligation step.

The CMV-SOCS3-EGFP plasmid was subjected to a double digestion with *Nhe*I and *Afl*II as above then the digested plasmid was run on a 1% agarose/TAE gel for 45 min at 120 V, and visualised on a Dark Reader transilluminator (Clare Chemical Research Ltd). The SOCS3-EGFP backbone was excised from the gel and extracted using the QIAquick Gel Extraction kit (Qiagen) and its DNA concentration measured.

The digested *ppSOCS3* sequence and the SOCS3-EGFP plasmid were ligated together using 1 Unit T4 DNA Ligase (Roche Applied Science, UK) at a ratio of 3:1 insert to backbone, according to the instructions, and the mixture was left overnight in an ice bath, warming from 4ºC to 16ºC overnight. The ligated product was transformed into DH5α *E. coli* cells by heat shock and plated out onto LB agar kanamycin plates to grow overnight at 37ºC. 20 colonies were mini-prepped and screened by *Not*I restriction digest (Roche). Samples resulting in the expected band sizes were sent for sequencing using the primers listed in Table 2.4 and a *ppSOCS3*-SOCS3-EGFP (hereafter ppSOCS3-EGFP) plasmid was successfully obtained. Mini-prepped DNA was aliquoted and stored at -20ºC for future use.

Name	Primer Sequence
SOCS3 cds Rvs	TCACTGCGCTCCAGTAGAAG
SOCS3 cds Fwd1	CTCCAAGAGCGAGTACCAG
SOCS3 cds Fwd2	CTTCGACTGCGTGCTCAAG
ppSOCS3 Rvs	CAGATTCCAGAGGGGAGACC
ppSOCS3 Fwd1	AGGGTTGGCAAAGAACCTG
ppSOCS3 Fwd2	AGGTCGGCCTCCTAGAACTG
ppSOCS3 Fwd3	CTCTCGTCGCGCTTTGTC
ppSOCS3 Fwd4	CGACTTGGACTCCCTGCTC

Table 2.4: List of sequencing primers for *ppSOCS3* cloning. Primers were designed to provide adequate coverage of the target sequence using Primer3.

2.1.4 SOCS3-firefly luciferase reporter

A SOCS3 proximal promoter firefly luciferase vector was constructed for use in live cell luminometry experiments to act as a marker of STAT3 transcriptional activity. The pGL4.12 firefly vector was used as its expression dynamics have been well characterised. The SOCS3 proximal promoter sequence used was the same as for the SOCS3 expression vector. The promoter was amplified from the SOCS3 BAC as before, using the ppSOCS3-LucF primers (Table 2.3). The PCR amplification was carried out with KOD polymerase as before, with an experimentally determined annealing temperature of 60°C in the presence of 5% v/v DMSO. The PCR products were run on a 1.2% agarose/TAE gel for 45 min at 120 V and the gel visualised. The band was excised from the gel and extracted with QIAquick Gel Extraction kit.

Both the amplicon and the pGL4.12 plasmid were digested with *Nhe*I and *Kpn*I in a double digest, as so: <1 µg DNA, 2 µl NE Buffer, 200 µg/ml BSA (final concentration), 5 Units *Nhe*I, 5 Units *Kpn*I, to a final volume of 20 µl with dd H_2O, incubated at 37°C overnight. The digested amplicon was cleaned using the QIAquick PCR cleaning kit. The plasmid digest products were run on a 1% agarose/TAE gel for 45 min at 100 V, the 4.4 kb band of the plasmid backbone was gel extracted, and the DNA concentration was determined. Digested *ppSocs3* and pGL4.12 were combined in a 3:1 ratio with 1 Unit T4 DNA Ligase, and 2 µl 10 x Ligase Reaction Buffer overnight in an ice bath. The products were

checked by running them on a gel, and 5 µl ligation mix was transformed into DH5α cells via heat-shock. Colonies were streaked out onto 30 µg/ml ampicillin LB agar plates and mini-prepped. Samples were sent for DNA sequencing to confirm the ligation.

2.1.5 Plasmid Maxi-preps for Transfection

Once sequences of constructs were confirmed, single colonies from the streak plates were used to inoculate 5 ml LB broth starter cultures, which were grown at 37°C in a shaking incubator for 6 h. The 5 ml cultures were used to inoculate flasks of 500 ml LB broth, which were then grown overnight in a 37°C shaking incubator. The overnight cultures were spun down at 4000 x *g* rcf in a Beckman Avanti J26XP Centrifuge using the F10BA6 rotor for 15 min at 4°C. Cell pellets were maxi-prepped using the Invitrogen PureLink® HiPure Maxi-prep Kit (#K2100-06) as per the instructions. DNA pellets were resuspended in Milli-Q H_2O and diluted to a final concentration of 1 µg/µl, using the NanoDrop to measure the DNA concentration and purity. DNA was split into 20 µl aliquots which were frozen at -20°C for future use.

2.3 Fluorescent Fusions in Bacterial Artificial Chromosomes

2.3.1 Introduction to Bacterial Artificial Chromosomes

The Bacterial Artificial Chromosome (BAC) system, developed by Shizuya et al (1992), is based upon the F' plasmid. This plasmid is used by certain bacterial species to replicate and horizontally transfer chromosomal material between species members in times of great stress. The F' plasmid was cleaned up and only the sections needed for replication, translation and antibiotic resistance were retained. This enabled the vector to contain an additional 300 kbp of DNA, enough for one or more complete eukaryotic genes and their surrounding DNA sequences. Fluorescent protein expression cassettes can be seamlessly introduced into specific gene loci to create a fusion gene. There are numerous advantages to expressing fluorescent fusion proteins in the context of a native gene structure, especially compared to typical expression plasmids driven by a strong viral promoter.

The main advantages result from being able to express the gene of interest under the control of its own promoter while also retaining the gene's intron/exon structure. Expression dynamics are maintained by signalling through the gene's native promoter, via known and unknown transcription factor binding sites. Furthermore, because the intron/exon structure is maintained, the pre- mRNA transcript will be processed according to its integral regulatory sequences, which may be intronic or within the 5'- and 3'-UTRs. These sequences confer additional levels of control, affecting splice variants, mRNA half-life, copy number and stability etc. By preserving these regulatory processes, any fusion protein expressed under these conditions will much more accurately reflect the endogenous system. This is particularly useful for investigating labile inducible repressors such as SOCS3 and IκBα, which are only induced under particular circumstances and may adversely affect the signalling network if constitutively over-expressed.

The BACs large size however presents several technical difficulties compared to expression plasmids. Standard *in vitro* molecular biology techniques are insufficient for manipulating BACs so new *in vivo* techniques were developed. These included modifying homologous recombination to make it inducible through temperature-sensitivity and a two-step selection procedure based upon galactose metabolism in E. coli.

2.3.1.1 Inducible Homologous Recombination

A temperature-sensitive form of homologous recombination was developed so that large segments of DNA could be introduced into a BAC. Homologous recombination is used by bacteria to repair double-stranded DNA breaks. It is also used by bacteriophages to insert their single-stranded DNA into the host bacteria's chromosome so that they can replicate. Phages hijack the host's RecBCD enzyme that performs homologous recombination using three proteins of their own, *gam*, *exo* and *bet*. G*am*, inhibits RecBCD's exonuclease function which would otherwise destroy the viral single-stranded DNA. *Exo*, a 5'-3' exonuclease, produces 3' overhangs whilst *bet* binds the 3' overhangs to mediate annealing and homologous recombination with complementary DNA (Court et al, 2002). The genes for these three proteins are encoded by the

defective λ Red prophage, which was stably integrated into *E. coli* to produce the SW102 strain (Warming et al, 2005). The λ Red prophage was placed under the control of the pL strong phage promoter, which in turn was stringently regulated by the temperature-sensitive repressor, c1857 (Yu et al, 2000; Lee et al, 2001). C1857 is stable at 32°C but breaks down at 42°C, allowing the genes to be rapidly expressed thus facilitating highly efficient homologous recombination. Consequently this temperature-sensitive system is inducible, facilitating specific, targeted modification of BAC vectors.

2.3.1.2 The GalK Selection Process

The λ Red prophage system was subsequently combined with a two-step screening procedure utilising galactose metabolism to improve the efficiency of the recombination process (Warming et al, 2005). *E. coli* can grow with galactose as its only carbon source if its Gal operon is fully functional and contains all four genes, *galE*, *galT*, *galK* and *galM*. *GalK* encodes galactokinase which phosphorylates galactose into the metabolite galactose-1-phosphate whereas phosphorylation of the galactose analogue, 2-deoxy-galactose, results in a toxic non-metabolite, 2-deoxy-galactose-1-phosphate (Alper & Ames, 1975). SW102 cells lack the *GalK* gene but adding it *in trans* via a BAC enables the cells to grow on minimal media containing galactose as the carbon source. The GalK gene is inserted into the BAC at the point where you want to put your desired gene e.g. for a fluorescent protein. After replacing *GalK* with the desired DNA sequence the E. coli are grown on minimal media containing 2-deoxy-galactose and glycerol to select for cells that have lost *GalK*. Cells that haven't replaced *GalK* through homologous recombination preferentially metabolise 2-deoxy-galactose and die from the accumulation of the toxic non-metabolite. The sequential positive and negative selection steps significantly reduce the number of false positives, simplifying the screening process and making the development of a suitable BAC much swifter than before.

2.3.2 Overview of BAC Engineering

The Galactokinase selection process for generating a seamless fluorescently tagged BAC expression vector could be broadly divided into three stages. Firstly, the appropriate BAC vector should be selected and transformed into the SW102 *E. coli* strain. Next, the Galactokinase gene must be introduced at a specific locus by homologous recombination. Finally, the desired fluorescent protein coding sequence replaces the Galactokinase coding sequence.

At each stage extensive screening is required to ensure the correct vector has been selected. The first stage can be further subdivided into four steps: i) selection of suitable BACs, ii) extraction of BAC DNA from supplied library strain, iii) transformation of BAC DNA into the SW102 strain, and iv) screen of transformed SW102 colonies for accurate DNA up-take and propagation. These steps are discussed in detail in the following sections.

2.3.3 Selecting SOCS3 and STAT3 BACs

Two Bacterial Artificial Chromosomes were selected using the UCSC Genome Browser and ordered from Invitrogen. The RP11-183K18 BAC contained the SOCS3 gene and the PGSI gene for Phosphatidylglycerophosphate synthase I, required for the biosynthesis of an essential phospholipid. Located on the RP11-102M17 BAC are the STAT3 and PTRF genes. The latter's product, Polymerase I and Transcription Release Factor, is involved in ribosomal RNA synthesis. Both BACs, being based upon pBACe3.6, contained four genes from the *E. coli* F-plasmid to regulate transcription: *ori*S and *rep*E to mediate unidirectional replication and *par*A and *par*B to limit the BAC copy number per cell. Maps were constructed and annotated in SimVector (Premier Biosoft) (Figure 2.2).

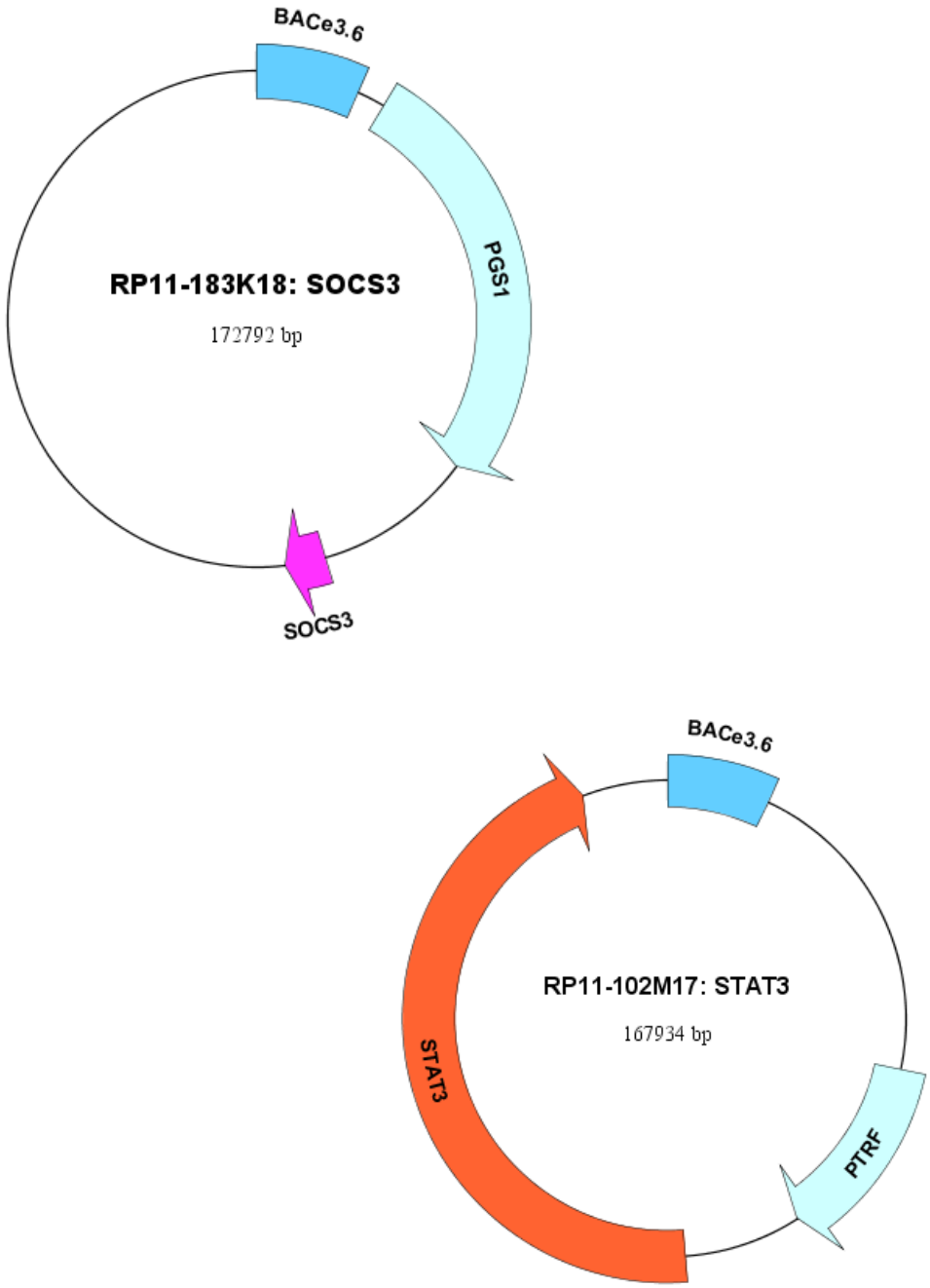

Figure 2.2: Maps for RP11-183K18 SOCS3 and RP11-102M17 STAT3 BACs. The pBACe3.6 sequence, common to both BACs, contains a pUC link, *SacB*I (from the BAC library preparation techniques) and the CM^R gene for chloramphenicol resistance, and the *par*A, *par*B, *rep*E and *ori*S genes for replication. The SOCS3 BAC contains the PGS1 gene whilst the STAT3 BAC contains the PTRF gene, in addition to the genes of interest.

2.3.4 BAC DNA Maxi-prep

The BACs were supplied in DH10B *E. coli* cells as glycerol stocks and were streaked onto LB agar plates under chloramphenicol selection and incubated at 37°C overnight. After incubation, a single BAC colony was inoculated into 5 ml LB broth supplemented with 12.5 µg/ml chloramphenicol and was incubated at 37°C for 8 h in a shaking incubator. The 5 ml starter culture was then used to inoculate 500 ml LB broth with chloramphenicol selection which was kept at 37°C in a shaking incubator overnight.

The Nucleobond BAC 100 maxi-prep kit (Macherey-Nagel, supplied by Fisher Scientific, Loughborough, UK) was used to extract the BAC DNA from the 500 ml culture, as per the manufacturer's protocol for low-copy plasmid purification. The purified BAC DNA was resuspended in sterile deionised H_2O and the yield was determined by UV spectroscopy on the NanoDrop spectrophotometer.

2.3.5 Transformation of Cold-competent SW102 Cells

2.3.5.1 Inducing Competency by Cold-Shock

Tetracycline-resistant SW102 cells were streaked from a glycerol stock onto an LB agar plate under tetracycline selection and incubated overnight at 32°C. 5 ml LB broth with 10 µg/ml tetracycline was inoculated with one colony from the streak plate and incubated with shaking at 32°C overnight. 1 ml of the starter culture was used to inoculate 50 ml LB broth with tetracycline in a baffled flask and was incubated with shaking for 3-5 h at 32°C until an OD600 of 0.5 - 0.6 was reached, when the flask was quickly cooled on ice. The culture was centrifuged at 6,000 g for 10 min at 4°C and the supernatant was discarded. The pellet was resuspended in 1 ml ice-cold dd H2O, to which another 9 ml ice-cold ddH_2O was added. This step was repeated and the bacteria resuspended in 1 ml of ice-cold ddH_2O before being transferred to pre-chilled 1.5 ml Eppendorf tubes. The samples were centrifuged at 6,000 *g* and 4 °C for 1 min in a bench-top centrifuge and the pellets resuspended in 1 ml ice-cold dd H_2O. This step was repeated twice more. After the final centrifugation step the supernatant was discarded and the pellet of competent cells kept on ice until required.

2.3.5.2 Transforming with BAC DNA by Electroporation

The pellet of competent cells was resuspended in 40 µl ice-cold ddH_2O and transferred to a p1mm gap electroporation cuvette (Cell Projects, Kent, UK). 100 ng of BAC DNA was added and the cells electroporated at 25 uF, 1.8 kV and 200 ohms. The cells were immediately rescued in 1 ml S.O.C. medium (Invitrogen), transferred to a 15 ml Falcon tube and incubated with shaking for 90 min at 32°C. Following this recovery period, 100 µl of the cell suspension was spread onto an LB agar plate supplemented with 1.25 µg/ml chloramphenicol and 10 µg/ml tetracycline (these concentrations used throughout). The reserved 900 µl cell suspension was spun down at 5,000 *g* for 1 min in a microcentrifuge, 800 µl of supernatant was removed and the pellet resuspended in the remaining media. This was spread onto another LB agar plate supplemented with chloramphenicol and tetracycline. The plates of transformed SW102 cells were incubated overnight at 32°C.

2.3.6 Characterisation of BAC-Transformed SW102 Cells

2.3.6.1 BAC Mini-prep of Transformed SW102 Cells

5 cultures of 5 ml LB broth supplemented with chloramphenicol and tetracycline, each inoculated with an individual colony from the plate of transformed SW102 cells, were incubated with shaking overnight at 32°C. One colony of the original BAC DH10B cells was also used to inoculate 5 ml LB broth + 1.25 µg/ml chloramphenicol and was incubated with shaking overnight at 37°C. Following the over-night growth, LB agar plates were streaked for each culture under chloramphenicol and tetracycline selection.

The cultures were centrifuged at 2,500 *g* for 5 min and the supernatant discarded. Cell pellets were resuspended in 250 µl P1 Resuspension Buffer (cat. no. 19051). 250 µl of P2 Lysis Buffer (cat. no. 19052) was added and mixed by inversion before incubating for 5 min at room temperature. 250 µl P3 Neutralisation Buffer (cat. no. 19053) was then added and the samples inverted to mix and incubated on ice for 5 min. (All three buffers supplied by Qiagen).

The lysates were centrifuged at 4°C and 6,000 *g* for 5 min, the supernatant transferred to new Eppendorfs and the spin step repeated. 750 µl of isopropanol was added to the DNA suspension and the samples left on ice for 10

min before centrifugation at 6,000 *g* for 10 min at 4°C. The supernatant was then discarded and the DNA pellet washed in 1 ml 70% ethanol. Samples were centrifuged at 6,000 *g* for 5 min at 4°C and the ethanol carefully removed. Pellets were air dried next to a Bunsen flame DNA and finally resuspended in 52 µl ddH_2O and stored at 4°C.

2.3.6.2 Restriction Digests

Three restriction digests were performed, using the frequent cutter *Eco*RI enzyme, and the infrequent cutters *Xho*I and either *Sal*I or *Not*I, for the SOCS3 and STAT3 BACs respectively. 15 µl DNA was digested with 5 µl enzyme master mix (enzyme, Buffer H and water) overnight at 37°C. In a 20µl reaction 5 Units of *Eco*RI and 10 Units of *Xho*I, *Sal*I or *Not*I were used.

2.3.6.3 Agarose Gel Electrophoresis

The *Eco*RI-digested samples were run on a 1% agarose gel for 18 h, 25 V in a gel electrophoresis unit (Bio-Rad, Hemel Hempstead, UK). The gel was made with 1% Agarose/TAE buffer. Since the *Xho*I, *Sal*I and *Not*I enzymes generated fragments larger than 20kbp these samples were separated out using the CHEF DRII Bio-Rad Pulsed Field Agarose Gel Electrophoresis apparatus. The samples were run on a 1% agarose gel (PGFE-approved agarose from Bio-Rad) in 0.5x TBE (diluted from 10x TBE buffer: 108 g Tris base, 55g Boric acid, 9.3 g EDTA, adjusted to 1 L with dH_2O) for 18 h at 6 V/cm power, 6 s switching time, with the running buffer cooled to 14°C. The markers used were the Mid Range PFG Marker I and Mid Range PFG Marker II (New England Biolabs, Hitchin, UK). Following the completion of the run the gel was stained with 30 µl SYBR Safe for 1 h to reveal the DNA bands for visualisation.

An illustrative example of the gels from this process are shown below in Figure 2.3 below, the digests grouped first by gene of interest and then by restriction enzyme. Obvious differences in the digest pattern between the BACs extracted from the transformed cells and the parent BAC are highlighted by an orange box. It was clear that while the STAT3 BAC was not altered by the transformation step, the SOCS3 BAC was. Two bands were missing from the *Xho*I digest, while in the *Sal*I digest the largest band was much smaller than expected after the transformation step. The *Eco*RI digest also reveals

differences; there is a double band where there should be one, and a small band is missing entirely. This incorrect pattern was seen on multiple attempts, suggesting that there was a particular sequence the bacteria were responding to. The STAT3 BAC was successfully transformed into the SW102 cells but the SOCS3 BAC transformation was not successful, even after many attempts.

2.3.6.4 BAC Glycerol stocks

The successfully transformed STAT3 BAC SW102 cells were stored as glycerol stocks at -80ºC for future use. A 5 ml overnight LB broth (with chloramphenicol and tetracycline) culture of the transformed cells, grown at 32ºC, was mixed with 5 ml 80% sterile glycerol, to give a 40% glycerol stock, from which 1 ml aliquots were made.

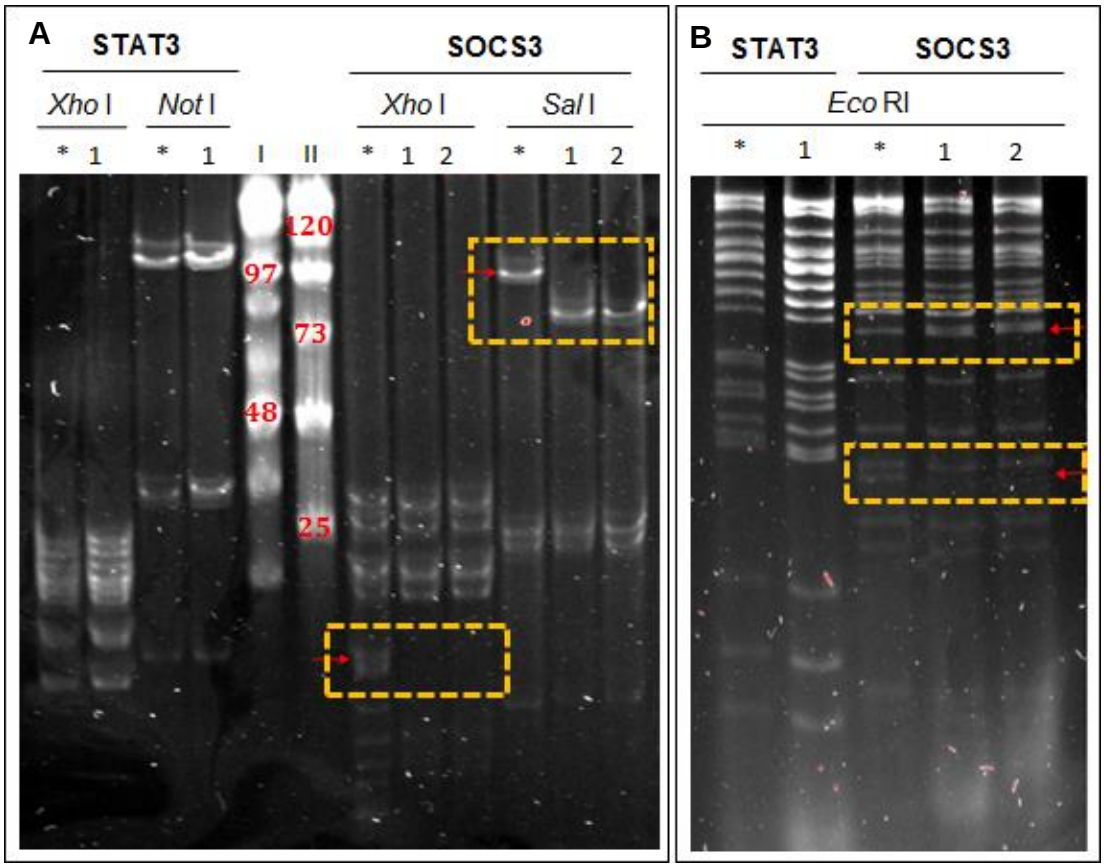

Figure 2.3: Restriction digest gels of STAT3 and SOCS3 BAC DNA obtained from SW102 cells, using **A** the infrequent cutters *Xho*I, *Sal*I and *Not*I, and **B** the frequent cutter *Eco*RI. I and II are the pulsed-field ladders, sizes in kbp. 1 and 2 were individual colonies of transformed SW102 cells while * indicates DNA from the original DB10.B strain. Red arrows and orange dashed boxes indicate where the bands are different or missing.

2.4 Cell Culture

SK-N-AS human neuroblastoma cells (cat. no. 94092302) and HepG2 human hepatoma cells (cat. no. 85011430) (obtained from the European Collection for Cell Cultures, Porton Down, UK) were cultured as a monolayer and grown in Earles's Minimum Essential Media (MEM) (Gibco, Paisley, UK) supplemented with 10% Foetal Calf Serum (Harlan Sera-lab, Loughborough, UK) and 1% NEAA (Gibco) in T75 flasks (Corning, Scientific Laboratory Supplies Ltd, Nottingham, UK) at 37 °C with 5 % CO_2 in a humidified incubator. SK-N-AS and HepG2 cells were passaged at 60-80 % confluencey, up to 15 and 25 times respectively, for use in experiments.

2.4.1 Subculturing Cells

Cells were washed with Mg^{2+} and Ca^{2+}-free Phosphate-Buffered Saline (PBS; Gibco) and incubated with 1 ml of 0.05 % (w/v) trypsin in 0.48 mM EDTA (Gibco) at 37 °C and 5 % CO_2 for 5 min to detach the monolayer from the flask. Since HepG2 cells are very resistant to tyrpsinisation, 2ml Trypsin was used and they were pipetted up and down multiple times to break up the cell clumps. Cells were resuspended in media to a final volume of 10 ml and centrifuged at 150 x *g* for 5 min in a Centrifuge 5804 (Eppendorf, Cambridge, UK). The supernatant was discarded and the cell pellet was resuspended in 10 ml media. Cells were counted using a Z2 Coulter Particle Count and Size Analyzer (Beckman Coulter, High Wycombe, UK) and seeded as required.

2.4.2 Cryogenic Storage of Cell Lines

For freezing, after cells were spun down the cell pellet was resuspended in FCS with 10% v/v DMSO to a final concentration of $1x10^6$ cells/ml. 1.5 ml aliquots in externally threaded cryovials (Sigma-Aldritch) were placed into a NALGENE™ Cryo 1ºC freezing container filled with 100% Isopropanol and transferred into an -80ºC freezer for at least 24 h before being transferred to gas-phase liquid Nitrogen cryostorage.

2.4.3 Thawing of Cryogenically Stored Cell Lines

Aliquots of cells were removed from liquid Nitrogen storage onto wet ice for transfer to Tissue Culture. The aliquot was thawed in a 37°C water bath until only a small ice crystal remained then 1 ml media (EMEM, 10% FCS, 1% NEAA) was slowly added to the cells. This mixture was added to 2.5 ml media and the cells were centrifuged. The cell pellet was resuspended in 5 ml media and was transferred to a T25 flask and the flask kept in the incubator as above. One to two days later, once 70-80% confluencey was reached, the cells were subcultured as above.

2.4.4 Seeding and Transfecting Cells

HepG2 cells were seeded at a density of approximately 12000 cells/cm^2, 72 h in advance for use in confocal microscopy, immunoblotting, luminometry and RNA extraction. 30 mm diameter glass-bottomed dishes (Greiner Bio-One Ltd, Stonehouse, UK) were used for microscopy, 60 mm dishes for protein and RNA lysates and 100 mm dishes for luminometry. Dishes were transfected 24 h after seeding. For luminometry, 48 h after transfection the cells were harvested and reseeded into 24 well clear tissue culture plates at a density of 1.2 x 10^6 cells in 500 µl media per well for use the following day.

To transfect SK-N-AS cells Fugene 6 (Promega, Southampton, UK), was used in a 2 µl:1 µg ratio with DNA in 100 µl serum-free MEM per approx. 1 x 10^6 cells in 3 ml media. Transfection of HepG2 cells was optimised by a luminometry assay (Section 2.6) which led to a 5:1 Fugene 6:DNA ratio being used for all transfections. Where two plasmids were being transfected together, equal amounts were used to a total of 1 µg DNA. The transfection efficiency in HepG2 cells ranged between 5 and 15%, compared to 70-80% in SK-N-AS cells, as assessed by fluorescence microscopy.

2.5 Generation of Stable Cell Lines

The generation of a stable HepG2 cell line expressing p65-dsRedXP was attempted. The p65-dsRedXP plasmid contains a resistance marker for geneticin®/G418 (Invitrogen). However HepG2 cells are well known to be highly resistant to G418/geneticin therefore a kill curve was carried out as

follows to determine a feasible geneticin dose. HepG2 cells were seeded in 6-well plates and grown for 24 h prior to treatment with increasing concentrations of geneticin, from 200 μg/ml to 800 μg/ml, where the typical dose for non-resistant cells is around 200 μg/ml. The cells were incubated for two weeks, changing the media and replenishing the geneticin every 2-3 days. At the end of the two week period, the cells were trypsinised and collected in 5 ml PBS, then counted using the Cell Counter. Even at the highest dose of geneticin, there was no significant decrease in cell numbers compared to untreated controls. Because of this, plans to make stable HepG2 cell lines were abandoned. To make stable cell lines possible, the existing plasmids would have to be reverse engineered to replace the geneticin resistance marker, or new plasmids would have to be constructed using a parent plasmid backbone with a different mammalian antibiotic marker.

2.6 Stimulation with Cytokines and Wash Protocols

The cytokines used were human Interleukin-6 (IL-6), human Tumour Necrosis Factor-alpha (TNFα) and human Interleukin-1β (IL-1β) and were all sourced from Calbiochem (Merck Millipore, UK). 10 μg lyophilised IL-6 was reconstituted in 1 ml filter-sterilised 100 mM Acetic acid. 20 μl aliquots were stored at -80ºC and were diluted to a working stock concentration of 20 ng/ml with serum-free MEM. Lyophilised IL-1β and TNFα were reconstituted in filter-sterilised 0.1% v/v BSA in H_2O to a stock concentration of 100 ng/ml. Aliquots were stored at -80ºC and were diluted before use with serum-free MEM to a working concentration of 10 ng/ml.

IL-6, TNFα and IL-1β were all used for continuous stimulation of cells, whereby the cytokines were added and left on for the duration of the experiment. IL-6 was also applied for shorter periods, commonly 30 min but also for 15 and 5 min, after which time the media would be aspirated off the cells, the dish washed with 4 ml 37ºC MEM and an appropriate volume of media added. Microscopy dishes were washed 3 times with 1 ml fresh MEM warmed to 37ºC whereas 6 cm dishes for protein and RNA lysates were washed once with 5 ml MEM. After washing the media was replaced with either the appropriate volume of fresh MEM or culture conditioned media. Culture-conditioned media was

obtained by growing cells in the same sized dish for the same length of time concurrently to the dishes that were to be imaged or lysed and using the media from that dish to replace the media on the washed cells.

2.7 End-point Luminometry

End-point luminometry was used to optimise the transfection protocol and to compare the function of the plasmid constructs to the endogenous STAT3 and SOCS3 proteins. HepG2 cells were seeded and transfected as described in 2.4.4. Transfected cells were grown for 48 h before being harvested and re-seeded into clear 24 well plates at a density of 120,000 cells/well. Plates were used 15 h later and were treated for 3 h. At the end of each experiment, cells were washed with 1 ml cold PBS, prior to the addition of 250 µl lysis buffer (Table 2.5). Plates were shaken for 20 min at room temperature to ensure complete lysis and homogenisation. Afterwards plates were frozen at -20°C for up to a week before being used in the luminometry assay. Triplicate technical repeats were conducted within each plate and each plate was repeated at least 3 times.

Luminometry Lysis Buffer	
25 mM	Tris Phosphate, pH 7.75
10 mM	$MgCl_{2\ (aq)}$
5 % v/v	0.5 M EDTA, pH 8.0
15 % v/v	Glycerol
0.1 % v/v	Triton X-100
0.1 mg/ml	BSA
Final vol. 100 ml	dd H_2O

Table 2.5: Luminometry Lysis Buffer

For the luminometry assay, ATP was added to a final concentration of 1mM to each lysate, then duplicate 80 µl lysate aliquots were transferred to a white 96-well Lumitrac™ plate (Greiner). The plate was loaded into a FLUOstar Omega plate reader (BMG Labtech, Aylesbury, UK) and readings were taking every 0.1 s. After 0.5 s of background readings, 80 µl 2.5 mM Firefly D-luciferin (Biosynth, Fisher Scientific, UK) (dissolved in 25mM Tris-PO_3 pH 7.75) was added to the wells by automated injection. Data analysis consisted of calculating the

mean of the post-stimulation readings collected between 2.0 and 3.0 s for each well, minus the averaged pre-luciferin background reading, then averaging the technical duplicate wells. The means of within-plate technical triplicate wells were calculated, before being converted to the fold-change relative to the untreated sample. Finally the results of biological replicate plates were averaged and the standard deviation calculated.

To optimise the HepG2 transfection protocol, a range of Fugene 6 (µl) to SOCS3-lucF DNA (ng) ratios were tested: 1:1, 2:1, 3:1, 4:1, 5:1, 6:1. Cells were stimulated with 20 ng/ml IL-6 for 3 h. This demonstrated that the 5:1 ratio was best (data not shown). Dose-response experiments were carried out to confirm the optimum IL-6 dose. Concentrations tested were 0, 0.5, 2, 20, 40 and 100 ng/ml IL-6 and were applied for 3 h. The saturating dose in HepG2 cells was 20 ng/ml IL-6 (data not shown). To test the function of the plasmid constructs, the SOCS3-lucF reporter was transfected in with an equal amount of plasmid DNA. An empty fluorophore expression plasmid was used in the endogenous control. Cells were treated with 20 ng/ml IL-6 for 3 h.

2.8 Immunoblotting

2.8.1 Cytokine Stimulation Time Courses

Time courses of cytokine stimulation were carried out in SK-N-AS and HepG2 cells. Saturating doses were determined by dose-response luminometry assays (data not shown), which for IL-6 was 20 ng/ml and 10 ng/ml for TNFα. Time-courses included i) 30 min intervals for up to 3.5 h, generating samples at 0, 30, 60, 90, 120, 150, 180 and 210 min, ii) a 24 h time course, weighted to early time points: 0, 0.25, 0.5, 0.75, 1, 1.5, 2, 4, 6, 8, 24 h, and iii) others as specified in the text. Cytokine exposure was either continuous (IL-6 and/or TNFα) or pulsatile (IL-6).

2.8.2 Cell Lysate Preparation

Cells were grown in 6 cm dishes as described in 2.4.4 and treated as described in 2.7.1 above. After treatment, the media was aspirated off and the cells washed with 4 ml ice-cold PBS. 250 µl Western Lysis Buffer was added to the dish and the cells scraped into it. HepG2 cell lysates were boiled in a heat block set to

104ºC for 8 min whereas SK-N-AS lysates were boiled for 4 min. Lysates were rapidly cooled on ice and stored at -20ºC until use.

Western Lysis Buffer	
% v/v	In dd H_2O
10	10 % SDS (aq)
10	100% Glycerol
10	0.1% β-mercaptoethanol
8	0.5 M Tris Base pH 6.8
1	0.1% Bromophenol Blue

Table 2.6: Western Lysis Buffer

2.8.3 Immunoblotting

Samples were subjected to Acrylamide SDS-PAGE for ~1.5 h at 100 V. Gels were cast using buffers in Tables 2.8-9, and the running buffer is given in Table 2.10. A combination of Colour Plus Protein and Biotin ladders were used (Cell Signaling and New England Biolabs, respectively). Proteins were transferred to nitrocellulose membranes (Whatman, Kent, UK) by the wet method at 300 mAmps for ~1.5 h, (transfer buffer – Table 2.11). Membranes were blocked in 5% skimmed milk powder/TBS/Tween20 (TBST) for 1 h and then washed for 3 x 5 min in TBST. Incubation with primary antibodies was overnight at 4°C as per Table 2.7 in either 5% Skim milk/TBST or 5% Bovine Serum Albumin/TBST (both skimmed milk powder and BSA from Sigma Aldritch).

After a further three 5 min washes in TBST, the secondary antibodies were applied for 1 h. Membranes were washed for 3 x 5 min in TBST, then ~1 ml of LuminataTM Crescendo Western HRP Substrate (Millipore, Merck Watford, UK) was applied to each membrane and incubated at room temperature for 2 min before the excess was drained off. CL-XPosure™ films (Thermo Scientific, Loughborough, UK) were exposed to the membranes for 30 s to 10 min and developed.

Antibody	Source	Catalogue ID	Dilution Factor	Buffer
STAT3	Mouse	#9139S	1:2000	Skim milk
STAT3	Rabbit	#4904	1:2000	BSA
pY-705-STAT3	Mouse	#9138	1:2000	Skim milk
SOCS3	Rabbit	#2923S	1:1000	BSA
α-Tubulin	Rabbit	#2144S	1:2500	
GAPDH - 14C10	Rabbit	#2118	1:2500	
Cyclophilin A	Rabbit	#2176	1:1000	
Anti-mouse IgG	-	#7076	1:1000	Skim milk
Anti-rabbit IgG	-	#7074	1:1000	
Anti-biotin	-	#7075	1:1000	

Table 2.7: All Antibodies supplied by Cell Signaling Technology (New England Biolabs, Hertfordshire, UK)

Stacking Gel Buffer	0.5 M Tris-HCl pH 6.8
Resolving Gel Buffer	1.5 M Tris-HCl pH 8.8

Table 2.8: Resolving and Stacking Gel Buffers

Western Gels	Resolving Gel	Stacking Gel
Acrylamide	10 % w/v	0.04 % w/v
Buffer (Table 2.8)	25 % v/v	25 % v/v
dd H_2O	40 % v/v	60 % v/v
SDS	0.1 % w/v	0.1 % w/v
APS	0.06 % w/v	0.06 % w/v
TEMED	0.06 % v/v	0.012 % v/v

Table 2.9: Resolving and Stacking Gels

Running Buffer	In dd H2O
SDS	3.47 µM
Glycine	0.19 mM
Tris Base	25 µM

Table 2.10: SDS-PAGE Running Buffer

Transfer Buffer	In dd H2O
Glycine	0.19 mM
Tris Base	25 µM
100 % Methanol	20 % v/v

Table 2.11: Transfer Buffer

2.9 Quantitative Real-Time-PCR

2.9.1 Primer Design

Primers were designed using the CDS for the relevant genes in Ensembl (www.ensembl.org) and the Primer3 software. The primers were around 18-22 bases long with a melting temperature (Tm) value of around 60°C. Their suitability in terms of GC percentage, Tm, risk of single and dinucleotide base runs, GC clamp and hairpin formation, and self-annealing ability was checked using PCR Primer Stats. Potential primers were checked for selectivity against other DNA features in BLASTn and were ordered from Invitrogen. Primer pairs used are listed in Table 2.12.

2.9.2 Cytokine Stimulation Time Course

SK-N-AS and HepG2 cells were seeded into 6 cm dishes in 5 ml media as described in Section 2.4.4. Cells were stimulated with either 10 ng/ml TNFα, 20 ng/ml IL-6 (continuous exposure or 30 min pulse) or co-stimulated with both 10 ng/ml TNFα and 20ng/ml IL-6, 24 h after seeding as in Section 2.5. Each condition was repeated three times. Time points were 0, 0.25, 0.5, 0.75, 1, 1.5, 2, 4, 6, 8 and 24 h. After stimulation, the media was aspirated off and the cells washed with 5ml ice-cold PBS, lysed and the mRNA extracted as described below.

cDNA Target	5' Left	3' Right
GAPDH	ACCCAGAAGACTGTGGATGG	TTCAGCTCAGGGATGACCTT
Cyclophilin A	GCTTTGGGTCCAGGAATGG	GTTGTCCACAGTCAGCAATGGT
β-tubulin	ACCTTCAGTGTGGTGCCTTC	TGGTGTGGTCAGCTTCAGAG
POLR2A	GTCGTCCTCCCCTGTAACCT	GGTCATCCCCATTCACAATC
STAT3	GTCCTGAGCTGGCAGTTCTC	CACACCAGGTCCCAAGAGTT
SOCS1	GCCAGAACCTTCCTCCTCTT	GAACGGAATGTGCGGAAGT
SOCS2	GTGCAAGGATAAGCGGACAG	GTAAAGGCAGTCCCCAGATG
SOCS3	CCTCAAGACCTTCAGCTCCA	TCACTGCGCTCCAGTAGAAG
SOCS5	ACCCAGAGTTCATTGGATGC	GGAAAACACAAGCCCACAGT
SOCS7	TGGTGTCATCCCAAGTTTGA	GTGCTGGAGGGATTTGACAT
IL-6	AAAGAGGCACTGGCAGAAAA	TTTCACCAGGCAAGTCTCCT
IL6R	AAAGGCTGTGCTCTTGGTGA	CTGAACTTGCTCCCGACACT
gp130	ACACCAAGTTCCGTCAGTCC	CTGGGCAAAATACCATCACC
IL-10	AGGAGGTGATGCCCCAAG	TGGCTTTGTAGATGCCTTTCTC
IL-15	GTTCACCCCAGTTGCAAAGT	TACTTGCATCTCCGGACTCA
A2M	TTCGCTGTCCCAAAGTCTTC	TCTTGGGTTGGTCCTTTCAC
FGG	CTAAACAGAGCGGGCTTTAC	CATCCATTTCCAGACCCATC
SAA1	CCAATTACATCGGCTCAGAC	TGGCATCGGTGATCACTTC
Hepcidin	TGGCTCTGTTTTCCCACAAC	GCAGCAGAAAATGCAGATGG
IkBα	TGGTGTCCTTGGGTGCTGAT	GGCAGTCCGGCCATTACA
IkBε	GGACCCTGAAACACCGTTGT	CCCCAGTGGCTCATTCAGA
A20	GCCCTCATCGACAGAAACAT	CACAAGCTTCCGGACTTCTC
RANTES	GTCGTCTTTGTCACCCGAAAG	TCCCGAACCCATTTCTTCTCT

Table 2.12: qPCR primer sequences

2.9.3 mRNA Extraction

RNA was extracted from the cells using the High Pure RNA Isolation Kit (Roche). Washed cells were resuspended in 200 µl ice-cold PBS, using a plastic scraper to detach them from the dish. Next 400 µl Lysis/-Binding Buffer was added and the lysate vortexed for 15 s. The resulting lysates were processed according to the kit's instructions. RNA was eluted from the columns in 70 µl Elution Buffer and the concentrations determined using the NanoDrop.

2.9.4 cDNA Conversion

Using the VILO Superscript kit (Invitrogen), 2.5 µg mRNA was converted to cDNA, according to the manufacturer's instructions. Samples were heated in a Px2 Thermal Cycler (Thermo Electron Corporation, UK) as follows: 10 min at 25ºC for annealing, 1 h at 42 ºC for synthesis and 85 ºC for 5 min to terminate the reaction. For qPCR using the LightCycler® 480 (Roche), aliquots were diluted 1 in 40 and stored at -20 °C until required. For qPCR using the Fluidigm® Bio-Mark™ System, the cDNA concentration was determined using a Qubit® Fluorometer (Invitrogen) and the Quant-iT™ ssDNA Assay Kit (Invitrogen) according to the manufacturer instructions, before being diluted to a working stock concentration of 10 ng/µl. For the primer efficiency standard curves, aliquots of cDNA from different samples and conditions were combined and a 10-fold serial dilution was performed using the pooled cDNA, to give relative concentrations of 1, 0.1, 0.01 and 0.001.

2.9.5 Quantitative PCR using the LightCycler 480 System

Initial quantitative real-time PCR (qPCR) experiments were performed on the LightCycler™ 480 platform with the SYBR Green I fluorescent dye (Roche). A 96 well format was utilised. In each well, 2 µl 1:40 diluted cDNA was incubated with 10 µl SYBR Green (Roche), 0.25 µM forward primer and 0.25 µM reverse primer, with RNase-free H_2O added to a total volume of 20 µl. Included on each qPCR plate was the target gene, reference gene (cyclophilin A) and non-template control, along with cDNA dilution standard curves for both target and reference genes. Each sample was plated out in technical triplicate. The cycling parameters are listed in Table 2.13.

Step	Cycles	Temperature °C	Hold	Ramp Rate °C/s
Pre-Incubation	-	95	5 min	4.4
Amplification	45	95	10 s	4.4
		58	30 s	2.2
Melt curve	-	95	5 s	4.4
		65	1 min	2.2
		97	-	0.06
Cooling	-	40	10 s	1.5

Table 2.13: Cycling parameters for LightCycler 480 qPCR

Data analysis for LightCycler 480 qPCR was performed using the supplied Roche LightCycler 480 software, version 1.5. Melt-curve analysis was performed for each run to check specificity of amplification, then standard curves were calculated for the primer pairs within each run to determine primer amplification efficiency and ensure they were at least 85% effective. Advanced relative quantification was performed using the calculated primer efficiency, accounting for any background noise from the non-template controls, normalising first to the reference gene and then to the untreated control samples. Normalised data and calculated error values were exported into Excel for further analysis. Biological triplicates for each condition and gene were averaged and the errors propagated through to account for variation between repeats and the error from the sample measurement.

2.9.6 Quantitative PCR using the Fluidigm System

The Fluidigm BioMark System performs semi-quantitative RT-PCR in the same way as the LightCycler 480, allowing the SYBR Green dye, primer sets and cDNA samples to be used. Its advantage over the LightCycler 480 system is its 48 x 48 multiplex format which allows 48 primer pairs to be tested against 48 samples in a single run. Plates were set up to include three sets of samples, a serial dilution for the calculation of standard curves for primer efficiency, inter-run controls, water-only and non-template controls. The serial dilution included 1:1, 1:10, 1:100 and 1:1000 dilutions of a pooled set of cDNA samples, each plated out in four technical replicates to improve the accuracy of the standard curve. A

separate plate was set up with the primer pairs for the 24 selected genes in duplicate so that technical replicates of each gene-sample pairing could be obtained. Prepared sample and primer plates were processed and run in-house by Core Services on the BioMark System and the resulting data files were analysed using Biogazelle's qBase+ software on a premium licence (www.biogazelle.com/qbaseplus, accessed September 2013).

2.9.7 qBase+ Analysis of Fluidigm Gene Expression Data

Biogazelle's qBase+ software imports and automatically detects sample annotations from CSV files and also permits additional sample labelling. Once the data were fully annotated with test conditions, time-points, test or reference target status etc. the calculation parameters, quality control and normalisation steps were determined. The data were presented as Cq (quantification cycle) values, also known as Ct (cycle threshold) or Cp (crossing point) values. The quality control settings first exclude any samples with Cq values below 0, any too close to the negative control values (within 5 units) and then samples whose technical duplicate Cq values were more than 1 cycle out. For the remaining samples, the arithmetic mean of the duplicates was used to calculate the Cq value.

The MIQE Guidelines (Bustin et al, 2009) for qPCR analysis recommend using the efficiency corrected delta-delta-Ct method described by (Pfaffl, 2001) for accurate analysis. This method generates standard curves to calculate PCR efficiency for each target from a serial dilution of a representative sample template, in this case pooled cDNA from multiple sample sets, and the qBase+ software will also make the analysis run-specific as well as target specific. The calculated efficiency values were checked for each target to ensure it was between 80% and 110% efficient, otherwise it was excluded from the rest of the analysis.

Further to the recommendation of the efficiency-corrected delta-delta-Ct method, the MIQE guidelines also recommend using more than one reference target for normalisation purposes. The limited plate size for the LightCycler 480 qPCR means that only one reference target could be used but with the Fluidigm

system multiple genes could be selected. Four potential reference genes were included: PolR2A, GAPDH, β-Tubulin, and Cyclophilin-A. The GeNorm feature of qBase+ determined that all four genes were stable across all samples and were therefore suitable reference genes (data not shown). Normalisation factors were calculated for each sample according to the reference targets, and were compared to highlight any potential issues; a variation of 2-3 fold was considered acceptable and only one sample was flagged at this stage as unsuitable for further analysis.

The last quality control consideration was the Inter-Run Calibration (IRC). Inter-run variability is an under-estimated cause of error so including a normalisation step to account for it increases accuracy. Consequently one sample was chosen to be included on every plate as the inter-run calibrator. The software used the IRC result to normalise the plates to each other so that their Cq values were comparable.

Normalisation and scaling strategies were applied after the quality control steps. The unknown samples' relative quantities were normalised to the geometric mean of the reference targets and then the data were scaled to the average of all unknown samples per target, since several genes were undetectable under unstimulated conditions. This is in contrast to the LightCycler 480 analysis where the samples were normalised to the unstimulated, zero time-point control. Finally the normalised relative quantities for all samples and all targets were exported to Excel. At this stage the mean and standard deviation could be calculated using the biological repeats of the four time series test conditions (continuous IL-6, 30 min IL-6, continuous TNFα, and continuous IL-6 + TNFα). GraphPad Prism was used to plot the results.

2.10 Fluorescence Confocal Microscopy

Cells for fluorescence confocal microscopy were seeded in glass-bottomed dishes and transiently transfected as described in Section 2.4.4 two to three days before use. A Zeiss LSM510 Confocal microscope was used to image the cells at 5 minute intervals for up to 24 h using a Fluar 40x 1.3NA oil immersion objective. The pinhole was set to capture light from a 4.0 μm optical slice. EGFP was excited using an argon ion laser at 488 nm and the emitted light was reflected through a 505-530 Band Pass filter from a 545 nm dichroic mirror. A green helium neon laser (543 nm) was used to excite dsRedXP and was detected through a 560 Long Pass filter. The Ellenberg macro (Rabut & Ellenberg, 2004) was used to automatically focus the microscope prior to each image capture. After completion, data files were concatenated and visualised using the LSM Zeiss Image Browser version 4.2, and were processed to extract quantified fluorescence intensity of the nuclear and cytoplasmic compartments using the methods described next.

2.11 Cell Tracking Approaches for Image Analysis

Three different methods for extracting quantitative fluorescence data from microscopy images were compared. Region of Interest (ROI), manual and automatic whole cell tracking methods (Fig. 2.4) were performed using the Cell Tracker software (Shen et al, 2006). Automated whole cell tracking was previously found to be the most appropriate method for detecting low amplitude p65 nuclear translocations because it gave the best signal-to-noise ratio (Dr D. Turner, personal communication). However, the majority of this project focuses on STAT3 and uses the HepG2 cell line, both of which behave differently to p65 and SK-N-AS cells, therefore the suitability of automated whole cell tracker was in doubt. Re-evaluation of the three approaches regarding their suitability for STAT3 dynamics in HepG2 cells led to the conclusion that ROI tracking was the most appropriate method.

2.11.1 Description of the Tracking Approaches

In 'whole cell' tracking (Fig. 2.4A), compartments for the cytoplasm and nucleus are demarcated by drawing precise boundaries for the cell membrane and

nuclear envelope. In manual whole cell tracking, the boundaries are marked by hand, frame by frame, which is a very laborious, time-consuming process. Automated whole cell tracker meanwhile uses an algorithm to determine where the cytoplasmic and nuclear boundaries are based on a pre-set threshold for fluorescence intensity. The threshold level and sensitivity options can be set on a case-by-case basis, within a certain range. The cytoplasm is defined as any fluorescence above a pre-determined level while the nucleus is identified as the region of lowest fluorescence within the cytoplasmic area. The algorithm was designed this way for optimal analysis of p65 which is absent from the nucleus in the resting state.

In comparison, ROI analysis involves demarcating two sample areas, one within the cytoplasm and the other in the nucleus (Fig. 2.4B). Ideally the nuclear sample region is just a fraction smaller than the nucleus since there is often some fluorescence spill-over from the cytoplasm. The cytoplasmic ROI is, at a minimum, the same size as the nuclear ROI in order to capture as much of the cytoplasm as possible whilst simplifying boundary selection and reducing operator selection bias. The ROIs are then copied from frame to frame and adjusted as necessary to ensure only the appropriate regions are sampled.

In all three methods, once the boundaries had been marked for all frames, the software calculated the average fluorescence in the nuclear and the cytoplasmic regions, and exported the quantified data into Excel for further analysis.

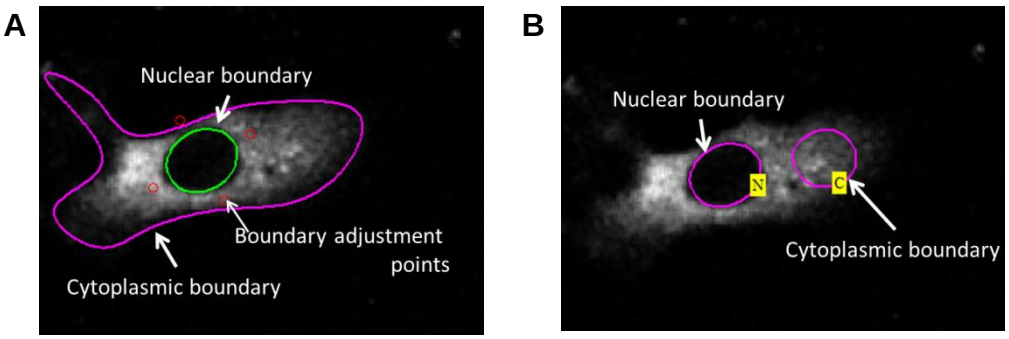

Figure 2.4: **Comparison of Cell Tracking methods.** **A** An example of "whole cell tracker" and **B** an example of ROI cell tracker. The nuclear and cytoplasmic boundaries are labelled, and the small red circles in A are the points used to manually adjust a boundary.

2.11.2 Cost-Benefit Analysis of Tracking Methods

The three methods have different advantages and disadvantages and were therefore suited to different situations. The whole cell tracker methods provided a slightly better signal-to-noise ratio than ROI analysis but they had significant draw-backs. The manual approach was very labour intensive, taking up to four times per cell as long as the other two methods, making it the appropriate choice only for difficult analyses e.g. where two or more cells were in very close proximity or frequently changed their morphology or location. The automated tracking algorithm had the potential to be the quickest approach but it was very susceptible to confounding factors in the images, such as neighbouring fluorescent cells and auto-fluorescent debris. In addition, since it was optimised for p65, it identified the nucleus as any area of low fluorescence within the cytoplasm. However, since STAT3 is evenly distributed between the nucleus and the cytoplasm in unstimulated cells, and in stimulated cells is predominantly nuclear, the algorithm failed to identify the nucleus in STAT3-expressing cells, necessitating manual tracking of the nuclei. It could also be confused by the oil vesicles often present in HepG2 cells as these would appear as dark regions within the area of EGFP fluorescence. This slowed down the "automated" tracking considerably and made it entirely unsuitable for tracking cells expressing STAT3 alone. It was however useful for analysing cells expressing p65-dsRedXP, either alone or with STAT3-EGFP, and therefore was used for many of the cells in the p65-based microscopy experiments.

In contrast to these difficulties with whole cell tracking approaches, ROI tracking was very fast and labour efficient. Side-by-side comparisons of cells analysed with both automated whole cell tracking and ROI tracking indicated that ROI tracking had a sensitive enough signal-to-noise ratio to detect STAT3 and p65 nuclear translocations in HepG2 cells. Although the ROI data was somewhat noisier than whole cell tracking, the use of a 3-point moving average reduced the noise sufficiently to enable feature detection in the output fluorescence graphs. ROI tracking was also very useful for HepG2 cells due to their highly variable, non-uniform morphology, both between cells and within cells over time. Whilst HepG2 cells are considerably less mobile than the SK-N-

AS or HeLa cell lines, they prefer to grow in clumps, even if sparsely seeded. This clumped growth pattern meant the HepG2 cells had a tendency to crawl over and around each other as the island of cells proliferates. This can make cell boundary detection difficult, especially when fluorescence levels were low. By using ROI tracker, selection of nuclear and cytoplasmic regions was more straightforward, even for 'difficult-to-track' cells that the 'whole cell' algorithms could not accurately process, thereby increasing the number of analysed cells.

In conclusion, since both semi-automated whole cell tracking and ROI tracking had different advantages and disadvantages, it was necessary to identify the best approach for each given cell or experiment. ROI tracker was used for preference, particularly for experiments on cells expressing EGFP-STAT3 alone, or where cells were more crowded or mobile than usual, since it was by far the fastest method for processing such images. Automated whole cell tracking was used for 'easy-to-track' cells, particularly for those expressing p65-dsREdXP. Ideally, use of good nuclear markers, such as Hoechst stain or a fluorescent marker using an ubiquitous nuclear protein e.g. H2B, a histone protein, would speed up the analysis by simplifying identification of the nucleus – several colleagues have recently had success with this approach (Dr Bagnall and Dr Spiller, personal communication). Alternatively, development of a new, up-to-date analytical software would represent a significant step forward, and would have streamlined this project considerably, especially given the lack of a stable cell line.

2.11.3 Analysis of Processed Image Data

Two normalisation methods were considered for processing the raw fluorescence values of the nuclear and cytoplasmic compartments in order to give the clearest indication of the localisation dynamics. These were the ratio of nuclear to cytoplasmic fluorescence (N/C) and the nuclear fluorescence as a proportion of the total cellular fluorescence (N/T). The N/T ratio gave clearer results than the N/C ratio when the nuclear region was close to the upper threshold detection limit, which was often the case with EGFP-STAT3. Furthermore, since it has been repeatedly demonstrated that STAT3 levels do

not change significantly due to turn-over, degradation or induction under the tested conditions and time scales (Siewert et al, 1999; Wormald et al, 2006), the N/T ratio represents how much of the total STAT3 pool is in the nucleus and therefore can be considered transcriptionally active.

The cytoplasmic and nuclear fluorescence intensity values exported into Excel were used to calculate the N/T ratio. A 3rd order moving average of the N/T fluorescence was calculated and plotted over time in hours. This pre-processed data was imported into a spreadsheet tool constructed by Drs Bagnall and Boyd to subject it to a peak-detection protocol as a way to expedite quantification of the fluorescence time series data and ensure consistency. Prior to the development of this spreadsheet tool, peak detection was performed manually by the experimenter. For the purposes of this thesis, a 'peak' is a transient but significant increase in transcription factor occupancy of the nucleus; each 'peak' or 'nuclear translocation' has an associated time and amplitude value. It was the purpose of the spreadsheet tool to extract these values and also calculate the intervals between sequential peaks.

Within the spreadsheet itself, peaks were identified by searching for the highest N/T fluorescence value above a pre-determined amplitude and within a given window of time. These amplitude and window values were empirically determined and optimised separately for STAT3 and p65. In this way peaks could be identified via amplitude thresholding and a minimum peak-to-peak timing interval.

The peak amplitude, peak appearance time and peak to peak interval data extracted from the Excel analysis were transferred into GraphPad Prism, version 6.02 for Windows, (GraphPad Software, La Jolla California USA, www.graphpad.com) for statistical analysis.

Chapter 3
Setting up the Model System

3.1 Introduction

IL-6 is a functionally pleiotropic cytokine and is a critical instigator of the acute phase response to infection. IL-6-activated STAT3 induces transcription of SOCS3, which inhibits activation of STAT3 thus setting up a delayed negative feedback loop (Bode et al, 2012a). This has the potential to create oscillatory dynamics within the system. Indeed, phospho-STAT3 and SOCS3 protein oscillate out of phase in a population of serum-synchronised cells, and their oscillations were mechanistically interdependent (Yoshiura et al, 2007). Based on experience in other systems, such as NF-κB (Nelson et al, 2004; Ashall et al, 2009) and p53 (Lahav et al, 2004), it seemed likely that oscillations would be more obvious at the single cell level. Live cell fluorescence microscopy was used for these studies as it is a very effective tool for studying protein dynamics at the single cell level. It provides detailed time-resolved data for individual cells and so can reveal complex dynamics and intercellular heterogeneity that would otherwise confound population-based data.

A key aim of this project was to investigate IL-6-induced STAT3/SOCS3 dynamics in single cells using time-lapse fluorescence confocal microscopy. The second aim was to investigate cross-talk between the potential oscillations of STAT3-SOCS3 system and the known oscillatory dynamics of p65, an NF-κB transcription factor (Ashall et al., 2009). To address these aims, various molecular and cellular tools needed to be developed and validated, which is the subject of the current chapter.

3.1.1 Objectives

The overall objective of this chapter is to establish a system for the investigation of STAT3 and SOCS3 single cell dynamics and subsequently the investigation of STAT3-NF-κB cross-talk. To achieve this objective, a cell line with functional IL-6 and TNFα signalling first needed to be selected from a number of possible candidates, including the SK-N-AS and HepG2 cell lines. The TNFα-induced NF-κB dynamics in the HepG2 cell line were characterised for comparison to the SK-N-AS cell line, which has been previously used to study NF-κB dynamics (Nelson et al, 2004; Ashall et al, 2009). Secondly, in order to try and visualise STAT3 and SOCS3 dynamics, fluorescent protein fusion plasmid expression vectors for

STAT3 and SOCS3 were constructed. STAT3 and SOCS3 BACs were also attempted. A SOCS3 proximal promoter-driven luciferase vector was constructed to report on STAT3 transcriptional activity. The biological function of the STAT3 and SOCS3 fluorescence fusion proteins were investigated, and the effect of placing the fluorescent protein at either the N- or C-terminus of STAT3 was also assessed.

3.2 Selecting an IL-6 and TNFα Responsive Cell Line

A cell line with functional IL-6 – STAT3 and TNFα – p65 signalling was necessary for being able to investigate cross-talk between p65 and STAT3 later in the project. Previous work has used cell lines such as SK-N-AS and HeLa (Nelson et al., 2004), and HepG2 and HEK-293 (Kretzschmar et al., 2004). The SK-N-AS neuroblastoma cell line has previously been used as a key model to study p65 and IκBα single cell dynamics (Nelson et al., 2004; Ashall et al., 2009). The data generated with this cell line was used to build and parameterise various models of NF-κB dynamics (Paszek et al., 2010; West et al., 2014). Stable NF-κB BAC transfected SK-N-AS lines are also available (A. Adamson, University of Manchester, unpublished), which would be advantageous for studying NF-κB and STAT3 cross-talk as only STAT3 constructs would need to be transiently transfected into the cells, making them a better choice than HeLa cells. However, the SK-N-AS ability to respond to IL-6 was unknown. Meanwhile, HEK-293 cells lack the IL-6 receptor and have to be transfected with an IL6R expression vector, making them unsuitable for studying IL-6-induced signalling. The hepatoma HepG2 cell line was a strong candidate, as it has been used extensively in the study of STAT3 signalling (Wegenka et al., 1993), including imaging studies (Pranada et al., 2004; Hermann et al., 2007). The HepG2 line has also been used to study aspects of NF-κB signalling (Albretch et al., 2007). However, the long-term single cell NF-κB dynamics were unknown. Therefore the first step was to test IL-6 signalling in the SK-N-AS line and compare it to that in the HepG2 line, using a combination of Western blotting and qPCR.

STAT3 activation by IL-6 in SK-N-AS and HepG2 cells was assessed by blotting for transcriptionally active pY705-STAT3 and by measuring mRNA induction of SOCS3, a target gene of STAT3. SK-N-AS cells showed no increase in pY705-STAT3, despite having a similar amount of STAT3 to HepG2 cells (Fig. 3.1A & B). That there was no observable change following IL-6 stimulation, even though SK-N-AS cells had some degree of basal STAT3 tyrosine-phosphorylation, suggested these cells lack a functioning IL-6 receptor complex, probably due to a lack of IL6R subunit expression. Conversely, the HepG2 cells displayed a large increase in pY705-STAT3 within 30 min of stimulation that was sustained over the 3.5 h period studied (Fig. 3.1B). The absence of IL-6-induced STAT3 signalling in SK-N-AS cells was confirmed by qPCR analysis of SOCS3 mRNA expression, which did not increase in response to IL-6 (Figure 3.1C). In contrast, SOCS3 was strongly induced in HepG2 cells, increasing 18-fold by 1 h. The unresponsiveness of SK-N-AS cells to IL-6 makes them unsuitable for studying IL-6-induced STAT3 single cell dynamics.

Having established that the SK-N-AS line did not respond to IL-6, it was necessary to determine the HepG2 response to TNFα and compare it to that of SK-N-AS cells. Western blotting of IκBα and pS536-p65 and qPCR analysis of IκBα mRNA induction revealed minor differences between the cell lines (Fig. 3.2). IκBα was degraded more slowly in HepG2 cells upon TNFa stimulation, but was resynthesized more rapidly (Fig. 3.2B). The induction of IκBα mRNA expression was similar in timing and amplitude in both cell lines (Fig. 3.2C), and was sustained in SK-N-AS but transient in HepG2 cells. These slight differences were not considered to be functionally important for the present studies.

In conclusion, the p65/IκBα population dynamics of the two cell lines appeared very similar. However, only the HepG2 line responded to IL-6; this cell line was therefore used for the rest of the project. The next step was to define the p65 and IκBα dynamics in detail at the single cell level in HepG2 cells to see if they showed the typical oscillatory dynamics previously been seen in several cell lines and studied in most detail in SK-N-AS cells.

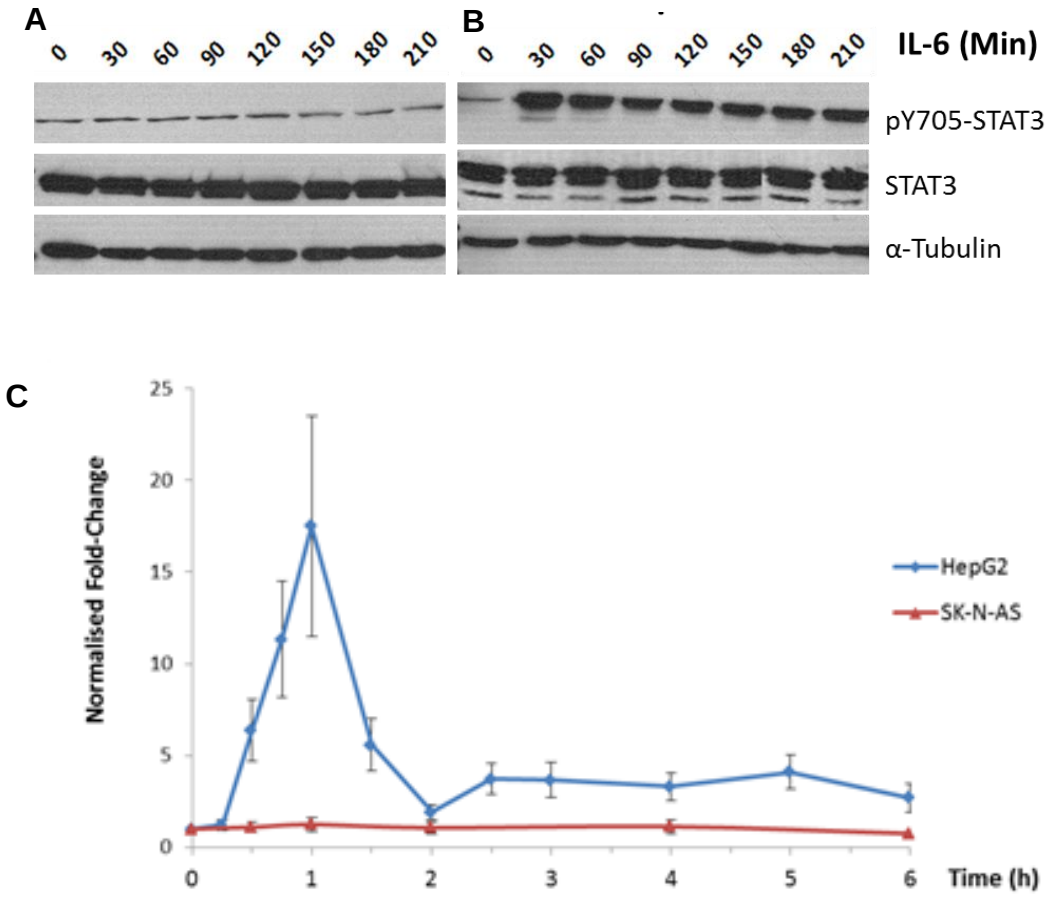

Figure 3.1: Comparison of SK-N-AS and HepG2 cell line responses to continuous 20 ng/ml IL-6. Western blots for pY705-STAT3, STAT3 and α-tubulin from whole cell lysates collected at times indicated from **A** SK-N-AS and **B** HepG2 cells, representative of n=3 blots. **C** qPCR graph of relative fold-change in SOCS3 mRNA, normalised to t=0 min, over a 6 hour period. Error bars represent the standard deviation of n=3 independent biological repeats.

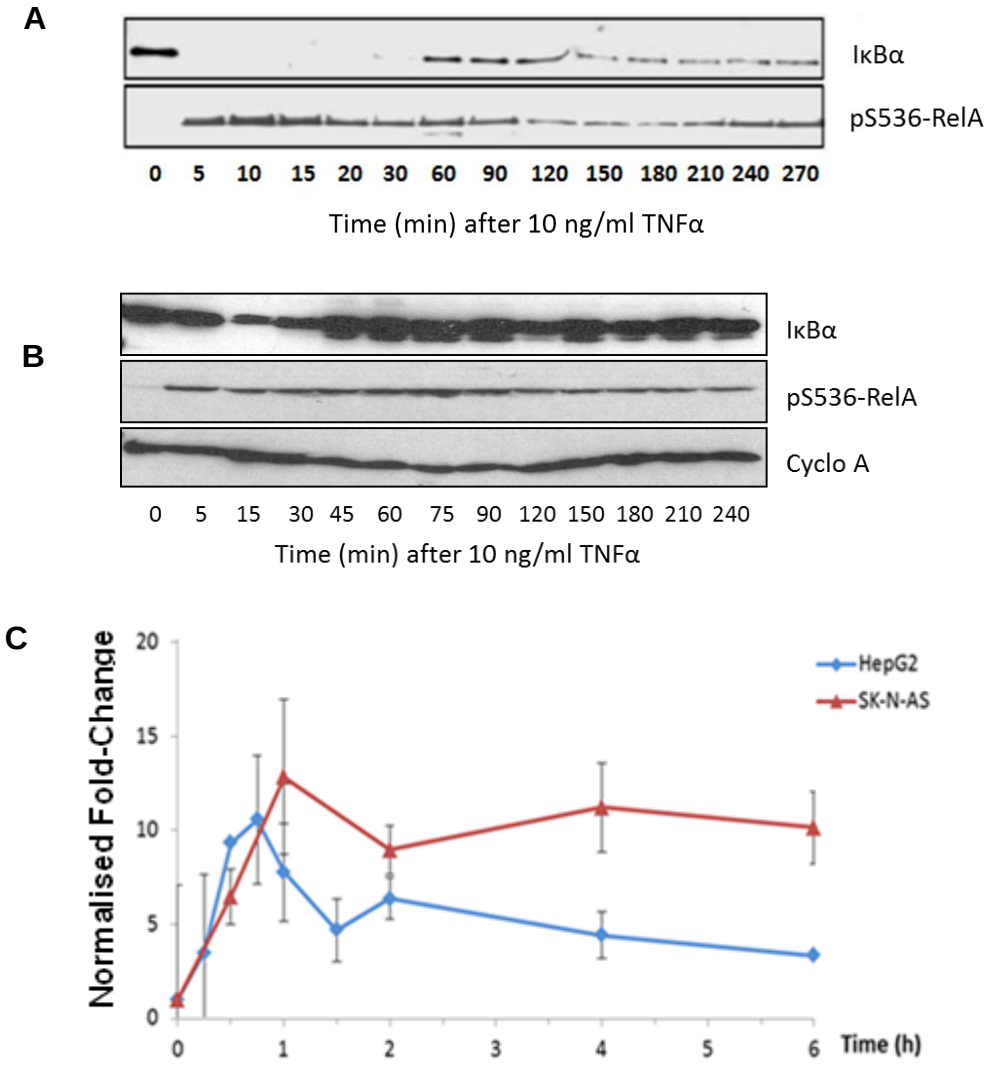

Figure 3.2: Comparison of SK-N-AS and HepG2 responses to continuous stimulation with 10 ng/ml TNFα. Western blots for IκBα, pS536-RelA (p65) and Cyclophilin A on cell lysates collected at indicated times. **A** SK-N-AS cell line (reproduced from Nelson et al 2004). **B** HepG2 cell line. Western blots representative of n=3. **C** qPCR of relative fold-change in IκBα mRNA, normalised to t=0 min, over a 6 hour period. HepG2 data from Fluidigm qPCR and SK-N-AS data from LightCycler480 qPCR. Mean ± SEM from n=3 replicates.

3.3 Live-Cell Imaging of p65 and IκBα in HepG2 Cells

The previous section established that the population dynamics of p65 and IκBα of HepG2 cells reflected those seen in SK-N-AS cells. The next step was to study the behaviour of p65 and IκBα in individual HepG2 cells using fluorescence confocal microscopy. This served the dual purposes of determining whether the Ashall model of NF-κB signalling in SK-N-AS cells is applicable to HepG2 cells, as well as providing experimental control data for NF-κB – STAT3 cross-talk work in Chapter 5.

This was accomplished by transiently transfecting HepG2 cells with either the CMV-driven p65-dsRedXP plasmid or the IκBα-EGFP BAC, as per Section 2.4.4. Images from microscopy experiments were analysed using ROI Cell Tracking to calculate the Nuclear/Total (N/T) Fluorescence (Section 2.10). Amplitude and time of peak maxima values were extracted from the data using an Excel tool and the peak-to-peak intervals were calculated (Section 2.10.3). A representative p65-dsRedXP cell trace with the timing, amplitude and interval of the nuclear peaks marked is given in Fig. 3.3. The recurring peaks of p65 nuclear translocation form an oscillatory pattern and period of oscillation can be calculated from the average of all peak intervals from a sample population of cells.

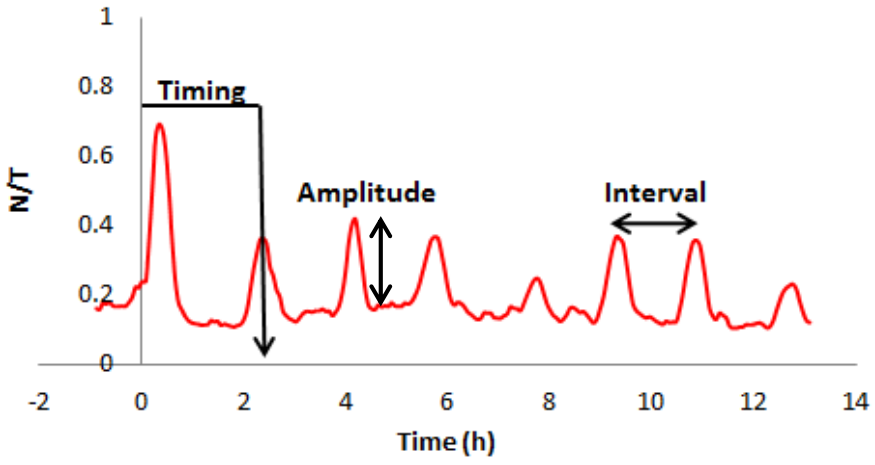

Figure 3.3: Oscillations in p65-dsRedXP Nuclear/Total Fluorescence in a single HepG2 cell. 10 ng/ml TNFα added at t = 0. Timing of nuclear translocation, amplitude of translocation and peak-to-peak interval are labelled on the graph.

3.3.1 Single Cell p65 Dynamics

Oscillations in p65 nuclear-cytoplasmic movement were detected in HepG2 cells following continuous TNFα stimulation (Fig. 3.4). Sustained oscillations in p65 nuclear translocation occurred in over 95% of cells, as previously seen in the SK-N-AS cell line (Nelson et al., 2004). Nuclear peaks were asynchronous between cells after the first peak. This heterogeneity is an observed feature of the NF-κB system, posited as a deliberate design feature and hypothesized to control a robust population immune response (Paszek et al., 2010). This is also seen at the tissue level (A. Adamson, C. Walker and E. Borysiewicz, University of Manchester, unpublished observations).

The variability of the HepG2 p65 oscillatory period in response to TNFα stimulation was investigated. The average period and standard deviation of p65 oscillations were calculated for each individual HepG2 cell (Fig. 3.5). The mean p65 oscillatory period was 98 $\pm$ 25 min in HepG2 cells and the cell periods were normally distributed, according to the D'Agostino & Pearson omnibus normality test (performed in Prism). No outliers were identified using the ROUT method in Prism. The standard deviations of the cell periods were very variable, ranging from 4 to 45 min, with a median of 17 min. This large variability between cells could be caused by differences in the timing of feedback loops such as A20 or IκBε (Paszek et al., 2010).

The peak intervals from oscillating p65 transfected cells were pooled and HepG2 cells were found to have a mean oscillation period of 98 $\pm$ 25 min whilst the SK-N-AS oscillatory period was 102 $\pm$ 17 min (Fig. 3.6) (SK-N-AS data courtesy of Dr C. Harper, University of Manchester). The population mean and distributions were compared using the two-sample t-test assuming unequal variances and no significant difference was found between the cell lines ($P<0.01$) (Fig. 3.6). This test was used to compare the population means for SK-N-AS and HepG2 cell lines because the Kruskal-Wallis test confirmed that the data were normally distributed while the F-test determined that the variances were unequal. A probable cause of this difference is the difference in sample size. On average only 3.1 translocations were imaged per SK-N-AS cell whereas

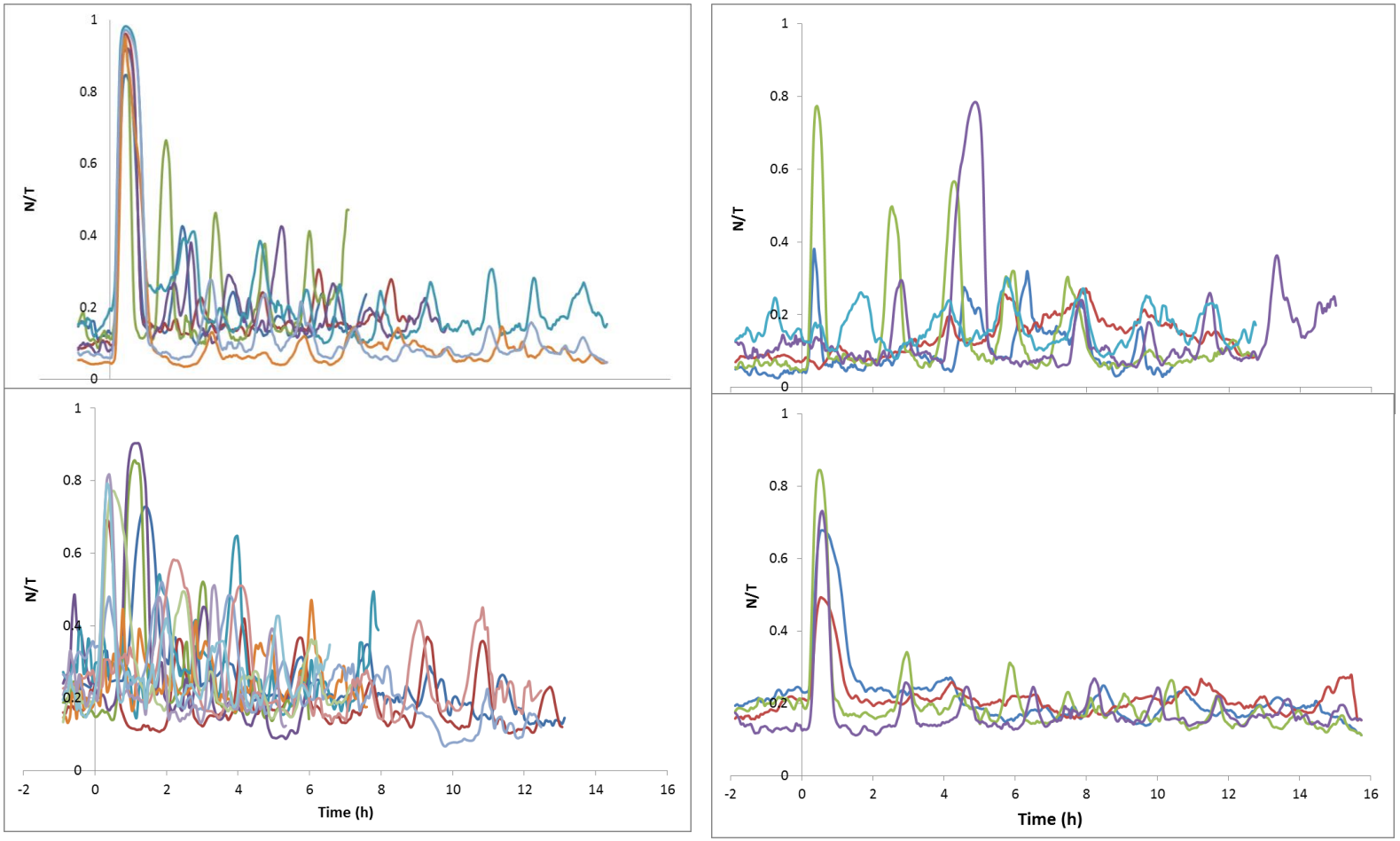

Figure 3.4: p65 Localisation in Response to Continuous TNFα Stimulation. Individual traces of p65 localisation, defined as Nuclear/Total Fluorescence (N/T), in HepG2 cells in response to continuous 10 ng/ml TNFα, grouped by biological repeat (n=4).

for HepG2 cells this number was 5.4. In conclusion, p65 oscillated at the same frequency in the two cell lines following TNFα stimulation

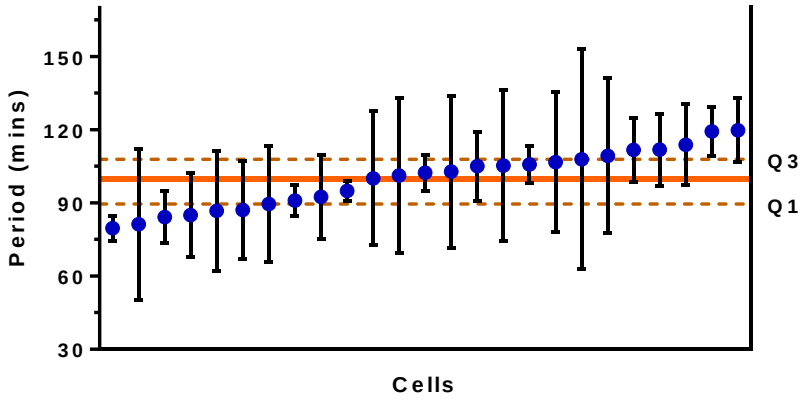

Figure 3.5: Mean period of p65 oscillations in transiently transfected p65-dsRedXP HepG2 cells. (●) = Average period ± 1 S. D. per cell. Cells ordered by oscillatory period. Solid orange line = mean period of all cells. Orange dashed lines: Upper (Q3) and Lower (Q1) quartiles..

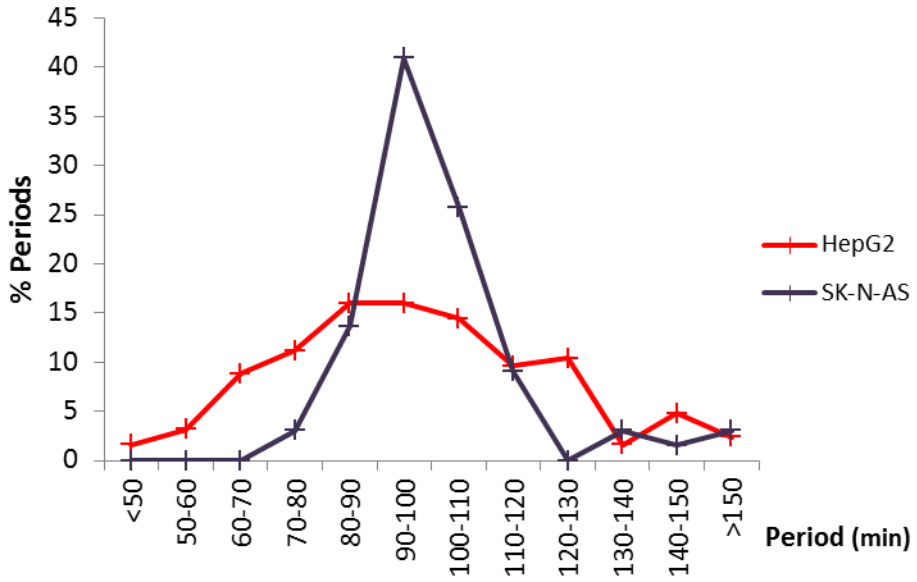

Figure 3.6: Histogram of p65 peak intervals pooled from all cells to compare the HepG2 (red) and SK-N-AS (purple) cell lines, expressing p65-dsRedXP and treated with continuous 10 ng/ml TNFα. Peak periods grouped in 10 minute intervals and expressed as a percentage of total number of peaks. HepG2: cells n= 25, peaks n= 135. SK-N-AS: cells n= 21, peaks n=66.

3.3.2 Single Cell IκBα Dynamics

To complement the p65 data, IκBα degradation and resynthesis dynamics were investigated. SK-N-AS and HepG2 cells transiently transfected with the IκBα-EGFP BAC were treated with 10 ng/ml TNFα and the degradation and resynthesis of IκBα followed by confocal microscopy (Fig. 3.7A, data provided by Dr. A. Adamson).

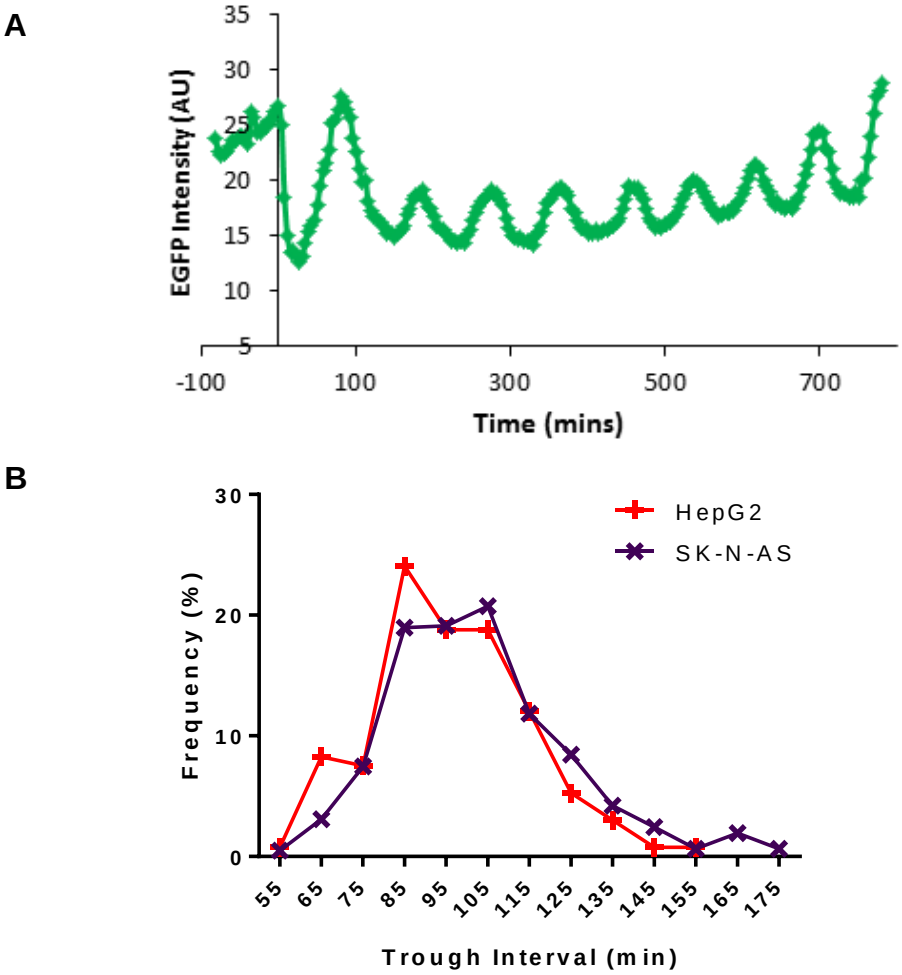

Figure 3.7: IκBα-EGFP oscillations compared in HepG2 and SK-N-AS cells treated with 10 ng/ml TNFα. A Example of EGFP-IκBα fluorescence intensity in a single SK-N-AS cell (Arbitrary Units) over time (minutes) adjusted so that TNFα addition is at t=0. **B** Histogram of IκBα trough intervals in transiently transfected HepG2 (red) and SK-N-AS (purple) cells. HepG2: cells n = 20, peaks n = 133. SK-N-AS: cells n = 43, peaks n = 617.

The troughs indicate IκBα degradation while the peaks are periods of resynthesis. Trough appearance times and trough-to-trough intervals were calculated for individual cells as for p65. Trough intervals were pooled to form a histogram (Fig. 3.7B), comparing HepG2 and SK-N-AS cells. The mean period for IκBα oscillations in HepG2 cells was 98.9 min $\pm$ 25.7 and was 101.9 min $\pm$ 21.2 in SK-N-AS cells (A. Adamson, unpublished). This suggests IκBα signalling dynamics are not significantly different between the cell lines.

3.3.3 Combining p65 and IκBα Dynamics

Work utilising the p65-dsRedXP and IκBα-EGFP BACs has conclusively shown that IκBα and p65 oscillate out of phase with each other in response to TNFα treatment, as can be seen in Figure 3.8 (A. Adamson, unpublished). Given these out of phase oscillations in SK-N-AS cells, it could be expected that the mean period and peak interval distributions for p65 and IκBα in HepG2 cells would be virtually indistinguishable, assuming they are oscillating likewise. In HepG2 cells, IκBα oscillated at 99 $\pm$ 26 min and p65 oscillated at 98 $\pm$ 25 min, while a histogram demonstrated that p65-dsRedXP and IκBα-EGFP peak and trough interval distributions aligned precisely (Fig. 3.9). This strongly implied that p65 and IκBα were oscillating out of phase with each other in HepG2 cells also. It would be very interesting if the same pattern could be seen for STAT3 and SOCS3, hence the work to construct the fluorophore constructs described below.

In summary, the previous sections on p65 and IκBα dynamics established that the HepG2 and SK-N-AS cells lines oscillated at the same frequency in response to TNFα stimulation. In conjunction with the strong response to IL-6 signalling, the HepG2 cell line was the preferred candidate for studying STAT3 and NF-κB signalling cross-talk. The next stage of the project was to make and test the STAT3 and SOCS3 expression constructs in the HepG2 cells.

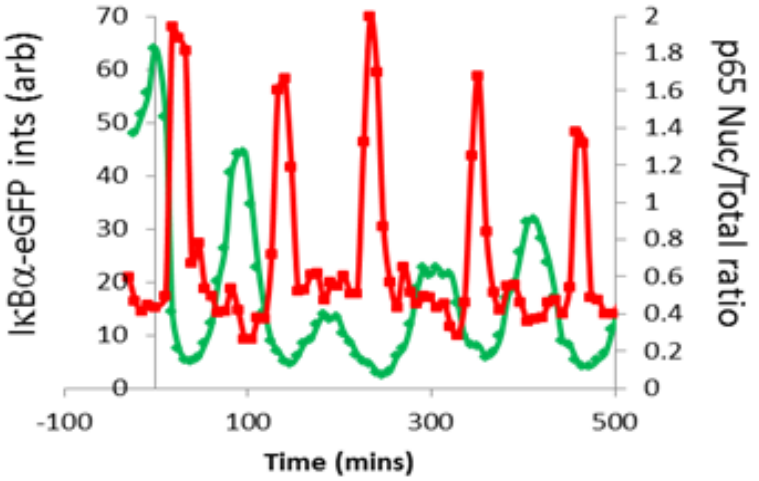

Figure 3.8: Out of phase oscillations of p65 and I κ Bα in a single cell. Stable BAC transfection of SK-N-AS cell, expressing p65-dsRedXP (red) and IκBα-EGFP (green) in response to 10 ng/ml TNFα (A. Adamson, unpublished).

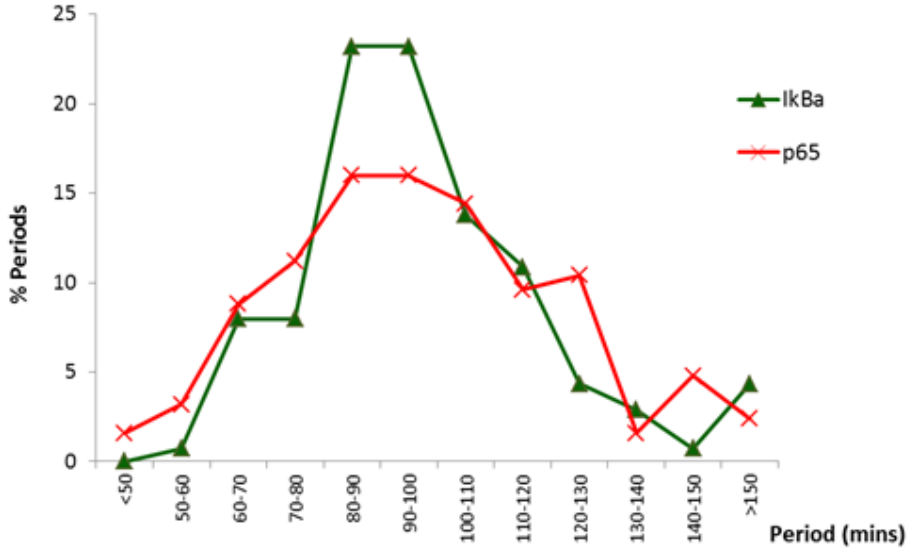

Figure 3.9: Comparing the distribution of peak intervals for p65 and IκBα. p65-dsRedXP plasmid and IκBα-EGFP BAC transiently transfected HepG2 cells treated with 10 ng/ml TNFα. IκBα: cells n = 20, peaks n = 133. P65: n= 25, peaks: n= 135.

3.4 Overview of Expression Vector Cloning

A key goal of the project was to investigate the single cell signalling dynamics of the STAT3 and SOCS3 proteins by imaging their bulk subcellular movements in real time using live cell fluorescence confocal microscopy. Therefore the first aim was to assess the fluorescent protein fusions expressed from transiently transfected plasmid vectors. There was a concern that the position of the fluorescent protein might affect the functionality of the STAT3 protein, based on previous work with STAT6 (Nelson et al., 2002). This study found that N-terminal tagged STAT6 was more transcriptionally active than the C-terminal tagged version. Consequently two versions of STAT3 were generated placing the EGFP moiety at either the N- or C-terminal (Fig 3.10B), using the Invitrogen Gateway® cloning system (Section 3.4.1).

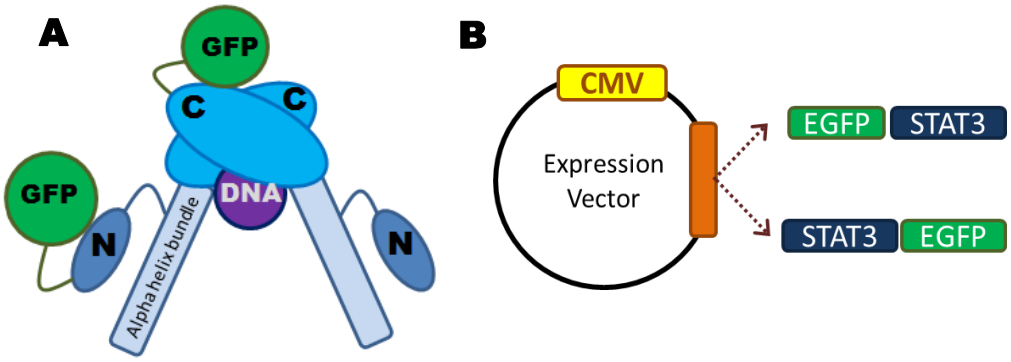

Figure 3.10: EGFP positions on STAT3. A Illustration of the active STAT3 dimer conformation bound to DNA with the two locations for the EGFP tag indicated (GFP). N-terminal domain (N). C-terminal domain (C), including the DNA-binding region, and the regulatory phosphorylation sites. Based on the published structures of STAT3β (Becker et al., 1998) and STAT1 (Chen 1998). **B** Schema of the two STAT3 expression plasmids, ordered from 5' to 3'.

The structure of the active STAT3 dimer bound to DNA (Fig. 3.10A) and knowledge of the roles of the different domains of STAT3 suggested that C-terminal placement of EGFP could obstruct access to the phosphorylation sites in the C-terminal region, affecting activation and/or deactivation of the dimer. A fluorescent protein tag at the N-terminal domain should have less risk of functional effects, but constitutive basal shuttling and subcellular localisation could potentially be affected. These concerns necessitated the evaluation of the EGFP-STAT3 and STAT3-EGFP constructs, after which a decision about the best location for the fluorescent protein in the STAT3 BAC could be made.

An expression vector for SOCS3 under the control of the inducible SOCS3 promoter was a key target because it should be a good reporter of STAT3 signalling dynamics. Initially, a CMV-promoter driven SOCS3 expression vector tagged with EGFP was generated. Only a C-terminal tagged construct was made because the SOCS3 protein structure did not suggest any major functional problems would arise from a C-terminal tag. However, constitutive expression of CMV-driven SOCS3 could prevent STAT3 activation. Therefore a SOCS3 fluorescent protein fusion BAC was attempted. STAT3 and SOCS3 BACs would allow the fluorescent fusions to be expressed under the control of the appropriate native promoters and other regulatory sequences, increasing the likelihood of visualising realistic expression dynamics of single cells. The methods for this work are described in Section 2.3. In addition to the BACs, a SOCS3-EGFP plasmid driven by the SOCS3 proximal promoter sequence was constructed as an intermediate measure.

3.5 Production of STAT3 Fusion Vectors

The Gateway protocols described in Section 2.2 were used to generate STAT3 expression vectors tagged with EGFP at the N- and C-terminals, hereafter defined as EGFP-STAT3 and STAT3-EGFP respectively. The STAT3 coding sequence was amplified from SK-N-AS cells to generate cassettes with and without a STOP codon. These were integrated into empty entry vectors. The STAT3 entry vectors were combined with EGFP destination vectors to produce the final expression vectors, driven by the viral CMV promoter to ensure high expression levels.

3.6 Examining the Functionality of the EGFP-tag Orientations for STAT3 Expression Plasmids

To address the potential issues on STAT3 functionality caused by the position of the EGFP-tag outlined in the cloning overview, the STAT3 fluorophore fusions were compared by size, phosphorylation in response to a pulse of IL-6 and ability to induce the SOCS3 promoter luciferase. Finally cellular expression was investigated by live cell fluorescence microscopy.

3.6.1 Pulsed IL-6 Treatment Protocol Optimisation

A stimulation protocol able to uncover phosphorylation kinetics was needed to assess the effect of the EGFP tag on activation and deactivation of the STAT3 constructs. Continuous IL-6 stimulation was insufficient for evaluating the constructs because it led to sustained phosphorylation (Figure 3.11A) of STAT3, which would mask any dephosphorylation effects. Therefore a 30 min pulse of IL-6 was tested (Figure 3.11A) as per Section 2.5. This is a common protocol for IL-6 stimulation of HepG2 cells (Pranada et al, 2004; German et al, 2011) and it resulted in transient phosphorylation of endogenous STAT3, that peaked at 30 min and returned to initial levels within 90 min. The transient phosphorylation made the 30 min IL-6 pulse ideal for assessing the impact of EGFP tag position on STAT3 activation and deactivation.

The washing process for the 30 min pulse was tested to control for any effects on basal STAT3 phosphorylation. Washing followed by non-conditioned media replacement (Fig. 3.11B) caused a rapid drop in STAT3 phosphorylation that lasted for at least 6 h, so washing followed by replacement with conditioned media (i.e. from a matched but untreated dish of cells) was tried. Adding conditioned media prevented the drop in phospho-STAT3, indicating that differences between the conditioned and non-conditioned media were responsible, rather than the wash protocol itself. The nature of the difference was not investigated further since it was sufficient to know that conditioned media prevented the down-regulation of STAT3 signalling. In light of this finding, all subsequent pulsed treatments of the HepG2 cells were carried out using conditioned media replacement.

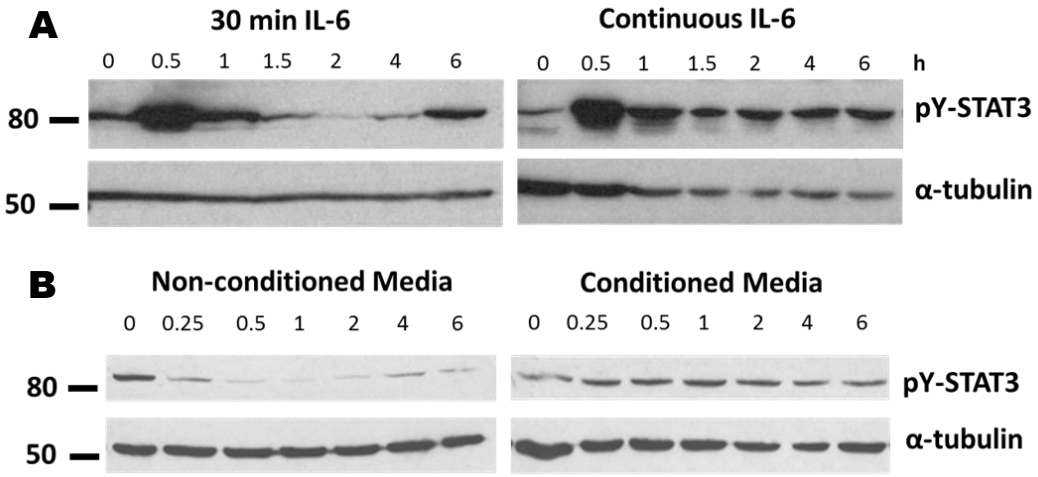

Figure 3.11: Optimisation of pulsed stimulation protocol for assessing phosphorylation of STAT3 constructs. A STAT3 Y705-phoshporylation in HepG2 cells exposed for 30 min or continuously to 20 ng/ml IL-6 over 6 hours. **B** The effect of washing untreated cells with MEM and replacing with either non-conditioned or conditioned media. Blots representative of three independent repeats.

3.6.2 Phosphorylation of EGFP-tagged STAT3 Proteins in Response to Pulsed IL-6

The EGFP-tagged STAT3 constructs were the expected size, approx. 130 kDa, by Western blot and did not differ from each other (Fig. 3.12A). However the constructs did differ significantly in their pattern of Y705-phosphorylation in response to a 30 min pulse of IL-6. EGFP-STAT3 followed the phosphorylation of endogenous STAT3 closely, but exhibited a slightly slower dephosphorylation rate (Fig. 3.12B).

STAT3-EGFP on the other hand was not appreciably dephosphorylated (Fig. 3 12C). Instead it maintained a high phosphorylation level for the 8 h period studied, even though the endogenous STAT3 returned to its original phosphorylation level by 2 h. That STAT3-EGFP was not being dephosphorylated suggested that it might remain transcriptionally active long after the original stimulus had been removed. By contrast it could be hypothesized that the endogenous STAT3 were not transcriptionally active

between 1.5 and 8 h because Y705 phosphorylation is responsible for maintaining the active dimer conformation. Consequently the STAT3-EGFP protein perturbed the endogenous system, which could confound any experiments performed with it. To test this, luminometry assays were performed and the construct imaged by confocal microscopy.

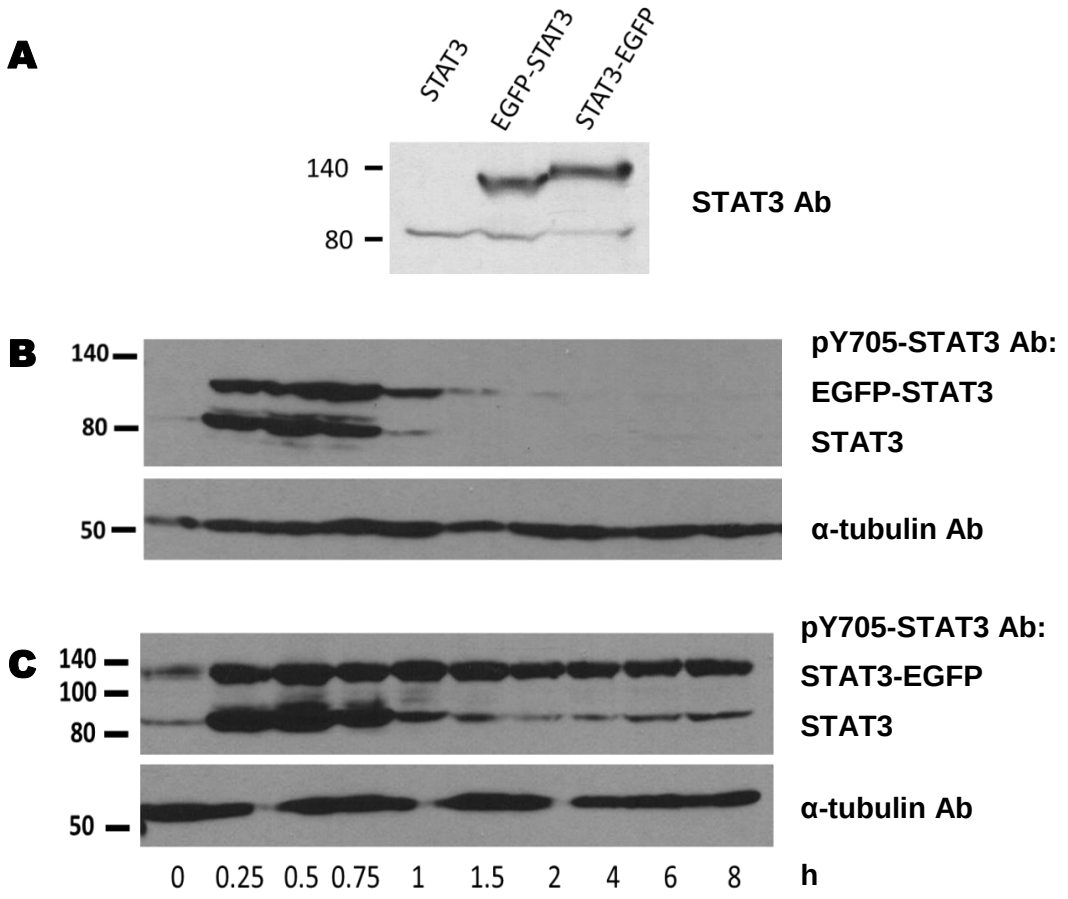

Figure 3.12: Comparing IL-6 induced phosphorylation of EGFP-STAT3 and STAT3-EGFP to endogenous STAT3. Western blots representative of n=3 replicates for **A** STAT3 protein from untransfected HepG2 cells, and HepG2 cells transfected with either EGFP-STAT or STAT3-EGFP 24 h after seeding. Blotted with STAT3 Ab; HepG2 cells expressing **B** EGFP-STAT3 and **C** STAT3-EGFP, stimulated with 20 ng/ml IL-6 for 30 min and lysed at indicated intervals. Blotted with pY705-STAT3 and α-tubulin.

3.6.3 Transcriptional Activity of EGFP-tagged STAT3 Proteins

The transcriptional activity of the EGFP-tagged STAT3 constructs was examined by end-point luminometry (Section 2.6) using the SOCS3-proximal promoter

driven firefly luciferase (SOCS3-lucF) construct generated in Section 2.2.5. The effect of the expression vectors upon unstimulated cells was assessed by comparison of SOCS3-lucF induction in cells transfected with EGFP-STAT3, STAT3-EGFP or EGFP alone (Fig. 3.13A), in accordance with the transfection protocols in Section 2.4.4. The STAT3 expression plasmids significantly altered basal SOCS3 induction, with EGFP-STAT3 lowering induction ($P<0.01$) and STAT3-EGFP increasing induction ($P<0.001$) (2-way ANOVA). Induction of SOCS3 in response to 30 min of 20 ng/ml IL-6 was also assessed (Fig. 3.13B). IL-6 stimulated samples were normalised to their unstimulated controls and then all samples were normalised to the EGFP untreated control. This was to highlight the fold-induction in transcription caused by IL-6 stimulation. IL-6 caused approximately a 2-fold increase in SOCS3 transcription, regardless of EGFP expression vector. Both EGFP-STAT3 and STAT3-EGFP expressing cells significantly increased SOCS3 induction over the EGFP control ($P<0.05$), however there was no significant difference between the STAT3 expression vectors.

There was considerable inter-replicate variation across the four biological replicates performed. The variation was largely due to the poor transfection rates of HepG2 cells (Section 2.4.4), leading to extremely low luminescence levels. Averaging the replicates masked the degree of conflict between them so only the most internally reliable biological replicate with the strongest luminescence readings is presented (Fig. 3.13).

Only two trends were consistent across all replicates. Firstly, STAT3-EGFP increased basal SOCS3 induction above that of EGFP and EGFP-STAT3 cells in the untreated case. It was not possible to determine the effect of EGFP-STAT3 relative to the EGFP control, as it was seen to both increase and decrease basal transcriptional activity. Secondly, EGFP-STAT3 and STAT3-EGFP expressing cells induced SOCS3 more strongly than the EGFP control when stimulated with IL-6. The increase in transcription could be primarily attributed to over-expression of EGFP-tagged STAT3. However, it was not possible to identify a difference between the two constructs in response to IL-6. This was unexpected, based on the Western results where STAT3-EGFP was phosphorylated at a

higher rate for longer than EGFP-STAT3. In conclusion, the poor reproducibility of the data meant that the differences seen between the IL-6-induced transcriptional activity of the N- and C-terminal EGFP-tagged STAT3 constructs could not be reliably confirmed.

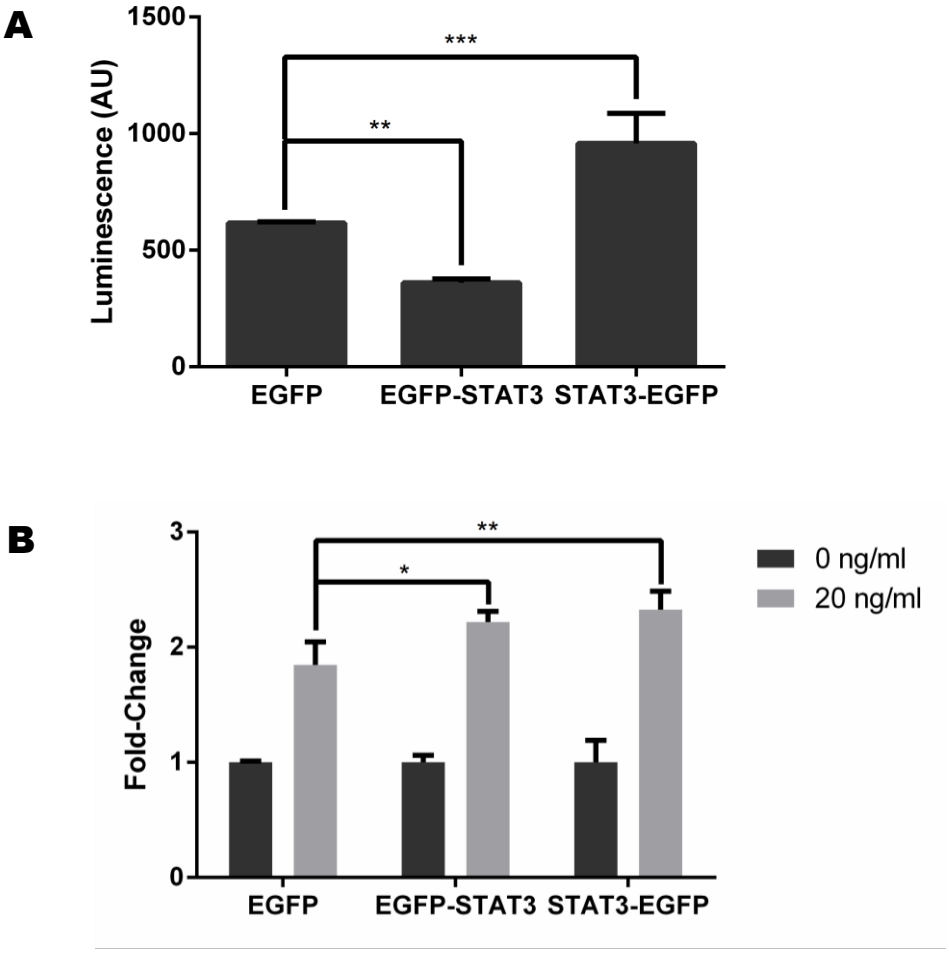

Figure 3.13: ppSOCS3-lucF Induction before and after IL-6 treatment. Cells transfected with ppSOCS3-lucF in a 1:1 ratio with either EGFP, EGFP-STAT3 or STAT3-EGFP. **A** Raw luminescence values for untreated cells, in arbitrary units. **B** Luminescence 3 h after 30 min of 20 ng/ml IL-6 treatment. Statistical analysis of the results was performed in GraphPad Prism, using two-way ANOVA with multiple comparisons. * = $P<0.05$, ** = $P<0.01$, *** = $P<0.001$. Error bars represent 1 standard deviation. Results obtained from n=1 biological replicate.

3.6.4 Cellular Localisation of Fluorescent STAT3 Proteins

The final stage in identifying the best fluorescent STAT3 construct was to study the subcellular localisation of the two constructs. This could reveal protein expression abnormalities and any obstacles to trafficking and movement within the cell, as well as confirming their fluorescence.

Cells expressing EGFP-STAT3 and STAT3-EGFP were classified according to observed pattern of subcellular localisation. Several differences in localisation became apparent between the two constructs. EGFP-STAT3 was evenly distributed between the nucleus and cytoplasm in all cells (Fig. 3.14A), in line with published immunocytochemistry reports of endogenous STAT3 in HepG2 cells (Meyer et al, 2002). However many STAT3-EGFP expressing cells displayed additional features (Fig. 3.14B). Some contained bright fluorescent protein aggregates, while others had a bright ring surrounding the nucleus, termed a perinuclear ring. These features were often found together. An additional observation was that the level of STAT3-EGFP aggregation varied over time. In some cells the volume of aggregates decreased, with a few losing them entirely. Other cells however accumulated aggregates and underwent apoptosis, suggesting that their presence could affect cell fate. The cells with the expected spatial distribution were usually the very faintest ones, suggesting there may be some link between the amount of STAT3-EGFP expressed and the abnormal localisation. The percentages of cells displaying each phenotype were calculated (Fig. 3.14C) and over 75% of STAT3-EGFP cells were found to exhibit abnormal features whereas none of the EGFP-STAT3 cells were affected.

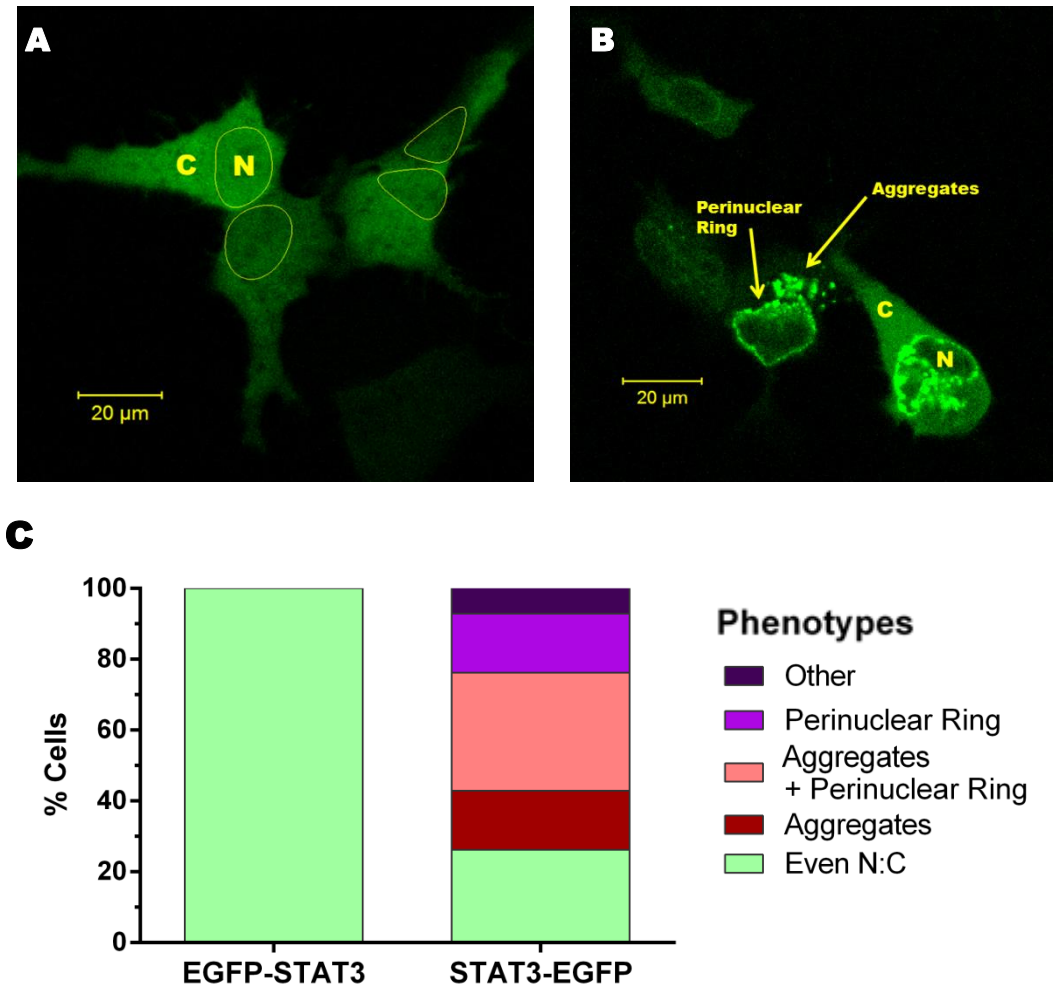

Figure 3.14 Comparison of N- and C-terminal EGFP-tagged STAT3 subcellular localisation phenotypes. Representative pictures of untreated HepG2 cells expressing **A** EGFP-STAT3, with nuclei ringed in yellow. N = Nucleus, C = Cytoplasm; **B** STAT3-EGFP. Nucleus and cytoplasm are marked, as are a Perinuclear Ring and Aggregates. Scale bar is 20 µm. **C** Graph of percentage of cells showing each of the spatial characteristics: even STAT3 distribution between N and C; aggregates; perinuclear ring; aggregates and perinuclear ring; and 'other'. At least 50 cells were counted for each expression plasmid, from n=3 independent replicates.

The perinuclear ring phenomenon noted in Figure 3.15 was briefly studied using z-stack imaging (Fig. 3.15). It was observed that the bright spots of fluorescence were apparently evenly distributed around the nucleus, enclosing it. One possible explanation is that STAT3-EGFP becomes trapped at the Nuclear Pore Complex, although whether it is inside or outside of the nuclear envelope cannot be determined from the z-stacks. It is also unknown from these studies whether these spots were dynamic and exchanging with their surroundings or whether they were static features.

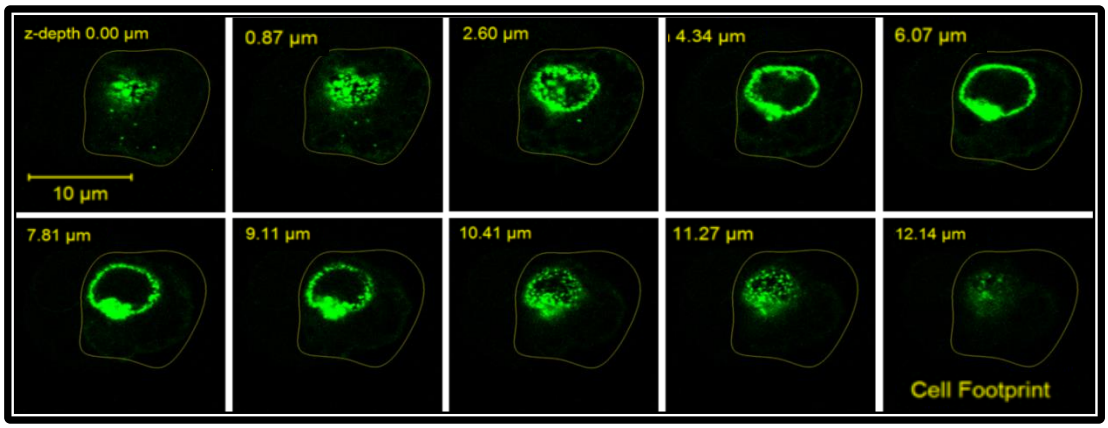

Figure 3.15: Z-stack of a HepG2 cell expressing STAT3-EGFP displaying the perinuclear ring phenotype. 10 slices, each 0.6 µm thick, from a 25 slice stack 15 µm deep, starting at the base of the cell. Thin yellow ring marks the footprint of the cell where it is attached to the glass dish. Inside the bright green fluorescent ring is the nucleus. Scale bar represents 10 µm.

The presence of aggregates and perinuclear rings in the majority of STAT3-EGFP expressing cells, versus their complete absence in EGFP-STAT3 cells, indicates that the C-terminal localisation of EGFP affects the basal expression and nucleocytoplasmic shuttling of STAT3 in a way that the N-terminal tag does not. It is unlikely to be a problem with post-translational folding as the fusion is fluorescent; the most likely explanation is that a C-terminal EGFP tag affects the formation of the U-STAT3 dimer. Combined, these data indicate that the STAT3-EGFP construct is unsuitable and that the EGFP-STAT3 fusion should be used for imaging STAT3 signalling dynamics. Furthermore, an N-terminal fluorescent protein tagged STAT3 BAC should be constructed (Section 3.8).

3.7 Cloning and Expressing the CMV-driven SOCS3-EGFP Expression Vector

The SOCS3 coding sequence was amplified from HepG2 cells stimulated for 2 h with 20 ng/ml IL-6 because it is an inducible and labile mRNA. Gateway cloning protocols were followed as for STAT3. Only a C-terminal tagged version was produced because the protein structure (Babon et al., 2006) locates the SH2 binding domain in the middle of the protein and the Kinase Inhibitory Region towards N-terminus, suggesting that the fluorescent tag would not interfere with the function of SOCS3. The CMV-SOCS3-EGFP construct was expressed in HepG2 cells and was observed mainly in the cytoplasm (Fig. 3.16), in agreement with published reports (Ben-Yair et al., 2002; Babon et al., 2006). Given this positive result, cloning of the SOCS3 BAC began.

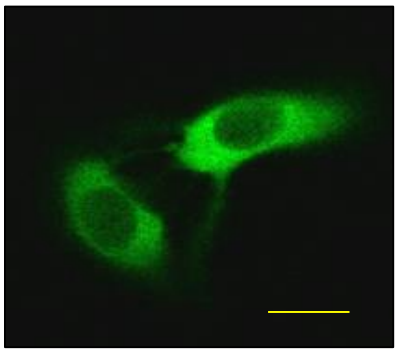

Figure 3.16: Untreated HepG2 cells expressing SOCS3-EGFP under the control of the CMV promoter. Yellow scale bar represents 20 μm.

3.8 SOCS3 and STAT3 Bacterial Artificial Chromosomes

The BACs were intended to supersede the plasmid constructs for EGFP-STAT3 and SOCS3-EGFP, as they would allow protein expression to be controlled by the endogenous promoters and downstream regions. The methods used to engineer the BACs are described in detail in Section 2.3. Briefly, two BACs were selected, one for SOCS3 and one for STAT3, so that the gene of interest was towards the middle of the BAC vector. This was to ensure that as much of the upstream and downstream regulatory regions as possible were included. The BACs were maxi-

prepped and transformed into the SW102 bacterial strain by electroporation of cold-competent SW102 cells, with chloramphenicol and tetracycline selection for presence of the BAC. BAC DNA was prepared from multiple selected colonies and was screened by Pulse-Field Agarose Gel Electrophoresis of restriction digest fragments (Fig. 2.3 in Section 2.3.5).

The STAT3 BAC was successfully transformed into SW102 cells after multiple attempts. Since the EGFP-STAT3 fusion was identified as the best orientation (Section 3.6), primers to introduce the EGFP cassette at the N-terminal of STAT3 had to be designed. However, by this stage, the EGFP-STAT3 plasmid was producing very promising results in response to IL-6 signalling. In order to devote more time to these microscopy experiments, work on the STAT3 BAC was temporarily suspended. The EGFP-STAT3 plasmid microscopy experiments worked well and are discussed further in Chapter 4.

In contrast to the STAT3 BAC, attempts to transform the SOCS3 BAC into SW102 cells were unsuccessful. It appeared that the SOCS3 BAC was undergoing homologous recombination events during the transformation process, causing regions of the BAC to be lost. Although the cultures were grown at 32°C to inhibit the recombination machinery, this process is not always completely efficient.

Problems in the early stage of the BAC engineering process are associated with subsequent difficulties with the introduction of the fluorescent protein cassette (A. Adamson, personal communication). In light of this and the successful EGFP-STAT3 plasmid, the decision was made to cease further attempts with the SOCS3 BAC. However, in order to provide a means to investigate SOCS3 expression and to support the STAT3 work, a STAT3-inducible SOCS3 expression plasmid was produced.

3.9 Cloning and Expression of *Socs3* Proximal Promoter-driven SOCS3-EGFP

SOCS3 inhibition of STAT3 signalling depends on its induction by STAT3 (Babon et al, 2014). Therefore it was necessary to place the expression of the SOCS3-EGFP fusion protein under the control of the SOCS3 promoter (as opposed to constitutive expression from the CMV promoter). The existing SOCS3-EGFP plasmid was manipulated further to place expression of the fusion protein under the sole control of 1 kb of the SOCS3 proximal promoter. The selected promoter sequence contained the TATA box, Transcription Start Site and conserved STAT3 and NF-κB binding sites, and was also used in the construction of the SOCS3 Firefly luciferase reporter used the validation of the STAT3 plasmids.

The proximal promoter was amplified from the SOCS3 BAC using specific primers. A series of restriction digests and a ligation step (Section 2.2.4 and Fig. 3.17) successfully generated a SOCS3 proximal promoter-driven SOCS3-EGFP fusion. The construct was verified by restriction digest and sequencing. This plasmid is hereafter referred to as ppSOCS3-EGFP.

Imaging HepG2 cells transfected with the ppSOCS3-EGFP construct showed that it was expressed predominantly in the cytoplasm (Fig. 3.18), as per CMV-driven SOCS3-EGFP. This was a positive outcome, however the poor transfection efficiency of HepG2 cells coupled with the inducible SOCS3 proximal promoter meant that identifying cells transfected with the construct prior to imaging them was extremely difficult. Furthermore, transfection event during mitosis was enough to induce SOCS3-EGFP expression, because the cells became fluorescent after mitosis. This is a known potential issue with transient plasmid transfections (Pellegrin et al, 2002) and it limited the usefulness of the ppSOCS3-EGFP construct. Use and optimisation of other transfection techniques may have improved transfection efficiency and partially overcome this issue. The ideal solution would have been to develop a stable cell line with the plasmid.

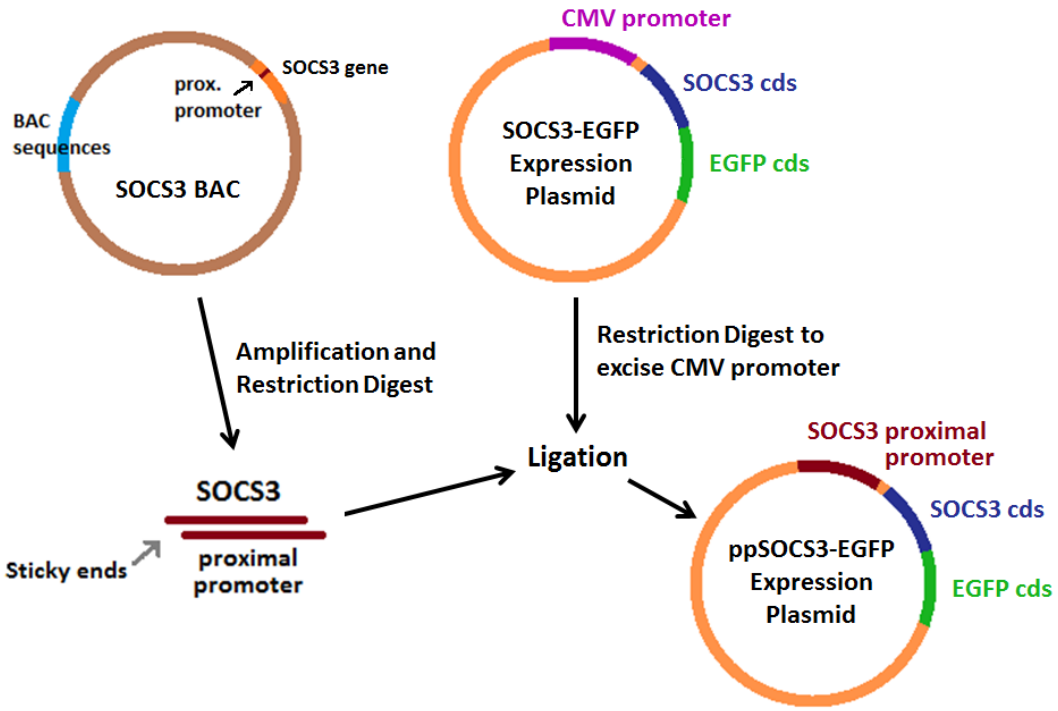

Figure 3.17: Schematic of cloning steps necessary to convert SOCS3-EGFP into ppSOCS3-EGFP. SOCS3 proximal promoter was amplified from the SOCS3 BAC then subjected to a two-step restriction digest to create sticky ends. Pre-existing SOCS3-EGFP expression vector was similarly digested. Ligation of digested vector and SOCS3 proximal promoter cassette generated the ppSOCS3-EGFP expression vector.

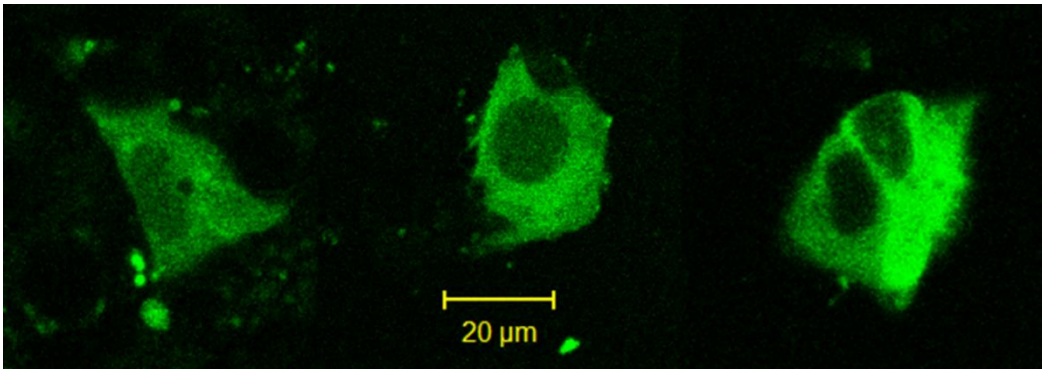

Figure 3.18: Untreated HepG2 cells expressing ppSOCS3-EGFP, 12 h after transfection. Scale bar represents 20 µm.

3.10 Discussion

3.10.1 General Summary

This chapter covered the groundwork of the thesis, detailing the choice of cell line and the generation of the fluorescent fusion proteins needed to investigate STAT3 and SOCS3 signalling through fluorescence microscopy. The HepG2 cell line was selected because it was responsive to both IL-6 and TNFα, which would allow cross-talk between STAT3 and p65 to be investigated at a later point. Signalling dynamics in response to TNFα were characterised in detail at the single cell level to compare the HepG2 cell line to the well defined SK-N-AS line. This demonstrated that p65 and IκBα oscillated at the same frequency in the two cell lines and also revealed that oscillations in HepG2 cells were more heterogeneous.

Following this work, several fluorescent fusion protein expression vectors were constructed. The effect of fluorescent tag position on STAT3 activity was assessed, showing that the N-terminal placement of the EGFP-tag had fewer effects than the C-terminal alternative; therefore the EGFP-STAT3 construct was selected for STAT3 imaging. Two SOCS3-EGFP constructs were developed, one under the control of a constitutive CMV promoter, and the other under the control of the SOCS3 proximal promoter. These constructs were forerunners to a SOCS3 BAC that unfortunately did not progress past the first engineering stage. Work on a STAT3 BAC was halted at a similar stage because by that point the EGFP-STAT3 plasmid was producing good preliminary data; these results are discussed in the next chapter.

3.10.2 Cell Line Cytokine Responsiveness

Comparison of IL-6 responsiveness of the HepG2 and SK-N-AS cell lines revealed that only the HepG2 cell line responded to IL-6. STAT3 was phosphorylated on Tyr705 in HepG2 cells in response to IL-6 but this did not occur in SK-N-AS cells. SOCS3 mRNA transcription was also induced in HepG2 but not SK-N-AS cells, indicating a lack of STAT3-mediated transcriptional activity in the latter. This lack of IL-6 response made the SK-N-AS cell line unsuitable for the intended study on IL-6 and TNFα cross-talk, but the HepG2

cell line could be used. Investigation of TNFα signalling in HepG2 cells showed that p65 and IκBα temporal dynamics were similar to those in SK-N-AS cells, whose NF-κB dynamics are relatively well understood (Ashall et al., 2009). There were minor differences in IκBα dynamics between the cell lines, where IκBα protein was degraded more slowly in HepG2 cells but was also resynthesized more rapidly. This difference could perhaps be attributed to greater heterogeneity at the single cell level, which could be explored through fluorescence imaging of NF-κB.

3.10.3 SOCS3 Expression Vectors

An inducible expression vector for SOCS3 under the control of the SOCS3 promoter was expected to be the best reporter of STAT3 signalling dynamics. This was because work with IκBα, the inducible repressor of p65 signalling, only produced useful results regarding long-term p65 activity when expressed under its own promoter from a BAC expression vector (A. Adamson, personal communication). Early attempts with constitutive IκBα expression plasmids could only capture the initial IκBα degradation event and not the subsequent cycles of resynthesis and degradation (Nelson et al, 2004, and unpublished observations). Unfortunately the SOCS3 BAC was unsuccessful very early on and as expected the CMV-driven plasmid and the proximal promoter-driven plasmids were of limited use.

A successfully constructed SOCS3 BAC could have provided evidence for the hypothesized SOCS3 oscillations in single cells. Ideally the experiments would be performed in stably transfected HepG2 cells, overcoming the issues related to transient transfection and enabling higher throughput microscopy experiments. Furthermore BAC transgenic mice could have been generated. In the future, SOS3 transgenic mice could be made without using BACs, instead utilising the new "genome editing" technologies of Zinc-Finger Nucleases, TALENs and CRISPR/Cas9 (reviewed Doudna & Charpentier, 2014; Gupta & Musunuru, 2014). These technologies can be used to introduce a fluorescent protein cassette at a specified locus within the genome and thus do not disturb copy number of the target gene, removing the negative effects of over-expression and also reducing or eliminating endogenous protein expression.

However these techniques require specific expertise or use of commercial applications and may have other drawbacks.

Transgenic mice expressing a SOCS3 fluorescent protein fusion would have many uses. They would enable the study of SOCS3 in infection and inflammation (reviewed in Rottenberg & Carow, 2014), and for investigating LIF/STAT3 signalling in embryogenesis (Sekkaï et al, 2005; Xie et al, 2009). They would also facilitate investigation into cross-talk between STAT3 signalling with other STATs and other signalling networks such as MAPK (Bode et al, 2001; Ehlting et al, 2007) and NF-κB (McFarland et al, 2013). These are just some of the potential applications of a SOCS3 transgenic mouse.

3.10.4 STAT3 Phosphomutants and phosphomimetics

In addition to the SOCS3 constructs and the fluorescent protein-tagged STAT3 constructs, the use of STAT3 phosphomutant and phosphomimetic proteins was considered. A STAT3 phosphomutant (STAT3-Y705F) has a dominant negative function, and was crucial to the discovery that Tyr^{705} phosphorylation is essential for STAT3 nuclear translocation and transcriptional activity in response to cytokines (Nakajima et al, 1996; Bhattacharya & Schindler, 2003; Pranada et al, 2004). Given that the dominant negative phosphomutant completely abrogates cytokine-induced STAT3 nuclear translocation, it would be futile to use it in this study of STAT3 nuclear translocation dynamics. Furthermore, there are no STAT3-Y705 phosphomimetics available in the literature, probably due to the general difficulty in mimicking phospho-tyrosine. Whereas phospho-serine and phospho-threonine can be successfully mimicked with glutamate, tyrosine usually cannot because of the aromatic ring in its side chain. Consequently using phosphomimetics and phosphomutants as line of approach was discounted.

3.10.5 Fluorescent-tag Effects on STAT3 Function

The structure of the STATs and the functions of the domains are well understood, and were reviewed in the Introduction. The domains each have different roles and the N-terminal domain, and the C-terminal SH2 domain and Transactivation Domain (TAD) are particularly important to dimerisation of

both unphosphorylated and phosphorylated STATs. Therefore the position of the EGFP tag, itself bigger than either the TAD or the N-terminal domain, could impact the function of the STAT3 fusion. Investigation of the orientation of the EGFP tag relative to the STAT3 protein revealed that the N-terminal position had few apparent effects on STAT3 function, whilst the C-terminal tagged STAT3 construct, STAT3-EGFP, was considerably perturbed. As a result the EGFP-STAT3 construct was selected for the project.

The first difference between the EGFP-tagged STAT3 constructs was in their tyrosine phosphorylation kinetics. STAT3-EGFP exhibited persistent tyrosine phosphorylation, even as the endogenous STAT3 was dephosphorylated, whilst EGFP-STAT3 only showed a minor delay in dephosphorylation of approximately 30 min. Dephosphorylation of the STAT3 dimer requires a switch from the parallel to antiparallel configuration (Mao et al, 2005; Zhong et al, 2005) and the Tyr705 phosphorylation site is located at the C-terminal domain interface. In both cases, the perturbation could be due to the EGFP moiety interfering with dimer switching between the parallel and antiparallel conformations, or from direct steric hindrance effects, thus inhibiting phosphatase activity (Zhong et al, 2005).

Further issues were seen in imaging STAT3-EGFP. Whereas EGFP-STAT3 had a subcellular distribution that matched endogenous STAT3 (Meyer et al, 2002), the majority of STAT3-EGFP cells had perinuclear rings and aggregates. These phenotypes suggest that nuclear trafficking, a constitutive process requiring NLS and NES motifs in the coiled-coil domain (Vinkemeier, 2004), of U-STAT3 was affected. These effects may be explained through the effects of the C-terminal tag on dimer conformation switching, possibly as a result of the size of the EGFP moiety, which is larger than the TAD and the N-domain.

In the antiparallel conformation, the C-terminal domain is close to the coiled-coil domain, where the NLSs and NESs of STAT3 are located (Vinkemeier, 2004). EGFP could hinder importin and exportin access to these sequences (Komeili & O'Shea, 2001). An inability to readily change conformation could also cause issues with transport through the Nuclear Pore Complex, leading to the speckled appearance of the perinuclear ring. Interestingly, this effect has not been

reported elsewhere so it is possible that these negative effects on STAT3-EGFP are due to the specific linker sequence being too short or inflexible, or incompatibility with this cell type, as these are generally known issues with artificial linker sequences. To determine whether this is the case, different linker sequences could be tested. Regardless of whether these problems with STAT3-EGFP dephosphorylation and subcellular distribution and transport are specific to this particular construct or all such C-terminal tagged STATs, EGFP-STAT3 was the most suitable construct for the rest of the project.

Chapter 4
Modelling Observed STAT3:SOCS3 Dynamics

4.1 Introduction

In Chapter 3, different cell lines were tested to establish a good model system for the analysis of the dynamics and function of STAT3 signalling. The HepG2 cell line was chosen because it gave a good STAT3 response, unlike the SK-N-AS cells. In addition, HepG2 cells exhibited robust NF-κB oscillations in response to TNFα stimulation. Plasmids that expressed STAT3 fluorescent fusion proteins at N- and C-termini were examined to determine their behaviour. The N-terminal fusion was found to mimic the phosphorylation dynamics of endogenous STAT3 at the population level and exhibited a cellular localisation that closely matched the endogenous protein. The optimal media for STAT3 pulse stimulation experiments was also determined.

Having developed a good model system, the next aim was to investigate whether STAT3 oscillations could be observed in single cells by time-lapse fluorescence microscopy. This could confirm biochemical experiments that had suggested such oscillations might occur (Yoshiura et al, 2007). To achieve this, live cell confocal microscopy was performed on cells treated with IL-6, under conditions similar to those successfully used to analyse NF-κB dynamics (Nelson et al, 2004). In addition to studying the response to constant IL-6 stimulation, the cells were subjected to different length pulses of cytokine treatment. The aim was to determine the minimum stimulation time needed to induce a full STAT3 translocation to the nucleus, to gain a better understanding of receptor and STAT3 activation dynamics and to decide whether a repeat pulsing protocol would be suitable.

Further to the experimental microscopy work, a small gene expression study was carried out using Fluidigm qPCR technology to investigate the HepG2 response to IL-6. This was to serve two purposes. Firstly, to study in detail core components of the STAT3 signalling pathway, some of which are key to the model, by building upon experimental results published elsewhere. Secondly, to give context to the microscopy data from the continuous and pulsed IL-6 treatments by establishing whether the length of IL-6 stimulation may alter gene expression patterns. If changes were found, this could be correlated to any

treatment-dependent differences seen in STAT3 signalling dynamics, thus highlighting their importance.

At the very start of this project, a mathematical model of STAT and SOCS oscillations had been developed by Dr Núria Domedel-Puig in the laboratory of Prof. Jordi Garcia-Ojalvo. This generic model was subsequently adapted for IFN-β signalling through STAT1, with negative feedback from SOCS1, by fitting to population-level data, under which circumstances STAT1 demonstrated transient oscillatory dynamics (Pertsovskaya et al, 2013). The availability of quantitative, single-cell microscopy data presented an opportunity for an improved parameterisation of the generic STAT:SOCS model, leading to a deeper understanding of STAT3-SOCS3 signalling at the single-cell level, leading to further predictions. This work was performed in collaboration with Dr N. Domedel-Puig, Dr E. Abad, and Prof. J. Garcia-Ojalvo, Universitat Pompeu Fabra, Spain.

4.2 Imaging EGFP-STAT3 Dynamics in HepG2 Cells

HepG2 cells were prepared for time-lapse confocal fluorescence microscopy and transfected with EGFP-STAT3 as described in Section 2.4.4. Cells were imaged for up to 20 h and the data analysed according to Sections 2.9-.10. The results for untreated cells and cells treated with 20 ng/ml IL-6 (Section 2.5) for 5, 15 and 30 min with a conditioned media chase, or continuously, are presented in the following sections.

4.2.1 Untreated EGFP-STAT3

Untreated HepG2 cells expressing EGFP-STAT3 showed no significant change in fluorescence over time (Figure 4.1). Part A shows a single HepG2 cell expressing EGFP-STAT3 over a 5 h period. Cell traces of Nuclear/Total Fluorescence were grouped by independent biological replicate (B, C, and D). This showed that ROI tracker produced somewhat noisier data (B and C) than whole cell tracker (D) but the techniques gave similar standard deviations for the N/T ratio over all. The average of all cells over time was calculated (E) and a line of best fit determined (black dashed line in E), giving the equation $y = 0.001x + 0.50$. This indicated that STAT3 fluorescence remained stable over time and was

evenly distributed between the cytoplasmic and nuclear compartments, on average (N/T = 0.5 ± 0.05). This is in line with a previous study that indicated that in unstimulated HepG2 cells 50.4 ± 7.4 % of STAT3 was nuclear (Meyer et al., 2002).

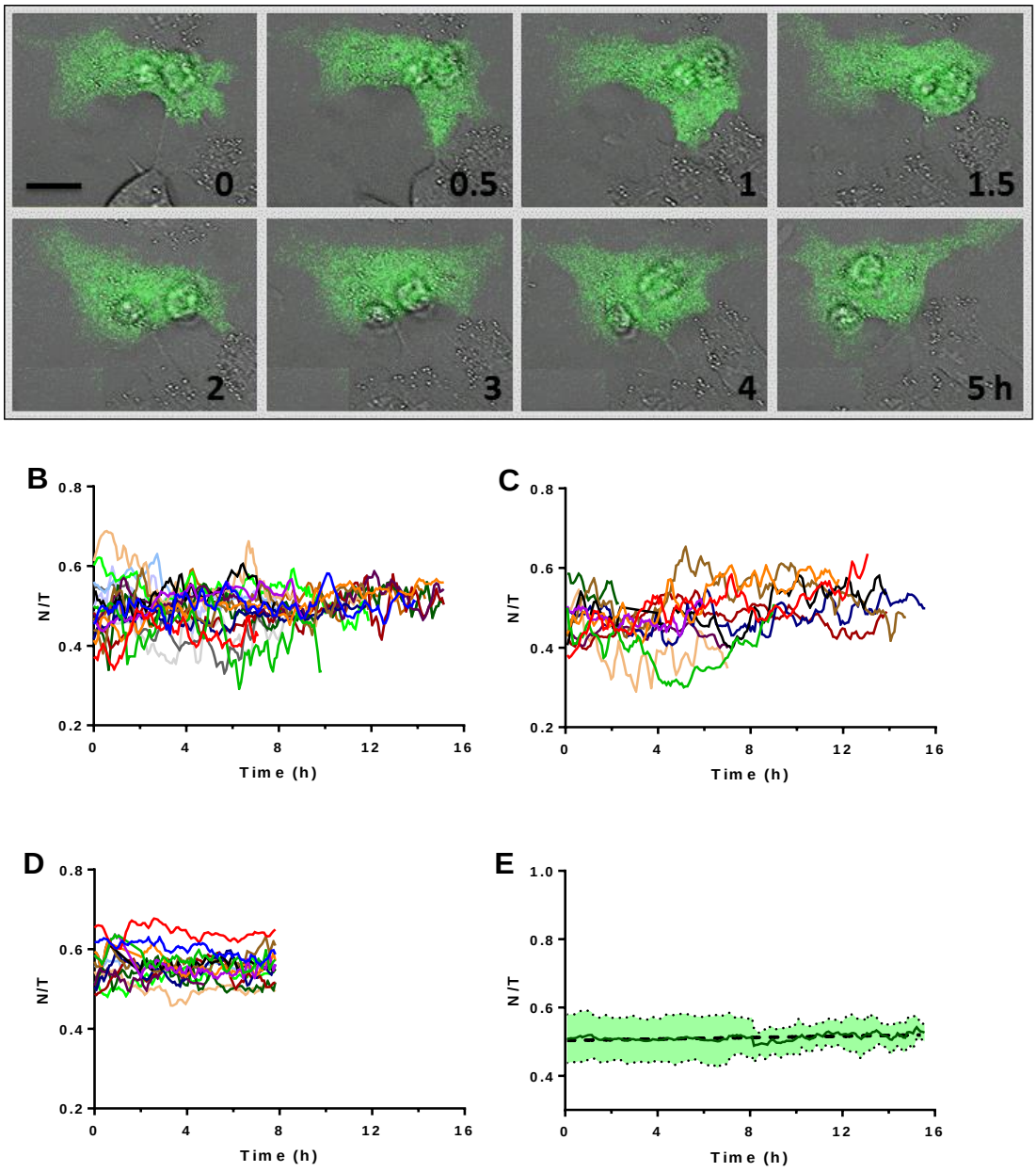

Figure 4.1: Analysis of untreated HepG2 cells expressing EGFP-STAT3.
A Untreated HepG2 cell expressing EGFP-STAT3, imaged over a 5 h period. Scale bar:20 µm. **B-C** Nuclear/Total fluorescence (N/T) for all cells from three independent experiments over time (h). **B** and **C** tracked by ROI, **D** tracked using Whole Cell method. **E** Average of all cells. Thin green line is experimental average. Green shaded area is equal to ± 1 S.D. Black dashed line is the line of best fit.

4.2.2 30 min IL-6 Stimulation

A 30 min pulse of IL-6 triggered a transient net movement of EGFP-STAT3 into the nucleus of HepG2 cells (Figure 4.2 and 4.3). As with unstimulated cells, most displayed an even N:C distribution before treatment. Addition of IL-6 caused EGFP-STAT3 to shift rapidly to a predominantly nuclear localisation (0.8 ± 0.05 N/T) which peaked at 35 min (Fig. 4.3F). Fitting the increase gave the rate equation $y = 0.55\ e^{\,0.91t}$. After 35 min, nuclear occupancy by EGFP-STAT3 started to decline, returning slowly to the unstimulated resting state over a ~6 h period. This decrease could be fitted to a first order decay equation of $y = 0.47\ e^{\,-0.66t}$, giving a half-life of 1.05 h, which is slightly longer than the P-STAT3 half-life from the Westerns in Section 3.6.2.

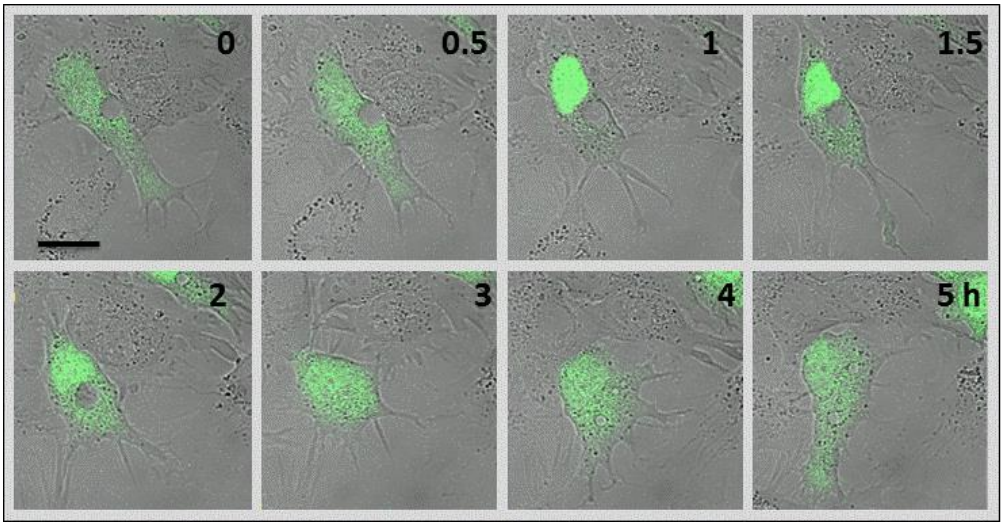

Figure 4.2: Transient nuclear translocation of EGFP-STAT3 in a HepG2 cell after 30 min IL-6 treatment. HepG2 cell expressing EGFP-STAT3, imaged over a 5 h period. 20 ng/ml IL-6 added at t = 0.5 h for 30 min before conditioned media replacement. Scale bar:20 μm.

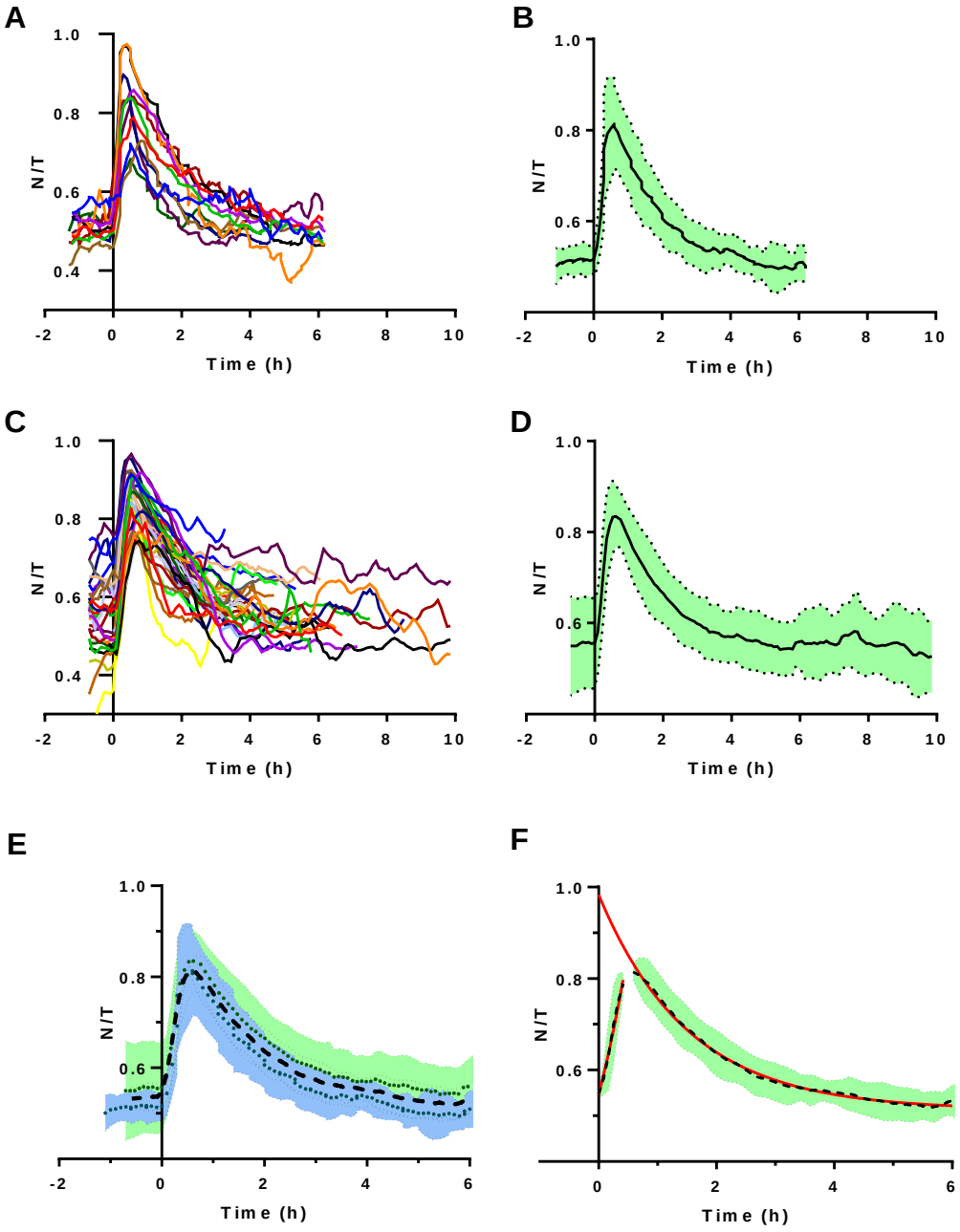

Figure 4.3: N/T EGFP-STAT3 in response to 30 min pulse IL-6 (20 ng/ml) followed by conditioned media replacement.

A and **C** display traces from all cells analysed in an experimental replicate. **B** and **D** show the average of all cells in that experiment (black line), ± 1 S.D (green shaded area). **E** shows the two replicates together and their interpolated average (black dashed line). **F** Fitting of first order exponential growth and decay equations (red lines) to the population average. All x-axes adjusted so that t_0 represents the time of IL-6 addition.

4.2.3 Comparing 5 and 15 min IL-6 Pulses to the 30 min Pulse

Cells expressing EGFP-STAT3 and responding to a 5 or 15 min pulse of IL-6 responded with the same strength nuclear translocation as for 30 min IL-6 (Fig. 4.4A). STAT3 translocated to the nucleus and returned to the resting distribution after a 5 or 15 min IL-6 pulse with the same temporal dynamics as for a 30 min pulse. However the percentage of cells responding to a 5 or 15 min pulse was only around 33 %, compared to 73 % for a 30 min pulse (Fig. 4.4B). This 2.2-fold increase in the number of responding cells between 15 and 30 min implies that in order for the majority of the population to respond, additional signalling events, requiring IL-6 to be present at the cell membrane, occur between 15 and 30 min after stimulation.

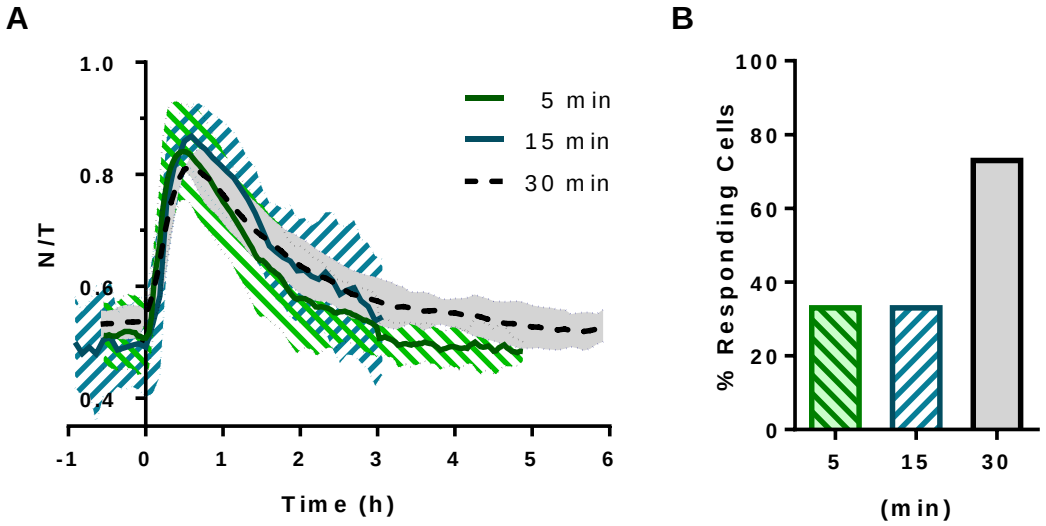

Figure 4.4: Comparing effects of short IL-6 pulses on EGFP-STAT3 nuclear translocation in HepG2 cells. 20 ng/ml IL-6 added at t=0, and removed 5, 15 or 30 min later, followed by conditioned media replacement. N = 1 replicate for each condition. **A** Comparing different length pulses. Average N/T for all cells for each condition. Mean of cells indicated by solid or dashed line and shaded area represents ± 1 S.D. **B** Percentage of responding cells for each pulse length.

4.2.4 Continuous IL-6 Stimulation

HepG2 cells expressing EGFP-STAT3 and subjected to continuous IL-6 stimulation demonstrated a sustained nuclear translocation of EGFP-STAT3 (Fig. 4.5). Cells were analysed using Cell Tracker and the N/T fluorescence calculated from the raw cytoplasmic and nuclear fluorescence values (Fig. 4.6). This analysis revealed that the sustained presence of EGFP-STAT3 in the nucleus was oscillatory in nature. The nuclear EGFP fluorescence oscillated around a new, higher set point whilst the cytoplasmic fluorescence oscillations were the inverse of the nuclear oscillations (Fig. 4.6). Since it is known that STAT3 levels are stable over time even in the presence of IL-6 (Siewert et al, 1999; Wormald et al, 2006) and that it is the tyrosine phosphorylation state which controls STAT3 nuclear translocation rather than degradation and resynthesis (Bhattacharya & Schindler, 2003; Meyer et al, 2003), this finding strongly suggests that the nuclear EGFP-STAT3 oscillations were due fluctuating net tyrosine phosphorylation of EGFP-STAT3.

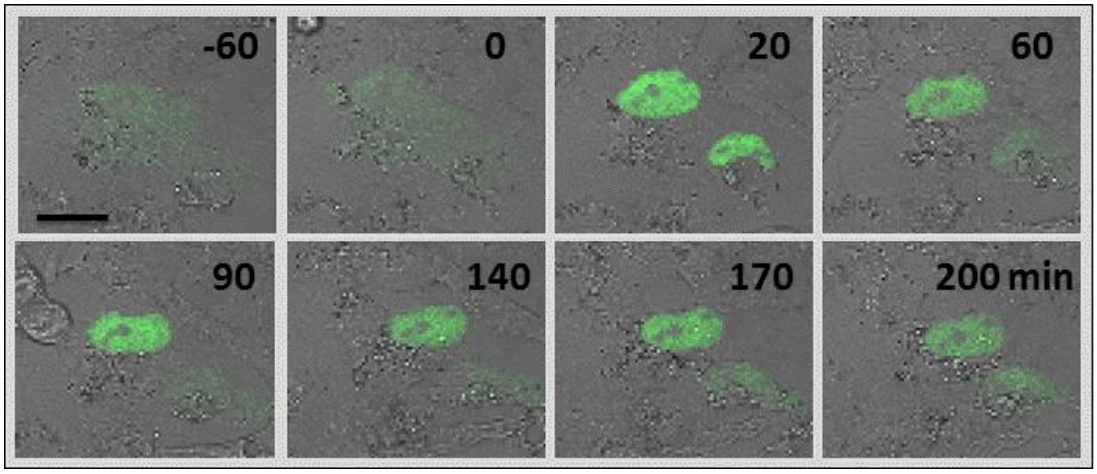

Figure 4.5: Sustained nuclear translocation of EGFP-STAT3 in a HepG2 cell under continuous IL-6 treatment. HepG2 cell expressing EGFP-STAT3, imaged over a 4 h period. 20 ng/ml IL-6 added at $t = 0$ h. Scale bar:20 μm.

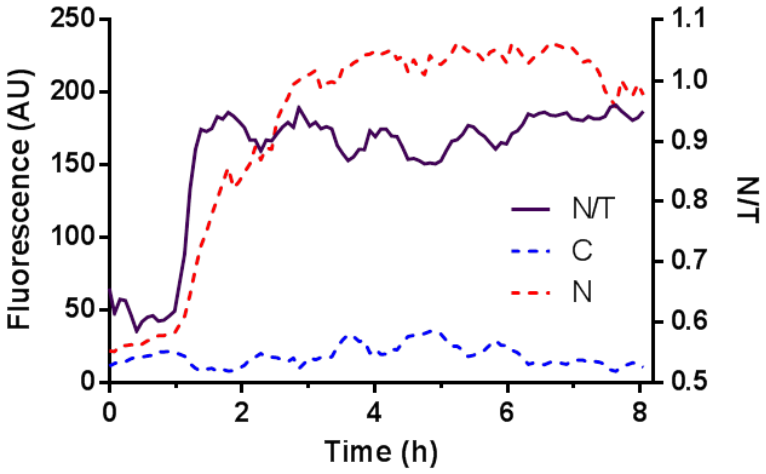

Figure 4.6: Sustained nuclear translocation of EGFP-STAT3 in a HepG2 cell under continuous IL-6 treatment. HepG2 cell expressing EGFP-STAT3, imaged over an 84 h period. 20 ng/ml IL-6 added at $t = 1$ h. Cytoplasm (C, blue), Nucleus (N, red) and Nuclear/Total (N/T, purple) fluorescence values.

Representative graphs of N/T ratios for IL-6 stimulated EGFP-STAT3 cells are presented in Figure 4.7A. Some cells became fluorescent after stimulation and so could not be used in determining first peak characteristics, however they provided good quality data for later time points. Other cells underwent mitosis after stimulation. Daughter cells which remained fluorescent were analysed, an example of which is included. Averaging the cells (n = 26) (Fig. 4.7B) obscured the nuclear oscillations of individual cells so cells were analysed individually using the peak detection tool (Section 2.11.2) to determine quantitative values for peak appearance, peak amplitude and peak-to-peak intervals. Fig. 4.7C illustrates one cell with the peaks of its nuclear oscillations marked.

The data revealed a sharp shift from the resting state to a predominantly nuclear localisation (0.9 N/T $\pm$ 0.05) that took 35 $\pm$ 9 min on average (Fig 4.8A), consistent with the 30 min pulse data. After the first peak, the proportion of nuclear EGFP-STAT3 dropped in all cells but not back to the resting level. Amplitude of peaks was relatively consistent within cells and less so between cells, varying by 0.05 to 0.20 points below the level set by the first translocation. Subsequent peaks and troughs could be seen in over 90% of cells analysed. Furthermore, the nuclear oscillations were sustained for up to 16 h after the addition of IL-6 in cells that were analysable at later time points.

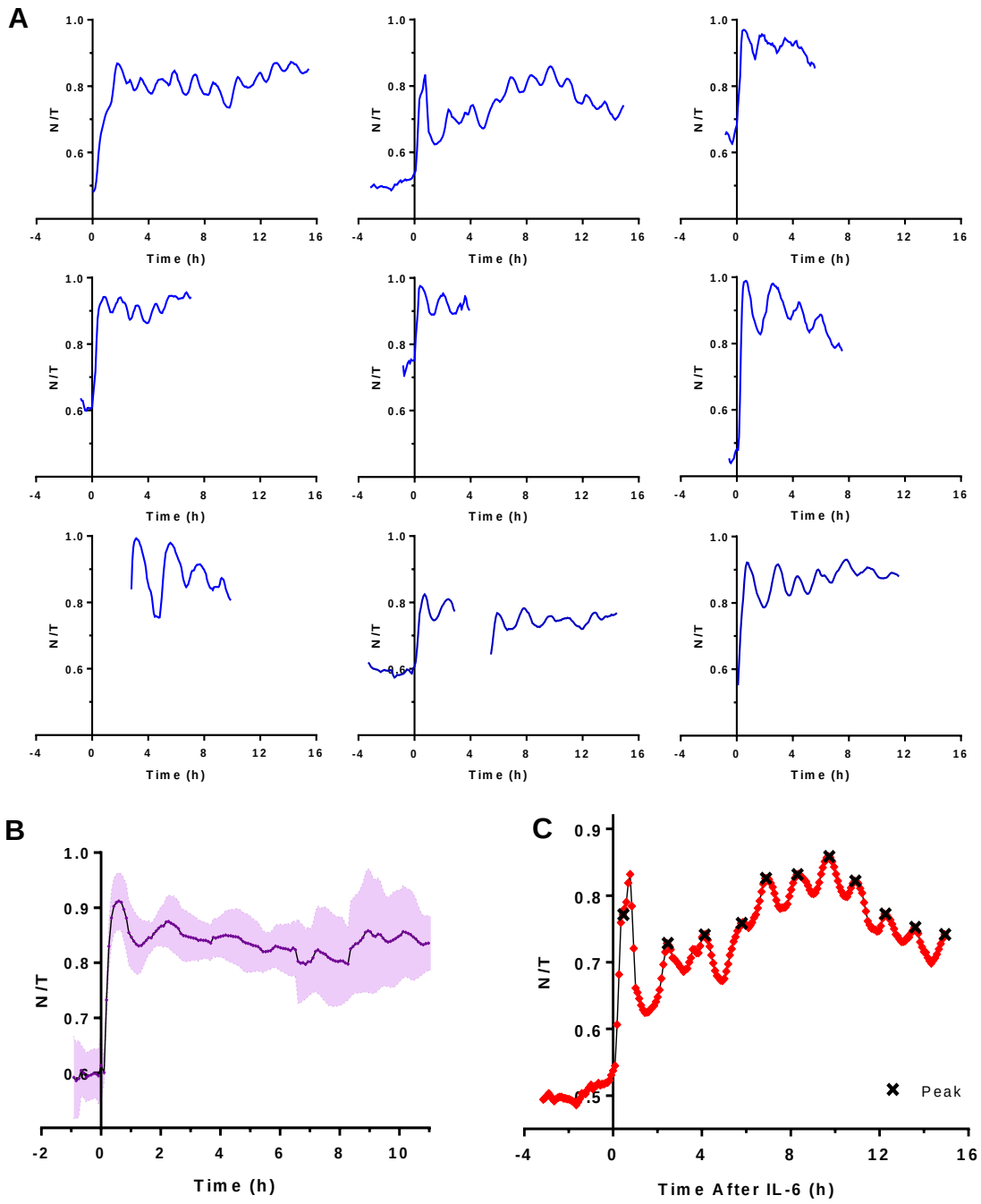

Figure 4.7: EGFP-STAT3 sustains nuclear oscillations over many hours in response to continuous stimulation with IL-6.

20 ng/ml IL-6 added at t_0. **A** Example N/T traces from individual cells expressing EGFP-STAT3 from n=4 biological replicates. Some cells have delayed starting points as they became fluorescent after IL-6 was added and others have gaps due to mitosis. **B** Average of all cell traces (n=26 cells), purple shaded area represents $\pm$ 1 S.D. **C** An N/T EGFP-STAT3 trace with position of peaks marked (black crosses). Peaks determined through use of Excel tool discussed in Section 2.11.2.

The nuclear oscillation peaks appeared to display a regular frequency and so were analysed in detail (Fig. 4.8B-D). The peak-to-peak intervals were grouped by cell (Figure 4.8B, each interval is represented by a circle), and no discernible differences between experimental replicates in the mean or variance of the intervals were found. To test whether order of the peaks affected the peak-to-peak interval, in each cell the peak 1 – peak 2 interval was compared to the mean of the subsequent peak-to-peak intervals using two-way ANOVA (Fig. 4.8C). No significant difference was found, suggesting that other factors contribute to the peak-to-peak interval variation. The intervals from all cells were displayed in a histogram (Fig. 4.8D). They ranged from 40 to 174 min, fitted a normal Gaussian distribution, and the mean interval was 93 ± 26 min. Intervals from 140 to 180 min could have been due to normal variation in period or due to noise leading to missed peaks, as an interval of 180 min is long enough to contain an additional peak, giving two intervals of approximately 90 min each.

STAT3 nuclear oscillations were observed before and after mitosis, and the translocations after mitosis were likely due to IL-6 still being present in the media at high concentrations. However cell numbers were not high enough to determine whether the cell cycle had any effect on timing. This might prove an informative line of enquiry in the future since the cell cycle is known to affect other signalling systems e.g. NF-κB (Dr J. Ankers, submitted for publication).

The consistent peak amplitudes, regular frequency and sustained nature of the repeated STAT3 nuclear translocations combined to form an oscillatory response to continuous IL-6 stimulation in single cells that has yet to be reported elsewhere. These oscillatory signalling dynamics were in line with the predictions from the initial iteration of the STAT3-SOCS3 model and the quantitative single cell data obtained will be used to improve it.

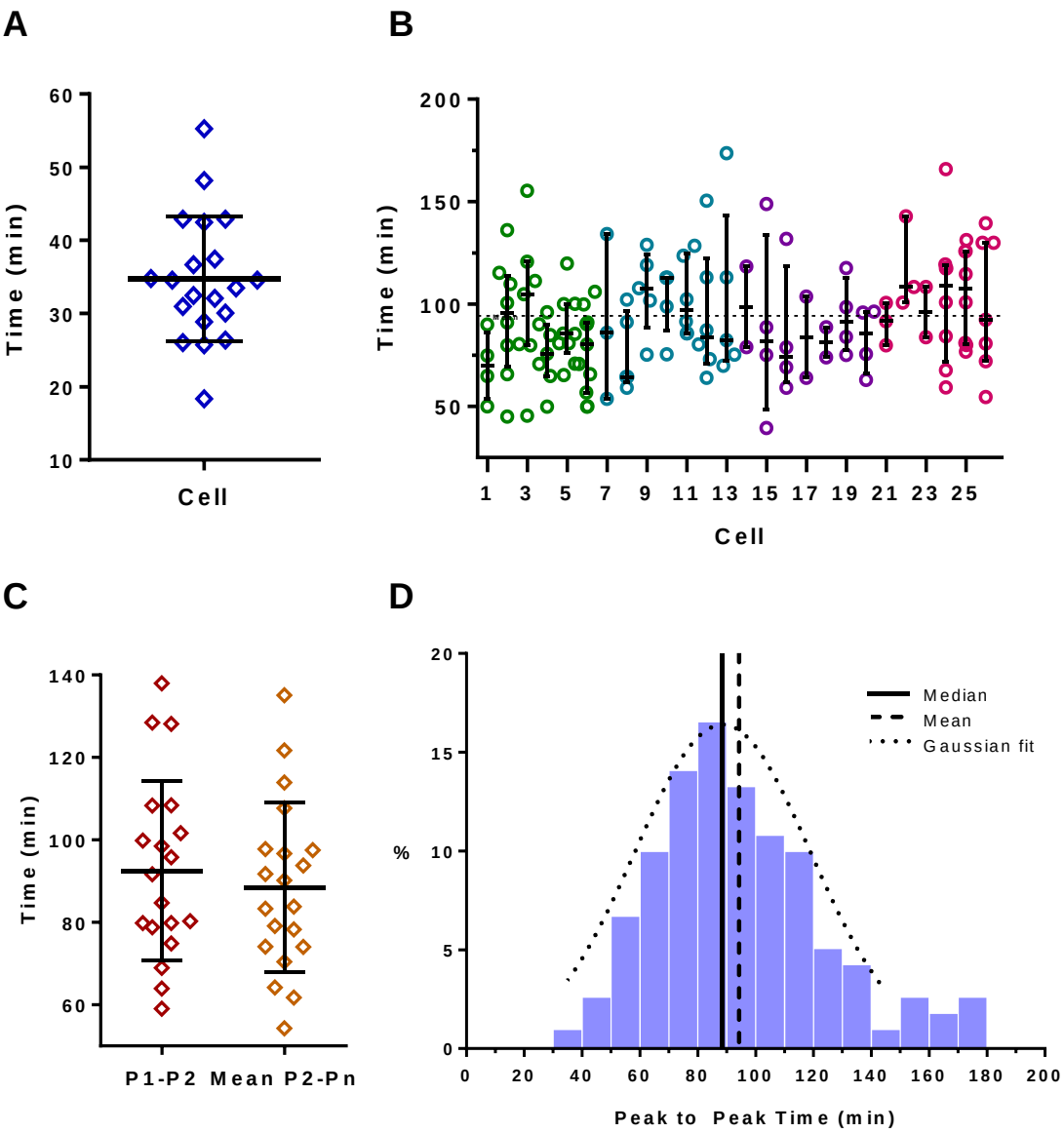

Figure 4.8: Timing the Peaks of EGFP-STAT3 Nuclear Translocations in response to continuous IL-6 stimulation.

Bars represent Mean ± 1 S.D. in A, B and C. **A** Appearance times of first peak (P1) for each cell in minutes. **B** Time between subsequent peaks (coloured rings) for each cell, excluding Peak 1 – Peak 2 (P1-P2). Each colour represents one biological replicate (n=4). Horizontal dashed line indicated mean peak-to-peak time across all cells. **C** Comparison of P1-P2 interval to mean of peak-to-peak timing for P2-P3 onwards. **D** Histogram of all peak-to-peak intervals. Median (solid line) and mean (dashed line) indicated. Dotted curve indicates Gaussian distribution of the data.

4.3 Transcriptional Responses to Differential IL-6 Stimulation

IL-6 is known to be a key driver of the Acute Phase Response, which occurs as a result of the liver responding to systemic infection (Moshage, 1997). The transcriptional responses of a variety of IL-6-induced target genes and STAT3-SOCS3 signalling components were investigated using qPCR to serve two purposes. Firstly, to provide detailed timing and amplitude information regarding mRNA transcription of various components of the STAT3 signalling network, particularly SOCS3, so that the STAT3-SOCS3 model parameters could be constrained accordingly. Secondly, to determine whether any genes responded differently to pulsatile versus continuous IL-6 stimulation. Since STAT3 oscillates under continuous but not pulsatile IL-6 stimulation, this would suggest that some genes could require sustained STAT3 oscillations for maximum expression. To these ends, a number of relevant genes were selected for detailed analysis.

4.3.1 Selecting Target Genes

The IL-6-Receptor (IL6R) and gp130, which together comprise the IL-6 receptor complex, were selected in case transcription dynamics of the receptor complex played a role in regulating IL-6 signalling. STAT3 was selected because it is self-induced in response to IL-6 (Ichiba et al, 1998) and the increased level of unphosphorylated STAT3 has been shown to be important for cross-talk with NF-κB (Yang et al, 2007). SOCS-1, 2 and 3, were selected because they are inducible inhibitors of STAT signalling, (reviewed in Krebs & Hilton, 2001). SOCS3 was of particular interest since Yoshiura et al., (2007) provided a very detailed time-course of SOCS3 mRNA oscillations showing a 2 h period. However their work was in a different cell line with a tendency to synchronise, so obtaining HepG2-specific data was essential. Whilst the SOCS1-3 proteins have previously been well characterised, less is known about SOCS-5 and 7, so they were included to determine whether they might also be linked to the IL-6 pathway response.

Two genes, hepcidin and γ-fibrinogen, were chosen, because as components of the liver's Acute Phase Response, they are part of the outcome of IL-6 signalling (Castell et al, 1989). They are also known to be differentially regulated by different cytokine combinations (Bode et al, 2012a), and so were potentially relevant for understanding any STAT3 - NF-κB cross-talk utilising IL-6, TNFα and IL-1β. Other genes included were IL-6, IL-10, and IL-15, as they were potential sources of paracrine and autocrine signalling, but they were not reliably detected in any of the samples. The reference genes were cyclophilin A, β-tubulin, GAPDH, and PolR2A, as discussed in Section 2.8.7.

4.3.2 Summary of Fluidigm qPCR Methods

HepG2 cells were stimulated either continuously or for 30 min with 20 ng/ml IL-6, as described in Section 2.8.2. The cells were lysed at the appropriate times to generate a detailed 24 h time-course. The early time points from 0 to 1.5 h were chosen to provide close coverage for early response genes, such as SOCS3. Lysates were collected at 2 h intervals between 2 to 8 h and a final 24 h sample was taken to capture mid and late responding genes. cDNA samples were prepared and subjected to Fluidigm qPCR (Sections 2.8.3-4, 6). Analysis was performed in qBase+ as described in Section 2.8.7. The mean $\pm$ 1 S.D. of n=3 independent repeats are presented in Figure 4.6. The reference genes did not change over time under any of the tested conditions so cyclophilin A is given as an example.

4.3.3 STAT3 Transcriptional Responses to IL-6

Looking first at the IL-6 receptor complex components, it was clear that the receptor complex was hardly affected by IL-6 signalling (Fig. 4.9). IL6R showed no change while gp130 was slightly up-regulated. Gp130 increased by approximately 1.5-fold in the first 1.5 h, which was sustained for the duration of the experiment, under both the 30 min pulse and continuous stimulation. This finding was in line with work by (Schooltink et al, 1992) in HepG2 cells that showed that IL-6 up-regulated gp130. STAT3 mRNA did not change during the first hour then increased to 1.5 fold at 2 h, which was sustained under continuous IL-6 but not the 30 min pulse. The increase seen with continuous IL-

6 is supported by work in hTERT-HME1 cells, an immortalised epithelial line, performed by (Yang et al, 2005).

Of the SOCS genes, SOCS1 detection was unreliable across replicates while SOCS5 and 7 did not change in response to IL-6 (data not shown). SOCS2 did not appear to distinguish between length of IL-6 stimulation, peaking between 45 and 90 min with a 3-fold increase before returning to initial levels between 2 and 4 h in both conditions (Fig. 4.9). SOCS3 however did distinguish between the 30 min pulse and continuous IL-6. In both cases, its mRNA was undetectable in unstimulated cells. However, it appeared within 15 min of IL-6 addition, rising sharply to peak at 45 min with a 10 to 20-fold increase, before returning to a low level by 2 h. From 2 to 8 h, SOCS3 was still detectible after the 30 min pulse, whereas it was present at a higher level under continuous IL-6 until 24 h. When combined with the knowledge that SOCS3 oscillates at the population level in synchronous cells (Yoshiura et al, 2007), this finding suggests that SOCS3 could be transcribed in a heterogeneous manner across the population. An analogous situation is found in SK-N-AS cells where oscillating levels of IκBα transcripts in single cells are averaged out across the population leading to a seemingly steady rate of transcription. Consequently, only the data for the first two hours of SOCS3 transcription will be used to refine the model (as this time frame contains the first peak in SOCS3 mRNA where the cells are far more likely to be synchronised).

Hepcidin and γ-fibrinogen confirmed the strong HepG2 response to IL-6 (Fig. 4.9). Hepcidin increased approximately 3-fold, peaking 2 h post stimulus, and did not differ between conditions. γ-fibrinogen did differ, showing a stronger and sustained response to continuous stimulation. After 1 h of IL-6 stimulation, γ-fibrinogen mRNA expression increased 2-fold in both conditions. Under continuous IL-6, expression slowly increased, reaching 3-fold induction at 24 h, whereas after the 30 min pulse expression was constant between 2h and 8 h, before decaying to the basal level at the 24 h time point.

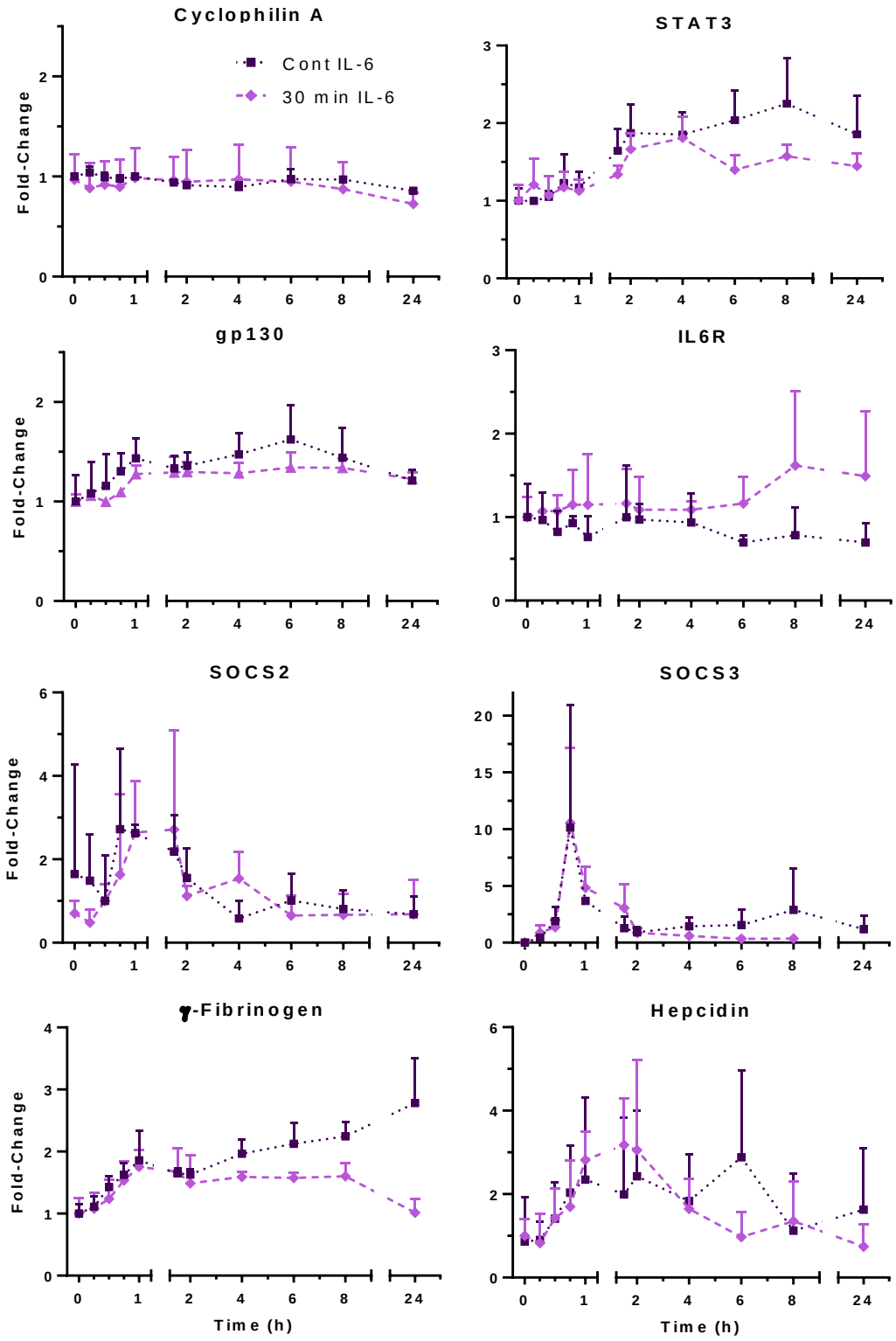

Figure 4.9: Normalised mRNA fold-change for selected STAT3 signalling components and target genes. HepG2 cells stimulated with 20 ng/ml IL-6 for 30 min (♦) or continuously (■). Mean + 1 S.D. for n=3 independent experiments.

The results for IL-6, IL-10 and IL-15 are not presented because they could not be consistently detected across biological replicates. Thus it appears that these genes were not responsive to IL-6 alone in HepG2 cells, despite indications in the literature that these genes and their products are involved in regulatory and cross-talk events downstream of IL-6 signalling in other cell types and tissues.

In summary, some genes were transcribed differently depending on whether a 30 min pulse or continuous IL-6 stimulation was given. These were STAT3, SOCS3, gp130 and γ-fibrinogen, and they showed either a stronger or more sustained induction in response to continuous IL-6. Conversely, the IL6R, SOCS2 and Hepcidin genes responded the same way to both conditions. In addition, the detailed, time-resolved information about early SOCS3 mRNA transcription will be used to constrain the parameter for the SOCS3 mRNA component of the model.

4.4 Modelling STAT3:SOCS3 Signalling Dynamics

4.4.1 The Initial Model

The first iteration of the STAT-SOCS model developed in Prof. J. Garcia-Ojalvo's group was based upon the work presented in (Yoshiura et al, 2007). Using Western blots to measure phospho-STAT3 and SOCS3 protein levels in serum synchronised cells, this study found they oscillated co-dependently with a 2 h period (Section 1.2.8). In order to capture these oscillations in phospho-STAT, a three-component ordinary differential equation (ODE) model describing STAT activation and its repression by SOCS was developed (Fig. 4.10) (Domedel-Puig, unpublished).

The three components of the generic STAT-SOCS model represented phospho-STAT, SOCS mRNA and SOCS protein (Fig. 4.10). Non-linear Hill terms were used to capture the induction of SOCS mRNA by active P-STAT and the repression of STAT phosphorylation by SOCS. Half of the parameter values were obtained from published works and the remainder were fitted manually (Table 4.3). Key constraints were the rates of STAT inactivation, degradation of SOCS mRNA and SOCS protein, and the rates of translation and transcription of SOCS mRNA. This basic representation was able to create a temporal delay that led to a stable limit cycle with robust, sustained oscillations in P-STAT and SOCS protein. The model was resistant to a range of parameter changes whilst stochasticity introduced through SOCS3 mRNA molecule numbers did not affect the oscillatory period (Domedel-Puig, unpublished). This resilience in the face of added noise suggested that STAT3/SOCS3 oscillations would be robust *in vivo*.

The intention was to test the generic model which predicted STAT oscillations in individual cells against the live single cell microscopy data and to expand the generic model so that the available single cell time-lapse microscopy data presented in Section 4.2 could be utilised effectively.

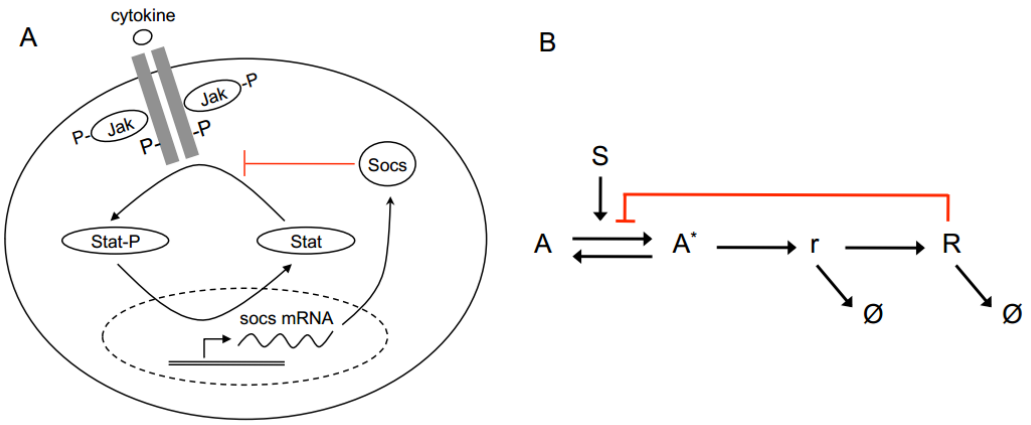

C

$$\frac{dA^*}{dt} = \beta_A S \frac{A/k_A}{1 + (A/k_A) + (R/k_I)^q} - \lambda_A A^*$$

$$\frac{dr}{dt} = \beta_r \frac{(A^*/k_r)^p}{1 + (A^*/k_r)^p} - \lambda_r r$$

$$\frac{dR}{dt} = \beta_R r - \lambda_R R$$

Figure 4.10: The initial STAT3-SOCS3 model, illustrating the SOCS3 negative feedback loop.

A Illustration of the model. **B** Model schematic. Components are: signal (S), inactive STAT (A), phosphorylated STAT (A*), SOCS mRNA (r) and SOCS protein (R). Ø = degradation. **C** Model equations. β = production rate, λ = decay rate, k = half-maximal constant, p and q = Hill coefficients. Figures and equations by N. Domedel-Puig (unpublished).

The primary limitation of the model was the lack of nuclear and cytoplasmic compartments, with active and inactive STAT levels being modelled instead. The microscopy data obtained does not differentiate between phosphorylated and unphosphorylated STAT3. Instead the key read-outs are the relative nuclear and cytoplasmic fluorescence levels. Whilst nuclear/total STAT3 could be used as a proxy for U/P-STAT3, this would not make the best use of the available data. In addition, the lack of compartmentalisation also meant that one reaction represented multiple biological processes that together regulate the balance of inactive cytoplasmic STAT3 and transcriptionally active nuclear STAT3. As described in Section 1.2.4-5, transcriptional activation and inactivation of

STAT3 requires its phosphorylation in the cytoplasm, shuttling of phospho-STAT3 into the nucleus, and dephosphorylation for subsequent nuclear export. This provided a strong motivation for the explicit modelling of nuclear and cytoplasmic portions, as well as phosphorylated and non-phosphorylated populations of STAT3. This additional complexity would also facilitate the inclusion of experimentally determined and published transport rates.

Another potential issue identified with the initial model was the presence of two relatively large Hill coefficients in the terms representing the activity of phospho-STAT3 and SOCS3. Essentially a large Hill coefficient acts as a sudden switch between two states at a given threshold whereas smaller coefficients produce a gradual shift from one state to the next. Inclusion of a large Hill coefficient is often an indication that the model has over-simplified some key aspect of the system being portrayed. In the first case, the transcription of SOCS mRNA presumed a high degree of cooperation at the promoter, suggesting multiple P-STAT dimers are required for transcription. The large Hill coefficient for the inhibitory effect of SOCS protein upon the production of active STAT implied a certain quantity of SOCS protein was required for inhibition. By implementing an expanded model of the STAT3-SOCS system, it may be possible to reduce non-linearity in the Hill terms for these two events. Hence the model could be made to better reflect the known biological situation.

4.4.2 Summary of Data Used to Re-fit the Model

The microscopy experiments presented earlier in this chapter allowed for the quantification of STAT3 behaviour under unstimulated and IL-6-stimulated conditions. It became clear early on that the initial model did not reflect STAT3 nucleocytoplasmic oscillations as visualised through fluorescence microscopy. Therefore we sought to update and expand the model, addressing the potential issues outlined in the previous section so that the characteristic features of the data could be used to constrain the model. Early experimental data (Fig. 4.11) was used in the first round of refitting, however it was derived from a very limited number of cells and only covered a 6 h period. Subsequently better quality data from experiments lasting up to 16 h became available. Statistical analysis quantified the spatio-temporal characteristics of the nucleocytoplasmic

STAT3 oscillations caused by continuous IL-6 stimulation. This detailed quantitative data (summarised in Table 4.1) was used to reproduce an idealised STAT3 oscillating cell (Fig. 4.12), against which an expanded and re-parameterised version of the STAT3-SOCS3 model could be tested. The 30 minute pulse data supplied a rate for the return of post-stimulus STAT3 nuclear occupancy to the resting condition after the removal of the stimulus, providing an additional constraint for the model.

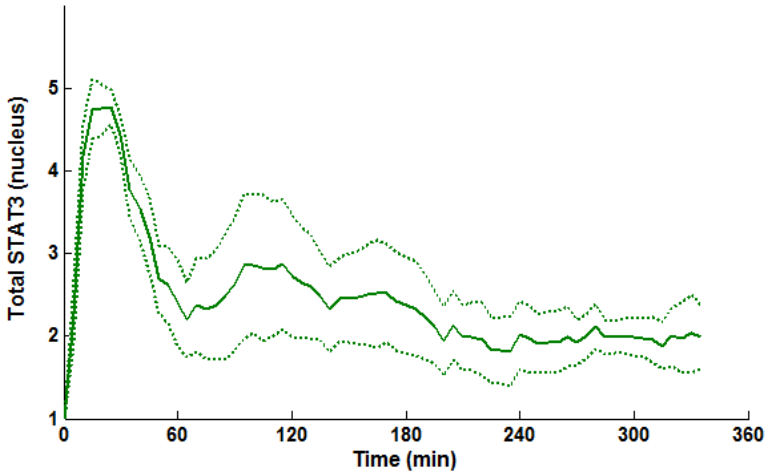

Figure 4.11: Average of total nuclear STAT3 from a limited number of HepG2 cells under continuous IL-6 stimulation. Solid green line = average, dotted line = ± 1 S.D.

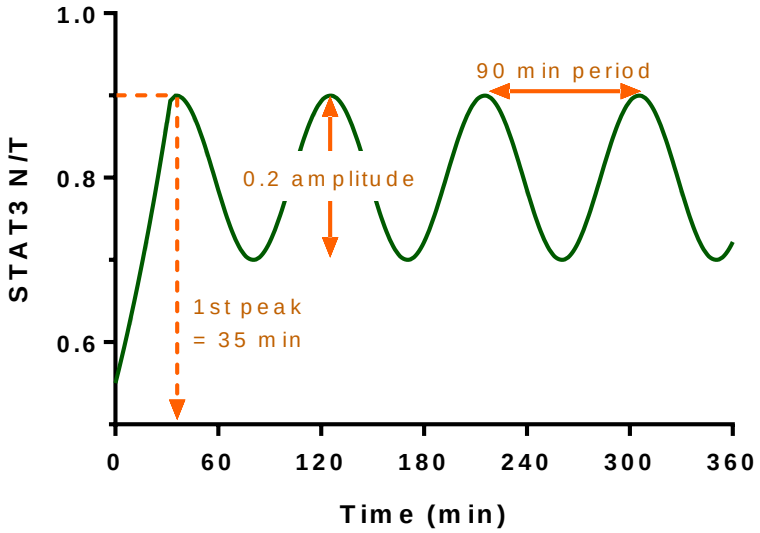

Figure 4.12: An idealised oscillating cell. Generated according to the average population characteristics described in Table 4.1, for the first 6 h post-IL-6 stimulation.

STAT3 Protein	Dynamic Behaviour	Time	N/T Localisation	Time to First Peak
Unstimulated	NA	NA	50 ± 7 %	NA
30 min IL-6	Half-life Decay	63 min	80 ± 0.5 %	35 min
Continuous IL-6	Period of Oscillation	93 ± 26 min	80 ± 0.5 %	35 min
SOCS3 mRNA Continuous IL-6	Transient peak	Max at 45 min Min at 1.5 h	NA	NA

Table 4.1: Key features of the data used to parameterise the model.

4.4.3 Extending the Initial Model

The initial model was extended so that the issues discussed earlier could be addressed and the average population characteristics (Table 4.1) used to constrain the model. The model was separated into nuclear and cytoplasmic compartments, necessitating the split of the non-linear equation for the production of P-STAT3 into equations 1 through 5, Table 4.2. Signal from the receptors was introduced (Equation 1), including a biologically meaningful number of Receptor molecules (R) and a decay rate (λ_R) so that receptor turnover could be included if necessary. Non-phosphorylated and phosphorylated populations of cytoplasmic STAT3 were explicitly modelled (Equations 2 and 3, respectively), as were the non-phosphorylated and phosphorylated populations of nuclear STAT3 (Equations 4 and 5, respectively). To achieve this, linear terms for phosphorylation of cytoplasmic STAT3 (k_{pC}) and the nuclear import rate for P-STAT3 (k_{imp}) were incorporated. Compartmentalisation meant that the basal nucleocytoplasmic shutting of latent STAT3 dimers (k_{impL}) could also be incorporated as a constitutive rate. This was important for the equal nucleocytoplasmic distribution of STAT3 of the resting state and modelling the 30 min pulse data. Additionally, dephosphorylation rates for cytoplasmic and nuclear P-STAT3 (k_{dpC} and k_{dpN} respectively) and a

nuclear export rate for STAT3 (k_{exp}) were introduced. These changes (Fig 4.13) meant the model more accurately reflected the biological STAT3 activation and deactivation processes and STAT3 nuclear transport. The new equations were developed by Dr E. Abad after discussions with myself and Prof. J. Garcia-Ojalvo. The parameters for the these new terms were drawn from the literature where possible or were fitted by Dr Abad.

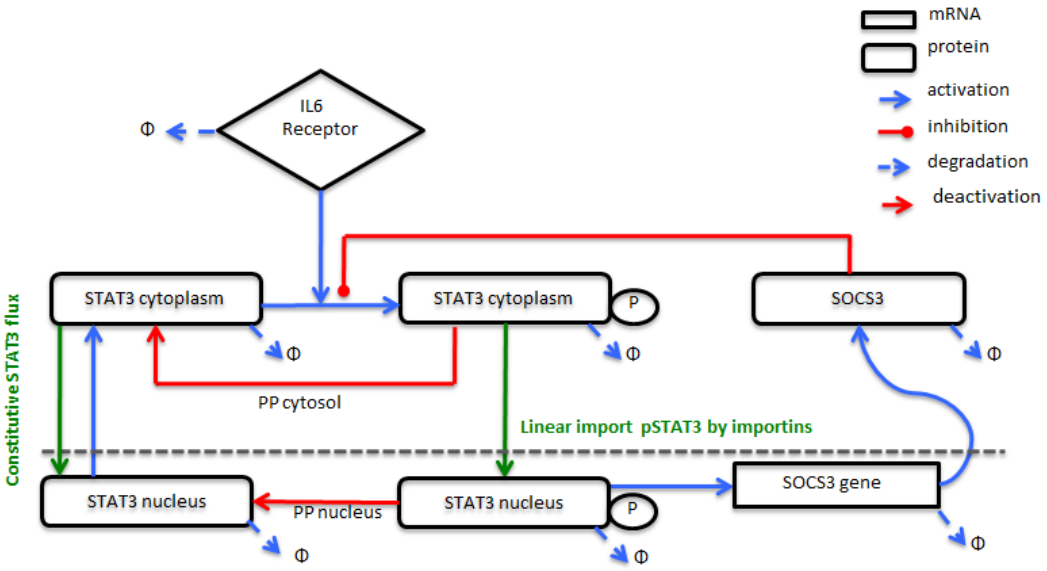

Figure 4.13: Schematic of the new compartmentalised STAT3-SOCS3 model, provided by Dr Abad.

$$\frac{dR}{dt} = S - \lambda_R \cdot R \tag{1}$$

$$\frac{dSTAT_C}{dt} = k_{exp} \cdot STAT_N - k_{impL} \cdot STAT_C + k_{dpC} \cdot pStat_C \ldots - k_{pC} \cdot R \cdot \frac{STAT_C}{STAT_C + W_A} + \frac{SOCS^q}{W_I^q} - \lambda_{STAT} \cdot STAT_C \tag{2}$$

$$\frac{dpSTAT_C}{dt} = k_{pC} \cdot R \cdot \frac{STAT}{STAT_C + W_A} + \frac{SOCS^q}{W_I^q} - k_{imp} \cdot pSTAT_C \ldots - k_{dpC} \cdot pSTAT_C - \lambda_{STAT} \cdot pSTAT_C \tag{3}$$

$$\frac{dSTAT_N}{dt} = k_{dpN} \cdot pSTAT_N - k_{exp} \cdot STAT_N - \lambda_{STAT} \cdot STAT_N + k_{impL} \cdot STAT_C \tag{4}$$

$$\frac{dpSTAT_N}{dt} = k_{imp} \cdot pSTAT_C - k_{dpN} \cdot pSTAT_N - \lambda_{STAT} \cdot pSTAT_N \tag{5}$$

$$\frac{dmSOCS}{dt} = k_T \cdot \frac{pSTAT_N^n}{pSTAT_N^n + W_{socs}^n} - \lambda_{mSOCS} \cdot mSOCS \tag{6}$$

$$\frac{dSOCS}{dt} = k_{SOCS} \cdot mSOCS - \lambda_{SOCS} \cdot SOCS \tag{7}$$

Table 4.2: Model Equations. $STAT$, $pSTAT$, $SOCS$ and $mSOCS$ represent levels of STAT3, phosphorylated STAT3, SOCS3, and SOCS3 mRNA respectively, formulated in terms of molecule numbers per cell. Cytoplasmic and nuclear species are denoted by the subscripts C and N. Parameter values are defined as in Table 4.3. Equations developed by Dr E. Abad.

4.4.4 Parameterisation of the Model

Parameters for the model were drawn from various published sources while others were fitted through local parameter searches (Table 4.3). Ultimately, two different parameter sets were required to capture both 30 min and continuous IL-6 stimulation (parameters different for 30 min IL-6 are highlighted in red). The total number of STAT3 molecules was assumed to be stable over the period modelled, and was based on the number of STAT1 molecules per cell ($1x10^5$) (Wenta et al., 2008). Therefore the STAT3 protein degradation rate (λ_{STAT}) was set to zero whilst STAT3 protein synthesis was not included. Nuclear import of latent STAT3 (k_{impL}) was drawn from Fluorescence Localisation After Photobleaching experiments in unstimulated HepG2 cells (Herrmann et al., 2007), (half-life recovery of fluorescence, 26 min). Rates for cytoplasmic phosphorylation (k_{pC}) and cytoplasmic and nuclear dephosphorylation of STAT3 (k_{dpC} and k_{dpN}) were fitted through local parameter searches. The rates used for the nuclear import of P-STAT3 (k_{imp}) and the nuclear export rate of STAT3 (k_{exp}) were determined experimentally by Cimica et al., (2011) (half-life import rate, 6 min; half-life export rate, 8-10 min). It should be noted that although the equations were compartmentalised, the nuclear and cytoplasmic compartments were not explicitly modelled so their volumes are implicitly assumed to be equal. The transcription rate for SOCS3 was adapted from Yu et al., (2002) whereas the translation rate for the production of SOCS3 protein was fitted. The SOCS3 mRNA degradation rate was obtained from Ehlting et al., (2007) (mRNA life-life, 17 min) and the SOCS3 protein degradation rate was set to match the mRNA stability so that protein and mRNA levels remained proportional over time. The Hill constant of half-maximal activation for the activity of phosphorylated STAT3 (W_A), the dissociation rate for SOCS3 inhibition (W_I), and the rate of SOCS3 transcription by active nuclear STAT3 (W_{SOCS3}) were manually determined through local parameter searches during fitting of the model.

Table 4.3: List of STAT3/SOCS3 model parameter values

Name	Symbol	Value Cont./Pulse (mean±SD)	Units	Reference
Receptor production rate (active by endogenous)	S	0	min^{-1}	NA
Transcription rate for SOCS3	k_T	19±12	min^{-1}	Yu et al, 2003
Translation rate for SOCS3	k_{SOCS}	13±6	min^{-1}	*
Phosphorylation STAT3 rate	k_{pC}	44±22	min^{-1}	*
Dephosphorylation STAT3 rate	k_{dpC}	0.12±0.04	min^{-1}	*
Maximum import rate (pSTAT3)	k_{imp}	0.026±0.007/ 0.018	min^{-1}	Cimica et al, 2011
Constitutive import rate (STAT3)	k_{impL}	0.043±0.02	min^{-1}	Hermann et al, 2007
Export rate (STAT3)	k_{exp}	0.04±0.02	min^{-1}	Cimica et al, 2011
Nuclear STAT3 Dephosphorylation rate	k_{dpN}	0.034±0.01 /0.017	min^{-1}	*
STAT3 phosphorylation activation (Hill's constant; half maximal activation)	W_A	38220±11956	molecules	*
Dissociation constant for the receptor - inhibitor SOCS3 (Hill's constant; half maximal activation)	W_I	48097±30800	molecules	*
SOCS3 transcription activation by nuclear pSTAT3 (Hill's constant; half maximal activation)	W_{socs}^n	12148±16220	molecules	*
Co-operativity of SOCS3 protein over STAT3 dimers	q	3±1.4	-	NA
Co-operativity of STAT3 on SOCS3 gene promoter	n	4±1	-	NA
Receptor internalization/degradation rate	λ_R	0	min^{-1}	NA
SOCS3 mRNA degradation rate	λ_{mSOCS}	0.035±0.01	min^{-1}	Ehlting et al, 2007
SOCS3 protein degradation rate	λ_{SOCS}	0.033±0.01	min^{-1}	Siewert et al, 1999
STAT3 protein degradation rate	λ_{STAT}	0	min^{-1}	NA
Total STAT3 level	$STAT_{total}$	1E5	molecules	Wenta et al, 2008
Total IL6 receptor level	R_{total}	500	molecules	Zöhlnhofer et al., 1992

* Parameter fitted manually using local parameter searches.

4.4.5 Model Simulations

Early attempts at expanding the model used one set of parameters to capture data for both the 30 min IL-6 pulse and continuous IL-6 stimulation. However, these attempts could not generate sustained STAT3 oscillations under continuous stimulation. Instead, two parameter sets were required, one for each stimulation regime. The most recent version of the model captured oscillations in N/T STAT3 with a 90 min period in response to continuous IL-6 stimulation, and SOCS3 mRNA and SOCS3 protein also oscillated (Fig. 4.14). Nuclear STAT3 oscillations were sustained over a 10 h period, in accordance with the imaging data.

Outputs from the extended model (Fig. 4.15) reflected the 30 min IL-6 pulse data well, generating single transient peaks in Nuclear STAT3, SOCS3 mRNA and SOCS3 protein levels. This was achieved by setting the level of active receptor to zero, 30 min after beginning simulation. The biological regulation of receptor activity is highly complex (Section 1.2.2.4) but IL-6-bound receptors are internalised within 5 min and subsequent activation and deactivation processes occur inside the cell. Therefore from a statistical perspective, removal of IL-6 from the media sets the active receptor level to zero. Although not an accurate reflection of receptor dynamics, it was sufficient for modelling IL-6 pulse data.

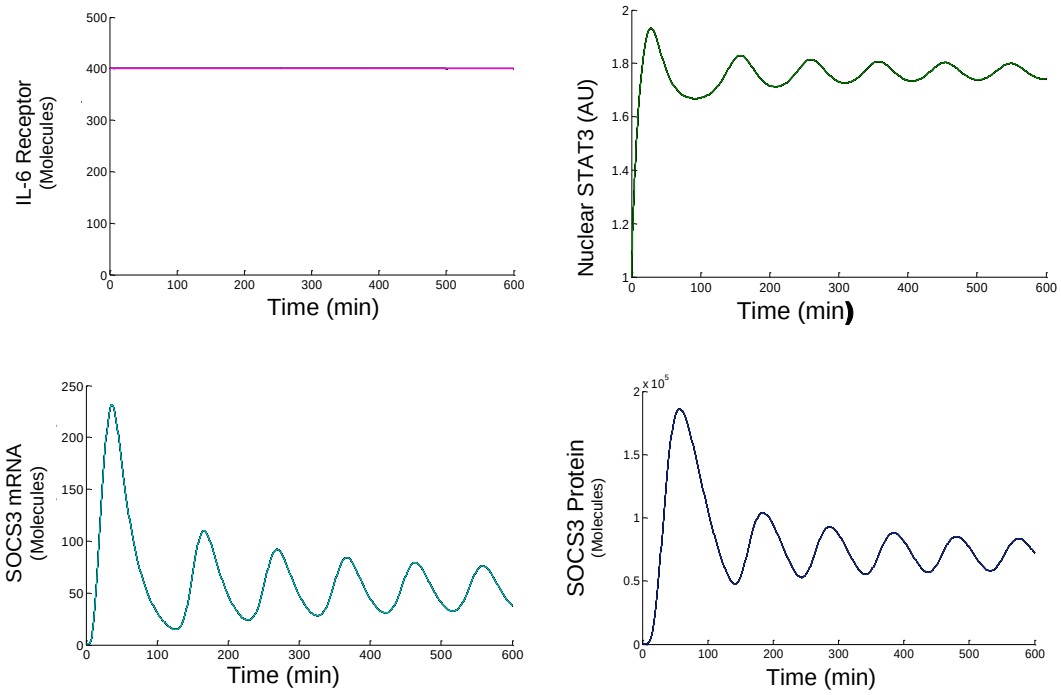

Figure 4.14: Simulation Outputs from the Expanded Model for Continuous IL-6 Stimulation in HepG2 cells. 10 h simulation. Graphs of IL-6 Receptor, Nuclear STAT3 Fluorescence, SOCS3 mRNA and SOCS3 protein.

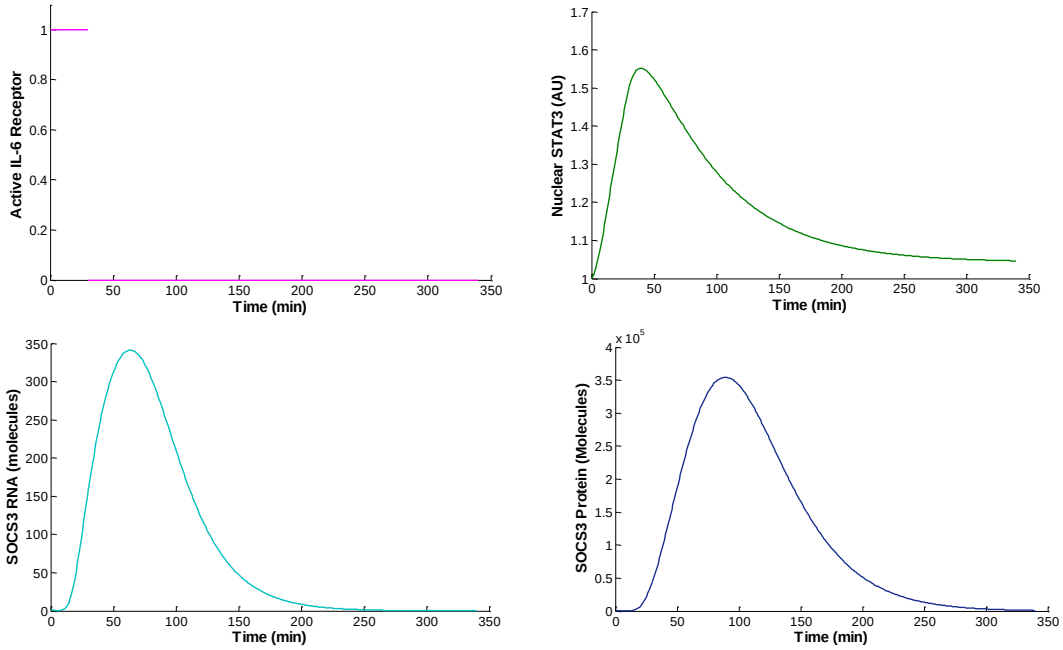

Figure 4.15: Simulation Outputs from the Expanded Model for 30 min Pulse IL-6 in HepG2 cells. Run time of 5 h. Graphs of IL-6 Receptor, Nuclear STAT3 Fluorescence, SOCS3 mRNA and SOCS3 protein

4.4.6 Observations on the Iterative Model Fitting

The simulations from the initial STAT:SOCS model created by Domedel-Puig did not reflect the newly available single cell STAT3 microscopy data. Therefore additional complexity representing STAT3 nuclear import/export was introduced into the model so that the model could use and capture the STAT3 data effectively. Even though the model has a small number of equations, it was complex enough to capture both oscillatory and transient dynamics in response to two different stimulation regimes. In doing so, two different solutions were generated. Values for half of the parameters were initially obtained from the literature, whilst the remainder were obtained by fitting to the data. Whilst refining the model to better reflect the data, certain parameters originally provided by the literature were significantly modified. These were the various import and export rates for the different STAT3 species, thus highlighting their central importance to the model.

4.4.6.1 Nuclear and Cytoplasmic Compartmentalisation

The first fundamental change to the initial model was introducing nuclear and cytoplasmic compartments. This allowed for separate populations of phospho- and non-phospho-STAT3 in the two compartments which in turn enabled nuclear import and export of both latent and active STAT3 to be modelled directly, making better use of the experimental data available. However, since no term was included for the relative sizes of the cytoplasmic and nuclear compartments, they are assumed to be the same size even though this is not the case in most cells. Experience from other models of oscillating systems (Ashall et al., 2009) suggests that an explicit representation of the compartment sizes is necessary for generating oscillatory dynamics. Therefore it may be useful to update the model so that compartment sizes are included.

4.4.6.2 Importance of U-STAT3 and Import/Export Rates

One novel feature of the model was the inclusion of nucleocytoplasmic transport of unphosphorylated STAT3 (U-STAT3). This phenomenon is functionally relevant, as U-STAT3 transcribes a specific subset of genes distinct from the targets of P-STAT3. Constitutive shuttling of U-STAT3, which also occurs with STAT5 and STAT6 (reviewed in Reich, 2013), was essential for

capturing the decay of the transient nuclear translocation under the pulse stimulus. Interestingly, the two parameter spaces together indicated that neither the absence nor presence of U-STAT3 trafficking affected the oscillatory dynamics under continuous stimulation, providing another possible role for U-STATs. Nuclear import of U-STAT3 was modelled at a rate approximately three times slower than for P-STAT3. There are conflicting reports in the literature regarding whether phospho- and non-phospho-STAT3 shuttle at the same rate (Herrmann et al, 2007; Cimica et al, 2011). Resolving this question experimentally is difficult because fluorescently-tagged proteins cannot distinguish between different phosphorylation states. Consequently existing studies have considered transport rates before and after stimulation of STAT3.

4.4.6.3 Receptor Dynamics

Experimentally, the temporal dynamics of the IL-6 receptor are complex, context-dependent and not fully understood. Much of the published work on receptor dynamics was obtained from population-based methods and thus does not account for intercellular variation, which could be significant given the level of heterogeneity seen in STAT3 oscillations. In light of the complex biology, a receptor turn-over rate was included. However it proved unnecessary for generating oscillatory dynamics in this model of STAT3:SOCS3 signalling. In the future it may prove beneficial to reconsider receptor dynamics in more detail, and perhaps move from a two-state active-inactive receptor model to a three state motif, similar to the IKK module (Ashall et al, 2009). Further pulsing experiments with repeat pulses with different length intervals could also shed light on receptor dynamics, perhaps indicating a refractory period for receptor activation.

4.5 Discussion

4.5.1 Live Cell Imaging of STAT3 Oscillatory Dynamics

The nucleocytoplasmic translocation dynamics of STAT3 were investigated by performing live cell imaging of the EGFP-STAT3 construct developed in the previous chapter. Four conditions were tested. EGFP-STAT3 in unstimulated HepG2 cells did not change its nuclear to cytoplasmic ratio over time, remaining evenly distributed between the two compartments, in line with published works (Meyer et al, 2002). A 30 min IL-6 pulse caused a single, transient nucleocytoplasmic translocation of STAT3, again in agreement with the literature (Pranada et al, 2004). However, this is the first study to quantify the dynamics of the translocation, including the rapid exponential accumulation in the nucleus and the first order exponential decay rate returning the cell to its resting state within 6 h. Interestingly the decay rate for the return of N/T STAT3 to the resting state was slightly longer than the half-life of P-STAT3, as determined by Western bot. This implies that N/T STAT3 does not directly correlate with P-STAT levels, one explanation for which might be that it takes some time for U-STAT3 to be exported from the nucleus after it has been dephosphorylated.

Continuous IL-6 stimulation resulted in STAT3 nucleocytoplasmic oscillations with an average period of approximately 90 min, confirming the prediction that STAT3 is capable of oscillating in single cells from the modelling of population-level oscillations (Yoshiura et al, 2007). The STAT3 oscillations were sustained over a long period (up to 16 h), indicating that the system can reach a robust limit cycle state. This study is the first to image and quantify STAT3 at a high time resolution for an extended period of time. Other studies have been of short duration (Pranada et al, 2004) or have focused on the specific mechanisms of nuclear import and export (Bhattacharya & Schindler, 2003; Cimica et al, 2011; Vogt et al, 2011), without considering the wider dynamics of the system. An early study in STAT1 imaged it at hourly intervals for up to 24 h but did not quantify the images, while the low time resolution means any dynamics would have been overlooked (Köster & Hauser, 1999). Meanwhile, early imaging studies of STAT6 were also for a period of less than 2 h (Nelson et al, 2002;

Nelson et al, 2003). It would be extremely interesting to repeat these studies with extended imaging, higher temporal resolution and image quantification to discover whether oscillatory dynamics are a feature of other STATs.

The characteristic shape of the STAT3 oscillations was different to those of p65/NF-κB (Section 3.3). Instead of sharp, clearly defined translocations to and from the nucleus, STAT3 oscillations were broad, and the majority of STAT3 remained in the nucleus after stimulation. In effect, STAT3 oscillated around a new, higher set point (around 80% nuclear/total STAT3). This made quantifying the oscillations more complex, introducing a potential source of error into the analysis. However, it should be remembered that bulk nuclear accumulation of STAT3 is a proxy for the transcriptionally active phospho-STAT3. It may be that nuclear STAT3 obscures more defined oscillations of the P-STAT3 population. Furthermore, since U-STAT3 has roles in transcription (Yang et al, 2007), it may be functionally relevant that STAT3 oscillates around a higher set-point after IL-6 stimulation, even if not all the STAT3 in the nucleus is phosphorylated. Also relevant is the existence of other signalling systems with complex and oscillatory dynamics, e.g. calcium signalling and the circadian clock, have differently shaped oscillatory responses (Meyer & Stryer, 1988; Goldbeter, 1995; Tyson et al, 1999).

A major hurdle with imaging STAT3 was the range of expression levels from the transient plasmid transfection, and the variable concentration of STAT3 in the nuclear and cytoplasmic compartments after IL-6 stimulation. Many fluorescent cells could not be imaged because they were too bright or too faint, whilst other cells exceeded the detection range of the microscope after stimulation due nuclear accumulation of STAT3. Often fluorescence in the nuclear compartment saturated the channel whilst other cells lost cytoplasmic fluorescence. This led to many cells having to be discarded during the image analysis due to the poor quality data produced. In an attempt to address this issue, two different detection channels were set up to capture overlapping ranges of fluorescence; unfortunately this was insufficient. The ideal solution would be the creation of a stable EGFP-STAT3 HepG2 cell line, which would enable more data to be collected more efficiently, and improve the statistical robustness of the data.

The effects of short IL-6 pulses on STAT3 were also considered. Pulses of 5 and 15 min resulted in far fewer cells responding with a nuclear translocation, however the cells that did respond, exhibited a full strength translocation. This suggests the existence of a threshold of activation. The pY705-STAT3 Western blots in Section 3.6.2 indicated that STAT3 was equally phosphorylated at 15 min as at 30 min. Furthermore some cells were able to produce a full STAT3 translocation after only 15 min of IL-6. Together these data suggest that additional signalling events, other than Y705-phosphorylation and occurring between 5 and 30 min after stimulation, are necessary for the induction of a full STAT3 nuclear translocation in the majority of cells. Indeed, it has been reported that whilst 80% of IL-6-bound receptors are internalised within 5 min of IL-6 treatment, IL-6-induced MAP Kinase signalling via Erk1/2 is essential for full S727 phosphorylation of STAT3, which is in turn needed for maximal gene transcription (German et al, 2011). S727 phosphorylation appears within 5 min of IL-6 addition but accumulates very slowly, reaching a maximum 30 to 45 min after IL-6. This time-scale fits with the hypothesis that signalling events occurring between 15 and 30 min post-stimulation with IL-6 are necessary for the majority of cells to respond with a STAT3 nuclear translocation.

An experiment with repeated short pulses of IL-6 was initially considered as it would have facilitated the investigation of a possible refractory period and the role of receptor dynamics. This approach was very successful for probing p65 responses to TNFα and generated data that considerably constrained the NF-κB model (Ashall et al, 2009). However the requirement for 30 min IL-6 stimulation for the majority of cells to respond made this a challenging approach, given the ~90 min period of STAT3 oscillations. Ideally a set of experiments would be performed where the cells are stimulated with IL-6 for 30 min, followed by media replacement and an increasingly long rest period, at intervals from 15 min after stimulation up to 120 min post-media-replacement, before the application of a second 30 min IL-6 pulse or continuous stimulation. This would cover the period between the first STAT3 nuclear peak and the second peak and would inform our understanding of SOCS3-dependent signalling deactivation and the proposed refractory period (Wormald et al, 2006), as well as the possible role of receptor dynamics in STAT3 activation.

Multiple repeat pulses would be difficult practically because of the 90 min STAT3 period and because of the significant cellular heterogeneity.

4.5.2 STAT3-Induced Gene Expression Study

The purpose of the qPCR study was to investigate whether there was any correlation between STAT3 signalling dynamics and the strength of transcriptional induction in response to differently timed IL-6 stimuli for a limited set of target genes. There were very few differences between the pulsed and continuous IL-6 protocols and those that were seen were small and limited to later time points. Due to the variability of the data, and the small fold-changes, these differences were unlikely to be significant. Consequently it was not possible to correlate the limited effects to the differences in STAT3 signalling dynamics. However the data was sufficient to indicate that there was IL-6 induced STAT3-mediated gene expression and the SOCS3 data was able to constrain the STAT3:SOCS3 model.

To re-address the question of whether gene expression can be related to signalling dynamics, it would be better to test a wider array of genes. This could be done using a microarray or Nanostring technology. It would be useful to perturb STAT3 signalling in different ways, such as performing repeat pulses, using different stimuli or adding inhibitors, as this could affect both STAT3 dynamics and gene expression. Finally single cell transcriptional data from a SOCS3 reporter would further inform on the dynamics of the system and could provide additional support for the STAT3:SOCS3 model.

4.5.3 Modelling STAT3:SOCS3 Signalling Dynamics

4.5.3.1 Summary

We sought to assess basic cellular responses to a strong STAT3 agonist, IL-6, by combining experimental and modelling approaches. The purpose of the model was to replicate the statistically determined key features of STAT3 nucleocytoplasmic translocation dynamics in response to differently timed stimulus regimes. By representing only the fundamental aspects of STAT3 signalling transduction and SOCS3 inhibition using a minimalist ODE approach, the STAT3 dynamics in response to continual and pulsed IL-6 stimulation were

modelled. In the course of the model fitting, the importance of the balance between nuclear import and export rates for P-STAT3 and U-STAT3 to STAT3 oscillations became apparent. Altering the import and export variables changed the amplitude and timing of STAT3 oscillations, however oscillatory dynamics were maintained across a range of parameters. The robustness of oscillation dynamics and the effect of SOCS3 negative feedback were not assessed in detail so this represents a key area for further work.

4.5.3.2 Future Approaches to Improve the Model

Models are inherently flawed so generating different solutions was not unlikely. It indicates that there may be more than one solution to the model and that conducting a sensitivity analysis is an important next step. One approach for sensitivity analysis entails changing specific parameters by fixed amounts on a case-by-case basis – this can lead to a better solution within a localised parameter space. Another option is to fit the model to the existing microscopy data on a cell-by-cell basis, constraining the parameters within a certain range and stopping the fitting once it approaches a certain level of best fit. This can give an indication of the range of reasonable values for key parameters. A much more intensive approach would be to perform a global sensitivity analysis. This searches the entire parameter space for possible results and so may identify non-intuitive solutions to the model (Rand, 2008).

Collecting more types of experimental data would also aid the modelling approaches aimed at identifying better solutions. Work within the NF-κB system has highlighted the importance of good quality data and perturbing experimental systems to constrain mathematical models. The first effort should be towards obtaining extensive good quality single cell data, and this is best achieved using stable cell lines. Secondly, perturbations to the experimental system can be particularly informative. In the NF-κB system, perturbations have included repeat pulsing protocols (Ashall et al, 2009), low dose stimulation (Turner et al, 2010), and temperature changes (C. Harper, unpublished), amongst others. In this STAT3 system, repeating short pulses of IL-6 with different intervals between pulses may be the most informative initially, and would aid understanding of the effect of receptor dynamics upon the system.

Another approach for the future would be to target specific measurements for key parameters such as the import and export rates for different STAT3 species, or for levels of SOCS3 mRNA or protein.

4.5.3.3 Future Investigation of STAT3 and NF-κB Cross-Talk

The ultimate goal was to investigate cross-talk between NF-κB/p65 and STAT3, with the intention of modelling any systemic effects on their respective nucleocytoplasmic translocation dynamics. In order for such modelling to be possible, it was necessary to have both the pre-existing Ashall NF-κB model and this STAT3:SOCS3 model defined in comparable terms. Compartmentalising the STAT3:SOCS3 model was one step towards this, as was converting the initial model into realistic molecular numbers, achieved by deriving the parameters from biologically meaningful data. However, although necessary, these steps are not sufficient for combining the two models into one. The number of possible interaction mechanisms (Section 1.4) is so large that testing all possible model combinations becomes unfeasible. The following chapter therefore considers the dynamic responses of STAT3 and p65 to dual IL-6 and TNFα stimulation and other stimulus regimes as a means to further constrain the two models, thus providing a way around the complexity of cross-talk between the two networks.

Chapter 5
Cross-Talk Between STAT3 and p65

5.1 Introduction

This chapter addresses the final key aim of the thesis which was to investigate the cross-talk between STAT3 and NF-κB in terms of their single cell dynamics in response to different cytokines. IL-6, TNFα and IL-1β drive the acute phase response and it is known that gene expression is affected by the interplay of these three cytokines (Schindler et al, 1990; Snyers & Content, 1992). The interaction of NF-κB/p65 and STAT3 is vital to the expression of a subset of APR genes, including Serum Amyloid A, whereas for other genes, the interaction between p65 and STAT3 is inhibitory (Bode et al, 2012a). The outcome also depends on which cytokines are activating, as TNFα and IL-1β may have different effects even though they both signal via p65. Although there are many different proposed mechanisms for STAT and NF-κB cross-talk (Section 1.4), the particular focus here is on intracellular cross-talk between STAT3 and p65. Both indirect and direct interactions have been recorded for p65, U-STAT3 and P-STAT3 (Bode et al, 1999; Yoshida et al, 2004; Hagihara et al, 2005; Yang et al, 2007; Lee et al, 2009), as a result of IL-6, TNFα or IL-1β signalling in combination. More recently, a mechanism for IL-1β inhibition of IL-6 signalling acting via MAPK as opposed to NF-κB was elucidated (Radtke et al, 2010).

NF-κB was already known as an oscillatory signalling system (Nelson et al, 2004; Ashall et al, 2009) whilst STAT3 was a suspected oscillator. Therefore, in light of the various direct and indirect interaction mechanisms, it was possible that they may function as a coupled oscillator (Wang et al, 2011). If that were the case, then the dynamics of one system might be able to modulate the dynamics of the other. In a strongly coupled oscillator, this could occur as synchronous oscillations. In a weakly coupled oscillator however, the interplay of the dynamics could be much more subtle and more difficult to detect.

In the previous chapter, STAT3 was established as a strong oscillator in HepG2 cells that responded to continuous IL-6 stimulation with sustained nucleocytoplasmic oscillations. In Chapter 3, the TNFα-induced NF-κB dynamics were characterised for HepG2 cells. This chapter therefore builds upon this work and seeks to investigate the interplay of STAT3 and p65 signalling dynamics in response to IL-6, TNFα and IL-1β. Numerous control experiments

were performed to assess the effects of co-transfection and co-stimulation of single transfections upon signalling dynamics. The importance of the timing of cytokine stimulation for transcription factor activation and cross-talk was also investigated. Cross-talk initiated by IL-6 and TNFα signalling was assessed first and a small gene expression study was carried out in an attempt to relate gene expression to the pattern of STAT3 and p65 interaction. The role of IL-1β signalling in HepG2 cells and its cross-talk with IL-6 was considered later.

5.2 Results

To assess the effects of cytokine cross-talk on STAT3 and p65 signalling dynamics, extensive experimental controls were necessary. Combinations of single and co-stimulation with single and co-transfections were tested because protein over-expression and altered expression ratios may affect protein interaction equilibria. The effect of Transcription Factor co-transfection on individual stimuli (IL-6 and TNFα) was assessed, as was the effect of co-stimulation (IL-6 + TNFα) on single TF expression. Continuous stimulation was used throughout. Once the controls were available, the STAT3:p65 co-transfection, co-stimulation experiments were performed. IL-6 and TNFα were applied simultaneously or separately with a pre-determined delay in order to assess the importance of the timing of cytokine stimulation upon cross-talk. IL-6 and TNFα were considered first in Section 5.3, while IL-6 and IL-1β were considered later in Section 5.5.

5.3 IL-6 and TNFα Induced STAT3 and p65 Cross-Talk

5.3.1 Controlling for Transcription Factor Activation Under Co-Transfection and Co-Treatment Conditions

5.3.1.1 STAT3 and p65 – Continuous IL-6 Stimulation

Continuous IL-6 stimulation of STAT3:p65 co-transfected HepG2 cells suggested that STAT3 oscillated as per the continuously IL-6 stimulated STAT3 results presented in Chapter 4, and also demonstrated that p65 did not exhibit nucleocytoplasmic oscillations (Fig. 5.1). However only two STAT3 oscillating cells were obtained. An additional 9 cells were analysed and they showed the initial STAT3 nuclear translocation, but subsequent oscillations could not be detected due to the limited dynamic range of the microscope's detector. No p65 response was observed in these responding cells. This extremely limited data set meant that no statistical analysis could be performed but it did confirm that STAT3 was capable of oscillating when co-expressed with p65 and that p65 did not respond when STAT3 was stimulated with IL-6.

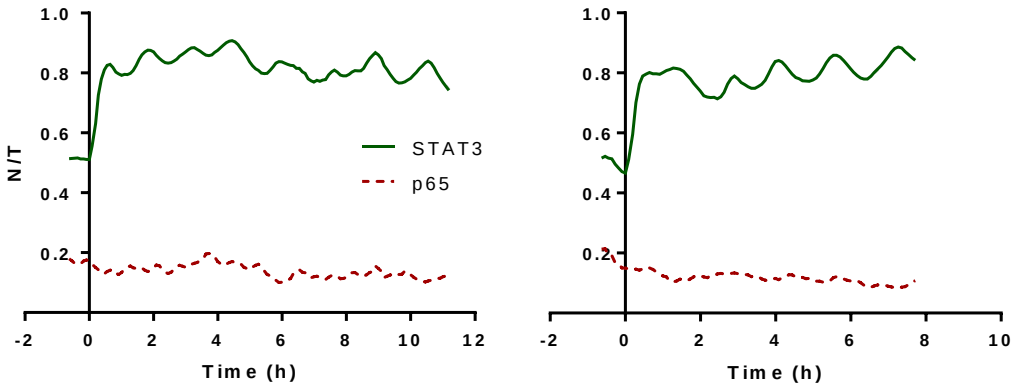

Figure 5.1: N/T Fluorescence Traces from EGFP-STAT3, p65-dsRedXP dual-transfected HepG2 cells stimulated with 20 ng/ml IL-6. Green solid line: STAT3, red dashed line: p65.

5.3.1.2 STAT3 – Continuous IL-6 and TNF α

Co-stimulation of EGFP-STAT3 singly transfected HepG2 cells with IL-6 and TNFα indicated that STAT3 was capable of oscillatory dynamics under these conditions (Fig. 5.2). However only one cell was successfully imaged and analysed, despite running multiple experimental replicates. This again meant that no statistical analysis could be performed so it was not possible to determine what effect, if any, p65 over-expression had on the dynamics of the STAT3 oscillations.

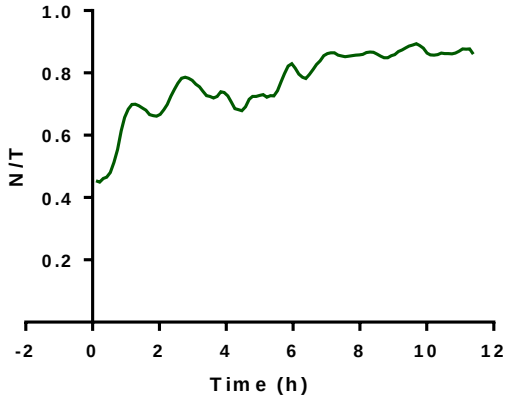

Figure 5.2: N/T Fluorescence Trace from an EGFP-STAT3 HepG2 cell, co-stimulated with 20 ng/ml IL-6 and 10 ng/ml TNFα. Green solid line: STAT3.

5.3.1.3 STAT3 and p65 – Continuous TNFα

Oscillations were observed for p65 when co-expressed with STAT3 and treated with TNFα, and no STAT3 response was detected (Fig. 5.3A). Peak intervals, mean cell period and average oscillatory period (Fig. 5.5C) were calculated from cell traces (Fig. 5.5B) as in Chapter 3. When p65 and STAT3 were co-expressed and only p65 was stimulated with TNFα, p65 oscillated with an average period of 87 ± 20 min. This was 12.5 ± 4 min faster than when p65 was expressed alone and treated with TNFα (period, 99 ± 15min), and was significantly different at the $P<0.05$ level (independent t-test) (Fig. 5.5D).

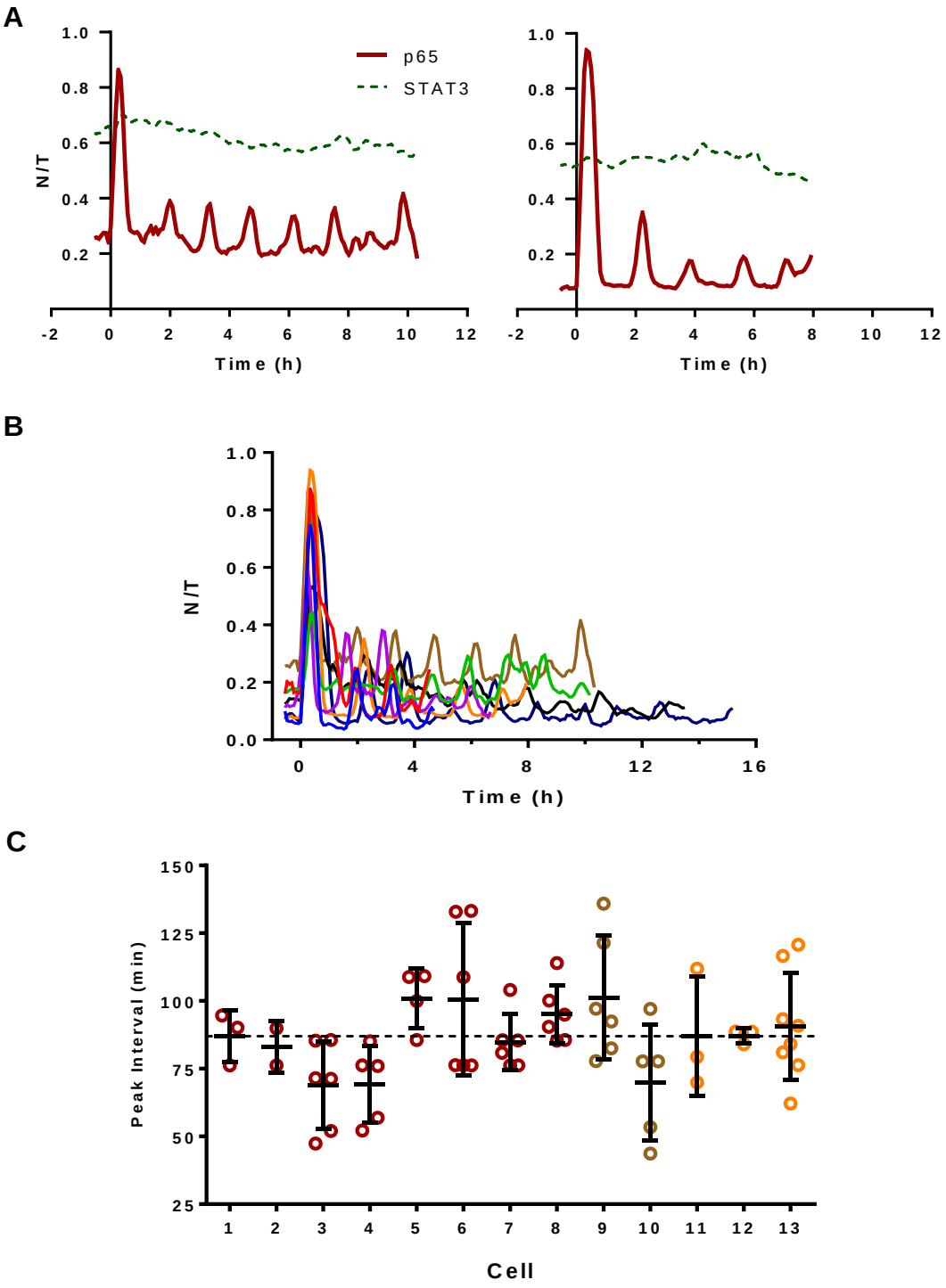

Figure 5.3: p65 Data from EGFP-STAT3, p65-dsRedXP dual-transfected HepG2 cells stimulated with 10 ng/ml TNFα. A Example N/T cell traces. STAT3: green dash, p65: solid red line. **B** All p65 cell traces, n = 13 cells. **C** Mean peak intervals by cell (n=13 cells) and colour-coded by replicate (n=3). Each circle represents one peak interval (min) (n=63 peaks). Error bars represent mean cell period ± S.D. Dashed horizontal line represents the mean of all cell periods.

5.3.1.4 p65 – Co-stimulation with Continuous IL-6 and TNFα

When p65 was expressed alone and co-stimulated with IL-6 and TNFα, it oscillated with a period of 93.5 ± 10 min, which was not significantly different to the response to TNFα stimulation alone (99 ± 15 min) (independent t-test with Welch's correction for unequal variance, P=0.15) (Fig. 5.5B).

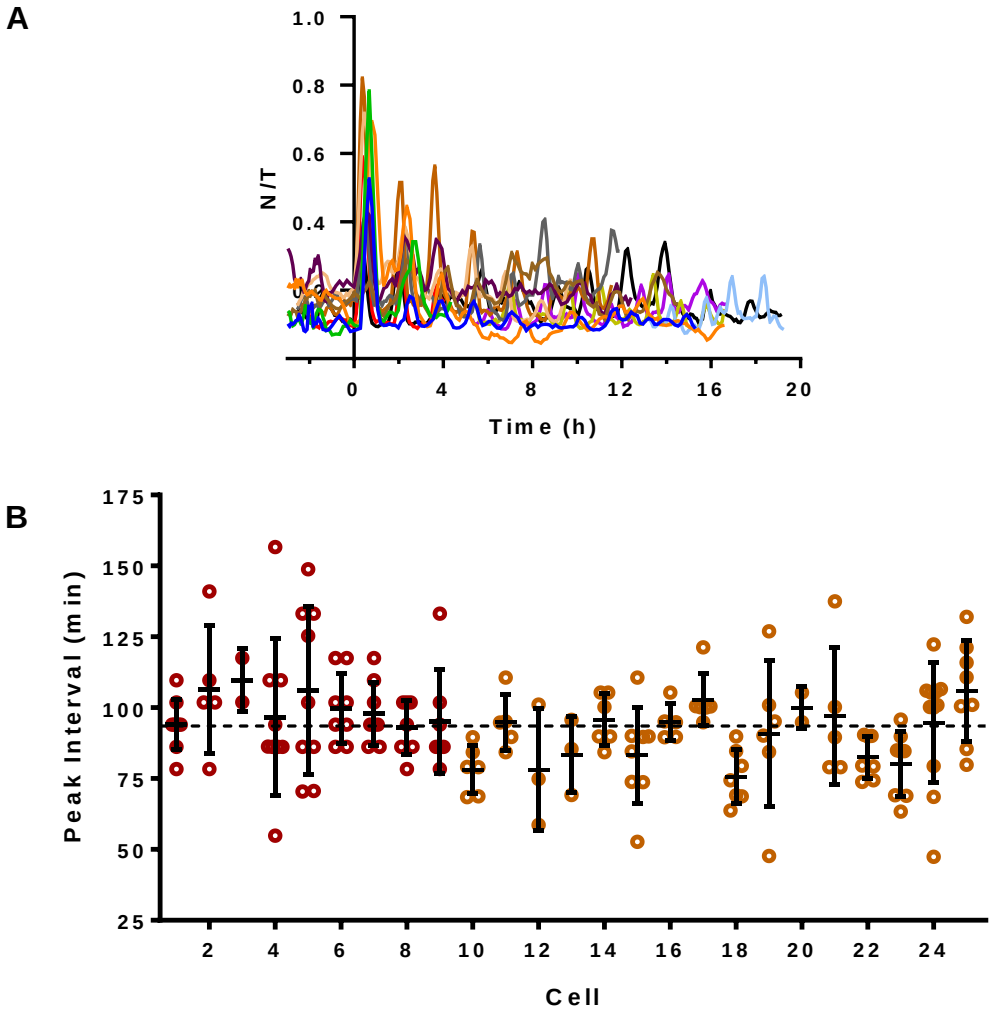

Figure 5.4: p65 Data from p65-dsRedXP singly-transfected HepG2 cells, stimulated with 10 ng/ml TNFα. **A** Selected p65 cell traces, n = 13 cells. **B** Mean of cell peak intervals by cell (n=25 cells) and colour-coded by experimental replicate (n=2). Each circle represents one peak interval (min), n= 160 peaks. Error bars represent mean cell period ± S.D. Dashed horizontal line represents the mean of individual cell periods.

5.3.1.5 Comparing p65 Dynamical Behaviour Across Control Experiments

The peak intervals (Fig. 5.5A and C) and cell periods (Fig. 5.5.B and D) from the p65:TNFα+IL-6 and p65+STAT3:TNFα were compared to the original p65+TNFα experiments presented in Section 3.3. Co-stimulating p65 with TNFα and IL-6 did not change the mean cell oscillatory period but did decrease the intercellular variance (Fig. 5.5 B), as measured with the F-test ($P<0.05$).

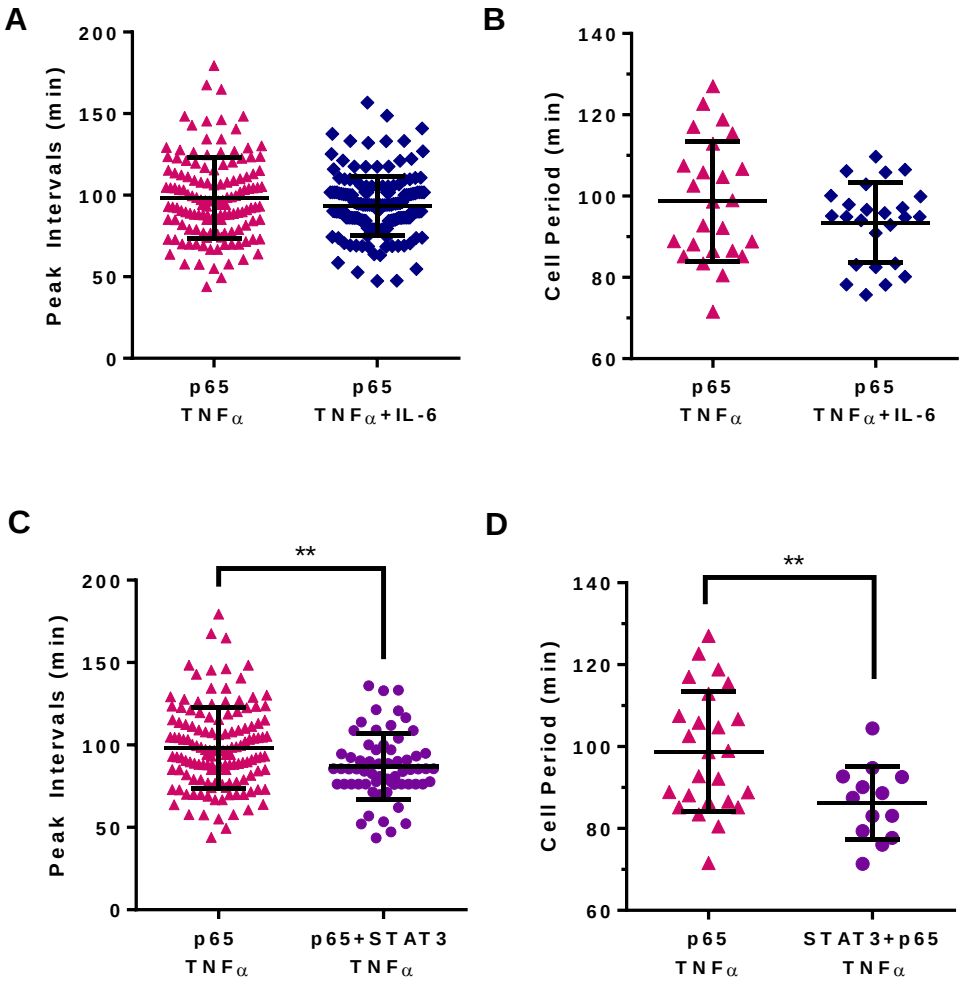

Figure 5.5: Comparing a) IL-6 and TNFα Co-stimulation to TNFα Stimulation and b) STAT3+p65 Dual Transfection to p65 Single Transfection. A and **C:** comparing pooled peak intervals (min) from all cells across all experiments. **B** and **D:** comparing individual mean cell periods (min). 10 ng/ml TNFα and 20 ng/ml IL-6. Each point represents a single peak interval or cell period and error bars in all graphs show population Mean ± S.D.

Co-expressing p65 with STAT3 did affect the p65 oscillatory period, decreasing it by 12.5 min to 87 min on average (Fig. 5.5.D), and this was also seen when all the peak intervals were pooled (Fig. 5.5C). This was a significant change but one possible explanation is that there were half as many cells for p65+STAT3:TNFα as for p65+TNFα so slower oscillating cells may not have been sampled. If however the difference remained after additional cells were collected then one explanation is that the excess STAT3 was able to interact with p65 and use its NLS to shift the p65 nuclear import/export equilibrium in favour of faster oscillations. This hypothesis is suggested by the work of various groups which have demonstrated that U-STAT3 and p65 can interact directly to drive gene transcription (Yoshida et al, 2004; Yang et al, 2007).

5.3.2 STAT3 and p65 Dynamics in Response to IL-6 and TNFα Co-stimulation in Co-Transfected Cells

HepG2 cells co-transfected with p65-dsRedXP and EGFP-STAT3 were co-stimulated with IL-6 and TNFα to determine whether the oscillatory dynamics of either protein were affected by the other when activated by cytokines. One hypothesis was that the two systems may be coupled and thus capable of re-enforcing their dynamics, leading to increased synchronisation in the oscillations. However, STAT3 and p65 oscillate with a very similar period when expressed alone and stimulated by one cytokine: 94 $\pm$ 12 min and 99 $\pm$ 15 min, respectively. The similarity in the average period, coupled with the degree of intracellular peak interval variation and intercellular period variation and also the wide STAT3 peaks, as opposed to the 'sharp' p65 peaks, could make it hard to classify the exact behaviour of the cells. Consequently, the systems synchronously oscillating could look very similar to the systems oscillating at their 'typical' speed but oblivious to each other, with a high degree of peak alignment in both cases. To attempt to address this issue, as well as applying the IL-6+TNFα simultaneously, they were applied with a 45 min delay between the IL-6 stimulation and TNFα stimulation. The 45 min delay was chosen because it is half of the 90 min STAT3+IL-6 oscillatory period. This should therefore start the oscillations precisely out of phase by 180°. If the systems were to synchronise, this could appear through a change in period over time, until the

oscillations were in phase. Alternatively the systems might be weakly coupled, in which case a number of different effects on the systems might be seen. To address this possibility, the population characteristics of peak interval distribution and mean oscillatory period were carefully considered, and statistically compared to the control experiments in Section 5.2.1.

5.3.2.1 IL-6 and TNFα Simultaneous Co-Stimulation

STAT3 and p65 oscillations were observed when co-transfected HepG2 cells were simultaneously stimulated with IL-6 and TNFα (Fig. 5.6). Shape and amplitude of the oscillations were similar to those seen previously for TNFα-stimulated (Fig. 3.4) and IL-6-stimulated (Fig. 4.5) HepG2 cells. Peak intervals and mean cell periods were determined as before (Fig. 5.7A, B) and the intervals from all cells were pooled (Fig. 5.7C) so that STAT3 and p65 could be compared across the sample population. The mean STAT3 peak interval was 103.8 $\pm$ 33.0 min and the median was 96.8 min, whilst the p65 mean interval was 93.1 $\pm$ 26.6 min and the median 91.1 min. The peak interval data were analysed using the Mann-Whitney test as the data were not normally distributed and this indicated that the 5.8 min difference between the medians was significant at the $P<0.05$ level. The mean STAT3 cell period was 103.6 $\pm$ 16.4 min and the p65 mean cell period was 96.0 $\pm$ 16.0 min (Fig. 5.7D). The p65 and STAT3 oscillatory periods were compared using the unpaired t-test (the data were normally distributed), and the 7.6 min difference in the means was not significant ($P=0.12$).

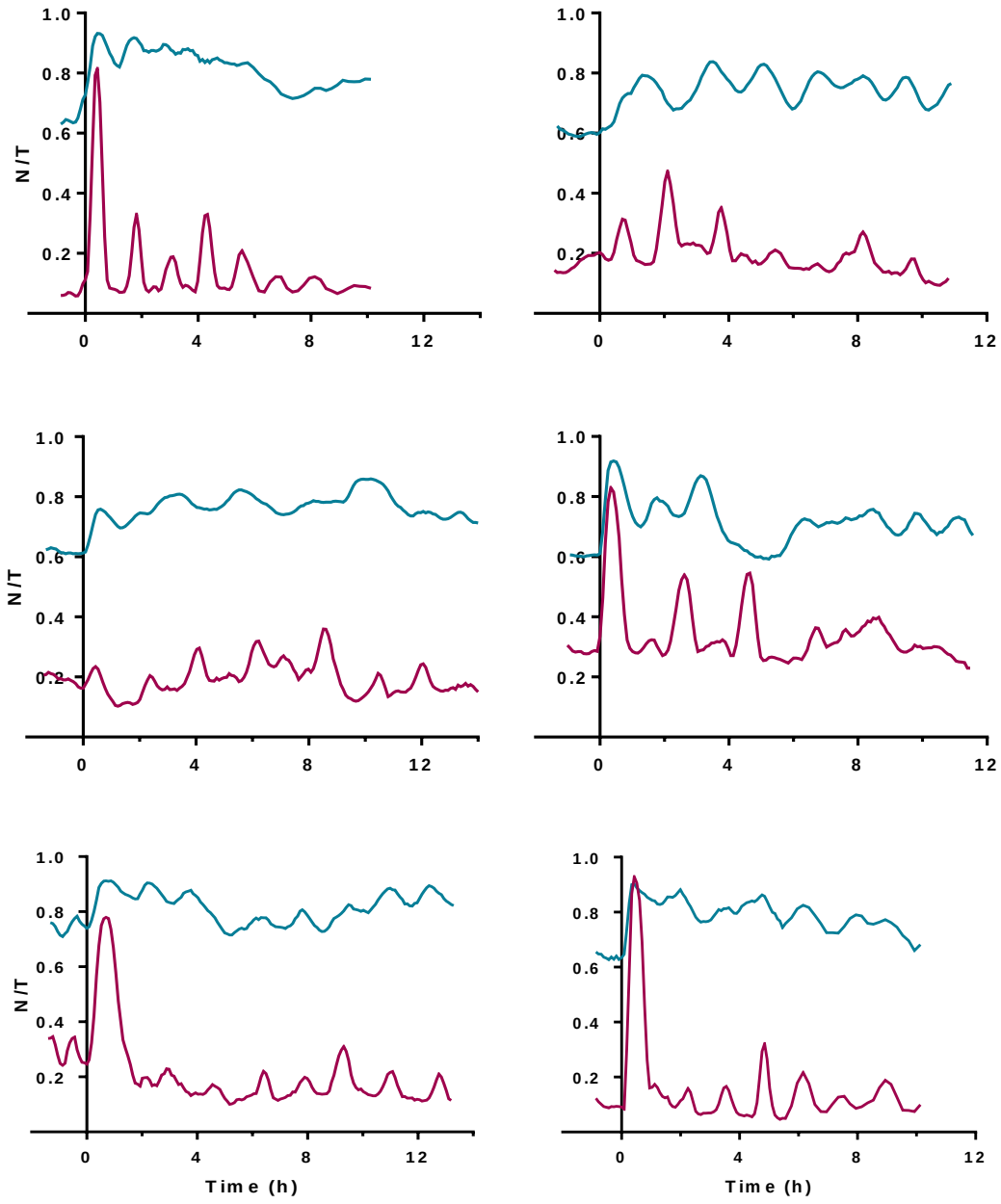

Figure 5.6: Example Cell Traces for simultaneously co-stimulated HepG2 cells co-expressing STAT3 and p65. Treated with 10 ng/ml TNFa and 20 ng/ml IL-6. STAT3 = blue line, p65 = pink line.

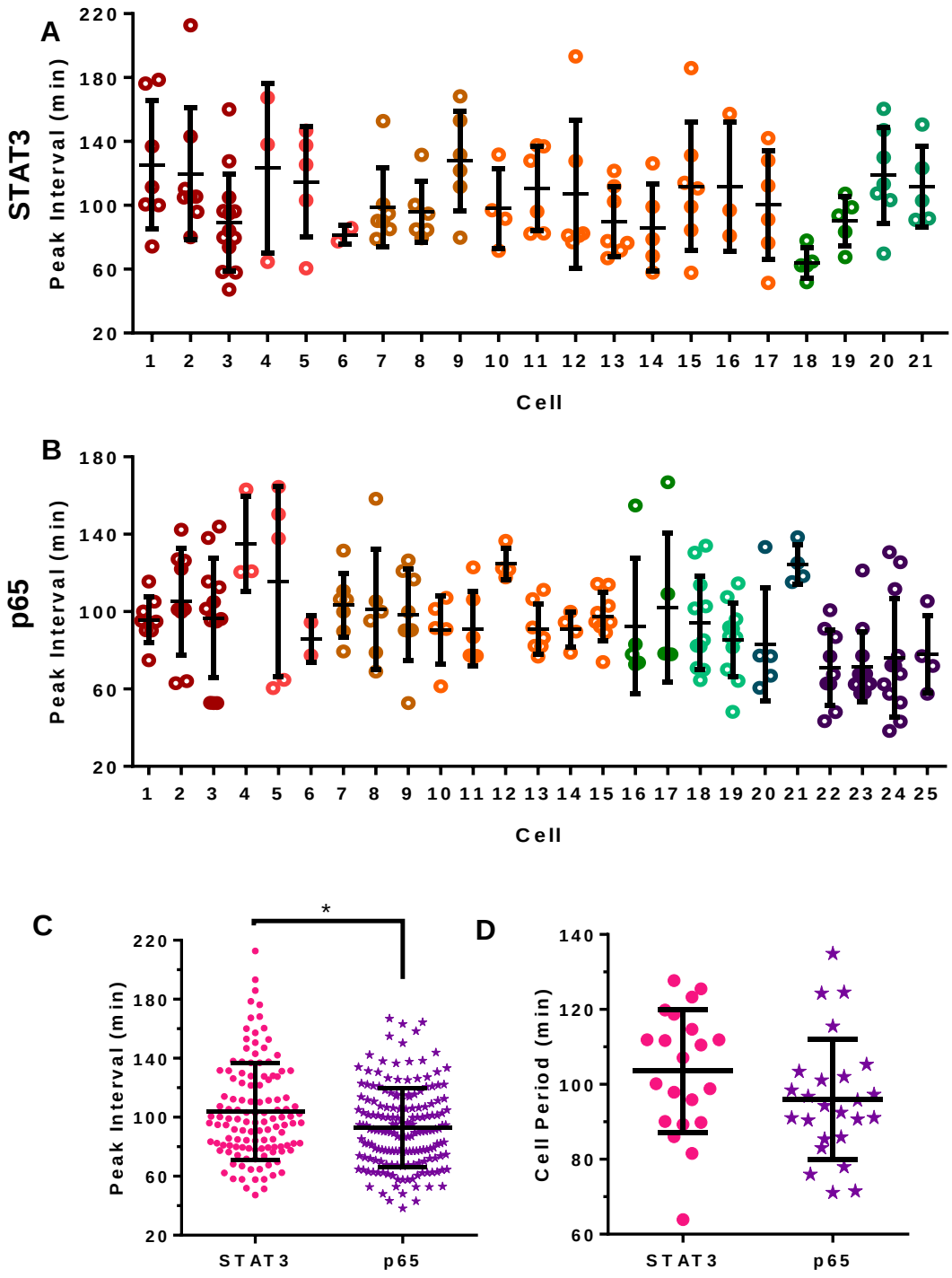

Figure 5.7: A) STAT3 and B) p65 Peak Intervals, C) pooled peak intervals and D) Cell Periods, for simultaneous IL-6 + TNFα co-stimulation of co-transfected HepG2 cells. 10 ng/ml TNFα and 20 ng/ml IL-6. **A, B)** Cells colour-coded by experimental replicate (A: n=6; B: n=8). Each circle represents one peak interval (A,B,C) or one cell period (D). Error bars represent mean cell period ± S.D. * = significantly different at P<0.95.

5.3.2.2 Comparison of IL-6 + TNFα Simultaneous Stimulation to Transfection and Stimuli Controls

The timings of p65 and STAT3 oscillations under IL-6 and TNFα simultaneous co-stimulation were compared to the single transcription factor, single stimulus data, and in the case of p65, to the IL-6+TNFα co-stimulated p65 cells and the TNFα stimulation of p65 and STAT3 co-expressing cells (Fig. 5.8 and 5.9).

There were no significant differences in the distributions of pooled peak intervals from all the p65 experiments (Fig. 5.8A and B). In all four experiments p65 oscillated with a mean peak interval frequency of approximately 98 min. When the cell periods were compared, no difference was found between the co-expression, co-stimulation p65 oscillatory period (96.0 $\pm$ 16.0 min, Fig. 5.7D) and the cells expressing only p65, whether TNFα or TNFα and IL-6 were applied. However, p65 was found to oscillate significantly faster ($P<0.05$) at 86.2 $\pm$ 9.0 min when co-expressed with STAT3 and stimulated with TNFα only, than under the other conditions. This was addressed in Section 5.2.1.5, in relation to Figure 5.5.

STAT3 oscillated more slowly when co-stimulated with IL-6 and TNFα and co-expressed with p65 than when expressed alone and stimulated with IL-6 (Fig. 5.9). The average period was 103.6 $\pm$ 3.6 (mean $\pm$ SEM) compared to 93.7 $\pm$ 2.4 min for STAT3 stimulated with IL-6, a significant difference of 9.9 $\pm$ 4.3 min, ($P=0.027$). The STAT3 period when co-expressed and co-stimulated was very similar to the p65 period from the same experiment (Fig. 5.7D), so it is possible that STAT3 oscillations were being slowed down by TNFα-induced p65 signalling.

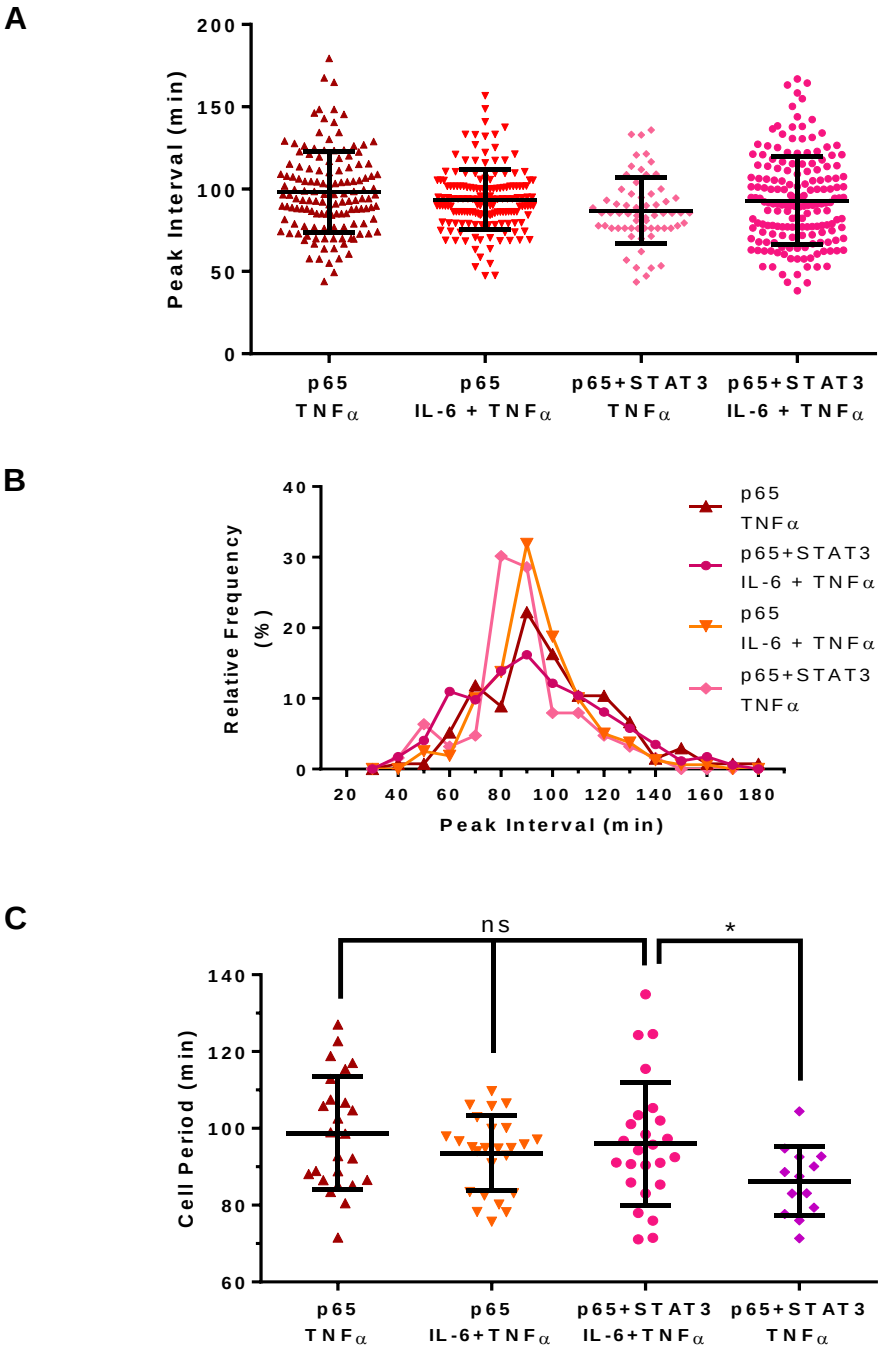

Figure 5.8: Comparison of TNFα Peak Intervals from IL-6+TNFα, co-transfected HepG2 cells to transfection and stimuli controls. **A** Pooled peak interval data with population mean ± S.D. by experiment. **B** Histogram of relative frequencies (%) of peak interval data by experiment. **C** Mean oscillatory period. Cell counts: p65+TNFα, n=25; p65, IL-6+TNFα, n=25; p65+STAT3, TNFα, n=13; p65+STAT3, IL-6+TNFα, n=25. Error bars = mean ± S.D. Two-tailed unpaired t-test with Welch's correction for unequal variance performed in Prism. * = significant at $P < 0.05$; 'ns' = not significant.

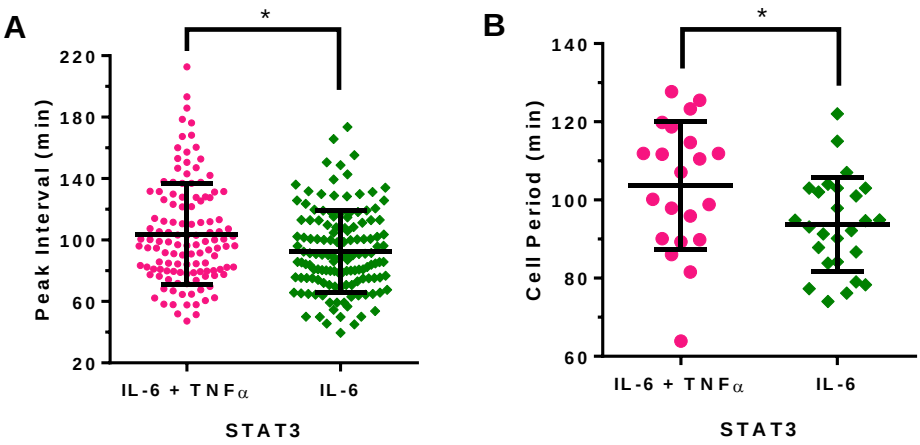

Figure 5.9: Comparing STAT3 data for simultaneous IL-6+TNFα stimulation of co-transfected HepG2 cells to IL-6-treated STAT3-transfected cells. A Peak interval data (mins). **B** Mean cell periods (min). Cell numbers: n=21 for IL-6+TNFα, STAT3+p65; n=26 for STAT3 + IL-6. Error bars = mean ± S.D. * = significant at $P < 0.05$. Statistical comparison performed in Prism using the Mann-Whitney test for peak intervals because data were non-parametric and the un-paired t-test for cell periods.

It is unfortunate that no data were obtained for the experiments of i) STAT3 alone co-stimulated with IL-6 and TNFα and ii) STAT3 co-expressed with p65 and stimulated with IL-6 only. This could have helped infer whether it was simply over-expression of p65 slowing down the STAT3 response, or whether it was an effect of oscillating TNFα-activated p65.

5.3.2.3 Studying Single Cell Effects on STAT3 and p65 Oscillations

Studying the effects on oscillation frequency at the sample population level suggested it was likely that p65 was affecting the period of STAT3. However, pooling the data masks effects at the single-cell level, even as it increases statistical power. Therefore the period of STAT3 and p65 oscillations were considered on a cell by cell basis (Fig. 5.10). First the mean period ± S.D. for STAT3 and p65 were plotted for each cell (Fig.5.10A).

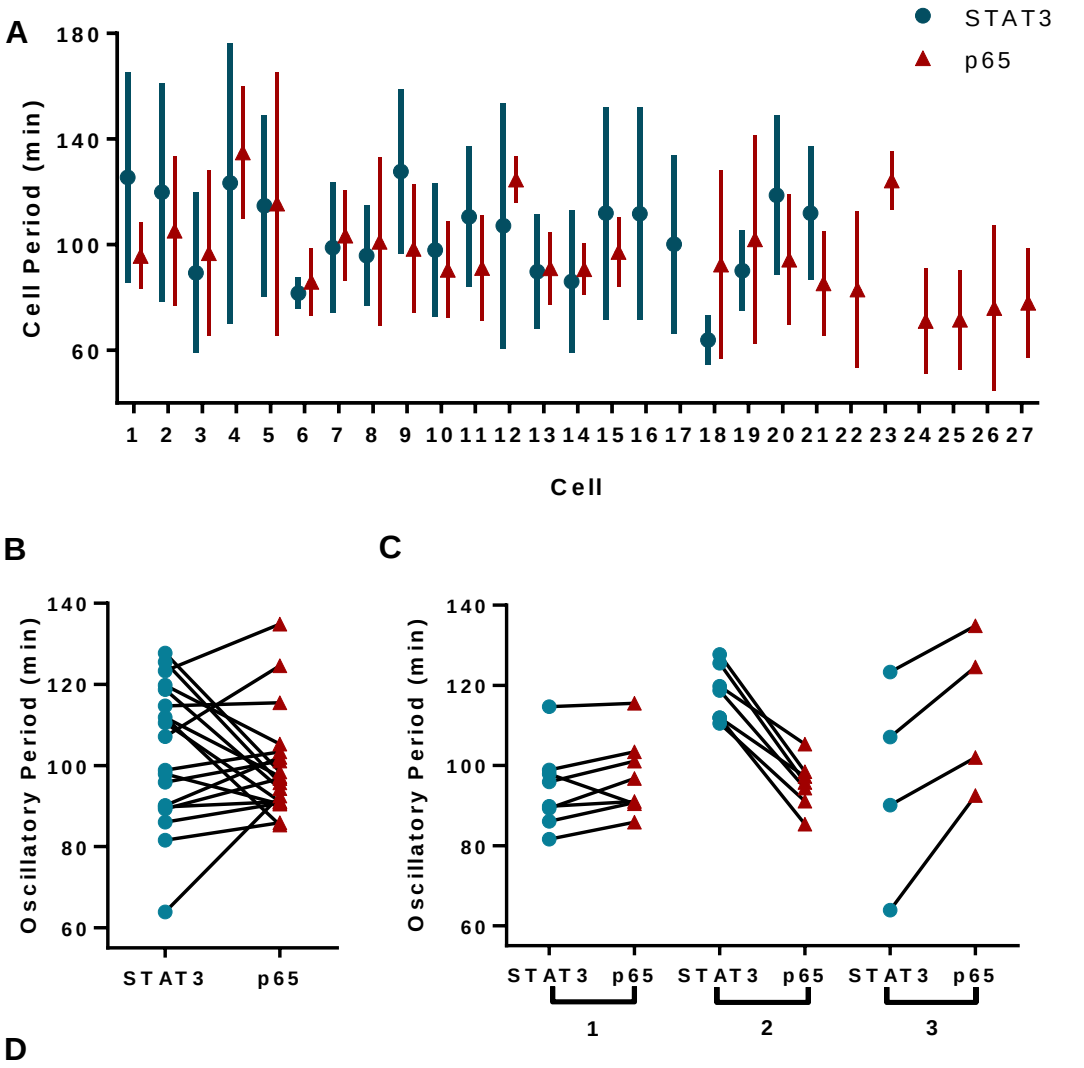

D

Group	1			2			3		
	Mean	SD	N	Mean	SD	N	Mean	SD	N
STAT3	94.3	10.2	8	118.0	6.9	7	96.1	25.4	4
p65	96.9	9.6	8	95.4	6.2	7	113.5	19.6	4

Figure 5.10: Mean Cell Periods for STAT3 and p65, paired by cell, for co-transfected, simultaneously co-stimulated HepG2 cells. 10 ng/ml TNFα and 20 ng/ml IL-6. Blue circle (STAT3) and red triangle (p65) = mean oscillatory period, error bars represent ± 1 S.D. **A** Mean ± S.D. period for STAT3 and p65 for each cell. **B** Linked STAT3 and p65 periods, n= 19 cells. **C** Cells split into groups according to characteristic features of the relationship between p65 and STAT3 periods. **D** Table of p65 and STAT3 mean period characteristics by group, time ± S.D. in mins.

From this, given the degree of variation, it was clear that there was not a simple correlation between p65 frequency and STAT3 frequency. The cell periods were plotted on a graph linking STAT3 and p65 together by cell (Fig. 5.10B). A by-eye analysis suggested that there might be a number of groups with different relations between p65 and STAT3 period. The magnitude and direction of the difference between the matched p65 and STAT3 periods were calculated. From this, three groups were identified: 1 – STAT3 oscillating slightly faster than p65; 2 – STAT3 oscillating markedly slower than p65; 3 – STAT3 oscillating markedly faster than p65 (Fig. 5.10C).

The mean STAT3 and p65 periods were calculated for each group (Fig. 5.10D). Whereas in Groups 1 and 2, p65 was oscillating close to it's 'basic' TNF-α frequency of 99 min, in Group 3 it oscillated approximately 14 min slower. In Group 1, STAT3 also oscillated at its 'basic' frequency of approx. 94 min. In Group 2, STAT3 oscillated approx. 25 min slower than STAT3 expressed alone and stimualted with IL-6. The average frequency in Group 3 was close to the 'basic' frequency but the variation was much larger.

In summary, in Group 1 both STAT3 and p65 oscillate as though they were expressed and stimulated alone. In Group 2, p65 likewise oscillated as though expressed and stimulated alone, however, STAT3 was slowed considerably. Group 3 was the inverse of Group 2, in that STAT3 oscillated as per STAT3+IL-6 and p65 was considerably slowed down, but in addition the variation between cells was greater. More widely, looking at the relationship between STAT3 and p65 signalling cell-by-cell revealed that there is not a simple, direct cross-talk effect betewen STAT3 and p65 when both are activated simultaneously within a cell. Rather there are at least three different possible outcomes for the relationship beween the two transcription factors. These different dynamic behaviour subsets were masked by the analysis performed on the pooled data sets for p65 and STAT3.

The number of cells was enough to identify the relationships described here, although it was not large enough for a thorough statistical analysis. In addition, the grouping analysis here was performed manually based on a visual inspection of the data. Ideally, a prinicple component analysis would be

performed on a larger set of cells to test the identified groups. For example, it is possible that Group 1 contains some cells that do not quite fit the group definition but which definitely do not belong in either group 2 or 3. With more cells for analysis, the groupings applied to the data set should be be more definitive.

This data raises several interesting questions about what the mechanisms of interaction are that enable the different dynamic relationships to emerge, what the biological differences are that result in the different oscillatory regimes and whether the biological outcomes differ between the groups. Group 1 also raises the question of whether STAT3 and p65 in these cells are oscillating at extremely similar frequencies because they have become entrained by each other, or whether they are acting completely independently and are oscillating at their 'basic' frequencies. To address this possibility, inhibitors that act at different points in the two signalling pathways could be used to identify differences between the groups of cells.

5.3.2.4 Staggered Co-Stimulation

To ascertain whether STAT3 and p65 were affecting each others' oscillatory dynamics, the cells were stimulated with a 45 min delay between the IL-6 and TNFα. Under this 'staggered stimulus' protocol, the first nuclear peaks of STAT3 and p65 were not synchronised (Fig. 5.11). Rather, STAT3 responded with a nuclear translocation within 30 min of IL-6 stimulation, then p65 translocated to the nucleus approximately 30 min after the addition of TNFα, giving a gap between their peaks of 35 min. It was difficult to determine the exact intervals between subsequent STAT3 and p65 nuclear peaks, due in part to the broad curves of the STAT3 peaks. Therefore STAT3 and p65 peaks were determined separately using the Peak Detection spreadsheet tool as before, and the population characteristics calculated independently (Fig. 5.12).

The variance between STAT3 and p65 peak intervals by cell appeared to be quite large (Fig. 5.12A and B respectively). When the peak intervals were pooled (Fig. 5.12C) and the populations analysed using to D'Agostino & Pearson omnibus normality test in Prism, the STAT3 peak intervals were normally distributed but the p65 peaks were not. The medians of the data sets were not

quite significantly different (Mann-Whitney test, P = 0.06). Comparison of the mean cell periods found that while p65 oscillated with a period of 84.7 ± 6.7 min, and STAT3 oscillated at 91.4 ± 17.5 min, the difference of 6.7 min was not significant (t-test with Whelch's correction for unequal variance) (Fig. 5.12D). However the difference in the variance of the data sets was significant, with the p65 data spread being much more compact (P<0.01).

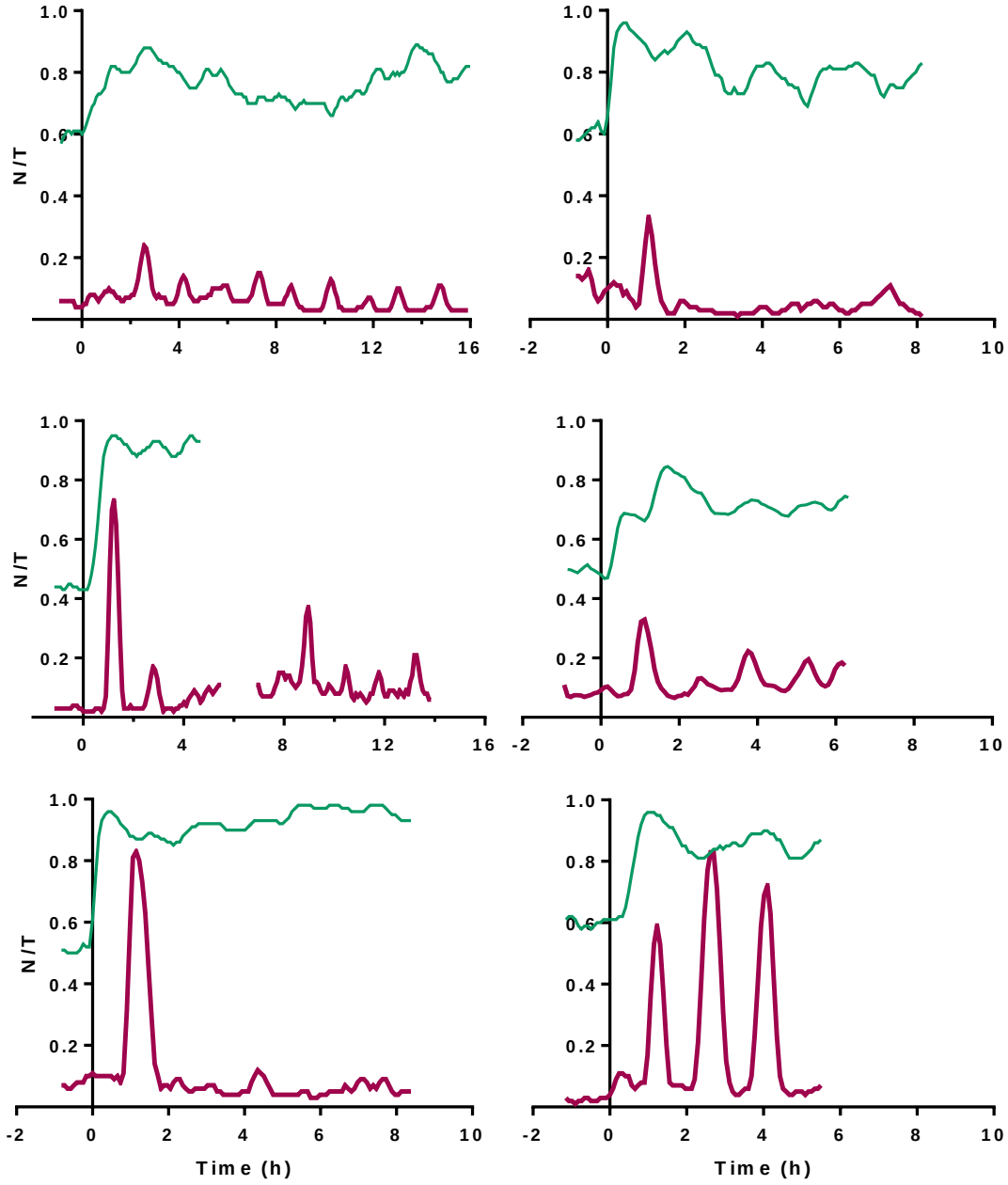

Figure 5.11: Example Cell Traces for co-transfected STAT3 and p65 HepG2 cells, staggered co-stimulation with 10 ng/ml TNFa and 20 ng/ml IL-6. STAT3 = green line, p65 = pink line.

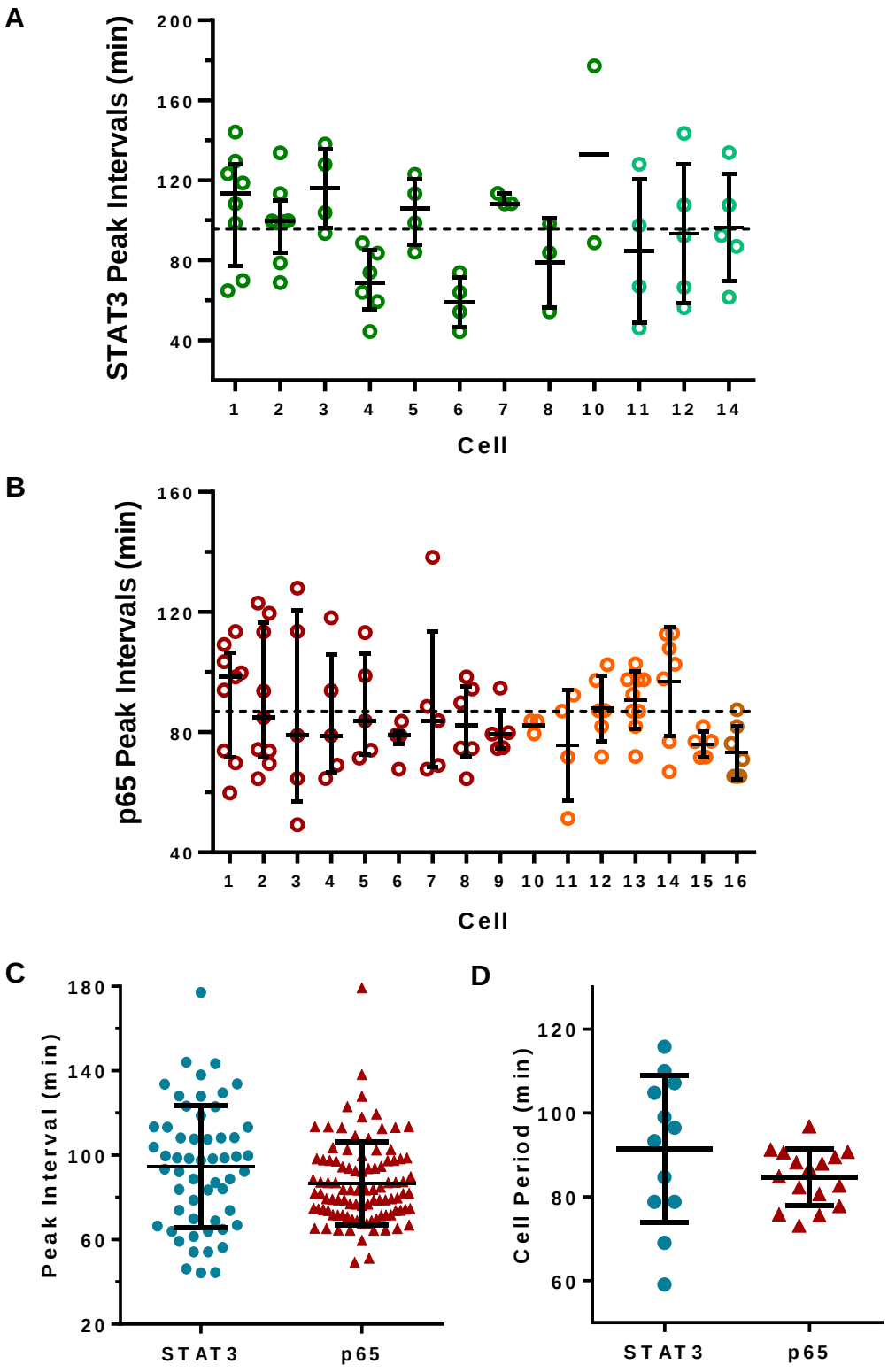

Figure 5.12: A) STAT3 and B) p65 Peak Interval Data, C) Pooled Interval and D) Cell Period data from co-transfected HepG2 cells, staggered co-stimulation with 10 ng/ml TNFα and 20 ng/ml IL-6. Cells colour-coded by experimental replicate (A: n=14; B: n=16). Each circle represents one peak interval (min). Error bars represent mean cell period ± S.D.

5.3.2.5 Comparing Staggered and Simultaneous Stimuli Protocols

Pooled p65 peak intervals from the staggered stimuli protocol were not found to be significantly different to TNFα alone or simultaneous IL-6 and TNFα on p65 and STAT3 co-transfected cells (Fig. 5.13 A). The STAT3 pooled peak intervals under the staggered protocol were not significantly different to the IL-6 stimulation of STAT3 transfected cells, or to the simultaneous stimulation of co-transfected cells (Fig. 5.13B). However, the simultaneous stimuli protocol was different ($P<0.05$) to the IL-6 stimulation of STAT3 alone (Fig. 5.13B).

A similar comparison was performed for the mean cell periods (Fig. 5.14). Although the pooled intervals were not significantly different for p65, the mean cell periods of the simultaneous and staggered stimuli conditions were significantly different ($P = 0.02$) (Fig. 5.14A). When p65 was stimulated 45 min after IL-6, it oscillated at 85.2 ± 2.6 min (mean $\pm$ SEM, N=16 cells), compared to 96.0 ± 3.2 min (Mean $\pm$SEM, N=25 cells) when stimulated simultaneously.

STAT3 oscillated 12.3 min faster under the staggered stimuli protocol than when simultaneously stimulated, however this did not quite reach significance ($P = 0.06$). The oscillation frequencies were: 91.4 ± 5.0 min (Mean $\pm$SEM, N=12 cells) for staggered stimuli vs. 103.6 ± 3.6 min (Mean $\pm$SEM, N=21 cells) for simultaneous stimulation.

Considering the STAT3 and p65 mean cell periods from the simultaneous and staggered stimuli protocols together, in both conditions a general trend of p65 oscillating faster than STAT3 could be seen. In addition, when the stimuli were staggered, both STAT3 and p65 oscillated faster than when the stimuli were added simultaneously. In both conditions the difference between STAT3 and p65 oscillation frequency verged on being significant; it is likely that with more cells for the staggered stimuli protocol (there were half as many cells available as for the simultaneous co-stimulation), that these differences would reach significance.

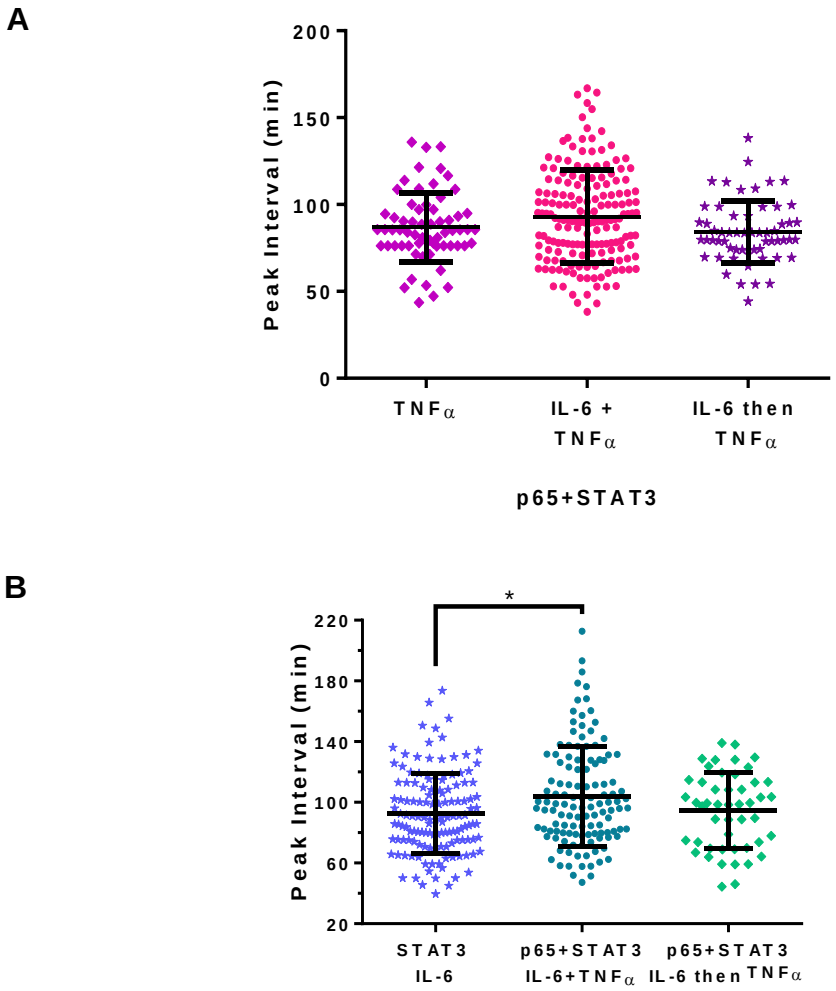

Figure 5.13: Comparing simultaneous and staggered co-stimulation Peak Intervals to single stimuli experiments. Pooled peak intervals with population mean ± S.D, by experimental condition. **A** p65 data for p65+STAT3 co-transfected cells, comparing simultaneous and staggered co-stimulation to TNFα alone. **B** STAT3 data for p65+STAT3 co-transfected cells, comparing simultaneous and staggered co-stimulation to STAT3 transfected cells, stimulated with continuous IL-6.

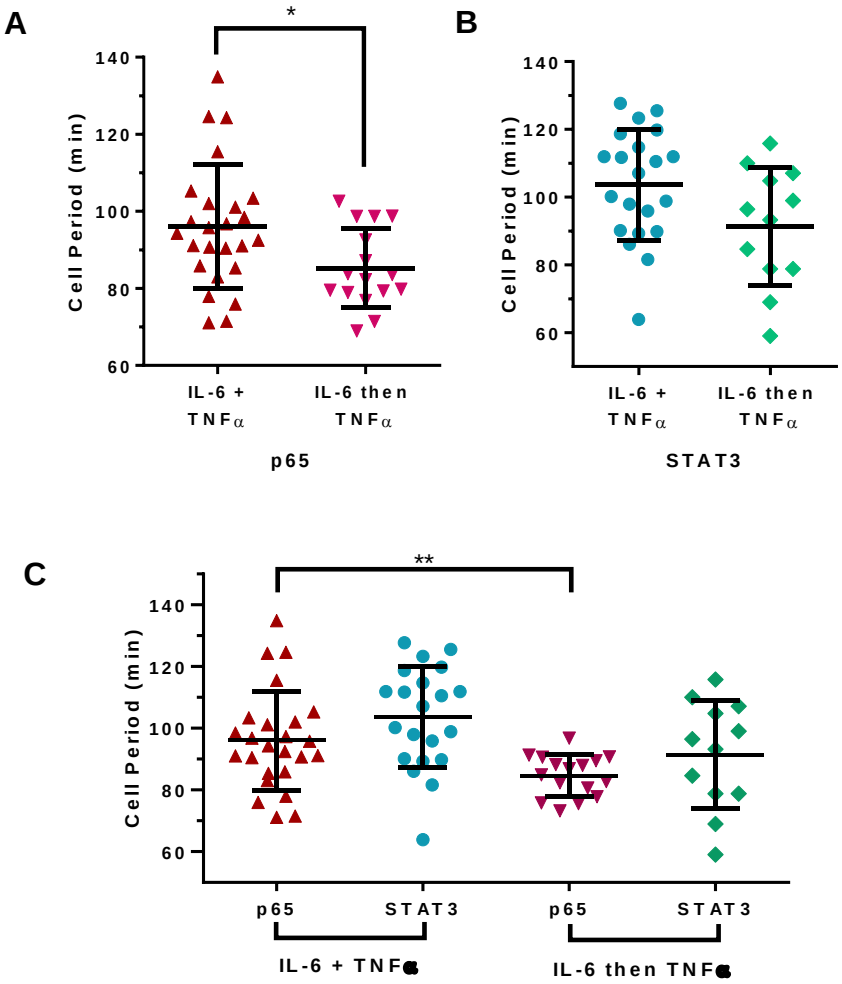

Figure 5.14: Cell Periods for A) p65 and B) STAT3 treated simultaneously (IL-6+TNFα) or staggered (IL-6 then TNFα), and combined in C). Error bars represent Mean ± S.D. * = P<0.05. ** = P<0.01.

5.3.2.6 Comparing Co-Stimulation Protocols to Single Stimuli and Transfection Controls

The co-stimulation protocols were compared to the single stimulus and transfection control experiments (Fig. 5.16). In general there appeared to be two main oscillation frequencies for p65 (Fig. 5.16A). TNFα alone and TNFα+IL-6 stimulation of p65 alone, and the simultaneous TNFα+IL-6 stimulation of p65 and STAT3 co-transfected cells, all oscillated at 96.0 min. On the other hand, STAT3 and p65 co-transfected cells, stimulated with TNFα alone, or with IL-6 followed by TNFα 45 min later oscillated 11 min faster, at 85.6 min.

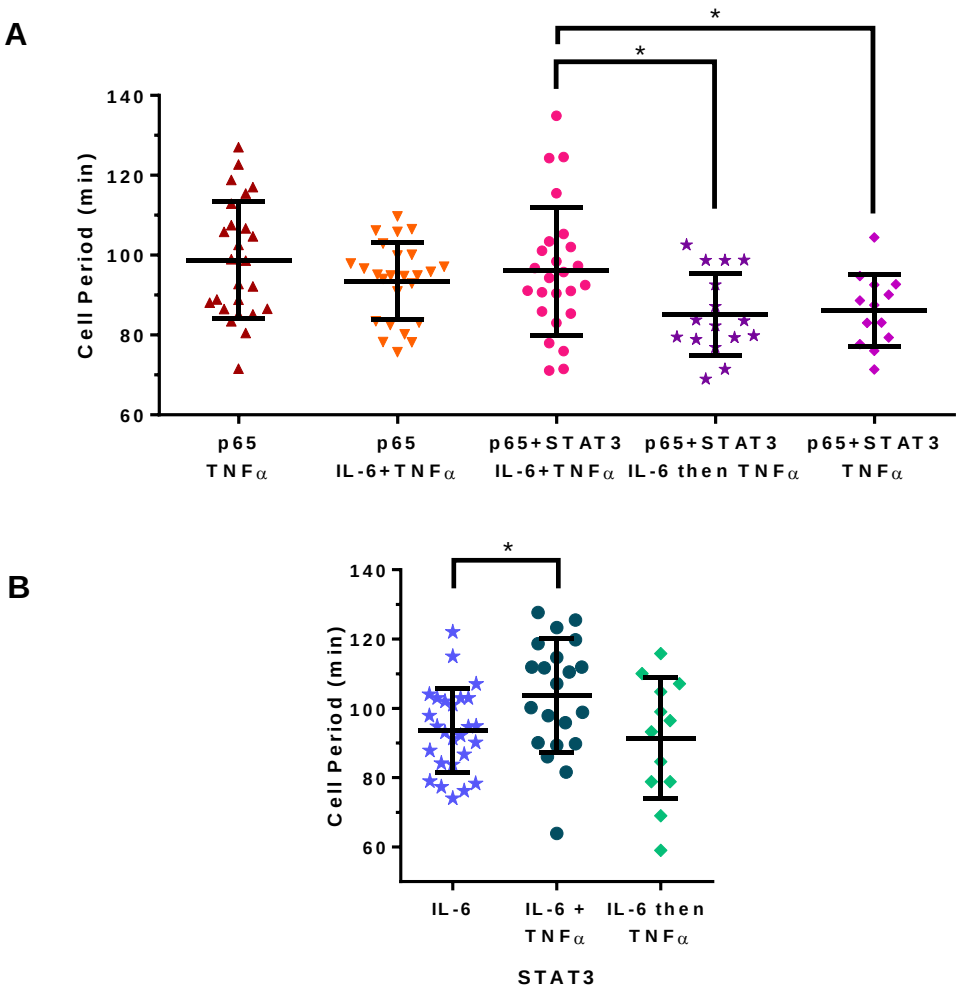

Figure 5.15: Comparing A) p65 and B) STAT3 oscillations under simultaneous and staggered co-stimulation conditions to all controls. Error bars represent Mean ± S.D. * = P<0.05.

This suggests that the difference between these two groups may be due to the availability of STAT3 when over-expressed. It is not a case of simple STAT3 over-expression because otherwise the co-transfected, simultaneously

stimulated p65 could have been expected to oscillate at the same speed as the co-transfection with TNFα experiment and the staggered stimuli experiment. Instead it oscillated at the same speed as the p65 alone experiments. It could be imagined that when STAT3 is over-expressed and activated by IL-6, there is less STAT3 available to affect p65 signalling. Instead, when it is not activated (co-transfected with TNFα only stimulation), or is activated at a different time (co-transfection, staggered stimulation), STAT3 is able to affect the oscillation frequency of p65. In order to test this, it would be necessary to express p65 alone then perform the staggered stimuli protocol. If the phenomenon was the effect of over-expressing STAT3, then the p65 alone, staggered stimuli experiment should oscillate at the same speed as p65 alone with TNFα and IL-6. If it were a direct effect of delaying the stimuli so the systems are asynchronous, then p65 should oscillate at the faster speed of 86 min.

STAT3 also displayed two main oscillation frequencies. STAT3 expressed alone and stimulated with continuous IL-6 oscillated at 93.7 $\pm$ 2.4 min, whilst STAT3 co-expressed with p65, and subjected to the staggered stimulus protocol oscillated at 91.4 $\pm$ 17.5 min, which was not different to STAT3+IL-6. Meanwhile, STAT3 co-expressed with p65 and simultaneously stimulated with IL-6 and TNFα oscillated considerably slower than these, with an oscillation frequency of 103.6 $\pm$ 16.4 min. Unfortunately, due to the lack of control data, particularly co-expressed STAT3 with IL-6 stimulation alone, it is not possible to make many deductions or inferences about the possible cause of these differences. It is unlikely to be a simple over-expression artefact, otherwise it would be expected that STAT3 under both the simultaneous and staggered stimuli protocol would oscillate at a similar, slower speed. Instead the results seem to suggest that initiating STAT3 signalling first through the application of IL-6 prior to the addition of TNFα allows the STAT3 signalling to occur independently of TNFα-p65 signalling, even once p65 signalling has started.

This is different to the behaviour of p65, which seems to be partially influenced by the over-expression of STAT3. It is interesting to note that the two systems, p65 and STAT3, are affected differently by the presence of the other system, which gives some indication of the complexity of their emergent dynamics.

5.3.2.7 Staggered Stimuli - Single Cell Effects on STAT3 and p65 Oscillations

The cells from the staggered stimuli protocol were analysed as per the simultaneous stimuli protocol, in Section 5.2.2.3. As with the simultaneous stimulation, it was clear from the paired STAT3 and p65 oscillatory periods (Fig. 5.15A), that there was no direct correlation between the average periods of STAT3 and p65. Linking the cells and considering the magnitude and direction of the difference between STAT3 and p65 periods (Fig. 5.15B) however did not reveal any obvious groupings because there were too few cells.

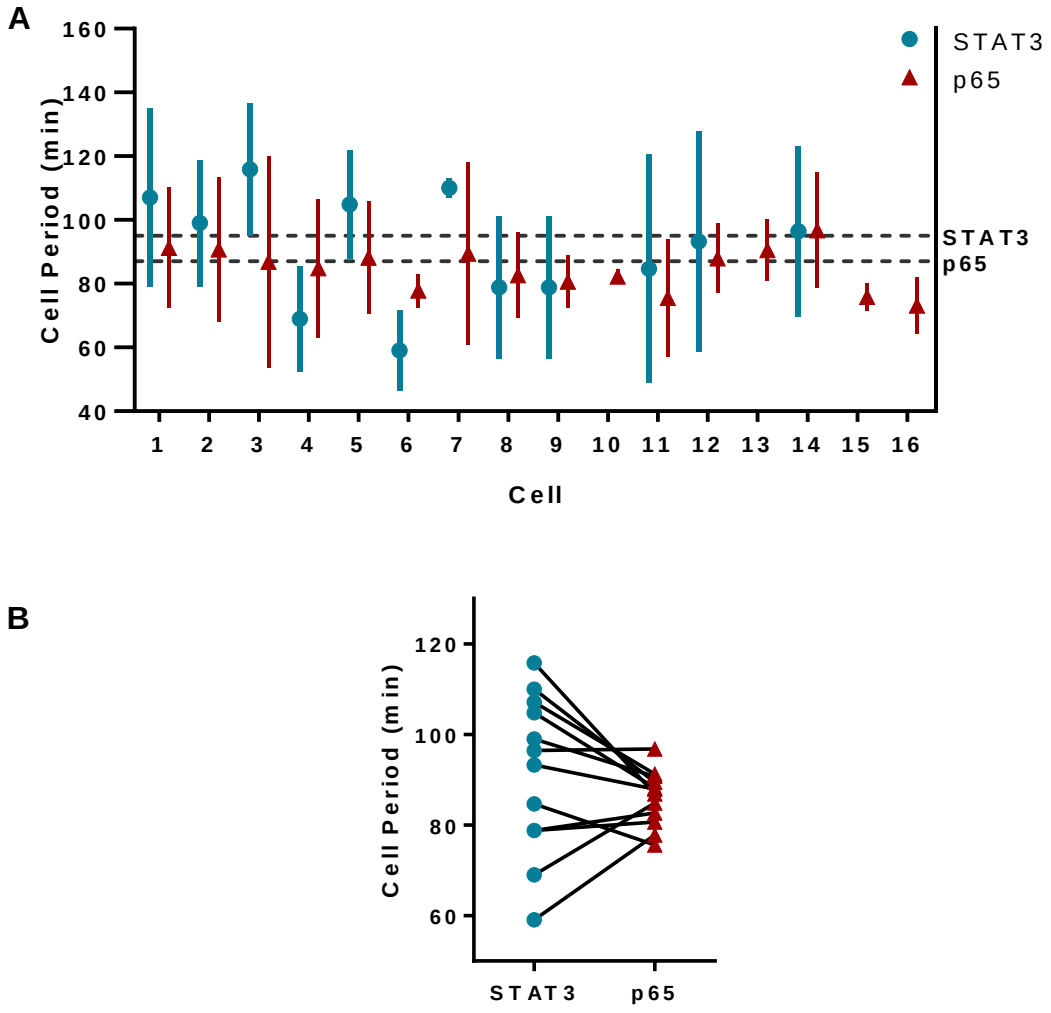

Figure 5.16: Mean Cell Periods for STAT3 and p65, paired by cell, for co-transfected, staggered co-stimulation HepG2 cells. 10 ng/ml TNFα and 20 ng/ml IL-6. Blue circle (STAT3) and red triangle (p65). **A** All cells with mean oscillatory period, error bars represent ± 1 S.D. Dashed lines indicated mean period for STAT3 and p65. **B** Cell periods paired by cell. N= 14 cells.

5.3.3 Summary of TNFα and IL-6 Co-Stimulation Experiments

This section of the chapter on the cross-talk between STAT3 and p65 when stimulated with IL-6 and TNFα demonstrates that the oscillatory period of the two signalling systems are more variable than suspected and that they can relate to each other in different ways. For example co-expressing STAT3 and p65 and stimulating simultaneously with IL-6 and TNFα slows down STAT3 oscillations whereas the p65 oscillatory period is unaffected on average. On the other hand, co-expressing p65 and STAT3 and stimulating them with IL-6 and delaying TNFα stimulation for 45 min allows STAT3 to oscillate at its 'primary' frequency yet speeds up p65 oscillations until they are faster than STAT3 on average. There also appear to be some complex effects on the frequency of p65 from over-expressing STAT3. Another important observation is that considering the behaviours of individual cells is critical for detecting complex and conflicting effects at the single cell level that are otherwise masked by population averages. For example, the different relationships between p65 and STAT3 oscillations in response to simultaneous stimulation.

5.4 IL-6 plus TNFα Simultaneous Co-stimulation Gene Expression Study

To gain a deeper understanding of the STAT3 and NF-κB dynamics in response to IL-6 and TNFα cross-talk, mRNA expression of a set of target genes was evaluated. Building on the continuous IL-6 mRNA expression study presented in Section 4.3, continuous TNFα and IL-6 plus TNFα stimuli were investigated. The previously selected STAT3 pathway and APR genes were included, as were three feedback genes for TNFα signalling, i.e. IκBα, IκBε and A20. The experimental and data analysis methods were as per Section 4.3, and the stimuli used were a) 20 ng/ml IL-6, b) 10 ng/ml TNFα and c) 20 ng/ml IL-6 plus 10 ng/ml TNFα. The pulsing protocol was not used, nor was the staggered stimuli protocol, consequently the results presented below are only relevant to the simultaneous IL-6 plus TNFα co-stimulation experiments.

The genes for the IL-6 receptor components i.e. IL6R and gp130 did not differ between stimulation protocols (Fig. 5.17). However the IL-6 responsive genes, STAT3, SOCS2 and SOCS3, were similar in that they responded to IL-6 alone and to IL-6 plus TNFα stimulation but not TNFα alone. Furthermore, SOCS3 had a weaker first peak under co-stimulation and did not maintain a lower sustained level after the initial wave of induction. STAT3 did show a sustained increase under co-stimulation but at a slightly lower level than for IL-6 alone (Fig. 5.17). These results suggest that TNFα co-stimulation dampens the response of certain IL-6 responsive genes slightly but does not eliminate the response all together.

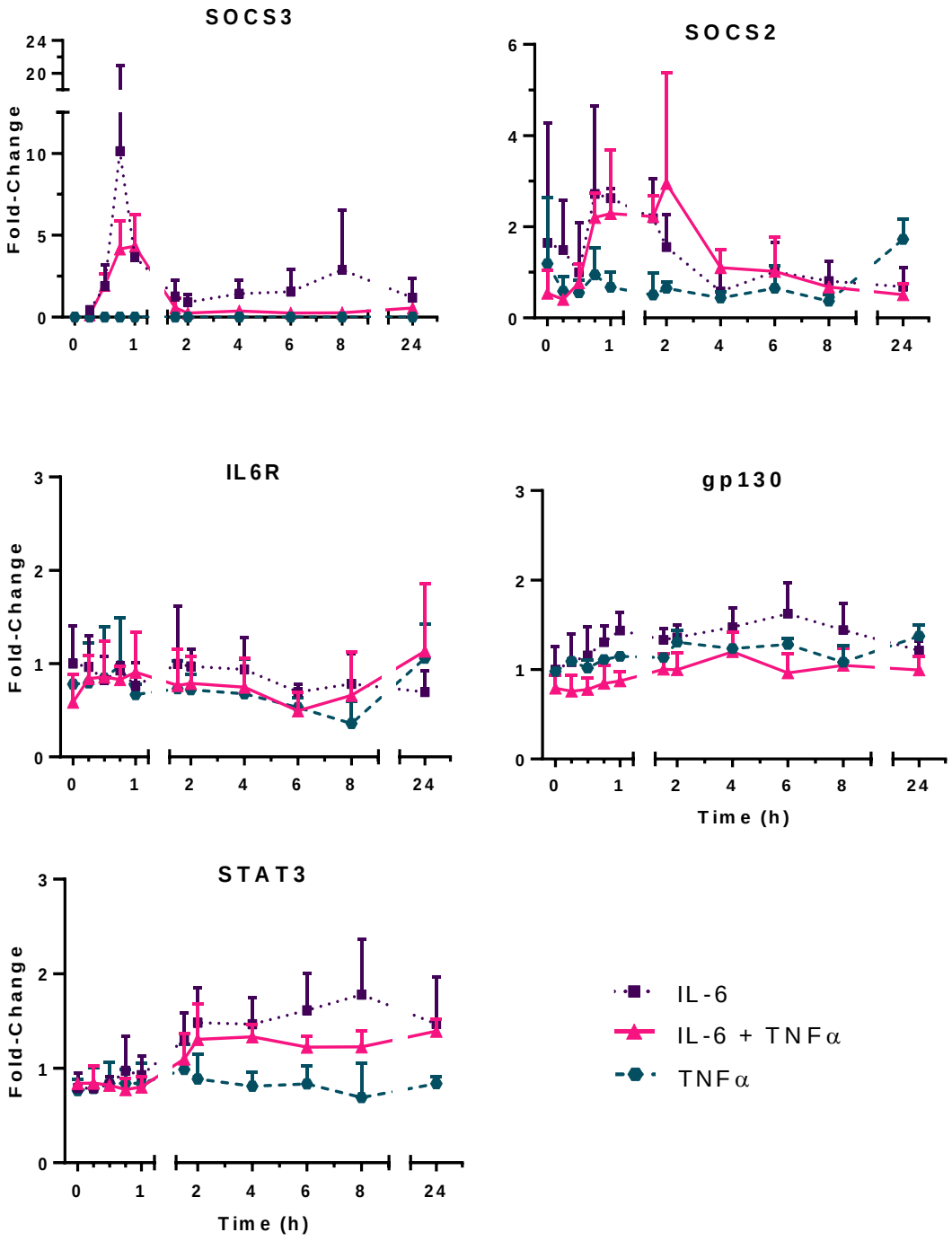

Figure 5.17: IL-6 Signalling and Feedback Genes. SOCS3, SOCS2, IL-6Receptor, gp130 and STAT3. HepG2 cells treated with continuous 20 ng/ml IL-6 (purple square, dotted line), continuous 10 ng/ml TNFα (teal hexagon, dashed line) or 20 ng/ml IL-6 with 10 ng.ml TNFα (pink triangle, solid line). Mean ± SEM, from N=3 independent replicates.

A similar effect was seen for the APR gene Hepcidin. Its initial response within the first 2 h was the same under both IL-6 and IL-6 plus TNFα but subsequently decreased faster under IL-6 plus TNFα than IL-6 alone (Fig. 5.18). On the other hand, γ-fibrinogen responded to IL-6 alone but was inhibited by TNFα even in combination with IL-6. Serum amyloid A was different to both γ-fibrinogen and hepcidin in that it could only be induced by IL-6 plus TNFα co-stimulation in HepG2 cells.

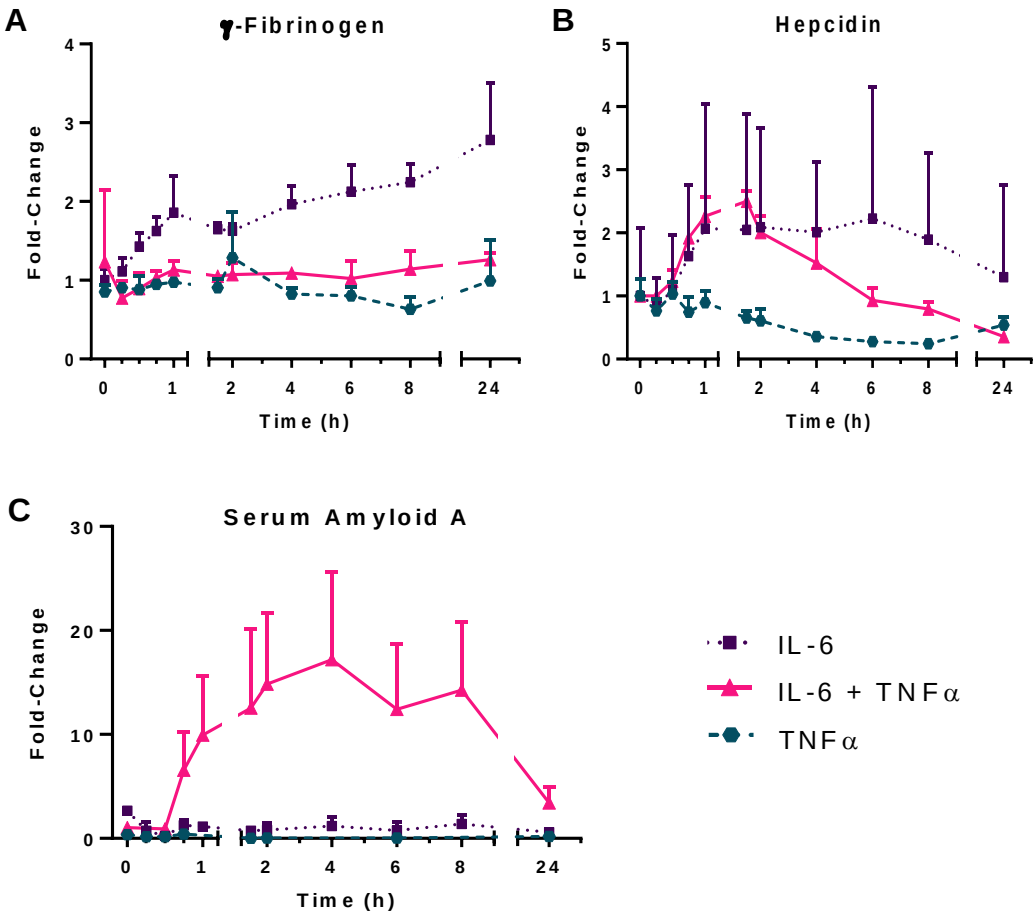

Figure 5.18: Acute Phase Response Genes. A γ-Fibrinogen**, B** Hepcidin, **C** Serum Amyloid A. HepG2 cells treated with continuous 20 ng/ml IL-6 (purple square, dotted line), continuous 10 ng/ml TNFα (teal hexagon, dashed line) or 20 ng/ml IL-6 with 10 ng.ml TNFα (pink triangle, solid line). Mean ± SEM, from N=3 independent replicates.

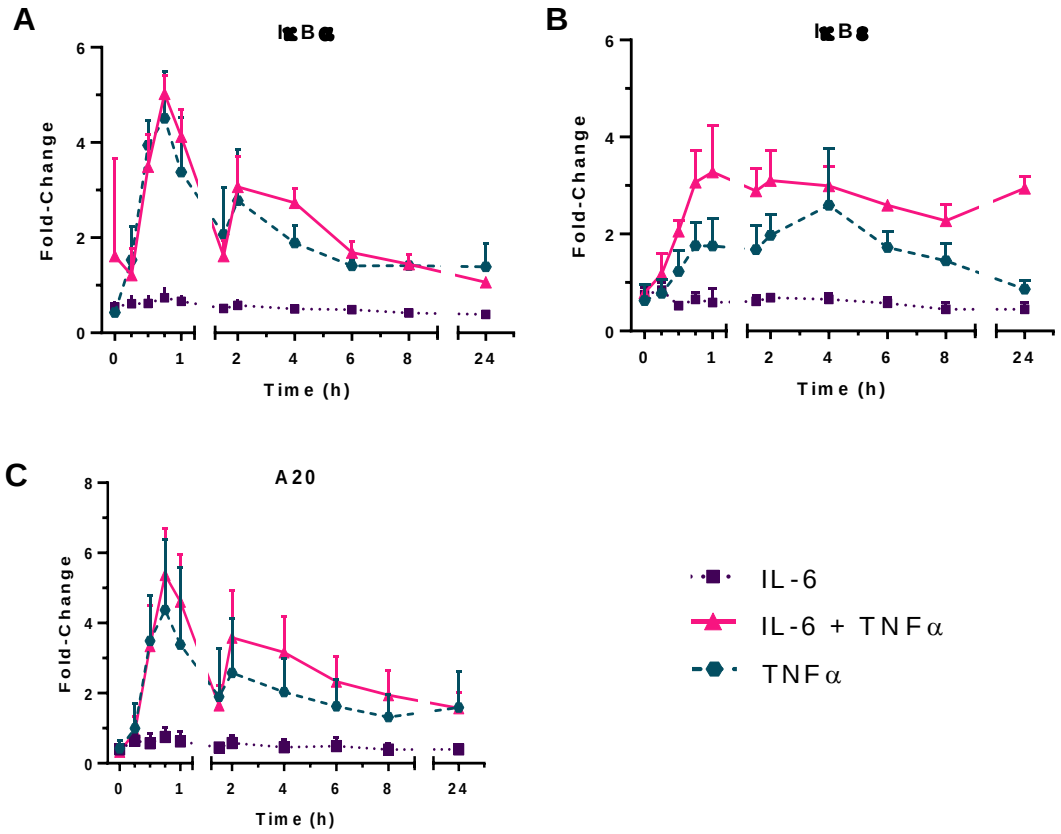

Figure 5.19: NF-κB Feedback loop genes. A IκBα, **B** IκBε, **C** A20. HepG2 cells treated with continuous 20 ng/ml IL-6 (purple square, dotted line), continuous 10 ng/ml TNFα (teal hexagon, dashed line) or 20 ng/ml IL-6 with 10 ng/ml TNFα (pink triangle, solid line). Mean ± SEM, from N=3 independent replicates.

The NF-κB feedback genes all responded similarly in that they responded to both TNFα alone and in conjunction with IL-6 but did not respond to IL-6 alone. The IκBα response had the same magnitude and timing for both TNFα alone and with IL-6 whereas both A20 and IκBε responded more strongly to the co-stimulation than TNFα alone. The difference for A20 was slight, and more pronounced between 2 and 6 h. IκBε was more strongly induced within 45 min of being co-stimulated and remained high for the duration of the time-course whereas under TNFα alone it dropped towards the baseline by 24 h.

5.5 IL-6 and IL-1β-Induced STAT3 and p65 Cross-Talk

IL-1β is another activator of the Acute Phase Response in hepatocytes. In addition to activating NF-κB/p65 signalling, it down-regulates IL-6 signalling via STAT3 by increasing degradation of phosphorylated gp130 (Radtke et al, 2010). This finding suggested that IL-1β signalling could significantly perturb the IL-6-induced oscillatory STAT3 dynamics and perhaps affect p65 dynamics. To this end, p65 dynamics in response to IL-1β were investigated, both with and without STAT3 over-expression, and STAT dynamics in response to IL-6 plus IL-1β were investigated, using the same approach as for IL-6 plus TNFα co-stimulation.

5.5.1 IL-1β Oscillations are Faster than TNFα in HepG2 Cells

IL-1β stimulation of p65 transfected HepG2 cells gave the surprising result that p65 oscillated 23 min faster on average under IL-1β stimulation than in response to TNFα stimulation (Fig. 5.20). The median period was 76.7 min in response to IL-1β, which was significantly faster ($P<0.0001$) than for TNFα-induced p65 oscillations. In this instance, due to data having a significantly non-parametric distribution, the medians and interquartile ranges are presented instead of the mean $\pm$ SD, and the medians were compared using the Mann-Whitney test in Prism. This result was unexpected because in the SK-N-AS cell line p65 oscillates at the same frequency in response to TNFα and IL-1β (Adamson, unpublished observations).

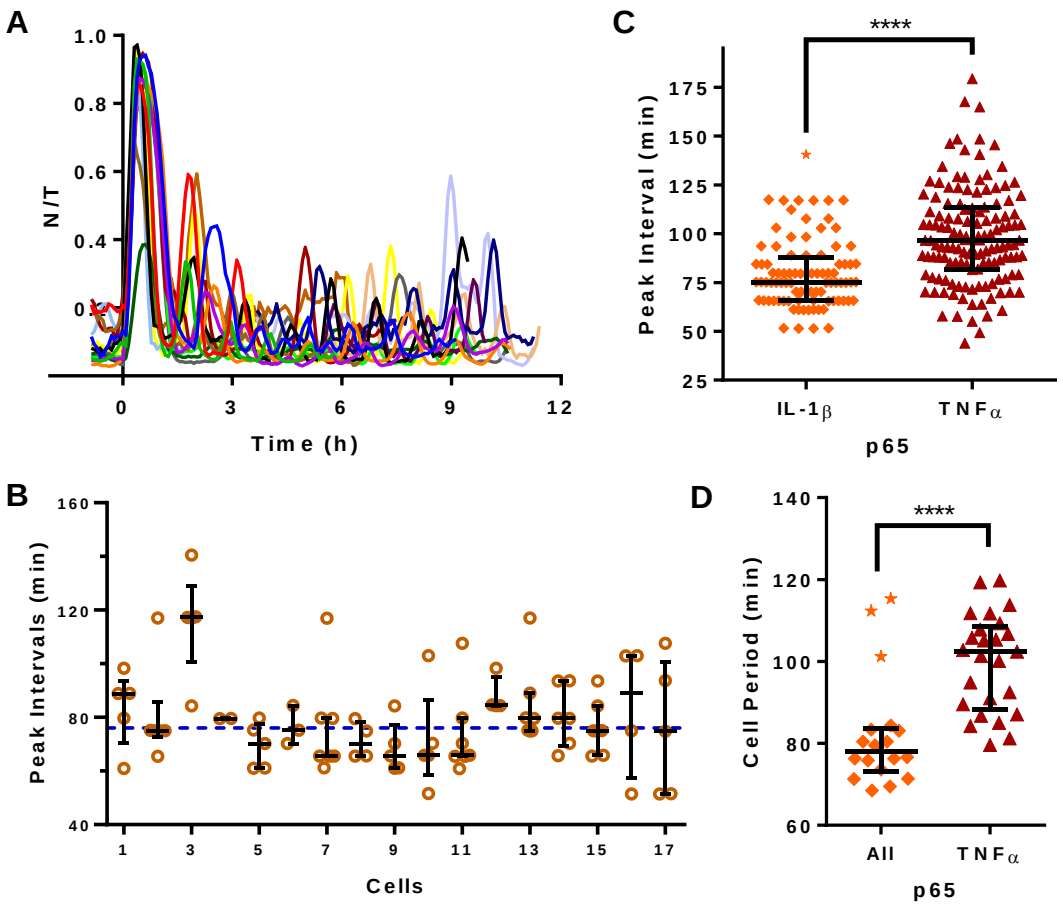

Figure 5.20: Results from p65-transfected HepG2 cells, stimulated with 10 ng/ml IL-1β, compared to 10 ng/ml TNFα stimulation. **A** p65 cell traces, n = 18 cells. **B** Median cell peak intervals by cell (n=17 cells, n= 1 experiment). Each circle represents one peak interval (min), n= 85 peaks. Dashed horizontal line represents the median of individual cell periods. **C** Pooled peak intervals (min) from all cells. **D** Individual median cell periods (min). Error bars show median with interquartile range. Data points represented by stars are outliers. Statistical comparison using Mann-Whitney test; **** = P<0.0001.

5.5.2 Effect of STAT3 Over-Expression on IL-1β Signalling

The effect of over-expressing STAT3 in HepG2 cells on IL-1β-induced p65 oscillations was assessed as for TNFα-induced oscillations (Fig. 5.21). Over-expression of STAT3 significantly slowed IL-1β-induced oscillations by 7.5 min, giving a median cell period of 84.0 min (Mann-Whitney test, exact P-value 0.015) (Fig. 5.22 A and B). Also of note is the cell with a doubled first peak where p65 does not rapidly exit the nucleus (Fig. 5.21A).

STAT3 over-expression also appeared to decrease intercellular heterogeneity of IL-1β-induced p65 oscillations in HepG2 cells. Visual comparison of the population means $\pm$ SD of individual cell traces for p65 alone to p65 with STAT3 transfected cells seemed to suggest that the nuclear translocations were more synchronous across the population from the second peak onwards when STAT3 was co-expressed with p65 (Fig.5.22C). Whilst the number of cells was comparatively small, there were a similar number of cells for each condition (17 vs. 18 cells). This suggests that it is not due to averaging vastly different number of cells. To test this further and with statistical significance, more cells should be imaged and analysed. A power calculation could be performed to indicate approximately how many cells would need to be analysed. To test the observation of an apparent decrease in intercellular heterogeneity in the co-expression experiment would require advanced mathematical and statistical analysis beyond the scope of this project.

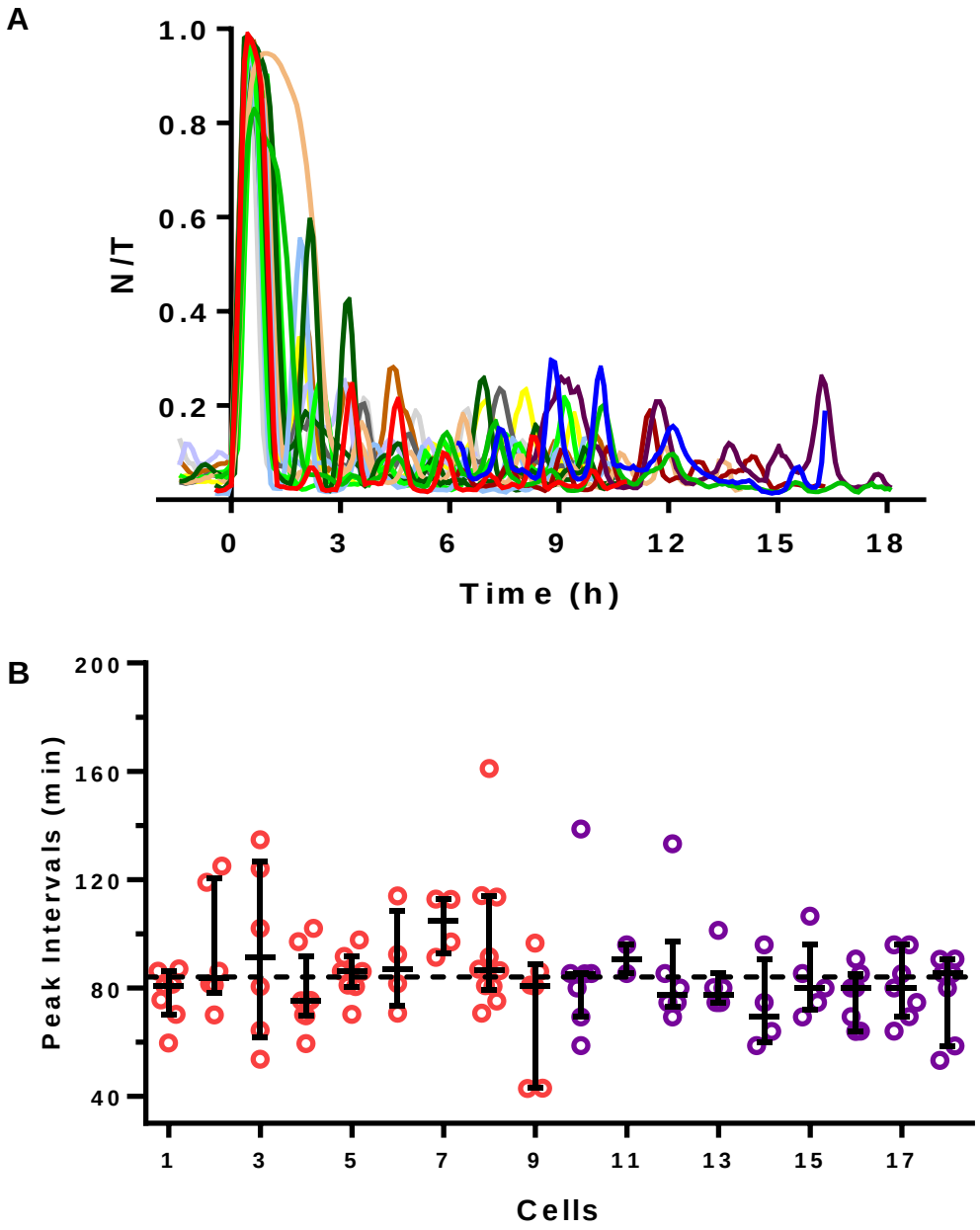

Figure 5.21: p65 Data from p65 and STAT3 co-transfected HepG2 cells, stimulated with 10 ng/ml IL-1β. A p65 cell traces, n = 18 cells. **B** Median cell peak intervals by cell (n=18 cells, n= 2 replicates). Each circle represents one peak interval (min), n= 87 peaks. Error bars represent median cell period with interquartile range. Dashed horizontal line represents the median of individual cell periods.

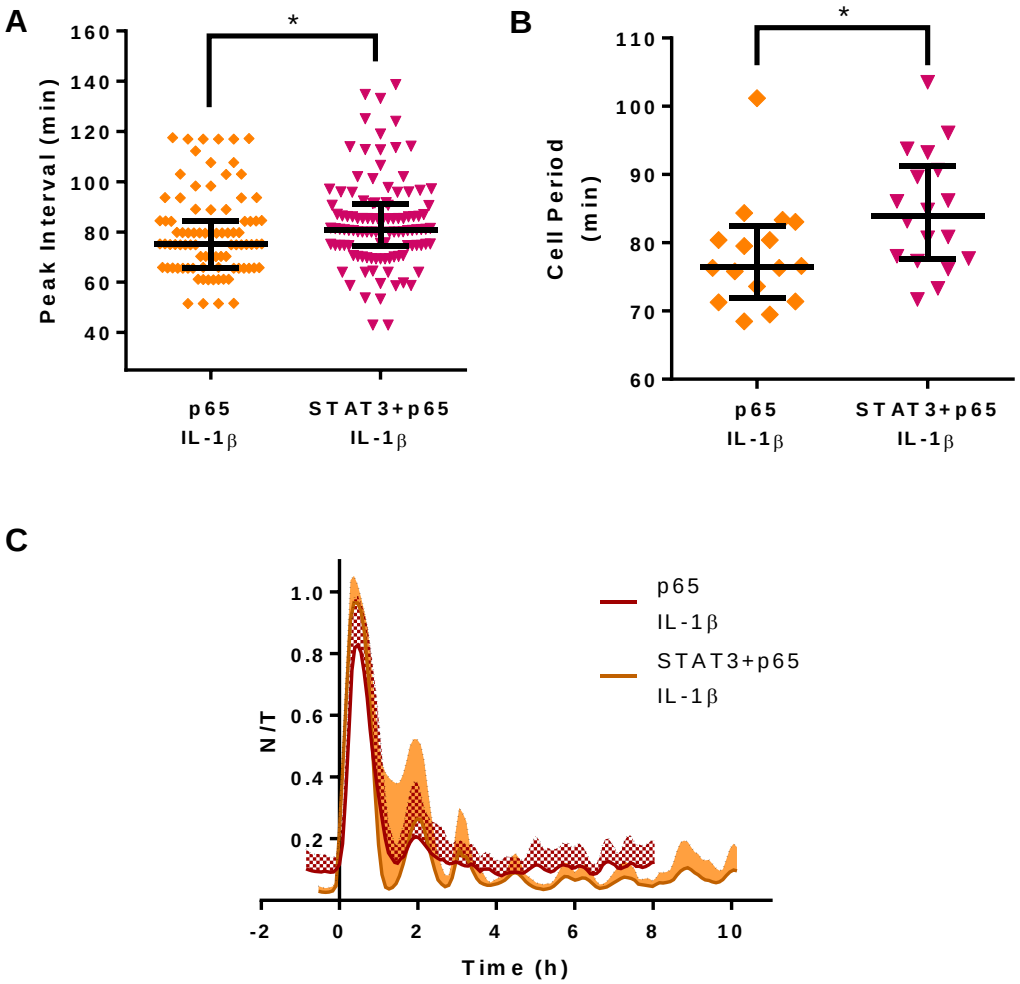

Figure 5.22: Comparing 10 ng/ml IL-1β stimulation of p65- and STAT3+p65-transfected HepG2 cells. A pooled peak intervals (min). **B** Individual mean cell periods (min). Each point represents a single peak interval or cell period and error bars show population Median ± Interquartile range * = P<0.05 **C** Average of all cell traces, for IL-1β+p65 (red) and IL-1β+p65 and STAT3 (orange). Solid line = average; shaded area to dashed line = +1 S.D.

The comparisons of p65 behaviour in response to IL-1β, both when expressed alone and with STAT3, with the equivalent TNFα experiments were compiled so that the general trends could be observed more easily (Fig.5.23). In addition the p65 and STAT3 co-expression IL-1β and TNFα experiments were compared using the Mann-Whitney test and were not found to be significantly different; in fact they were highly similar. In Section 5.2.1.5, it was suggested that excess STAT3 monomers may directly interact with p65 such that STAT3 NLS signals drive faster p65 oscillations. This additional finding that STAT3 slows down IL-1β-induced p65 oscillations however modifies this idea. It appears that STAT3 co-expression stabilises p65 oscillations at a frequency between the two extremes of TNFα and IL-1β stimulation of p65 expressed alone.

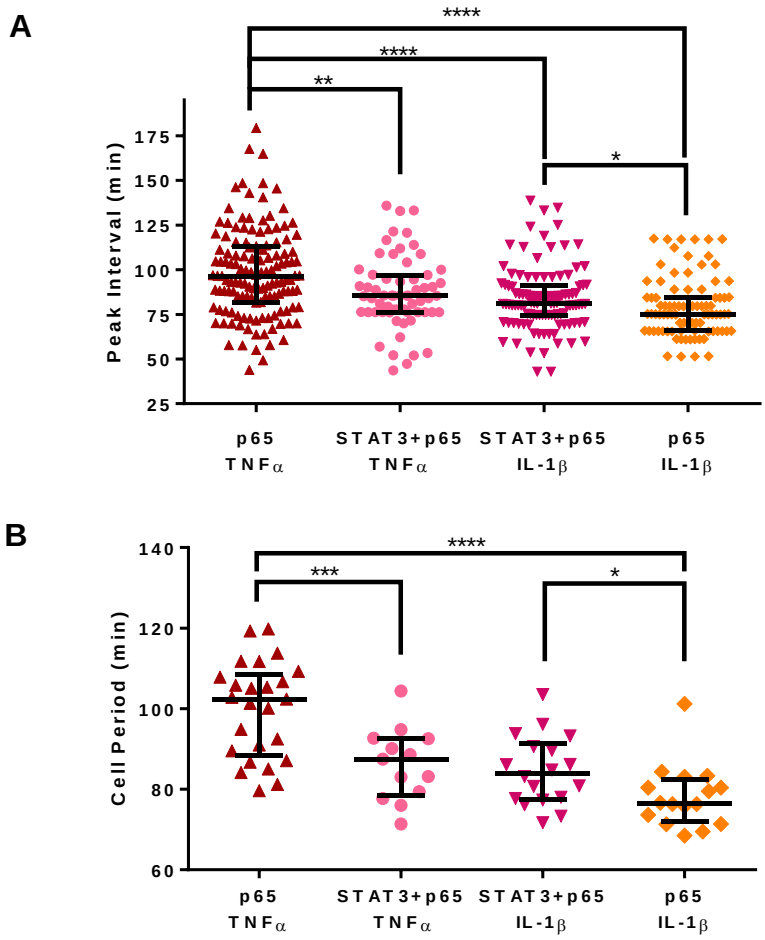

Figure 5.23: IL-1β vs TNFα experiments, with p65 alone vs. p65 and STAT3. A Pooled peak intervals (min). **B** Mean cell periods (min). Error bars show population median with interquartile range. * = P<0.05, ** = P<0.01, *** = P<0.005, **** = P< 0.001. The Mann-Whitney test with exact P-value calculations was performed in Prism due to non-parametric distributions.

The explanation is not as simple as STAT3 forcing p65 to oscillate at the same speed as STAT3 because the p65 oscillations are 5-10 min faster than STAT3 stimulated with IL-6. This suggests a synergistic effect upon nuclear trafficking. It is not possible to determine from the data available whether there is a direct interaction between STAT3 and p65 or whether an excess of U-STAT3 is altering other signalling events that affect p65 oscillations in turn. If there were a direct interaction, it could be possible to detect a correlation between the relative levels of STAT3 and p65 expression and the speed of the oscillations. However, many more cells would be needed to perform this analysis with any statistical power.

5.5.3 IL-1β and IL-6 Co-Stimulation of Co-Transfected HepG2 Cells

Cross-talk between STAT3 and p65 in response to IL-6 plus IL-1β was examined in HepG2 cells co-expressing STAT3 and p65. Initial visual inspection of the p65 and STAT3 cell traces from cells co-stimulated with 20 ng/ml IL-6 and 10 ng/ml IL-1β indicated that the relationships between the STAT3 and p65 responses were highly complex (Fig. 5.24-26). A variety of different responses were observed for both STAT3 and p65, including response patterns not seen in earlier experiments, and no obvious correlations could be identified between the different responses.

The responses seen were classified as follows: p65: early and late oscillators, and responders with a broad first peak, typically somewhat delayed. STAT3: non-responders, early oscillators, and late responders, which were further subdivided into mid, mid-late, and late responders. The characteristics of these groups are described in Table 5.1. Examples of: p65 responders (early, late and 'broad') with STAT3 non-responders (Fig. 5.24); p65 early and late oscillations with STAT3 early oscillations (Fig. 5.25); and examples of p65 responders (early, late and 'broad') with STAT3 late responders (mid, mid-late and late) (Fig. 5.26), are presented on the following pages. Due to the complexity of the responses, p65 and STAT3 cell traces are treated separately.

	Response	Description
p65	Early oscillations	Oscillations of typical amplitude. First peak median: 22 min post-stimulation
	Late oscillations	Oscillations of typical amplitude. First peak after 40 min post-stimulation; median response time 56 min.
	Broad first peak. Subsequent oscillations optional	Oscillations of typical amplitude. First peak wider than average, often doubled. First peak median: 52 min post-stimulus.
STAT3	None	N/T ratio did not increase above 60%
	Early oscillations	First peak around 35 min post-stimulation. Amplitude of first peak typically between 60 and 70%. Subsequent peak of increasing amplitude.
	Late: "mid"	Median peak time 82 min post-stimulus. Atypical oscillations.
	Late: "mid-late"	Median peak time 250 min post-stimulus. Not oscillatory, rather a gradual increase in N/T ratio is seen.
	Late: "late"	Median peak time 460 min post-stimulus. Not oscillatory, rather a gradual increase in N/T ratio is seen.

Table 5-1: Descriptions of STAT3 and p65 responses to IL-6 and IL-1β co-stimulation in STAT3 plus p65 co-transfected cells.

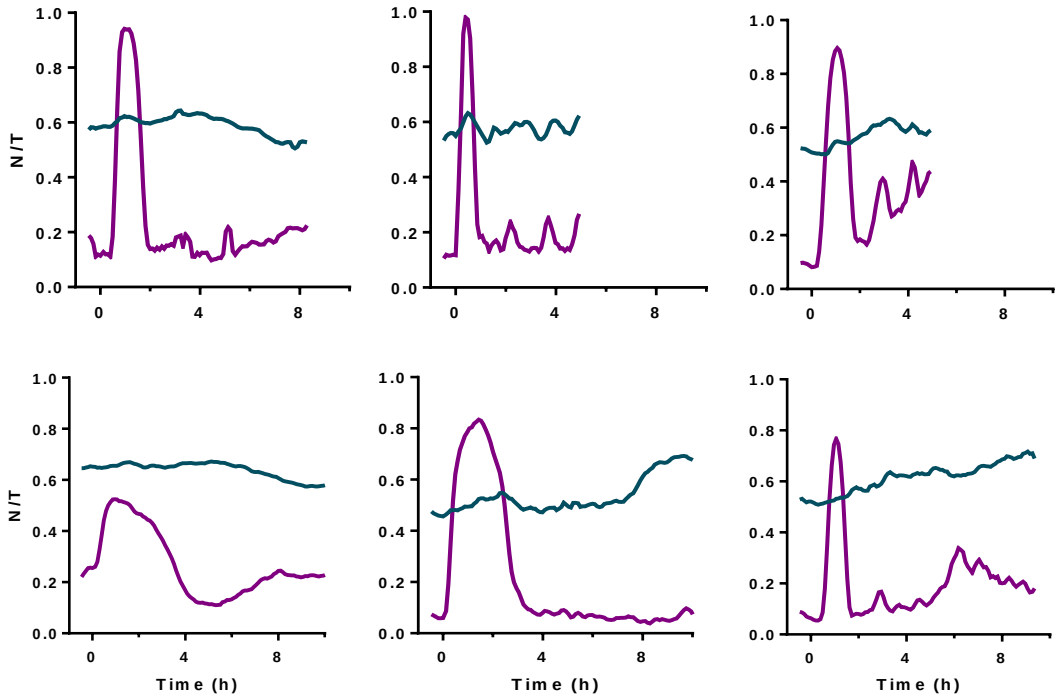

Figure 5.24: Example cell traces of p65-responsive, STAT3 non-responsive cells for 20 ng/ml IL-6 and 10 ng/ml IL-1β co-stimulated HepG2 cells expressing STAT3 and p65. STAT3: blue line, p65: purple line.

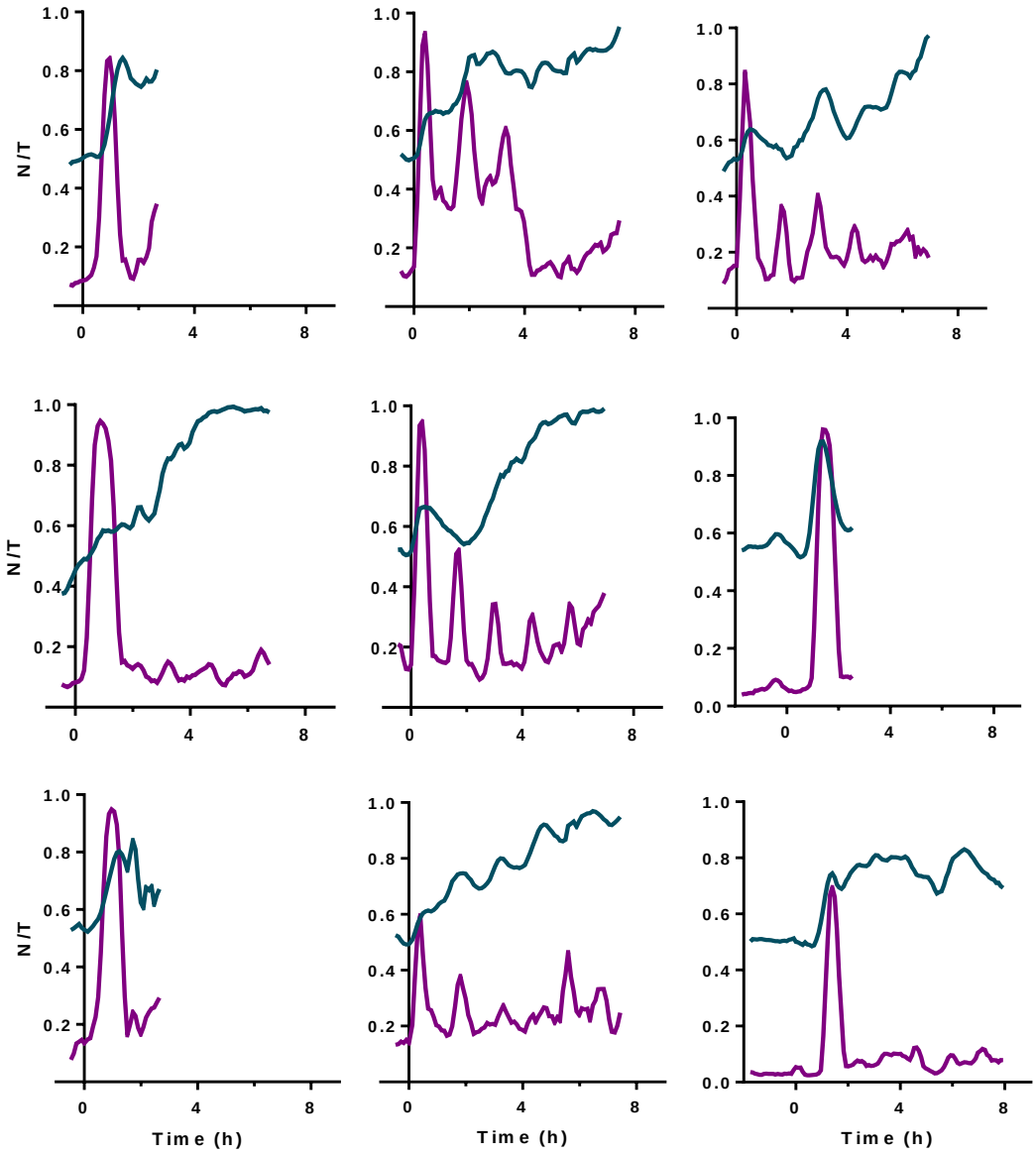

Figure 5.25: Example cell traces of p65-responsive, STAT3-responsive cells for 20 ng/ml IL-6 and 10 ng/ml IL-1β co-stimulated HepG2 cells expressing STAT3 and p65. STAT3: blue line, p65: purple line.

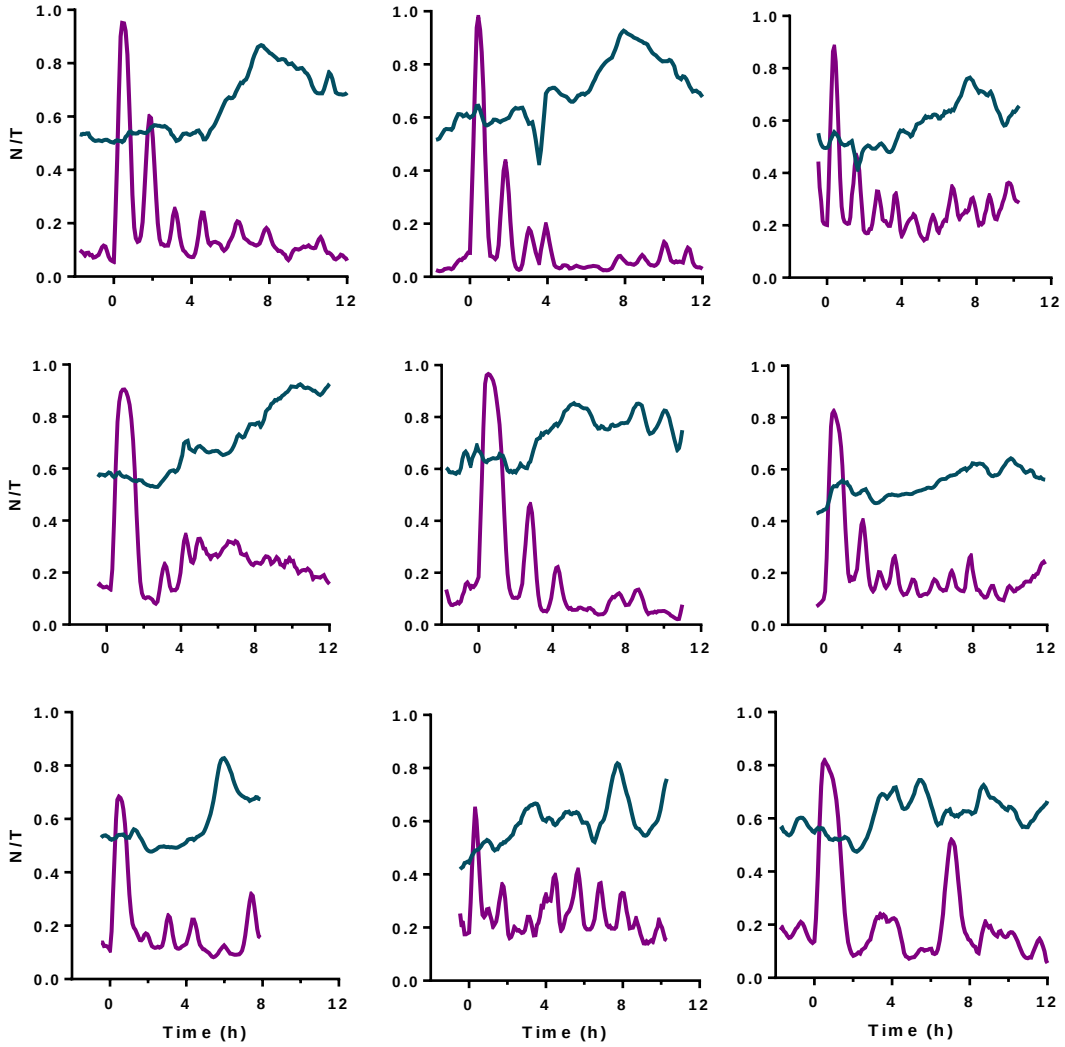

Figure 5.26: Example cell traces of p65-responsive, STAT3 late-responsive cells for 20 ng/ml IL-6 and 10 ng/ml IL-1β co-stimulated HepG2 cells expressing STAT3 and p65. STAT3: blue line, p65: purple line.

5.5.3.1 p65 Responses to IL-6 and IL-1β Co-stimulation

The p65 responses were categorised into three groups according to the time of the first peak maxima (Table 5.1; Fig. 5.28A). Peak intervals were calculated for each cell and the cells were grouped by time to first peak (Fig. 5.27). Comparison of the pooled peak interval groups (Fig. 5.28B) using the Mann-Whitney test did not reveal any significant differences however, comparison of the mean cell periods (Fig. 5.28C) identified some significant differences.

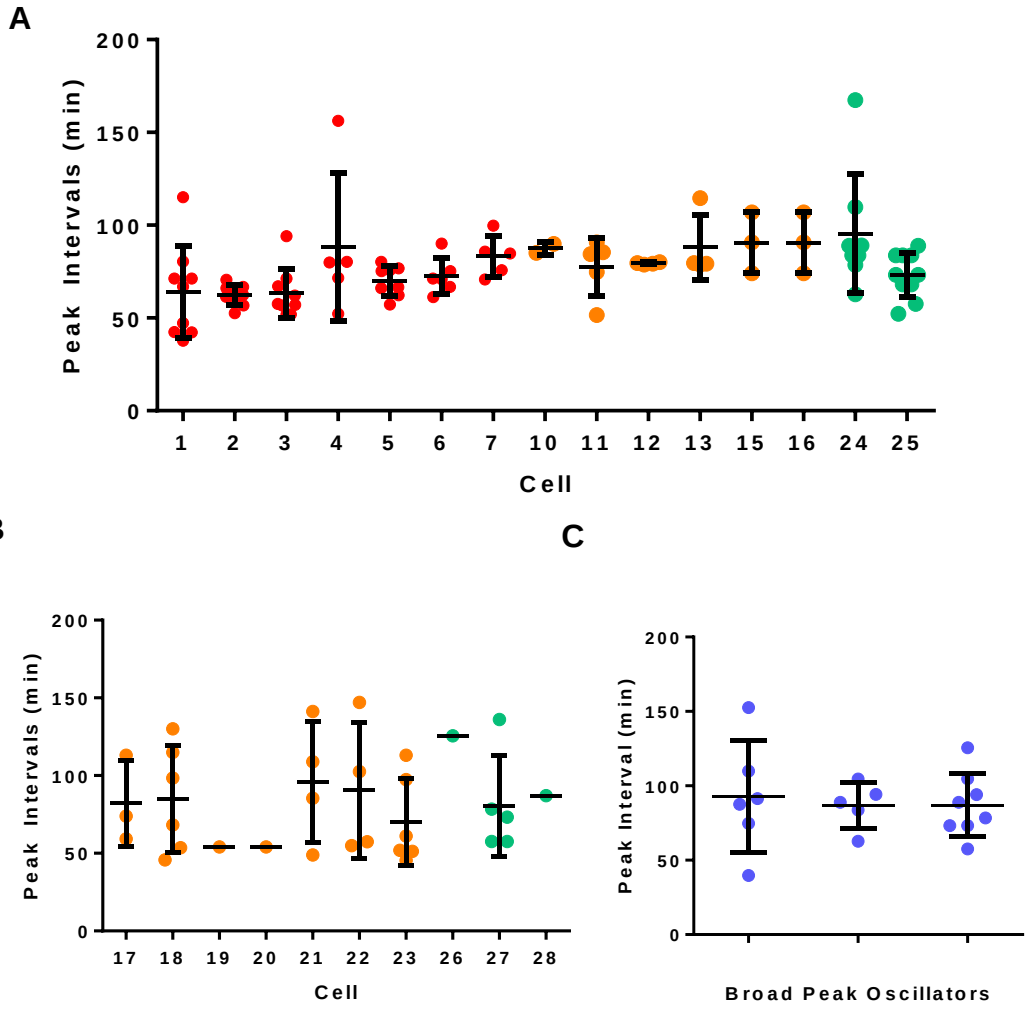

Figure 5.27: Peak interval data by cell for p65 from p65+STAT3 expressing HepG2 cells, stimulated with 20 ng/ml IL-6 and 10 ng/ml IL-1β. A Early responders, **B** Late responders, **C** Responders where the first peak is broad and there are subsequent oscillations.

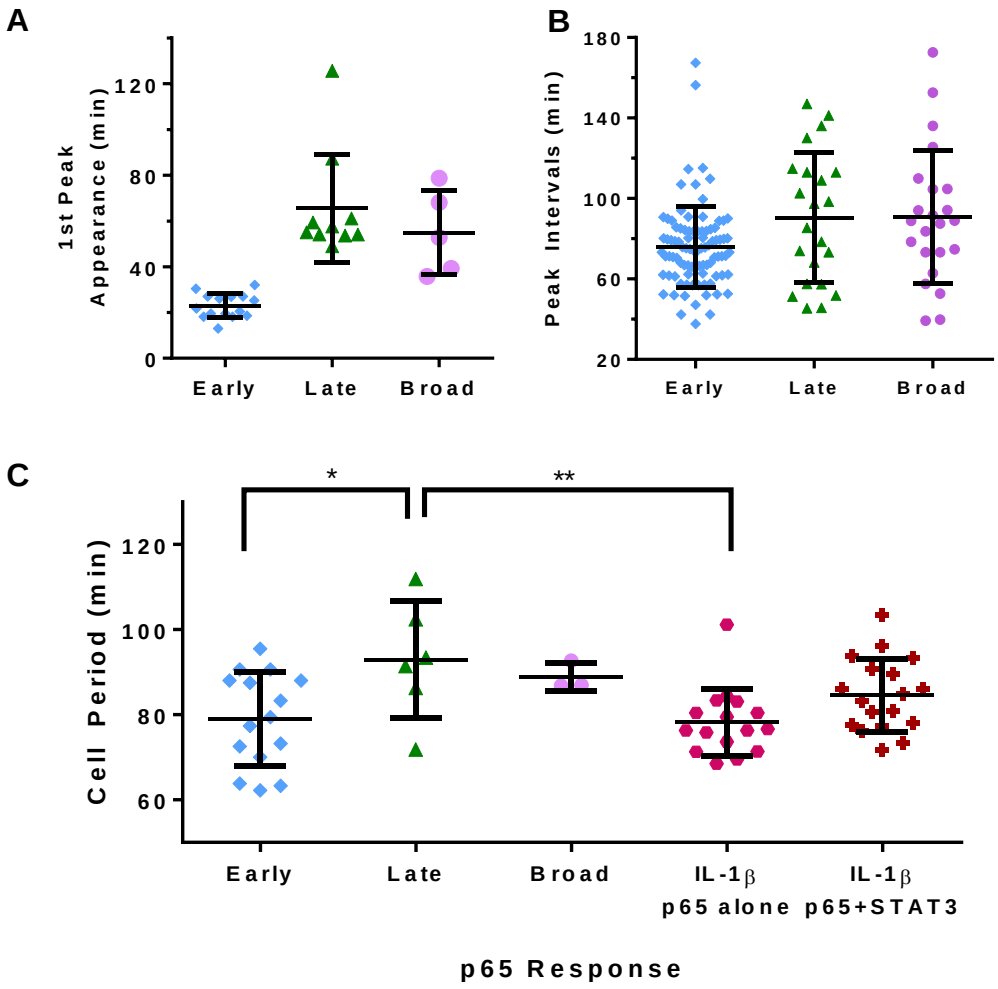

Figure 5.28: Characteristics of p65 responses to 20 ng/m, IL-6 and 10 ng/ml IL-1β co-stimulation. A Time of first peak appearance. **B** Pooled peak intervals. **C** Cell periods for early (15 cells), late (6 cells) and broad first peak (3 cells) p65 responders, compared to the IL-1β+p65 (16 cells) and IL-1β, p65+STAT3 controls (18 cells). * = P<0.05; ** = P<0.01.

The mean period of the early oscillators was 79.0 ± 11.0 min and they were significantly faster, by 13.8 min, than the late oscillators with a mean period of 92.9 ± 13.7 min (P<0.05). Neither group was significantly different to the IL-1β stimulation of p65 and STAT3 co-transfection experiment however the early oscillators were faster and the late oscillators slower. Whilst the late oscillators were 14.6 min slower than the p65 with IL-1β control (P<0.01), the early oscillators were not different to either the 'IL-1β, p65 alone' control group (mean cell period: 78.2 ± 7.9 min) or to the IL-1β stimulated p65 plus STAT3 co-transfected cells (mean cell period: 84.6 ± 8.5 min). Together, these results suggest that IL-6 can cause a subpopulation of co-transfected, co-stimulated

cells to oscillate at a slower rate, whilst leaving the other group seemingly unchanged. Finally, the 'broad peak' oscillators could not be statistically compared to the other groups because of the small sample size (n=3 cells).

Having examined p65 oscillatory dynamics in response to different stimuli when transfected into HepG2 cells alone and with STAT3, the distributions of p65 mean cell periods for all the different conditions tested were compared (Fig. 5.29). This highlighted the range of oscillation frequencies p65 can exhibit, from 76.5 min for 'IL-1β and p65' to 102.4 min for 'TNFα and p65'. It is particularly interesting that the extremes of oscillation frequency seen were from p65 expressed alone and stimulated with a single stimulus, whether TNFα or IL-1β.

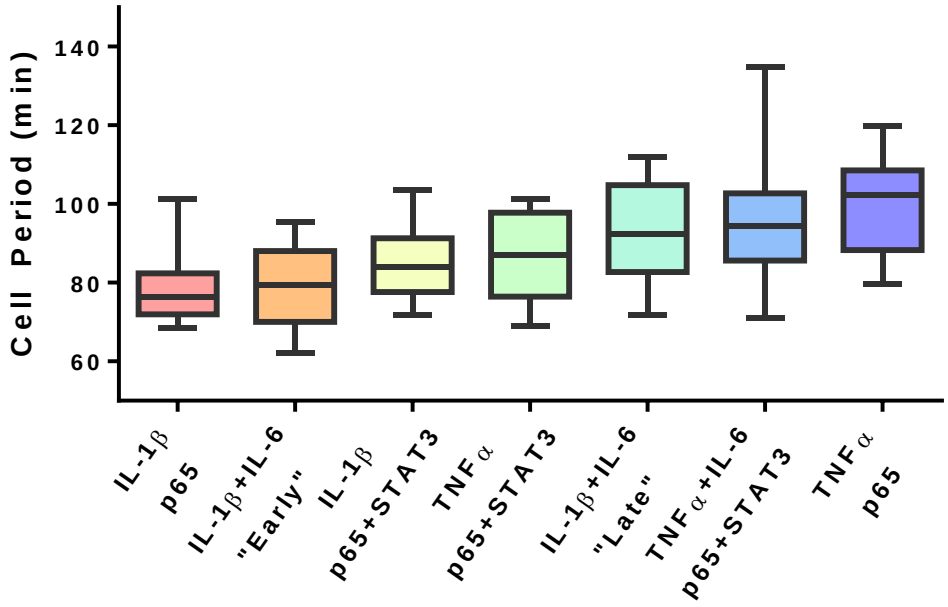

Figure 5.29: Variability of p65 responses to different stimuli and combinations thereof, when expressed alone or with STAT3. Min-to-max box plots indicating median oscillation frequency.

5.5.3.2 STAT3 Responses to IL-6 and IL-1β Co-stimulation

STAT3 responses under the IL-6 plus IL-1β regime were visually inspected and manually classified into groups (Fig. 5.30). Cells where STAT3 did not exhibit any net nuclear accumulation were classified as non-responders; they were the largest group (Fig. 5.30B). (For these purposes, net nuclear accumulation is defined as an N/T fluorescence ratio increase above 0.65 that could be confirmed by visual inspection. This was chosen based on the average fluctuations in non-stimulated controls, where the basal N/T ratio was between 0.4 and 0.6 (Chapter 4, Fig. 4.2).)

The second identifiable group was the 'early' responders. The first nuclear translocation in these cells occurred within 35 min of stimulation (Fig. 5.30A) as with IL-6 stimulation alone. However, the amplitude of the first peak was generally smaller, between 0.6 and 0.7, (Fig. 5.25) than under IL-6 stimulation alone, where the first peak is usually between 0.8 and 0.9 (Chapter 4, Fig. 4.3-4.5). Subsequent peaks increased in amplitude, eventually reaching N/T ratios between 0.8 and 1.

All cells that did not respond with a nuclear peak within 40 min were initially classed as 'late' responders (Fig. 5.30A) and were as numerous as the non-responders. Subsequent consideration of the time of first peak data suggested the presence of three subgroups. The Mid responders' first peak was 80-90 min after stimulation (lower and upper quartiles), and in addition their first peak was often 'full strength' i.e. N/T between 0.8 and 0.9. Several of these cells went through mitosis almost immediately after that first nuclear translocation, which raises the possibility of a cell cycle effect.

The final two classes were the 'mid-late' and 'late' cells, of which there were 8 in total (Fig. 5.26 and .30). The response pattern in these cells was very different to the early and mid responders and was completely different to anything seen in response to IL-6 or IL-6 plus TNFα. Instead of oscillatory dynamics, in these cells STAT3 gradually accumulated in the nucleus. For these cells, the peak detection spreadsheet tool was poor at identifying peak maxima, and as such the first peak appearance times may be inaccurate. However it was sufficient to give an indication of the cells' responses.

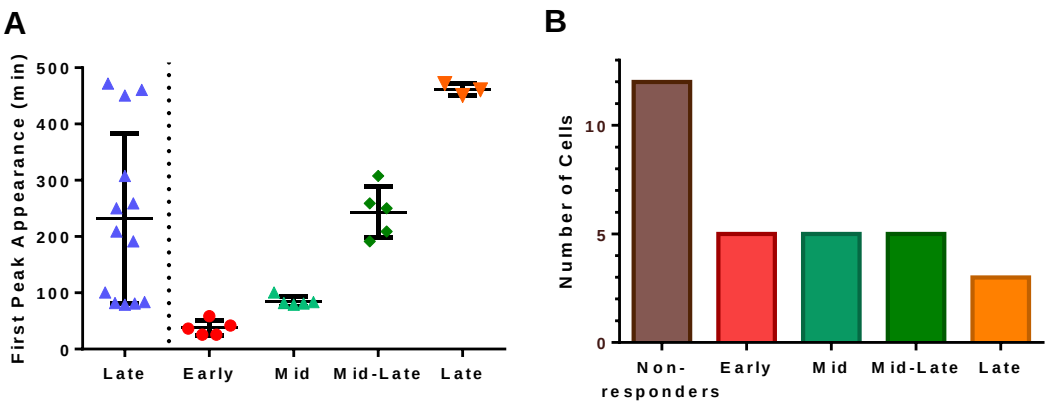

Figure 5.30: STAT3 Responses to IL-6+IL-1β in p65+STAT3 HepG2 cells. **A** Cells grouped according to time of first peak appearance. **B** Number of cells for each response.

Further to assessing first peak appearance time and peak amplitude, the peak intervals were determined for all cells, and are presented by group according to time to first peak (Fig. 5.31A-E). No additional distinctions could be made for the subgroups within the 'late' responders group based on the peak interval data. The variation between cells was much greater than for IL-6 stimulation of STAT3 alone, or indeed, for IL-6 with TNFα. The majority of cells were not reliable oscillators and so calculating the mean period of oscillation for each cell would have confounded the analysis. As such, only the pooled peak intervals for each condition are presented (Fig. 5.31). Due to the limited number of cells and peaks, statistical comparison of pooled peak data for each group to the IL-6-stimulated STAT3-expressing cells from Chapter 4 was not possible (Fig. 5.31F). However, visual inspection and a qualitative consideration of the data (Fig. 5.25 and 5.26) indicates that STAT3 signalling in response to IL-6 is severely curtailed in the presence of IL-1β. Less than a sixth of cells respond to IL-6 with regular oscillatory dynamics when co-treated with IL-1β, and those that do, do not exhibit full-strength translocations initially. 40% of cells exhibit a delayed response to IL-6, indicated by a gradual and time-delayed nuclear accumulation of STAT3, which may or may not also have had some oscillatory characteristics. Another 40% of cells did not respond to IL-6 at all (Table 5-2B).

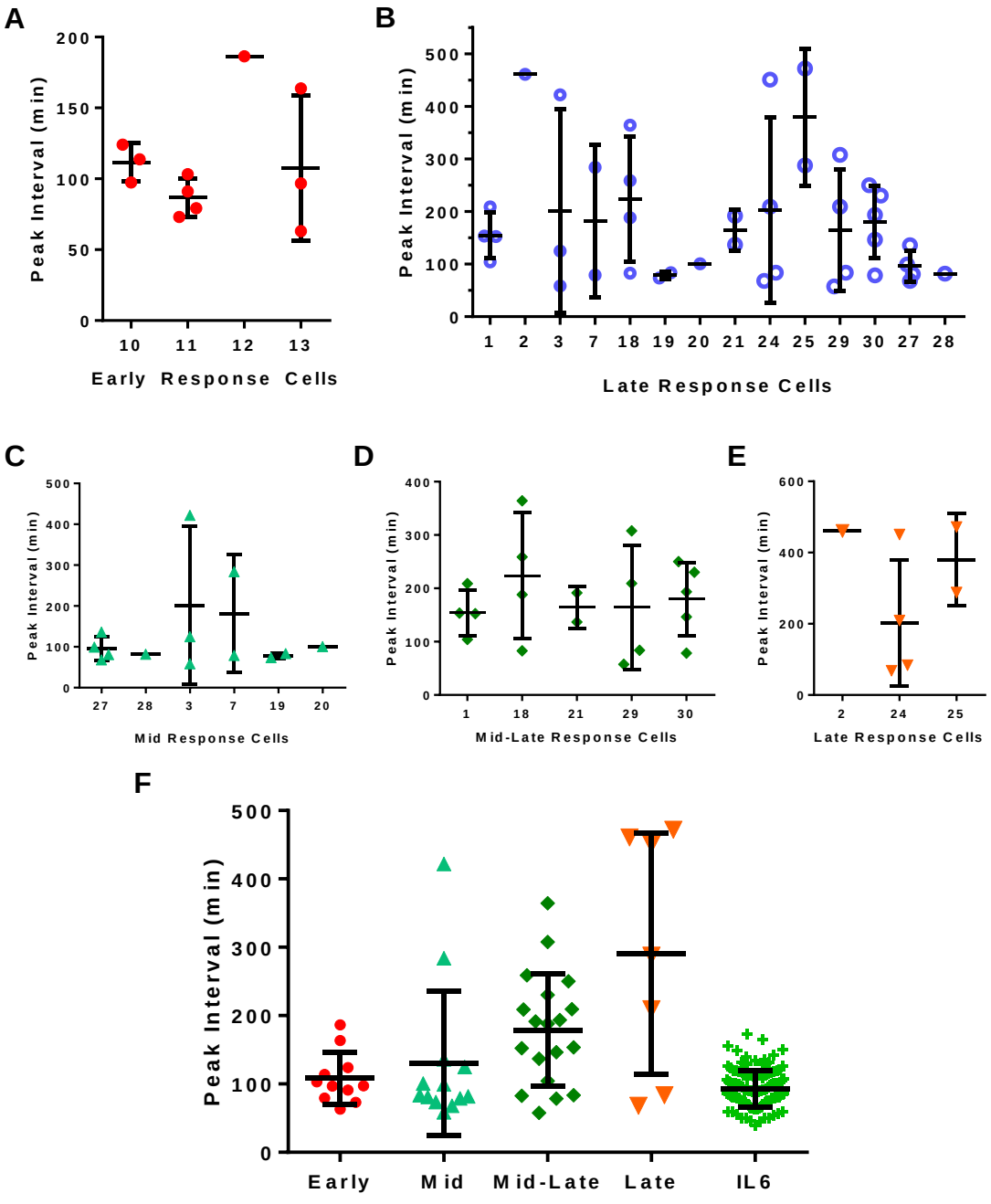

Figure 5.31: Peak interval data by cell for STAT3 from p65+STAT3 expressing HepG2 cells. Stimulated with 20 ng/ml IL-6 and 10 ng/ml IL-1β. **A** Early responders, **B** "Late" responders, **C-E** "Late" responders further divided according to appearance time of first peak: **C** Mid-responders, **D** Mid-Late responders and **E** Late responders. **F** Pooled Peak Intervals by response type, compared to STAT3 stimulated with IL-6. Error bars represent mean ± SD.

5.5.3.3 Combining p65 and STAT3 Responses to IL-6 plus IL-1β

After considering the p65 and STAT3 responses under the IL-6 plus IL-1β regime separately, it was possible to combine the data and investigate the possibility of correlation between the different behaviours. However all possible combinations of STAT3 and p65 response were well represented. The combinations were not equally represented but the number of cells in each group was too low for statistical analysis. Thus whilst there are discernible effects on the signalling dynamics of the two transcription factors at the population level, investigating whether there are any correlations between them will require a much larger data set than is currently available.

In the interim, the distribution of STAT3 and p65 responses were compared to the single transfection, single stimulus control experiments. I.e. the p65 data was compared to the IL-1β treatment of p65 (Table 5-2A), while the STAT3 data was compared to the IL-6 stimulation of STAT3 (Table 5-2B). For p65, the percentage of immediately responding cells halved, with the remaining cells either having a delayed start or a broad first peak. For STAT3, the percentage of non-responding cells increased from 25% to 40% and no cells oscillated in the same way as when under IL-6 stimulation alone. Instead 20% of cells had oscillatory dynamics that increased in amplitude over time. The final 40% of cells responded with either delayed, irregular and intermittent nuclear translocations or with a gradual nuclear accumulation that was delayed for 4 to 8 h after stimulation.

These comparisons indicate the strength of the inhibitory effect of IL-1β on IL-6-induced STAT3 signalling but also demonstrate that the inhibition of STAT3 dynamics is neither absolute nor consistent across the population. Furthermore, the p65 dynamics are also affected under this co-stimulatory cytokine regime in a way they are not when stimulated with IL-1β alone, whether co-expressed with STAT3 or not. These results indicate that there are complex synergistic effects between IL-6 and IL-1β and suggests that the outcome for each pathway depends on additional and unknown differences between individual cells.

A

	p65		
	Immediate	Late	Broad First Peak
Cell Count	15	10	5
Observed %	50	33.3	16.7
Expected† %	99	0	1

B

	STAT3			
	Strong Oscillator	Early	Late	Non-Responder
Cell Count	0	6	12	12
Observed %	0	20	40	40
Expected‡ %	75	0	0	25

Table 5-2: STAT3 and p65 Behaviours in Response to 20 ng/ml IL-6 plus 10 ng/ml IL-1β. A p65 behaviours and **B** STAT3 behaviours, by response type to IL-6 plus IL-1β co-stimulation. Displaying: Cell count; observed count as a percentage of the total number of cells (Observed %); and expected percentage based on control experiment (Expected %): † p65 stimulated with IL-1β alone, and ‡ STAT3 stimulated with IL-6 alone.

5.6 Discussion

5.6.1 General Summary

This chapter addressed the effects of cross-talk between STAT3 and NF-κB upon their dynamics. As described in Chapter 1 and Section 5.1, a large number of studies have found evidence of inter- and intra-cellular cross-talk between NF-κB and STATs, and a number of mechanisms have been proposed. The approach taken here was to ignore the mechanisms and instead look at the consequences for STAT3 and p65 dynamics in single cells. As described in Chapter 3, the HepG2 cell line was chosen for the cellular model because it showed independent responses to both IL-6 and TNFα. Therefore the results described here may only be applicable to this cell line and should be carefully considered if applied beyond this context.

The major observations of this chapter can be summarised as follows. Firstly, nucleocytoplasmic oscillations in STAT3 and p65 occur independently of each other under the various conditions tested. Secondly, there is considerable heterogeneity in the timing of individual p65 and STAT3 peaks within cells, indicating the two systems are mostly independent. Contrary to these observations however, stimulation of one pathway or the co-expression of the other fluorescent fusion protein can significantly affect the timing of responses in the first pathway when considered statistically at the population level. Different combinations of stimuli and TFs resulted in a range of p65 oscillatory periods observed. Interestingly, co-expression with STAT3 had a stabilising effect on the period of p65, keeping the average period within the upper and lower limits of TNFα and IL-1β stimulation of p65 alone, respectively. In addition, IL-6 stimulation was able to effect changes in the p65 dynamic response to IL-1β, an effect not noted by Radtke et al, (Radtke et al, 2010). No correlations could be identified between the STAT3 and p65 response to IL-6 plus IL-1β co-stimulation. In general, this suggests that STAT3 and p65 are weakly linked, most likely through one or more of the different mechanisms proposed for STAT3 and p65 interaction, in addition to the reported effects on gp130 receptor turn-over (Radtke et al, 2010). Only a large, carefully controlled

study would be able to elucidate further details regarding the effects of STAT3 and p65 cross-talk on their signalling dynamics.

5.6.2 Dynamics of p65 in Response to TNFα and IL-1β

One finding of note was that p65 oscillated at two vastly different frequencies depending on whether the stimulus was TNFα or IL-1β. Both these stimuli converge on the same point in the NF-κB signalling pathway, the IKK complex that ubiquitinates IκBα, resulting in the release of active p65. In SK-N-AS cells these stimuli result in the same p65 frequency of approximately 100 min (A. Adamson, unpublished observations). Since there are no molecular biology or qPCR data available for the IL-1β stimulation of HepG2 cells, it is not possible to determine a cause for the significantly faster IL-1β-induced oscillations. However it could be hypothesized that temporal or amplitude differences in the NF-κB feedback loops, such as IκBα, IκBε and A20, may account for the difference in oscillatory speed. Alternatively, there may be differences in the up-stream signalling events between the IL-1β and TNFα receptors and the IKK complex that are responsible.

An additional observation was of a few cells with a double-width first peak, also described as a 'broad first peak'. This was the first time it was seen in HepG2 cells, and it was only seen under IL-1β stimulation. Doubled first peaks have been intermittently observed in SK-N-AS and SHEP cells (Dr D. Spiller, University of Manchester, personal communication) but the cause is unknown. It was believed to be an artefact of the plasmid expression system or a problem with the incubation system on the microscope, however because it has now been seen in three unrelated cell lines it could be biologically important.

5.6.3 Limitations of the STAT3 Data

The data obtained for p65 were good in both quality and quantity, however the control experiments for STAT3 were lacking. This meant that while the effect of STAT3 on p65 dynamics was reasonably well quantified, the reverse was not true for STAT3 itself. Data were only obtained for STAT3 stimulated with IL-6, and for STAT3 co-expressed with p65 and stimulated with IL-6 and TNFα, simultaneously and staggered by 45 min. Even within this limited data set, it

was clear that the period of STAT3 could be perturbed to different degrees depending on the context. However, it would be very useful to know how exactly STAT3 responded to co-stimulation when expressed alone and to IL-6 when co-expressed with p65.

The STAT3 response to co-stimulation IL-6 and IL-1β was fascinating. IL-1β co-stimulation disrupted the STAT3 response but did not abolish it entirely. The proportion of non-responding cells increased in comparison to IL-6 stimulation alone but 60% of the cells responded in some fashion. A small set responded with oscillations similar to stimulation with IL-6 alone, except that the first peak was often significantly damped. In these cells, the strength of the oscillations increased over time. In a larger set of cells, the STAT3 response was delayed by anywhere between 4 and 8 h. Some of these cells oscillated erratically but in others, STAT3 accumulated in the nucleus over time. No correlation could be found between the STAT3 response and the p65 response which suggests that the causes may reside within a different pathway or be the result of complex interactions up-stream of p65.

5.6.4 Gene Expression in Response to IL-6 and TNFα

The differing STAT3 and p65 dynamics in response to IL-6 plus TNFα simultaneous co-stimulation compared to separate IL-6 and TNFα stimulation may have functional consequences for gene transcription, according to the results of the limited gene expression study performed here. Representatives of three different groups of genes were assayed. Genes for the components of the IL-6 signalling pathway, the early response NF-κB negative feedback genes, and the APR genes were sampled, and different trends were seen within each group.

The IL-6-responsive genes STAT3 and SOCS3 had similar responses at early time-points to IL-6 and TNFα as to IL-6 alone but the later dynamics were weaker under co-stimulation than IL-6 alone. SOCS2 responded similarly to both co-stimulation and IL-6. The NF-κB feedback genes responded similarly to both TNFα and IL-6 plus TNFα, indicating that IL-6 did not inhibit p65/NF-κB transcription. Instead IL-6 acted synergistically with TNFα, increasing the strength of A20 and IκBε transcription. This is interesting because IκBε has a

role in creating intercellular heterogeneity (Paszek et al, 2010), whilst A20 has been shown to decrease SOCS3 expression (da Silva et al, 2013). This could explain the effects of co-stimulation upon STAT3 signalling i.e. the longer STAT3 oscillation periods. The three selected APR genes each responded differently to co-stimulation. The responses were in line with published results in the literature (Hagihara et al, 2005; Pietrangelo et al, 2007; Asselin & Blais, 2011; Fish & Neerman-Arbez, 2012; Tiwari et al, 2013), and agree with the idea that TF binding sites in the promoters are more important for determining gene expression patterns (Grivennikov & Karin, 2010). It does not rule out the potential importance of nucleocytoplasmic shuttling dynamics in determining promoter occupancy however.

In order to thoroughly test the importance of spatiotemporal dynamics for gene expression in this context, a much larger study would need to be performed and different stimulation regimes tested. Ideally, the staggered stimulation protocol would be tested, as would IL-1β stimulation and IL-1β with IL-6. It would be interesting to investigate whether IκBα, IκBε or A20 transcription correlates with the variety of STAT3 and NF-κB dynamics in response to IL-6 plus IL-1β. A more representative gene set with additional reporters for NF-κB activity and the APR would be especially helpful. For this, a microarray or Nanostring set would be more efficient than the Fluidigm approach. Another option for correlating TF dynamics to transcriptional activity would be to obtain single cell transcription data, using single cell luminescence in conjunction with single cell fluorescence microscopy. This could be done with luciferase reporters for IκBα, IκBε and SOCS3. Transcriptional dynamics in response to cytokine signalling has been successfully characterised using this approach for prolactin signalling in pituitary cells (Harper et al, 2011; Featherstone et al, 2012).

Chapter 6
Final Discussion

6.1 Summary

In this thesis I investigated STAT3 localisation dynamics in single cells and intracellular cross-talk between STAT3 and NF-κB; a core hypothesis was that they might be interacting oscillatory systems. The work on STAT3 dynamics demonstrated that following cytokine activation, STAT3 is capable of oscillating in single cells. This supported and expanded upon previous work that had suggested the presence of oscillations at the cell population level (Yoshiura et al, 2007). Furthermore, whilst a number of reviews have recently been published summarising the possible mechanisms of interaction between the STAT and NF-κB systems and the biological importance thereof (Grivennikov & Karin, 2010; Bode et al, 2012a), no work has been published on the dynamical mechanisms or consequences that might underlie such interactions. In addition, the present work expands upon published studies looking at the mechanism of IL-1β inhibition of STAT3 signalling (Radtke et al, 2010; Bode et al, 2012a). It suggests that whereas the effects at the population level are relatively straightforward, at the single cell level the mechanisms of STAT3 inhibition are highly complex and variable between cells.

6.2 Cell Lines and Genetic Tools

A key issue at the beginning of the project was to identify the best cellular model and to generate new genetic tools needed to study the STAT3 pathway in single cells. The NF-κB tools were already available, including plasmids and BACs for p65 and IκBα, as well as stable p65 and IκBα BAC cell lines (SK-N-AS and HeLa) and later during the project, transgenic reporter mice. An IL-6-responsive cell line was required to study STAT3 signalling. In the initial studies it was found that the SK-N-AS cell line was unresponsive to IL-6. The HepG2 cell line had previously been extensively used for imaging STAT3 signalling (Pranada et al, 2004). In our experience this cell line was good for live cell imaging due to the large cell size, with an easy to identify nucleus as well as limited cell mobility. HepG2 cells can also be transiently transfected, with a rate of ~10%. The TNFα-induced NF-κB/p65 dynamics in HepG2 cells were found to be highly similar to those in the SK-N-AS cell line and so the HepG2 cell line was selected as the main cell line for the project.

STAT3 fluorescent fusion plasmids were successfully generated. Tagging at the N- and C-termini was investigated to check for effects on STAT3 expression, phosphorylation kinetics and transcriptional activity. Previous studies in our lab using STAT6 had shown that the choice of tag orientation affected the fusion protein's function (Nelson et al, 2004). Tagging at the C-terminus significantly perturbed STAT3 expression and phosphorylation kinetics whereas N-terminal tagged STAT3 was only mildly affected and, as far as could be measured, the behaviour of the fluorescent fusion protein was considered similar enough to the endogenous STAT3 to allow it to be valid for functional studies. Whether the results of the N- versus C-fusion proteins reflected a general difference or were specific to the linker of the cell line used remains to be clarified. There can be major potential issues with fluorescent fusion proteins and therefore tag orientation should always be considered when generating a new imaging construct.

Prior to these studies it was uncertain whether the STAT3 constructs would be able to capture the signalling dynamics of the system. It was possible that the only component that would move between the cytoplasm and nucleus would be phosphorylated STAT3. This might only be a minor fraction of the total STAT3, meaning that it might not be observable. Therefore SOCS3 reporters were thought to be necessary. Since SOCS3 is a short-lived inducible inhibitor of STAT3 signalling, plasmid constructs were not ideal for various reasons. Firstly, simple expression plasmids are usually under the control of a strong constitutive promoter and therefore gene induction dynamics are not captured by the reporter. Constitutive expression plasmids result in high expression levels of the reporter and so may perturb the system, especially in the case of an inhibitor such as SOCS3. It would therefore be necessary to incorporate the SOCS3 gene promoter. Furthermore, because plasmids use simple cDNA coding sequences as opposed to the endogenous gene structure, the duration of the half-lives of the mRNA and the protein might not reflect the endogenous gene products and so may alter the feedback dynamics, thus perturbing the overall dynamics of the system. Finally, there is a known issue with transient transfection of reporter plasmids where certain cell lines lose plasmids quickly.

Loss of the plasmid means that for short lived proteins with high turn-over rates such as SOCS3 or IκBα, subsequent rounds of expression may not be detected.

To overcome the limitations of the plasmid expression system, the construction of STAT3 and SOCS3 BACs was attempted. BACs enable a fusion protein to be expressed under the control of the native human gene promoter, and retain the native gene intron/exon structure and 5' and 3' sequences that direct mRNA processing and stability (Adamson et al, 2011). The SOCS3 BAC was found to be difficult to construct very early on in this project and this might have been a major problem. As an alternative, a SOCS3 fluorescent fusion under the control of the proximal SOCS3 promoter and a SOCS3-luciferase were constructed. Unfortunately the SOCS3-luciferase and the proximal promoter-SOCS3-EGFP construct were not very efficient and were affected by the transfection issues discussed above. Progress was made with cloning the STAT3 BAC, but by this point in the project the STAT3 plasmid was found to report STAT3 dynamics successfully. Due to time constraints, the proximal promoter SOCS3 fusion construct was not fully characterised and the STAT3 BAC was discontinued; instead the use of the STAT3 fluorescent fusion plasmid was made the focus of the project.

There are additional genetic tools that could be used in the future to overcome the limitations of the plasmid expression system. One approach is the generation of stable cell lines using the fusion expression plasmids. This would be useful for STAT3 but perhaps less so for the SOCS3 reporters. Stable transfection reduces the issues surrounding variable transfection rates, protein over-expression and the loss of the plasmid over time, leading to more stable protein expression levels. This was attempted for the STAT3 fusion plasmid however the HepG2 cell line is very resistant to the antibiotic geneticin, which was used as the selection marker in the expression plasmid. Reverse engineering to replace the resistance cassette in the plasmid would make this a feasible approach. Another option for the generation of stable cell lines might be lentiviral technology, although again this is less suitable for expression of inducible repressor proteins because there is not always sufficient room for the insertion of extensive promoter regions. More recent technologies for protein

expression include zinc-finger proteins, TALENS and CRISPR/cas9 to make specific changes to a target genetic locus (for review see Gupta & Musunuru, 2014). These technologies can enable a fluorescent protein cassette to be introduced directly into the target gene locus and so result in one or two copies of the fusion gene being expressed in the place of the endogenous gene (Gupta & Musunuru, 2014). This could be particularly useful for inducible repressors and if mouse genes are used, could allow the derivation of knock-in transgenic reporter mice.

6.3 Live Cell Imaging Approach

Live cell imaging formed the core technique used in this project because it has considerable advantages for studying longitudinal spatiotemporal signalling dynamics in single cells. This is in marked contrast to classical molecular biology techniques. It provides semi-quantitative time-resolved data for individual cells which overcomes population averaging effects that mask intercellular variation. This type of data also facilitates statistical analysis of a sample population and is excellent for testing and improving mathematical models of a dynamic system. In addition to live cell fluorescence microscopy other key techniques are Fluorescence Correlation Spectroscopy (FCS) and Fluorescence Cross-Correlation Spectroscopy (FCCS). These techniques can reveal whether different fluorescent proteins are associated together under particular conditions, and can determine dissociation constants. They can also infer how many fluorescent molecules there are within a cell and if used in conjunction with a stable cell line and Western blotting they can give an absolute quantification of both the fluorescent fusion protein and the endogenous protein. This can be very useful for mathematical models (for reviews see Ankers et al, 2008; Mullassery et al, 2008; Spiller et al, 2010).

There are some limitations to the live cell imaging techniques, both technical and analytical. Live cell imaging requires temperature-controlled microscopes capable of maintaining focus over extended periods of time, if experiments are to be run for between 8 and 48 h. Technological advances in microscopy and computing power have resulted in automated data collection and vastly improved image quality (Rabut & Ellenberg, 2004) but are financially costly

thus limiting availability. Furthermore, once the images are collected they must be processed and analysed. Image analysis is a very labour- and time-intensive process with the current software available (Shen et al, 2006; Du et al, 2010). In this project, over 350 cells were fully analysed. In addition a considerable number of cells were analysed but generated unusable data due to cell movement out of the field of view, overlaps between the cells or cell division or cell death during the experiment. Image analysis therefore requires considerably more time than running the microscopy experiments themselves and represents the biggest bottleneck in the live cell imaging workflow. Improved image analysis tools would therefore make a significant difference to the field.

Despite the data analysis limitations, this project generated a large quantity of unique data regarding cytokine-induced, temporally sustained STAT3 oscillations in single cells, which has not been reported elsewhere. It has also extended our knowledge of the implications of cross-talk between STAT3 and p65 for their respective signalling dynamics.

6.4 Modelling Dynamic Systems

The semi-quantitative, time-resolved data generated through single cell imaging lends itself to the mathematical modelling of system dynamics. We collaborated with a group of theoreticians in Spain, led by Prof. J. Garcia-Ojalvo, who had independently constructed a basic and generic mathematical model of STAT-SOCS signalling. In this case, the work presented in Chapter 4 that demonstrated and quantified the key characteristics of STAT3 oscillations disproved their existing generic model but indicated that it could be improved. I worked closely with Dr E. Abad as the model was updated and expanded to integrate the new findings. The improvements have not resulted in a single parameter set that captures both the pulsatile and continuous stimulation regimes, indicating that further work is required. Experimentally, more and better-quality STAT3 single cell data remains to be generated and a reporter for SOCS3 dynamics would be extremely beneficial. In association with improved global fitting of the model to the biological data and published literature, this would lead to a deeper

understanding of STAT3 signalling dynamics and to the generation of additional testable hypotheses for future biological experiments.

Despite models representing an abstraction, there is little doubt that they are an extremely useful tool for understanding biological systems and their interactions. Given the complexity of cytokine signalling within the immune system and the importance of understanding the molecular basis of disease, it is clear that an interdisciplinary, systems biology approach can contribute meaningfully to our understanding.

6.5 NF-κB Dynamics

The study of NF-κB nuclear translocation oscillatory dynamics only emerged within the last decade. There is a strong suggestion that the dynamics are functionally important for the temporal regulation of gene expression (Ashall et al, 2009). The published studies have only used a few cell lines, for example SK-N-AS and HeLa (Nelson et al, 2002; Nelson et al, 2004), fibroblasts (Tay et al, 2010) and macrophages (Sung et al, 2014). This project studied a different cell line, HepG2, and found it to be a strong oscillator with a similar period to previously characterised cell lines. Until now no published studies have considered perturbations of the period in different cell lines. I demonstrated that the period of NF-κB oscillations could be significantly perturbed in the HepG2 cell line through changing the stimulus used and by co-expressing STAT3 with NF-κB. Changing the period of oscillation by using different stimuli was particularly interesting; in the SK-N-AS cell line, TNFα and IL-1β result in the same period of 100 min (Dr A Adamson, personal communication) whereas in HepG2 cells, IL-1β stimulation caused NF-κB to oscillate 23 min faster than under TNFα. The cause of this cell line difference is unknown but two possible explanations are: firstly, differences in the pathway between the receptor and the IKK complex, and secondly, differences in the strength or timing of negative feedback loops. Furthermore the plasticity of the period in HepG2 cells is supported by observations in NF-κB transgenic mice, where the oscillatory period is as fast as 60 min in certain cell types (Dr C Walker, personal communication). The significant differences in oscillatory period with stimulus

are likely to be functionally relevant, given the role of frequency encoding of information with regards to gene expression patterns (Ashall et al, 2009).

6.6 STAT3 Dynamics

STAT3 shares many common features with other STATs, including constitutive nucleocytoplasmic shuttling (STAT1, STAT5 and STAT6), and negative feedback by SOCS1-3 and CIS. Whilst CIS, SOCS1-3 are not unique to each STAT, they do have strong preferences for classes of signals mediated by particular receptor types. Additionally, there is considerable evidence that feedback from multiple SOCS expressed at different levels can shape the nature of the STAT response, for example biasing IL-6 signalling via STAT3 towards a pro-inflammatory response, instead of the STAT1 anti-inflammatory response (Wormald et al, 2006). Therefore the core components necessary for oscillatory dynamics are present for several other STATs in conjunction with specific SOCS besides STAT3 and SOCS3.

The lack of a SOCS3 reporter was a big disappointment and might have presented significant problems for the project. Even so, a SOCS3 reporter alone may have generated incomplete data and been misleading. In the future, being able to report on SOCS3 and SOCS1 expression in addition to STAT3 would represent a major step forward. With accurate reporters in stable cell lines, it would be possible to perform knock-down experiments of SOCS feedback using siRNA to perturb STAT signalling. Data from such perturbation experiments would be especially useful for developing the STAT3:SOCS3 model presented here, for example by including multiple feedbacks as has been done for NF-κB signalling models (Paszek et al, 2010).

STAT3 was found to exhibit strong sustained nucleocytoplasmic oscillations in response to continuous IL-6 signalling at the single cell level in the HepG2 cell line. To our knowledge, this is the first demonstration of this phenomenon for any STAT in individual cells. Oscillatory STAT3 dynamics were observed at the population level in synchronised cells (Yoshiura et al, 2007) and attenuated transient oscillations have been seen for IFNγ-induced P-STAT1 and SOCS1 mRNA in macrophages (Pertsovskaya et al, 2013). The STAT3

nucleocytoplasmic oscillations were only seen under continuous stimulation; 30 min and shorter pulses of IL-6 triggered a single, transient nuclear accumulation of STAT3. It remains to be determined whether these STAT3 dynamics are biologically important, although evidence from signalling networks with strong oscillatory dynamics, such as p53 and ERK1/2 (Lahav et al, 2004; Shin et al, 2009), suggests that it is likely. A small gene expression study was performed but it was limited in scope and the differences seen between the 30 min and continuous data were small and as such, the significance could not be determined. This could be addressed by expanding the scope of the study to include more genes and test conditions, and other technologies such as Nanostring or RNA-Seq could be used.

6.7 Cross-talk Between STATs and NF-κB

Intercellular and intracellular cross-talk between STATs and NF-κB has been documented in various circumstances, involving different combinations of STATs, NF-κB dimers, cell lines and stimuli. The mechanisms for intracellular cross-talk are incompletely understood, due in part to the complexity and context-specific nature of the phenomenon. The known points of interaction between STAT3 and p65/NF-κB were discussed in Section 1.4 and are illustrated in Figure 6.1, with interactions through feedback loops and MAP Kinase signalling (Fig. 6.1A) and interactions at promoters of target genes (Fig. 6.1B) being shown. Efforts towards untangling cross-talk between the NF-κB and STAT networks have focused on the potential mechanisms and functional outcomes but have not generally considered the consequences on signalling dynamics of the transcription factors.

To limit the scope of the cross-talk question, this project focused on p65 and STAT3, joint mediators of the acute phase response to infection, in the HepG2 cell line, a model for the APR. The signalling dynamics of p65 have previously been studied in depth (Nelson et al, 2004) and have been found to be important for target gene transcription (Ashall et al, 2009), whilst STAT3 is capable of oscillatory dynamics at the population level (Yoshiura et al, 2007). At the beginning of the project, the dynamics of p65 were characterised in the HepG2 line whilst STAT3 was found to oscillate in single cells in response to IL-6.

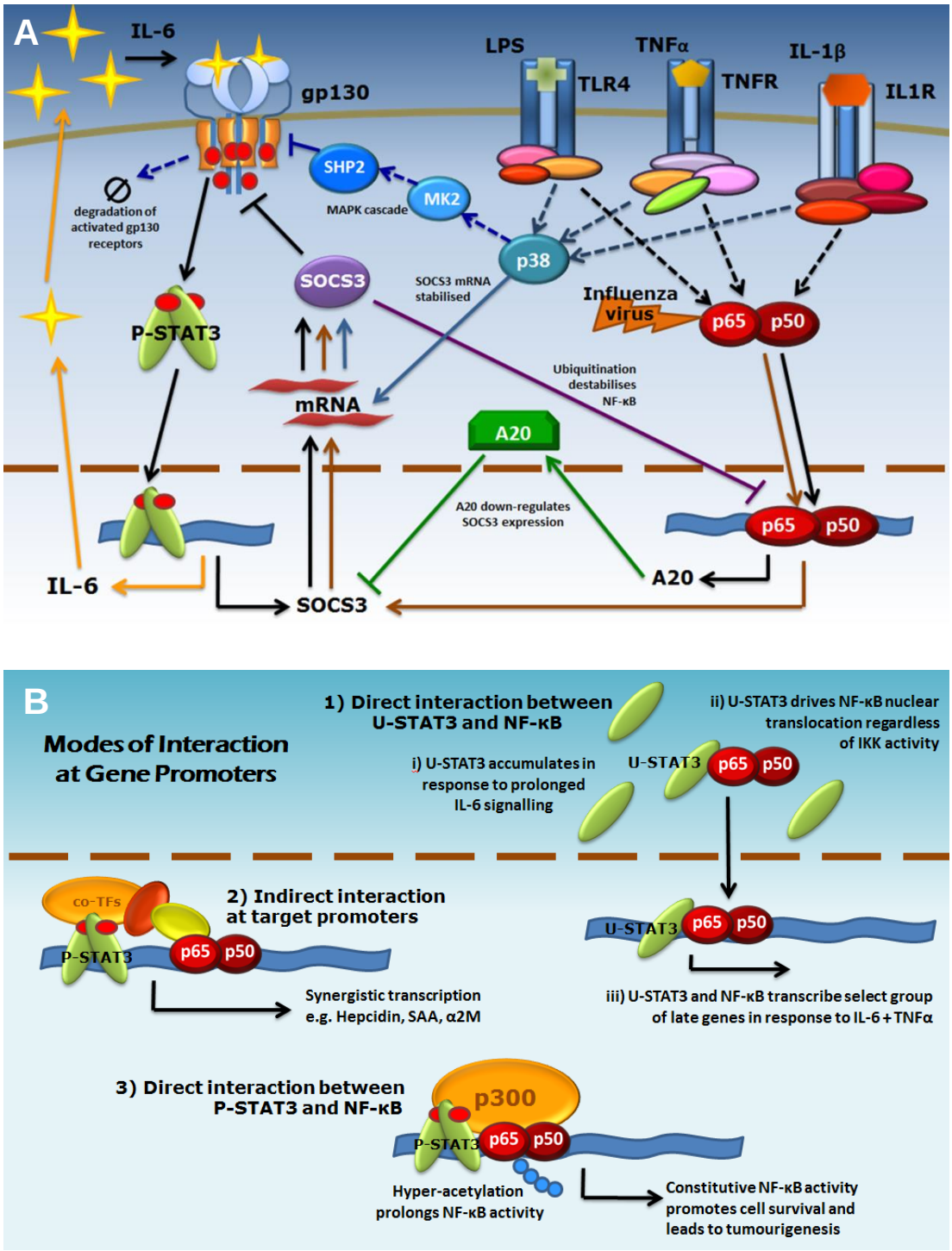

Figure 6.1: Known cross-talks between STAT3 and NF-κB. A Cross-talk mediated by feedback loops and other signalling events. Note the autocrine/paracrine IL-6 feedback, which is driven by STAT3 and NF-κB signalling. Various events lead to increased SOCS3 and therefore inhibit STAT3 signalling. SOCS3 can also limit NF-κB transcription. MAPK components and p38 are a critical link between STAT3 and NF-κB. **B** The three key modes of interaction at gene promoters, each driving a different subset of genes.

Therefore the final aspect of the project was to consider STAT3 and p65 together in HepG2 cells because if cross-talk did occur, their respective signalling dynamics could be perturbed.

In general, STAT3 and p65 dynamics were perturbed by cytokine co-stimulation. IL-6 co-stimulation with either TNFα or IL-1β produced different effects, both on p65 and STAT3 dynamics. The effects were not unidirectional; instead both transcription factors were perturbed. Additionally, TNFα and IL-1β affected IL-6-activated STAT3 in different ways. IL-1β significantly inhibited STAT3 signalling whereas TNFα did not inhibit STAT3, thus serving to highlight the importance of context in cross-talk studies. Interestingly, while subtle effects could be detected at the population level through the statistical analysis, there appeared to be no correlation under any stimulation protocol between the behaviour of the two pathways within individual cells. However, consideration of the population statistics also masked differences between groups of cells with similar dynamic responses. This was particularly noticeable under the simultaneous IL-6 and TNFα co-stimulation protocol and under IL-6 and IL-1β co-stimulation. Another interesting observation was the effect of delaying one cytokine stimulus in relation to the other. Staggered stimulation with 'IL-6 then TNFα' resulted in different signalling dynamics for p65 and STAT3 in comparison to simultaneous stimulation, suggesting that the order in which cells detect different cytokine signals is vital to the final outcome. This could be especially important in whole organisms where waves of different cytokines are responsible for moving the immune response through the different stages necessary to clear infection and repair tissue damage.

The inhibitory effect of IL-1β upon IL-6-induced STAT3 dynamics was in line with the work by Radtke et al., (2010). Whilst Radtke and colleagues elucidated the primary mechanism of inhibition, which entailed down-regulation of the IL-6 receptor, they were not able to consider the differences between cells, nor any differences that occurred later than 3 h after stimulation. Furthermore, they only provide an explanation for the effect on STAT3 signalling, whereas in the data presented here, p65 dynamics were also shown to be affected by co-stimulation. One possible mechanism might be via SOCS feedback (Park et al,

2003; Kiu et al, 2007; Strebovsky et al, 2011). RNAi experiments may help elucidate the role of SOCS feedback in the cross-talk between STAT3 and NF-κB, as may the use of inhibitors for MAPK components.

Future work should consider both the functional consequences of perturbing STAT3 and NF-κB dynamics and the possible mechanisms for the observed effects. Ideally, the gene transcription study should be extended to consider IL-1β, and the effects of staggering cytokine co-stimulation. RNA-seq might be a useful alternative to qPCR-based approaches. With regards to mechanistic studies for the effects of cross-talk, use of inhibitors for different pathway components could be informative if combined with traditional molecular biology approaches as well as advanced fluorescence microscopy techniques. Fluorescence cross-correlation spectroscopy could be used to detect any direct interactions between STAT3 and p65 proteins under different co-stimulation protocols. Ideally, such experiments would be performed in a dual-transfected stable cell line, as the biggest bottleneck for the cross-talk studies was obtaining enough cells with comparable fluorescence levels. Increased numbers of cells for the different conditions tested, including controls for STAT3, would improve the statistical strength of the observations presented here. Finally, it would be an interesting challenge to combine the existing models of STAT3 and NF-κB signalling dynamics in order to capture cross-talk effects.

6.8 Concluding Remarks

In summary, this investigation demonstrated oscillatory STAT3 dynamics in single cells and investigated the effects of cross-talk between STAT3 and NF-κB upon their respective dynamic profiles. STAT3 was found to be a strong oscillator under IL-6, and it is likely that the oscillatory dynamics are important in determining the biological outcome, given our understanding of other signalling networks. The characterisation of STAT3 oscillations enabled the re-fitting of an existing generic STAT:SOCS model into a specific STAT3:SOCS3 model that was able to capture two different dynamic STAT3 nuclear translocation profiles. The cross-talk effects were considerably complex, with a variety of subtle and conflicting results observed in addition to considerable intercellular variation. In general then, these findings highlight the flexible

nature of the STAT3 and NF-κB signalling networks and their ability to integrate signals from other pathways, whilst also reminding us that we have barely scratched the surface of the processes by which they interact. Furthermore, it emphasizes the importance of the cellular context, whether that be the cell type, the extracellular milieu, or the signals the cell has previously seen. In order to tease apart the interactions and dependencies of the cytokine signalling system, precise and thorough experiments must be performed in conjunction with detailed, quantitative analysis. Results so generated can then be used to define new models of cytokine-induced cross-talk with the aim of understanding the biological complexities of integrating multiple signalling systems.

Chapter 7
Bibliography

AARONSON DS, HORVATH CM (2002) *A road map for those who don't know JAK-STAT*. Science **296:** 1653-1655

ADAMSON AD, JACKSON D, DAVIS JRE (2011) *Novel approaches to in vitro transgenesis*. J Endocrin **208:** 193-206

ALBANESI C, FAIRCHILD HR, MADONNA S, SCARPONI C, DE PITA O, LEUNG DYM, HOWELL MD (2007) *IL-4 and IL-13 negatively regulate TNF-α and IFN-γ-induced α-Defensin expression through STAT-6, Suppressor of Cytokine Signaling (SOCS)-1, and SOCS-3*. J Immunol **179:** 984-992

ALBRECHT U, YANG X, ASSELTA R, KEITEL V, TENCHINI ML, LUDWIG S, HEINRICH PC, HAUSSINGER D, SCHAPER F, BODE JG (2007) *Activation of NF-kappaB by IL-1beta blocks IL-6-induced sustained STAT3 activation and STAT3-dependent gene expression of the human gamma-fibrinogen gene*. Cell Signal **19:** 1866-1878

ALON U (2007) *Network motifs: theory and experimental approaches*. Nat Rev Genet **8:** 450-461

ALPER MD, AMES BN (1975) *Positive selection of mutants with deletions of the gal-chl region of the Salmonella chromosome as a screening procedure for mutagens that cause deletions*. J Bacteriol **121:** 259-266

ALVAREZ JV, FRANK DA (2004) *Genome-wide analysis of STAT target genes: elucidating the mechanism of STAT-mediated oncogenesis*. Cancer Biol Ther **3:** 1045-1050

AMAN MJ, MIGONE TS, SASAKI A, ASCHERMAN DP, ZHU M, SOLDAINI E, IMADA K, MIYAJIMA A, YOSHIMURA A, LEONARD WJ (1999) *CIS associates with the interleukin-2 receptor beta chain and inhibits interleukin-2-dependent signaling*. J Biol Chem **274:** 30266-30272

ANKERS JM, SPILLER DG, WHITE MRH, HARPER CV (2008) *Spatio-temporal protein dynamics in single living cells*. Curr Opin Biotechnol **19:** 375-380

ARENZANA-SEISDEDOS F, TURPIN P, RODRIGUEZ M, THOMAS D, HAY RT, VIRELIZIER JL, DARGEMONT C (1997) *Nuclear localization of I kappa B apha promotes active transport of NF-kappa B from the nucleus to the cytoplasm*. J Cell Sci **110:** 369-378

ASHALL L, HORTON CA, NELSON DE, PASZEK P, HARPER CV, SILLITOE K, RYAN S, SPILLER DG, UNITT JF, BROOMHEAD DS, KELL DB, RAND DA, SÉE V, WHITE MRH (2009) *Pulsatile stimulation determines timing and specificity of NF-kB–dependent transcription*. Science **324:** 242-246

ASSELIN C, BLAIS M (2011) *Transcriptional regulation of Acute Phase Protein genes*.

BABON JJ, YAO S, DESOUZA DP, HARRISON CF, FABRI LJ, LIEPINSH E, SCROFANI SD, BACA M, NORTON RS (2005) *Secondary structure assignment of mouse SOCS3 by NMR defines the domain boundaries and identifies an unstructured insertion in the SH2 domain*. FEBS J **272:** 6120-6130

BABON JJ, MCMANUS EJ, YAO S, DESOUZA DP, MIELKE LA, SPRIGG NS, WILLSON TA, HILTON DJ, NICOLA NA, BACA M, NICHOLSON SE, NORTON RS (2006) *The structure of SOCS3 reveals the basis of the extended SH2 domain function and identifies an unstructured insertion that regulates stability*. Mol Cell **22:** 205-216

BABON JJ, LUCET IS, MURPHY JM, NICOLA NA, VARGHESE LN (2014) *The molecular regulation of Janus kinase (JAK) activation*. Biochem J **462:** 1-13

BAEUERLE P, BALTIMORE D (1988) *I kappa B: a specific inhibitor of the NF-kappa B transcription factor*. Science **242:** 540-546

BASAK S, BEHAR M, HOFFMANN A (2012) *Lessons from mathematically modeling the NF-κB pathway*. Immunol Rev **246:** 221-238

BAYLE J, LETARD S, FRANK R, DUBREUIL P, DE SEPULVEDA P (2004) *Suppressor of cytokine signaling 6 associates with KIT and regulates KIT receptor signaling*. J Biol Chem **279:** 12249-12259

BECKER S, GRONER B, MULLER CW (1998) *Three-dimensional structure of the STAT3[beta] homodimer bound to DNA*. Nature **394:** 145-151

BHATTACHARYA S, SCHINDLER C (2003) *Regulation of STAT3 nuclear export*. J Clin Invest **111:** 553-559

BILD AH, TURKSON J, JOVE R (2002) *Cytoplasmic transport of STAT3 by receptor-mediated endocytosis*. EMBO J **21:** 3255-3263

BODE JG, NIMMESGERN A, SCHMITZ J, SCHAPER F, SCHMITT M, FRISCH W, HÄUSSINGER D, HEINRICH PC, GRAEVE L (1999) *LPS and TNFα induce SOCS3 mRNA and inhibit IL-6-induced activation of STAT3 in macrophages*. FEBS Lett **463:** 365-370

BODE JG, LUDWIG S, FREITAS CA, SCHAPER F, RUHL M, MELMED S, HEINRICH PC, HAUSSINGER D (2001) *The MKK6/p38 mitogen-activated protein kinase pathway is capable of inducing SOCS3 gene expression and inhibits IL-6-induced transcription*. J Biol Chem **382:** 1447-1453

BODE JG, SCHWEIGART J, KEHRMANN J, EHLTING C, SCHAPER F, HEINRICH PC, HÄUSSINGER D (2003) *TNF-α induces tyrosine phosphorylation and recruitment of the Src Homology Protein-Tyrosine Phosphatase 2 to the gp130 signal-transducing subunit of the IL-6 receptor complex*. J Immunol **171:** 257-266

BODE JG, ALBRECHT U, HÄUSSINGER D, HEINRICH PC, SCHAPER F (2012a) *Hepatic acute phase proteins – Regulation by IL-6- and IL-1-type cytokines involving STAT3 and its crosstalk with NF-κB-dependent signaling*. Euro J Cell Biol **91:** 496-505

BODE JG, EHLTING C, HAUSSINGER D (2012b) *The macrophage response towards LPS and its control through the p38(MAPK)-STAT3 axis*. Cell Signal **24:** 1185-1194

BOLLRATH J, GRETEN FR (2009) *IKK/NF-[kappa]B and STAT3 pathways: central signalling hubs in inflammation-mediated tumour promotion and metastasis*. EMBO Rep **10:** 1314-1319

BONIZZI G, KARIN M (2004) *The two NF-kappaB activation pathways and their role in innate and adaptive immunity*. Trends Immunol **25:** 280-288

BOULANGER MJ, CHOW D-C, BREVNOVA EE, GARCIA KC (2003) *Hexameric structure and assembly of the Interleukin-6/IL-6 α-Receptor/gp130 complex*. Science **300:** 2101-2104

BOULTON TG, STAHL N, YANCOPOULOS GD (1994) *Ciliary neurotrophic factor/leukemia inhibitory factor/interleukin 6/oncostatin M family of cytokines induces tyrosine phosphorylation of a common set of proteins overlapping those induced by other cytokines and growth factors*. J Biol Chem **269:** 11648-11655

BRAUNSTEIN J, BRUTSAERT S, OLSON R, SCHINDLER C (2003) *STATs dimerize in the absence of phosphorylation*. J Biol Chem **278:** 34133-34140

BRAVO J, STAUNTON D, HEATH JK, JONES EY (1998) *Crystal structure of a cytokine-binding region of gp130*. EMBO J **17:** 1665-1674

BRUCE ALBERTS AJ, JULIAN LEWIS, MARTIN RAFF, KEITH ROBERTS, AND PETER WALTER. (2002) *Molecular Biology of the Cell*, New York: Garland Science.

BULLOCK AN, DEBRECZENI JE, EDWARDS AM, SUNDSTROM M, KNAPP S (2006) *Crystal structure of the SOCS2-elongin C-elongin B complex defines a prototypical SOCS box ubiquitin ligase*. Proc Natl Acad Sci USA **103:** 7637-7642

BUSTIN SA, BENES V, GARSON JA, HELLEMANS J, HUGGETT J, KUBISTA M, MUELLER R, NOLAN T, PFAFFL MW, SHIPLEY GL, VANDESOMPELE J, WITTWER CT (2009) *The MIQE guidelines: minimum information for publication of quantitative real-time PCR experiments*. Clin Chem **55:** 611-622

CARLOTTI F, DOWER SK, QWARNSTROM EE (2000) *Dynamic shuttling of Nuclear Factor kappa B between the nucleus and cytoplasm as a consequence of inhibitor dissociation*. J Biol Chem **275:** 41028-41034

CASTELL JV, GÓMEZ-LECHÓN MJ, DAVID M, ANDUS T, GEIGER T, TRULLENQUE R, FABRA R, HEINRICH PC (1989) *Interleukin-6 is the major regulator of acute phase protein synthesis in adult human hepatocytes*. FEBS Lett **242:** 237-239

CHEN H-C, REICH NC (2010) *Live cell imaging reveals continuous STAT6 nuclear trafficking*. J Immunol **185:** 64-70

CHEN LF, GREENE WC (2004) *Shaping the nuclear action of NF-kappaB*. Nat Rev Mol Cell Bio **5:** 392-401

CHEN X, VINKEMEIER U, ZHAO Y, JERUZALMI D, DARNELL JE, JR., KURIYAN J (1998) *Crystal structure of a tyrosine phosphorylated STAT-1 dimer bound to DNA*. Cell **93:** 827-839

CHEN X, BHANDARI R, VINKEMEIER U, VAN DEN AKKER F, DARNELL JE, JR., KURIYAN J (2003) *A reinterpretation of the dimerization interface of the N-terminal domains of STATs*. Protein Sci **12:** 361-365

CHUNG CD, LIAO J, LIU B, RAO X, JAY P, BERTA P, SHUAI K (1997) *Specific inhibition of STAT3 signal transduction by PIAS3*. Science **278:** 1803-1805

CIMICA V, CHEN H-C, IYER JK, REICH NC (2011) *Dynamics of the STAT3 Transcription Factor: nuclear import dependent on Ran and Importin-β1*. PLoS ONE **6:** e20188

COURT DL, SAWITZKE JA, THOMASON LC (2002) *Genetic engineering using homologous recombination*. Annu Rev Genet **36:** 361-388

CROKER BA, KREBS DL, ZHANG JG, WORMALD S, WILLSON TA, STANLEY EG, ROBB L, GREENHALGH CJ, FÖRSTER I, CLAUSEN BE (2003) *SOCS3 negatively regulates IL-6 signaling in vivo*. Nat Immunol **4:** 540-545

CROKER BA, KIU H, NICHOLSON SE (2008a) *SOCS regulation of the JAK/STAT signalling pathway*. Semin Cell Dev Biol **19:** 414-422

CROKER BA, MIELKE LA, WORMALD S, METCALF D, KIU H, ALEXANDER WS, HILTON DJ, ROBERTS AW (2008b) *SOCS3 maintains the specificity of biological responses to cytokine signals during granulocyte and macrophage differentiation*. Exp Hematol **36:** 786-798

DA SILVA CG, STUDER P, SKROCH M, MAHIOU J, MINUSSI DC, PETERSON CR, WILSON SW, PATEL VI, MA A, CSIZMADIA E, FERRAN C (2013) *A20 promotes liver regeneration by decreasing SOCS3 expression to enhance IL-6/STAT3 proliferative signals*. Hepatology **57:** 2014-2025

DECKER T, KOVARIK P, MEINKE A (1997) *GAS elements: a few nucleotides with a major impact on cytokine-induced gene expression*. J Interferon Cytokine Res **17:** 121-134

DECKER T, KOVARIK P (2000) *Serine phosphorylation of STATs*. Oncogene **19:** 2628-2637

DIF F, SAUNIER E, DEMENEIX B, KELLY PA, EDERY M (2001) *Cytokine-inducible SH2-containing protein suppresses PRL signaling by binding the PRL receptor*. Endocrinol **142:** 5286-5293

DOUDNA JA, CHARPENTIER E (2014) *Genome editing. The new frontier of genome engineering with CRISPR-Cas9*. Science **346:** 1258096

DU C-J, MARCELLO M, SPILLER DG, WHITE MRH, BRETSCHNEIDER T (2010) *Interactive segmentation of clustered cells via geodesic commute distance and constrained density weighted Nyström method*. Cytometry Part A **77A:** 1137-1147

EHLTING C, LAI WS, SCHAPER F, BRENNDÖRFER ED, MATTHES R-J, HEINRICH PC, LUDWIG S, BLACKSHEAR PJ, GAESTEL M, HÄUSSINGER D, BODE JG (2007) *Regulation of Suppressor of Cytokine Signaling 3 (SOCS3) mRNA stability by TNF-α involves activation of the MKK6/p38MAPK/MK2 cascade*. J Immunol **178:** 2813-2826

EHRET GB, REICHENBACH P, SCHINDLERI U, HORVATH CM, FRITZ S, NABHOLZ M, BUCHER P (2000) *DNA binding specificity of different STAT proteins. Comparison of in virto specificity with natural target sites*. J Biol Chem **276:** 6675-6688

ENDO T, SASAKI A, MINOGUCHI M, JOO A, YOSHIMURA A (2003) *CIS1 interacts with the Y532 of the prolactin receptor and suppresses prolactin-dependent STAT5 activation*. J Biochem **133:** 109-113

ENDO TA, MASUHARA M, YOKOUCHI M, SUZUKI R, SAKAMOTO H, MITSUI K, MATSUMOTO A, TANIMURA S, OHTSUBO M, MISAWA H, MIYAZAKI T, LEONOR N, TANIGUCHI T, FUJITA T, KANAKURA Y, KOMIYA S, YOSHIMURA A (1997) *A new protein containing an SH2 domain that inhibits JAK kinases*. Nature **387:** 921-924

FAN Y, MAO R, YANG J (2013) *NF-kappaB and STAT3 signaling pathways collaboratively link inflammation to cancer*. Protein Cell **4:** 176-185

FEATHERSTONE K, WHITE MR, DAVIS JR (2012) *The prolactin gene: a paradigm of tissue-specific gene regulation with complex temporal transcription dynamics*. J Neuroendocrinol **24:** 977-990

FENG ZP, CHANDRASHEKARAN IR, LOW A, SPEED TP, NICHOLSON SE, NORTON RS (2012) *The N-terminal domains of SOCS proteins: a conserved region in the disordered N-termini of SOCS4 and 5*. Proteins **80:** 946-957

FISH RJ, NEERMAN-ARBEZ M (2012) *Fibrinogen gene regulation*. Thromb Haemost **108:** 419-426

GADINA M, HILTON D, JOHNSTON JA, MORINOBU A, LIGHVANI A, ZHOU Y-J, VISCONTI R, O'SHEA JJ (2001) *Signaling by Type I and II cytokine receptors: ten years after*. Curr Opin Immunol **13:** 363-373

GERHARTZ C, DITTRICH E, STOYAN T, ROSE-JOHN S, YASUKAWA K, HEINRICH PC, GRAEVE L (1994) *Biosynthesis and half-life of the interleukin-6 receptor and its signal transducer gp130*. Euro J Biochem **223:** 265-274

GERMAN CL, SAUER BM, HOWE CL (2011) *The STAT3 beacon: IL-6 recurrently activates STAT 3 from endosomal structures*. Exp Cell Res **317:** 1955-1969

GERONDAKIS S, GRUMONT R, GUGASYAN R, WONG L, ISOMURA I, HO W, BANERJEE A (2006) *Unravelling the complexities of the NF-kappaB signalling pathway using mouse knockout and transgenic models*. Oncogene **25:** 6781-6799

GHOSH S, MAY MJ, KOPP EB (1998) *NF-kappa B and Rel proteins: evolutionarily conserved mediators of immune responses*. Annu Rev Immunol **16:** 225-260

GIESE B, AU-YEUNG CK, HERRMANN A, DIEFENBACH S, HAAN C, KUSTER A, WORTMANN SB, RODERBURG C, HEINRICH PC, BEHRMANN I, MULLER-NEWEN G (2003) *Long term association of the cytokine receptor gp130 and the Janus kinase Jak1 revealed by FRAP analysis*. J Biol Chem **278:** 39205-39213

GILMORE TD (1999) *The Rel/NF-kappaB signal transduction pathway: introduction*. Oncogene **18:** 6842-6844

GOLDBETER A (1995) *A model for circadian oscillations in the Drosophila period protein (PER)*. Proc Biol Sci **261:** 319-324

GOUILLEUX F, WAKAO H, MUNDT M, GRONER B (1994) *Prolactin induces phosphorylation of Tyr694 of Stat5 (MGF), a prerequisite for DNA binding and induction of transcription*. EMBO J **13:** 4361-4369

GRAEVE L, KOROLENKO TA, HEMMANN U, WEIERGRABER O, DITTRICH E, HEINRICH PC (1996) *A complex of the soluble interleukin-6 receptor and interleukin-6 is internalized via the signal transducer gp130*. FEBS Lett **399:** 131-134

GREENHALGH CJ, RICO-BAUTISTA E, LORENTZON M, THAUS AL, MORGAN PO, WILLSON TA, ZERVOUDAKIS P, METCALF D, STREET I, NICOLA NA, NASH AD, FABRI LJ, NORSTEDT G, OHLSSON C, FLORES-MORALES A, ALEXANDER WS, HILTON DJ (2005) *SOCS2 negatively regulates growth hormone action in vitro and in vivo*. J Clin Invest **115:** 397-406

GREENHILL CJ, ROSE-JOHN S, LISSILAA R, FERLIN W, ERNST M, HERTZOG PJ, MANSELL A, JENKINS BJ (2011) *IL-6 trans-signaling modulates TLR4-dependent inflammatory responses via STAT3*. J Immunol **186:** 1199-1208

GRIVENNIKOV SI, KARIN M (2010) *Dangerous liaisons: STAT3 and NF-κB collaboration and crosstalk in cancer*. Cytokine Growth Factor Rev **21:** 11-19

GUPTA RM, MUSUNURU K (2014) *Expanding the genetic editing tool kit: ZFNs, TALENs, and CRISPR-Cas9*. J Clin Invest **124:** 4154-4161

GUSCHIN D, ROGERS N, BRISCOE J, WITTHUHN B, WATLING D, HORN F, PELLEGRINI S, YASUKAWA K, HEINRICH P, STARK GR, ET AL. (1995) *A major role for the protein tyrosine kinase JAK1 in the JAK/STAT signal transduction pathway in response to interleukin-6*. EMBO J **14:** 1421-1429

HAAN C, HEINRICH PC, BEHRMANN I (2002) *Structural requirements of the Interleukin-6 signal transducer gp130 for its interaction with Janus Kinase 1: the receptor is crucial for kinase activation*. Biochem J **361:** 105-111

HAAN C, KREIS S, MARGUE C, BEHRMANN I (2006) *Jaks and cytokine receptors--an intimate relationship*. Biochem Pharmacol **72:** 1538-1546

HAAN S, HEMMANN U, HASSIEPEN U, SCHAPER F, SCHNEIDER-MERGENER J, WOLLMER A, HEINRICH PC, GRÖTZINGER J (1999) *Characterization and binding specificity of the monomeric STAT3-SH2 domain*. J Biol Chem **274:** 1342-1348

HAAN S, KORTYLEWSKI M, BEHRMANN I, MÜLLER-ESTERL W, HEINRICH PC, SCHAPER F (2000) *Cytoplasmic STAT proteins associate prior to activation*. Biochem J **345:** 417-421

HAAN S, FERGUSON P, SOMMER U, HIREMATH M, MCVICAR DW, HEINRICH PC, JOHNSTON JA, CACALANO NA (2003) *Tyrosine phosphorylation disrupts Elongin interaction and accelerates SOCS3 degradation*. J Biol Chem **278:** 31972-31979

HACKER H, KARIN M (2006) *Regulation and function of IKK and IKK-related kinases*. Sci STK **2006:** re13

HAGIHARA K, NISHIKAWA T, SUGAMATA Y, SONG J, ISOBE T, TAGA T, YOSHIZAKI K (2005) *Essential role of STAT3 in cytokine-driven NF-κB-mediated serum amyloid A gene expression*. Genes Cells **10:** 1051-1063

HARPER CV, FINKENSTADT B, WOODCOCK DJ, FRIEDRICHSEN S, SEMPRINI S, ASHALL L, SPILLER DG, MULLINS JJ, RAND DA, DAVIS JR, WHITE MR (2011) *Dynamic analysis of stochastic transcription cycles*. PLoS Biol **9:** e1000607

HAYDEN MS, GHOSH S (2008) *Shared principles in NF-kappaB signaling*. Cell **132:** 344-362

HE G, KARIN M (2011) *NF-kappa B and STAT3 - key players in liver inflammation and cancer*. Cell Res **21:** 159-168

HEBENSTREIT D, WIRNSBERGER G, HOREJS-HOECK J, DUSCHL A (2006) *Signaling mechanisms, interaction partners, and target genes of STAT6*. Cytokine Growth Factor Rev **17:** 173-188

HEINRICH PC, BEHRMANN I, MÜLLER-NEWEN G, SCHAPER F, GRAEVE L (1998) *Interleukin-6-type cytokine signalling through the gp130/Jak/STAT pathway*. Biochem J **334:** 297-314

HEINRICH PC, BEHRMANN I, HAAN S, HERMANNS HM, MULLER-NEWEN G, SCHAPER F (2003) *Principles of interleukin (IL)-6-type cytokine signalling and its regulation*. Biochem J **374:** 1-20

HERRMANN A, VOGT M, MONNIGMANN M, CLAHSEN T, SOMMER U, HAAN S, POLI V, HEINRICH PC, MULLER-NEWEN G (2007) *Nucleocytoplasmic shuttling of persistently activated STAT3*. J Cell Sci **120:** 3249-3261

HIBI M, HIRANO T (1998) *Signal transduction through cytokine receptors* Int Rev Immunol **17:** 75-102

HILTON DJ, RICHARDSON RT, ALEXANDER WS, VINEY EM, WILLSON TA, SPRIGG NS, STARR R, NICHOLSON SE, METCALF D, NICOLA NA (1998) *Twenty proteins containing a C-terminal SOCS box form five structural classes*. Proc Natl Acad Sci USA **95:** 114-119

HOESEL B, SCHMID JA (2013) *The complexity of NF-κB signaling in inflammation and cancer*. Mol Cancer **12:** 86-86

HOFFMANN A, LEVCHENKO A, SCOTT ML, BALTIMORE D (2002) *The IkappaB-NF-kappaB signaling module: temporal control and selective gene activation*. Science **298:** 1241-1245

HOFFMANN A, BALTIMORE D (2006) *Circuitry of Nuclear Factor-kappaB signaling*. Immunol Rev **210:** 171-186

HWANG M-N, MIN C-H, KIM HS, LEE H, YOON K-A, PARK SY, LEE ES, YOON S (2007) *The nuclear localization of SOCS6 requires the N-terminal region and negatively regulates Stat3 protein levels*. Biochem Biophys Res Commun **360:** 333-338

ICHIBA M, NAKAJIMA K, YAMANAKA Y, KIUCHI N, HIRANO T (1998) *Autoregulation of the Stat3 gene through cooperation with a cAMP-responsive element-binding protein*. J Biol Chem **273:** 6132-6138

IMADA K, LEONARD WJ (2000) *The Jak-STAT pathway*. Mol Immunol **37:** 1-11

JORDAN JD, LANDAU EM, IYENGAR R (2000) *Signaling networks: the origins of cellular multitasking*. Cell **103:** 193-200

KABIR NN, SUN J, RONNSTRAND L, KAZI JU (2014) *SOCS6 is a selective suppressor of receptor tyrosine kinase signaling*. Tumour Biol **35:** 10581-10589

KAPLAN MH, SCHINDLER U, SMILEY ST, GRUSBY MJ (1996) *STAT6 is required for mediating responses to IL-4 and for the development of Th2 cells*. Immunity **4:** 313-319

KARIN M (1999) *How NF-kappaB is activated: the role of the IkappaB kinase (IKK) complex*. Oncogene **18:** 6867-6874

KARIN M, BEN-NERIAH Y (2000) *Phosphorylation meets ubiquitination: the control of NF-kappaB activity*. Annu Rev Immunol **18:** 621-663

KARIN M (2008) *The IkappaB kinase - a bridge between inflammation and cancer*. Cell Res **18:** 334-342

KARIO E, MARMOR MD, ADAMSKY K, CITRI A, AMIT I, AMARIGLIO N, RECHAVI G, YARDEN Y (2005) *Suppressors of cytokine signaling 4 and 5 regulate epidermal growth factor receptor signaling*. J Biol Chem **280:** 7038-7048

KEARNS JD, BASAK S, WERNER SL, HUANG CS, HOFFMANN A (2006) *IkappaBepsilon provides negative feedback to control NF-kappaB oscillations, signaling dynamics, and inflammatory gene expression*. J Cell Biol **173:** 659-664

KENT WJ, SUGNET CW, FUREY TS, ROSKIN KM, PRINGLE TH, ZAHLER AM, HAUSSLER D (2002) *The human genome browser at UCSC*. Genome Res **12:** 996-1006

KERSHAW NJ, MURPHY JM, LIAU NP, VARGHESE LN, LAKTYUSHIN A, WHITLOCK EL, LUCET IS, NICOLA NA, BABON JJ (2013) *SOCS3 binds specific receptor-JAK complexes to control cytokine signaling by direct kinase inhibition*. Nat Struct Mol Biol **20:** 469-476

KERSHAW NJ, LAKTYUSHIN A, NICOLA NA, BABON JJ (2014) *Reconstruction of an active SOCS3-based E3 ubiquitin ligase complex in vitro: identification of the active components and JAK2 and gp130 as substrates*. Growth Factors **32:** 1-10

KHOLODENKO BN (2006) *Cell-signalling dynamics in time and space*. Nat Rev Mol Cell Bio **7:** 165-176

KILE BT, SCHULMAN BA, ALEXANDER WS, NICOLA NA, MARTIN HM, HILTON DJ (2002) *The SOCS box: a tale of destruction and degradation*. Trends Biochem Sci **27:** 235-241

KISSELEVA T, BHATTACHARYA S, BRAUNSTEIN J, SCHINDLER CW (2002) *Signaling through the JAK/STAT pathway, recent advances and future challenges*. Gene **285:** 1-24

KITANO H (2002) *Computational systems biology*. Nature **420:** 206-210

KIU H, HILTON DJ, NICOLA NA, ERNST M, MARQUEZ R, ALEXANDER WS, ROBERTS AW, MCMANUS EJ (2007) *Mechanism of crosstalk inhibition of IL-6 signaling in response to LPS and TNFalpha*. Growth Factors **25:** 319-328

KLIPP E, LIEBERMEISTER W (2006) *Mathematical modeling of intracellular signaling pathways*. BMC Neurosciences **7 Suppl 1:** S10

KOMEILI A, O'SHEA EK (2001) *New perspectives on nuclear transport*. Annu Rev Genet **35:** 341-364

KORESSAAR T RM (2007) *Enhancements and modifications of primer design program Primer3*. Bioinformatics **23**

KÖSTER M, HAUSER H (1999) *Dynamic redistribution of STAT1 protein in IFN signaling visualized by GFP fusion proteins*. Euro J Biochem **260:** 137-144

KREBS DL, HILTON D (2001) *SOCS proteins: negative regulators of cytokine signaling*. Stem Cells **19:** 378-387

KRETZSCHMAR AK, DINGER MC, HENZE C, BROCKE-HEIDRICH K, HORN F (2004) *Analysis of Stat3 (signal transducer and activator of transcription 3) dimerization by fluorescence resonance energy transfer in living cells*. Biochem J **377:** 289-297

LAHAV G, ROSENFELD N, SIGAL A, GEVA-ZATORSKY N, LEVINE AJ, ELOWITZ MB, ALON U (2004) *Dynamics of the p53-Mdm2 feedback loop in individual cells*. Nat Genet **36:** 147-150

LAVENS D, MONTOYE T, PIESSEVAUX J, ZABEAU L, VANDEKERCKHOVE J, GEVAERT K, BECKER W, EYCKERMAN S, TAVERNIER J (2006) *A complex interaction pattern of CIS and SOCS2 with the leptin receptor*. J Cell Sci **119:** 2214-2224

LEE EC, YU D, MARTINEZ DE VELASCO J, TESSAROLLO L, SWING DA, COURT DL, JENKINS NA, COPELAND NG (2001) *A highly efficient Escherichia coli-based chromosome engineering system adapted for recombinogenic targeting and subcloning of BAC DNA*. Genomics **73:** 56-65

LEE H, HERRMANN A, DENG J-H, KUJAWSKI M, NIU G, LI Z, FORMAN S, JOVE R, PARDOLL DM, YU H (2009) *Persistently activated Stat3 maintains constitutive NF-κB activity in tumors*. Cancer Cell **15:** 283-293

LEE J, NAKAGIRI T, OTO T, HARADA M, MORII E, SHINTANI Y, INOUE M, IWAKURA Y, MIYOSHI S, OKUMURA M, HIRANO T, MURAKAMI M (2012) *IL-6 Amplifier: NF-kappa B-triggered positive feedback for IL-6 signaling, in grafts is involved in allogeneic rejection responses*. J Immunol **189:** 1928-1936

LEHMANN U, SCHMITZ J, WEISSENBACH M, SOBOTA RM, HORTNER M, FRIEDERICHS K, BEHRMANN I, TSIARIS W, SASAKI A, SCHNEIDER-MERGENER J, YOSHIMURA A, NEEL BG, HEINRICH PC, SCHAPER F (2003) *SHP2 and SOCS3 contribute to Tyr-759-dependent attenuation of interleukin-6 signaling through gp130*. J Biol Chem **278:** 661-671

LEVY DE, DARNELL JE (2002) *Signalling: Stats: transcriptional control and biological impact*. Nat Rev Mol Cell Bio **3:** 651-662

LEVY DE, LEE C-K (2002) *What does Stat3 do?* J Clin Invest **109:** 1143-1148

LI S, WANG N, BRODT P (2012) *Metastatic cells can escape the proapoptotic effects of TNF-alpha through increased autocrine IL-6/STAT3 signaling*. Cancer Res **72:** 865-875

LINOSSI EM, BABON JJ, HILTON DJ, NICHOLSON SE (2013) *Suppression of cytokine signaling: The SOCS perspective*. Cytokine Growth Factor Rev **24:** 241-248

LUPARDUS PJ, ULTSCH M, WALLWEBER H, BIR KOHLI P, JOHNSON AR, EIGENBROT C (2014) *Structure of the pseudokinase-kinase domains from protein kinase TYK2 reveals a mechanism for Janus kinase (JAK) autoinhibition*. Proc Natl Acad Sci USA **111:** 8025-8030

MAO X, REN Z, PARKER GN, SONDERMANN H, PASTORELLO MA, WANG W, MCMURRAY JS, DEMELER B, DARNELL JR JE, CHEN X (2005) *Structural bases of unphosphorylated STAT1 association and receptor binding*. Mol Cell **17:** 761-771

MARG A, SHAN Y, MEYER T, MEISSNER T, BRANDENBURG M, VINKEMEIER U (2004) *Nucleocytoplasmic shuttling by nucleoporins Nup153 and Nup214 and CRM1-dependent nuclear export control the subcellular distribution of latent Stat1*. J Cell Biol **165:** 823-833

MATADEEN R, HON WC, HEATH JK, JONES EY, FULLER S (2007) *The dynamics of signal triggering in a gp130-receptor complex*. Structure **15:** 441-448

MCFARLAND BC, GRAY GK, NOZELL SE, HONG SW, BENVENISTE EN (2013) *Activation of the NK-κB pathway by the STAT3 inhibitor JSI-124 in human glioblastoma cells*. Mol Cancer Res

MEYER T, STRYER L (1988) *Molecular model for receptor-stimulated calcium spiking*. Proc Natl Acad Sci USA **85:** 5051-5055

MEYER T, GAVENIS K, VINKEMEIER U (2002) *Cell type-specific and tyrosine phosphorylation-independent nuclear presence of STAT1 and STAT3*. Exp Cell Res **272:** 45-55

MEYER T, MARG A, LEMKE P, WIESNER B, VINKEMEIER U (2003) *DNA binding controls inactivation and nuclear accumulation of the transcription factor Stat1*. Genes Dev **17:** 1992-2005

MEYER T, BEGITT A, VINKEMEIER U (2007) *Green fluorescent protein-tagging reduces the nucleocytoplasmic shuttling specifically of unphosphorylated STAT1*. FEBS J **274:** 815-826

MIHARA M, HASHIZUME M, YOSHIDA H, SUZUKI M, SHIINA M (2012) *IL-6/IL-6 receptor system and its role in physiological and pathological conditions*. Clinical Science (Lond) **122:** 143-159

MOORTHY AK, SAVINOVA OV, HO JQ, WANG VY, VU D, GHOSH G (2006) *The 20S proteasome processes NF-kappaB1 p105 into p50 in a translation-independent manner*. EMBO J **25:** 1945-1956

MOSHAGE H (1997) *Cytokines and the hepatic acute phase response*. J Pathology **181:** 257-266

MULLASSERY D, HORTON CA, WOOD CD, WHITE MRH (2008) *Single live-cell imaging for systems biology*. Essays Biochem **45:** 121

MURAKAMI M, HIBI M, NAKAGAWA N, NAKAGAWA T, YASUKAWA K, YAMANISHI K, TAGA T, KISHIMOTO T (1993) *IL-6-induced homodimerization of gp130 and associated activation of a tyrosine kinase*. Science **260:** 1808-1810

NAKA T, NARAZAKI M, HIRATA M, MATSUMOTO T, MINAMOTO S, AONO A, NISHIMOTO N, KAJITA T, TAGA T, YOSHIZAKI K, AKIRA S, KISHIMOTO T (1997) *Structure and function of a new STAT-induced STAT inhibitor*. Nature **387:** 924-929

NAKAJIMA K, YAMANAKA Y, NAKAE K, KOIJMA H, ICHIBA M, KIUCHI N, KITAOKA T, FUKADA T, HIBI M, HIRANO T (1996) *A central role for STAT3 in IL-6-induced regulation of growth and differentiation in M1 leukemia cells*. EMBO J **15:** 3651-3658

NECULAI D, NECULAI AM, VERRIER S, STRAUB K, KLUMPP K, PFITZNER E, BECKER S (2005) *Structure of the unphosphorylated STAT5a dimer*. J Biol Chem **280:** 40782-40787

NELSON DE, IHEKWABA AEC, ELLIOT M, JOHNSON JR, GIBNEY CA, FOREMAN BE, NELSON G, SEE V, HORTON CA, SPILLER DG, EDWARDS SW, MCDOWELL HP, UNITT JF, SULLIVAN E, GRIMLEY R, BENSON N, BROOMHEAD DS, KELL DB, WHITE MRH (2004) *Oscillations in NF-κB signaling control the dynamics of gene expression*. Science **306:** 704-708

NELSON G, WILDE GJC, SPILLER DG, SULLIVAN E, UNITT JF, WHITE MRH (2002) *Dynamic analysis of STAT6 signalling in living cells*. FEBS Lett **532:** 188-192

NELSON G, WILDE GJC, SPILLER DG, KENNEDY SM, RAY DW, SULLIVAN E, UNITT JF, WHITE MRH (2003) *NF-kappaB signalling is inhibited by glucocorticoid receptor and STAT6 via distinct mechanisms*. J Cell Sci **116:** 2495-2503

NG IH, NG DC, JANS DA, BOGOYEVITCH MA (2012) *Selective STAT3-alpha or -beta expression reveals spliceform-specific phosphorylation kinetics, nuclear retention and distinct gene expression outcomes*. Biochem J **447:** 125-136

NICHOLSON SE, DE SOUZA D, FABRI LJ, CORBIN J, WILLSON TA, ZHANG J-G, SILVA A, ASIMAKIS M, FARLEY A, NASH AD, METCALF D, HILTON DJ, NICOLA NA, BACA M (2000) *Suppressor of cytokine signaling-3 preferentially binds to the SHP-2-binding site on the shared cytokine receptor subunit gp130*. Proc Natl Acad Sci USA **97:** 6493-6498

NING Q, BERGER L, LUO X, YAN W, GONG F, DENNIS J, LEVY G (2003) *STAT1 and STAT3 alpha/beta splice form activation predicts host responses in mouse hepatitis virus type 3 infection*. J Med Virol **69:** 306-312

O'SHEA JM, PERKINS ND (2008) *Regulation of the RelA (p65) transactivation domain*. Biochem Soc Trans **36:** 603-608

OGURA H, MURAKAMI M, OKUYAMA Y, TSURUOKA M, KITABAYASHI C, KANAMOTO M, NISHIHARA M, IWAKURA Y, HIRANO T (2008) *Interleukin-17 promotes autoimmunity by triggering a positive-feedback loop via Interleukin-6 induction*. Immunity **29:** 628-636

P S (2000) *The Sequence Manipulation Suite: JavaScript programs for analyzing and formatting protein and DNA sequences*. Biotechniques **28:** 1102-1104

PARK SH, KIM KE, HWANG HY, KIM TY (2003) *Regulatory effect of SOCS on NF-kappaB activity in murine monocytes/macrophages*. DNA Cell Biol **22:** 131-139

PASZEK P, RYAN S, ASHALL L, SILLITOE K, HARPER CV, SPILLER DG, RAND DA, WHITE MR (2010) *Population robustness arising from cellular heterogeneity*. Proc Natl Acad Sci USA **107:** 11644-11649

PAULI EK, SCHMOLKE M, WOLFF T, VIEMANN D, ROTH J, BODE JG, LUDWIG S (2008) *Influenza A virus inhibits Type I IFN signaling via NF-κB-dependent induction of SOCS-3 expression*. PLoS Pathogen **4:** e1000196

PELLEGRIN P, FERNANDEZ A, LAMB NJC, BENNES R (2002) *Macromolecular iptake is a spontaneous event during mitosis in cultured Fibroblasts: implications for vector-dependent plasmid transfection*. Mol Biol Cell **13:** 570-578

PERKINS ND, SCHMID RM, DUCKETT CS, LEUNG K, RICE NR, NABEL GJ (1992) *Distinct combinations of NF-kappa B subunits determine the specificity of transcriptional activation*. Proc Natl Acad Sci USA **89:** 1529-1533

PERKINS ND (2006) *Post-translational modifications regulating the activity and function of the Nuclear Factor-kappaB pathway*. Oncogene **25:** 6717-6730

PERNIS AB, ROTHMAN PB (2002) *JAK-STAT signalling in asthma*. J Clin Invest **109:** 1279–1283

PERTSOVSKAYA I, ABAD E, DOMEDEL-PUIG N, GARCIA-OJALVO J, VILLOSLADA P (2013) *Transient oscillatory dynamics of interferon beta signaling in macrophages*. BMC Syst Biol **7:** 59

PFAFFL MW (2001) *A new mathematical model for relative quantification in real-time RT-PCR*. Nucleic Acids Res **29:** e45

PIETRANGELO A, DIERSSEN U, VALLI L, GARUTI C, RUMP A, CORRADINI E, ERNST M, KLEIN C, TRAUTWEIN C (2007) *STAT3 is required for IL-6-gp130-dependent activation of hepcidin in vivo*. Gastroenterol **132:** 294-300

PLATANIAS LC (2005) *Mechanisms of type-I- and type-II-interferon-mediated signalling*. Nat Rev Immunol **5:** 375-386

PRANADA AL, METZ S, HERRMANN A, HEINRICH PC, MULLER-NEWEN G (2004) *Real time analysis of STAT3 nucleocytoplasmic shuttling*. J Biol Chem **279:** 15114-15123

QUINTON LJ, BLAHNA MT, JONES MR, ALLEN E, FERRARI JD, HILLIARD KL, ZHANG X, SABHARWAL V, ALGUL H, AKIRA S, SCHMID RM, PELTON SI, SPIRA A, MIZGERD JP (2012) *Hepatocyte-specific mutation of both NF-kappaB RelA and STAT3 abrogates the acute phase response in mice*. J Clin Invest **122:** 1758-1763

RABUT GA, ELLENBERG J (2004) *Automatic real-time three-dimensional cell tracking by fluorescence microscopy*. J Microsc **216:** 131–137

RADTKE S, WULLER S, YANG XP, LIPPOK BE, MUTZE B, MAIS C, DE LEUR HS, BODE JG, GAESTEL M, HEINRICH PC, BEHRMANN I, SCHAPER F, HERMANNS HM (2010) *Cross-regulation of cytokine signalling: pro-inflammatory cytokines restrict IL-6 signalling through receptor internalisation and degradation*. J Cell Sci **123:** 947-959

RAM PA, WAXMAN DJ (2000) *Role of the cytokine-inducible SH2 protein CIS in desensitization of STAT5b signaling by continuous growth hormone*. J Biol Chem **275:** 39487-39496

RAND DA (2008) *Mapping global sensitivity of cellular network dynamics: sensitivity heat maps and a global summation law*, Vol. 5.

REICH NC (2013) *STATs get their move on*. JAK-STAT **2:** e27080

RICE NR, MACKICHAN ML, ISRAEL A (1992) *The precursor of NF-kappa B p50 has I kappa B-like functions*. Cell **71:** 243-253

ROTHWARF DM, ZANDI E, NATOLI G, KARIN M (1998) *IKK-gamma is an essential regulatory subunit of the IkappaB kinase complex*. Nature **395:** 297-300

ROTTENBERG ME, CAROW B (2014) *SOCS3, a major regulator of infection and inflammation*. Front Immunol **5**

RYO A, SUIZU F, YOSHIDA Y, PERREM K, LIOU YC, WULF G, ROTTAPEL R, YAMAOKA S, LU KP (2003) *Regulation of NF-kappaB signaling by Pin1-dependent prolyl isomerization and ubiquitin-mediated proteolysis of p65/RelA*. Mol Cell **12:** 1413-1426

SASAKI A, YASUKAWA H, SUZUKI A, KAMIZONO S, SYODA T, KINJYO I, SASAKI M, JOHNSTON JA, YOSHIMURA A (1999) *Cytokine-inducible SH2 protein-3 (CIS3/SOCS3) inhibits Janus tyrosine kinase by binding through the N-terminal kinase inhibitory region as well as SH2 domain*. Genes Cells **4:** 339-351

SASAKI A, INAGAKI-OHARA K, YOSHIDA T, YAMANAKA A, SASAKI M, YASUKAWA H, KOROMILAS AE, YOSHIMURA A (2003) *The N-terminal truncated isoform of SOCS3 translated from an alternative initiation AUG codon under stress conditions is stable due to the lack of a major ubiquitination Site, Lys-6*. J Biol Chem **278:** 2432-2436

SCHINDLER C, LEVY DE, DECKER T (2007) *JAK-STAT Signaling: From Interferons to Cytokines*. J Biol Chem **282:** 20059-20063

SCHINDLER R, MANCILLA J, ENDRES S, GHORBANI R, CLARK S, DINARELLO C (1990) *Correlations and interactions in the production of Interleukin-6 (IL- 6), IL-1, and Tumor Necrosis Factor (TNF) in human blood mononuclear cells: IL-6 suppresses IL-1 and TNF*. Blood **75:** 40-47

SCHMITZ J, WEISSENBACH M, HAAN S, HEINRICH PC, SCHAPER F (2000) *SOCS3 exerts its inhibitory function on Interleukin-6 signal transduction through the SHP2 recruitment site of gp130*. J Biol Chem **275:** 12848-12856

SCHOOLTINK H, SCHMITZ-VAN DE LEUR H, HEINRICH PC, ROSE-JOHN S (1992) *Up-regulation of the interleukin-6-signal transducing protein (gp130) by Interleukin-6 and dexamethasone in HepG2 cells*. FEBS Lett **297:** 263-265

SCHRÖDER M, KROEGER KM, VOLK H-D, EIDNE KA, GRÜTZ G (2004) *Preassociation of nonactivated STAT3 molecules demonstrated in living cells using bioluminescence resonance energy transfer: a new model of STAT activation?* J Leuk Biol **75:** 792-797

SCHROERS A, HECHT O, KALLEN KJ, PACHTA M, ROSE-JOHN S, GROTZINGER J (2005) *Dynamics of the gp130 cytokine complex: a model for assembly on the cellular membrane*. Protein Sci **14:** 783-790

SCHURINGA JJ, SCHEPERS H, VELLENGA E, KRUIJER W (2001) *Ser727-dependent transcriptional activation by association of p300 with STAT3 upon IL-6 stimulation*. FEBS Lett **495:** 71-76

SEHGAL PB (2008) *Paradigm shifts in the cell biology of STAT signaling*. Semin Cell Dev Biol **19:** 329-340

SEKKAÏ D, GRUEL G, HERRY M, MOUCADEL V, CONSTANTINESCU SN, ALBAGLI O, ROUX DT-L, VAINCHENKER W, BENNACEUR-GRISCELLI A (2005) *Microarray analysis of LIF/STAT3 transcriptional targets in Embryonic Stem Cells*. Stem Cells **23:** 1634-1642

SEN R, BALTIMORE D (1986) *Multiple nuclear factors interact with the immunoglobulin enhancer sequences*. Cell **46:** 705-716

SHAH M, PATEL K, MUKHOPADHYAY S, XU F, GUO G, SEHGAL PB (2006) *Membrane-associated STAT3 and PY-STAT3 in the cytoplasm*. J Biol Chem **281:** 7302-7308

SHEN H, NELSON G, NELSON DE, KENNEDY S, SPILLER DG, GRIFFITHS T, PATON N, OLIVER SG, WHITE MRH, KELL DB (2006) *Automated tracking of gene expression in individual cells and cell compartments*. J Royal Society Interface **3:** 787-794

SHIN SY, RATH O, CHOO SM, FEE F, MCFERRAN B, KOLCH W, CHO KH (2009) *Positive- and negative-feedback regulations coordinate the dynamic behavior of the Ras-Raf-MEK-ERK signal transduction pathway*. J Cell Sci **122:** 425-435

SHIZUYA H, BIRREN B, KIM UJ, MANCINO V, SLEPAK T, TACHIIRI Y, SIMON M (1992) *Cloning and stable maintenance of 300-kilobase-pair fragments of human DNA in Escherichia coli using an F-factor-based vector*. Proc Natl Acad Sci USA **89:** 8794-8797

SIEBENLIST U, FRANZOSO G, BROWN K (1994) *Structure, regulation and function of NF-kappa B*. Annu Rev Cell Biol **10:** 405-455

SIEWERT E, MÜLLER-ESTERL W, STARR R, HEINRICH PC, SCHAPER F (1999) *Different protein turnover of interleukin-6-type cytokine signalling components*. Euro J Biochem **265:** 251-257

SNYERS L, DE WIT L, CONTENT J (1990) *Glucocorticoid up-regulation of high-affinity interleukin 6 receptors on human epithelial cells*. Proc Natl Acad Sci USA **87:** 2838-2842

SNYERS L, CONTENT J (1992) *Enhancement of IL-6 receptor beta chain (gp130) expression by IL-6, IL-1 and TNF in human epithelial cells*. Biochem Biophys Res Commun **185:** 902-908

SOMMER U, SCHMID C, SOBOTA RM, LEHMANN U, STEVENSON NJ, JOHNSTON JA, SCHAPER F, HEINRICH PC, HAAN S (2005) *Mechanisms of SOCS3 phosphorylation upon Interleukin-6 Stimulation: Contributions of Src- and Receptor-Tyrosine Kinases*. J Biol Chem **280:** 31478-31488

SOW FB, ALVAREZ GR, GROSS RP, SATOSKAR AR, SCHLESINGER LS, ZWILLING BS, LAFUSE WP (2009) *Role of STAT1, NF-κB, and C/EBPβ in the macrophage transcriptional regulation of hepcidin by mycobacterial infection and IFN-γ*. J Leuk Biol **86:** 1247-1258

SPILLER DG, WOOD CD, RAND DA, WHITE MRH (2010) *Measurement of single-cell dynamics*. Nature **465:** 736-745

STARK GR, DARNELL JE, JR. (2012) *The JAK-STAT pathway at twenty*. Immunity **36:** 503-514

STARR R, WILLSON TA, VINEY EM, MURRAY LJ, RAYNER JR, JENKINS BJ, GONDA TJ, ALEXANDER WS, METCALF D, NICOLA NA, HILTON DJ (1997) *A family of cytokine-inducible inhibitors of signalling*. Nature **387:** 917-921

STREBOVSKY J, WALKER P, LANG R, DALPKE AH (2011) *Suppressor of cytokine signaling 1 (SOCS1) limits NF-kappaB signaling by decreasing p65 stability within the cell nucleus*. FASEB J **25:** 863-874

SUN SC (2011) *Non-canonical NF-kappaB signaling pathway*. Cell Res **21:** 71-85

SUNG MH, SALVATORE L, DE LORENZI R, INDRAWAN A, PASPARAKIS M, HAGER GL, BIANCHI ME, AGRESTI A (2009) *Sustained oscillations of NF-kappaB produce distinct genome scanning and gene expression profiles*. PLoS ONE **4:** e7163

SUNG MH, LI N, LAO Q, GOTTSCHALK RA, HAGER GL, FRASER ID (2014) *Switching of the relative dominance between feedback mechanisms in lipopolysaccharide-induced NF-kappaB signaling*. Science Signalling **7:** ra6

SUTHERLAND JM, KEIGHTLEY RA, NIXON B, ROMAN SD, ROBKER RL, RUSSELL DL, MCLAUGHLIN EA (2012) *Suppressor of cytokine signaling 4 (SOCS4): moderator of ovarian primordial follicle activation*. Journal of Cell Physiology **227:** 1188-1198

TAGA T, HIBI M, HIRATA Y, YAMASAKI K, YASUKAWA K, MATSUDA T, HIRANO T, KISHIMOTO T (1989) *Interleukin-6 triggers the association of its receptor with a possible signal transducer, gp130*. Cell **58:** 573-581

TAKEDA K, NOGUCHI K, SHI W, TANAKA T, MATSUMOTO M, YOSHIDA N (1997) *Targeted disruption of the mouse STAT3 gene leads to early embryonic lethality*. Proc Natl Acad Sci USA **94:** 3801-3804

TANAKA Y, TANAKA N, SAEKI Y, TANAKA K, MURAKAMI M, HIRANO T, ISHII N, SUGAMURA K (2008) *c-Cbl-dependent monoubiquitination and lysosomal degradation of gp130*. Mol Cell Biol **28:** 4805-4818

TAY S, HUGHEY JJ, LEE TK, LIPNIACKI T, QUAKE SR, COVERT MW (2010) *Single-cell NF-κB dynamics reveal digital activation and analogue information processing*. Nature **466:** 267-271

TENHUMBERG S, SCHUSTER B, ZHU L, KOVALEVA M, SCHELLER J, KALLEN KJ, ROSE-JOHN S (2006) *gp130 dimerization in the absence of ligand: preformed cytokine receptor complexes*. Biochem Biophys Res Commun **346:** 649-657

TERGAONKAR V, CORREA RG, IKAWA M, VERMA IM (2005) *Distinct roles of IkappaB proteins in regulating constitutive NF-kappaB activity*. Nat Cell Biol **7:** 921-923

THIEL S, DAHMEN H, MARTENS A, MÜLLER-NEWEN G, SCHAPER F, HEINRICH PC, GRAEVE L (1998) *Constitutive internalization and association with adaptor protein-2 of the interleukin-6 signal transducer gp130*. FEBS Lett **441:** 231-234

TIAN B, NOWAK DE, BRASIER AR (2005) *A TNF-induced gene expression program under oscillatory NF-kappaB control*. BMC Genomics **6:** 137

TIWARI P, TRIPATHI LP, NISHIKAWA-MATSUMURA T, AHMAD S, SONG SN, ISOBE T, MIZUGUCHI K, YOSHIZAKI K (2013) *Prediction and experimental validation of a putative non-consensus binding site for transcription factor STAT3 in serum amyloid A gene promoter*. Biochim Biophys Acta **1830:** 3650-3655

TURNER DA, PASZEK P, WOODCOCK DJ, NELSON DE, HORTON CA, WANG Y, SPILLER DG, RAND DA, WHITE MR, HARPER CV (2010) *Physiological levels of TNFalpha stimulation induce stochastic dynamics of NF-kappaB responses in single living cells*. J Cell Sci **123:** 2834-2843

TURPIN P, HAY RT, DARGEMONT C (1999) *Characterization of IkappaBalpha nuclear import pathway*. J Biol Chem **274:** 6804-6812

TYSON JJ, HONG CI, THRON CD, NOVAK B (1999) *A simple model of circadian rhythms based on dimerization and proteolysis of PER and TIM*. Biophys J **77:** 2411-2417

UNTERGASSER A, CUTCUTACHE I, KORESSAAR T, YE J, FAIRCLOTH BC, REMM M, ROZEN SG (2012) *Primer3--new capabilities and interfaces*. Nucleic Acids Res **40:** e115

USKOKOVIC A, DINIC S, MIHAILOVIC M, GRIGOROV I, IVANOVIC-MATIC S, BOGOJEVIC D, GRDOVIC N, ARAMBASIC J, VIDAKOVIC M, MARTINOVIC V, PETROVIC M, POZNANOVIC G (2007) *STAT3/NFkappaB interplay in the regulation of alpha2-macroglobulin gene expression during rat liver development and the acute phase response*. IUBMB life **59:** 170-178

VERDIER F, CHRETIEN S, MULLER O, VARLET P, YOSHIMURA A, GISSELBRECHT S, LACOMBE C, MAYEUX P (1998) *Proteasomes regulate erythropoietin receptor and signal transducer and activator of transcription 5 (STAT5) activation. Possible involvement of the ubiquitinated Cis protein*. J Biol Chem **273:** 28185-28190

VERSTREPEN L, VERHELST K, VAN LOO G, CARPENTIER I, LEY SC, BEYAERT R (2010) *Expression, biological activities and mechanisms of action of A20 (TNFAIP3)*. Biochem Pharmacol **80:** 2009-2020

VESTERLUND M, ZADJALI F, PERSSON T, NIELSEN ML, KESSLER BM, NORSTEDT G, FLORES-MORALES A (2011) *The SOCS2 ubiquitin ligase complex regulates Growth Hormone receptor levels*. PLoS ONE **6:** e25358

VINKEMEIER U, MOAREFI I, DARNELL JE, JR., KURIYAN J (1998) *Structure of the amino-terminal protein interaction domain of STAT-4*. Science **279:** 1048-1052

VINKEMEIER U (2004) *Getting the message across, STAT! Design principles of a molecular signaling circuit*. J Cell Biol **167:** 197-201

VOGT M, DOMOSZLAI T, KLESHCHANOK D, LEHMANN S, SCHMITT A, POLI V, RICHTERING W, MULLER-NEWEN G (2011) *The role of the N-terminal domain in dimerization and nucleocytoplasmic shuttling of latent STAT3*. J Cell Sci **124:** 900-909

WAKAHARA R, KUNIMOTO H, TANINO K, KOJIMA H, INOUE A, SHINTAKU H, NAKAJIMA K (2012) *Phospho-Ser727 of STAT3 regulates STAT3 activity by enhancing dephosphorylation of phospho-Tyr705 largely through TC45*. Genes Cells **17:** 132-145

WALLWEBER HJA, TAM C, FRANKE Y, STAROVASNIK MA, LUPARDUS PJ (2014) *Structural basis of IFNα receptor recognition by TYK2*. Nat Struct Mol Biol **21:** 443-448

WANG Y, FULLER GM (1994) *Phosphorylation and internalization of gp130 occur after IL-6 activation of Jak2 kinase in hepatocytes*. Mol Biol Cell **5:** 819-828

WANG Y, PASZEK P, HORTON CA, KELL DB, WHITE MR, BROOMHEAD DS, MULDOON MR (2011) *Interactions among oscillatory pathways in NF-kappa B signaling*. BMC Syst Biol **5:** 23

WARMING S, COSTANTINO N, COURT DL, JENKINS NA, COPELAND NG (2005) *Simple and highly efficient BAC recombineering using galK selection*. Nucleic Acids Res **33:** e36

WENTA N, STRAUSS H, MEYER S, VINKEMEIER U (2008) *Tyrosine phosphorylation regulates the partitioning of STAT1 between different dimer conformations*. Proc Natl Acad Sci USA **105:** 9238-9243

WHITESIDE ST, EPINAT JC, RICE NR, ISRAEL A (1997) *I kappa B epsilon, a novel member of the I kappa B family, controls RelA and cRel NF-kappa B activity*. EMBO J **16:** 1413-1426

WILLIAMS R, TIMMIS J, QWARNSTROM E (2014) *Computational models of the NF-KB signalling pathway*. Computation **2:** 131-158

WORMALD S, ZHANG JG, KREBS DL, MIELKE LA, SILVER J, ALEXANDER WS, SPEED TP, NICOLA NA, HILTON DJ (2006) *The comparative roles of suppressor of cytokine signaling-1 and -3 in the inhibition and desensitization of cytokine signaling*. J Biol Chem **281:** 11135-11143

XIE X, CHAN KS, CAO F, HUANG M, LI Z, LEE A, WEISSMAN IL, WU JC (2009) *Imaging of STAT3 signaling pathway during mouse embryonic stem cell differentiation*. Stem Cells Dev **18:** 205-214

XU Y, KERSHAW NJ, LUO CS, SOO P, POCOCK MJ, CZABOTAR PE, HILTON DJ, NICOLA NA, GARRETT TP, ZHANG JG (2010) *Crystal structure of the entire ectodomain of gp130: insights into the molecular assembly of the tall cytokine receptor complexes*. J Biol Chem **285:** 21214-21218

YAGIL Z, NECHUSHTAN H, KAY G, YANG CM, KEMENY DM, RAZIN E (2010) *The enigma of the role of protein inhibitor of activated STAT3 (PIAS3) in the immune response*. Trends Immunol **31:** 199-204

YAMAMOTO T, SEKINE Y, KASHIMA K, KUBOTA A, SATO N, AOKI N, MATSUDA T (2002) *The nuclear isoform of protein-tyrosine phosphatase TC-PTP regulates interleukin-6-mediated signaling pathway through STAT3 dephosphorylation*. Biochem Biophys Res Commun **297:** 811-817

YANG J, CHATTERJEE-KISHORE M, STAUGAITIS SM, NGUYEN H, SCHLESSINGER K, LEVY DE, STARK GR (2005) *Novel roles of unphosphorylated STAT3 in oncogenesis and transcriptional regulation*. Cancer Reseasrch **65:** 939-947

YANG J, LIAO X, AGARWAL MK, BARNES L, AURON PE, STARK GR (2007) *Unphosphorylated STAT3 accumulates in response to IL-6 and activates transcription by binding to NFkB*. Genes Dev **21:** 1396-1408

YANG J, STARK GR (2008) *Roles of unphosphorylated STATs in signaling*. Cell Res **18:** 443-451

YANG XP, ALBRECHT U, ZAKOWSKI V, SOBOTA RM, HAUSSINGER D, HEINRICH PC, LUDWIG S, BODE JG, SCHAPER F (2004) *Dual function of interleukin-1beta for the regulation of interleukin-6-induced suppressor of cytokine signaling 3 expression*. J Biol Chem **279:** 45279-45289

YEH TC, PELLEGRINI S (1999) *The Janus kinase family of protein tyrosine kinases and their role in signaling*. CMLS Cell Mol Life Sci **55:** 1523-1534

YOSHIDA Y, KUMAR A, KOYAMA Y, PENG H, ARMAN A, BOCH JA, AURON PE (2004) *Interleukin 1 activates STAT3/nuclear factor-kappaB cross-talk via a unique TRAF6- and p65-dependent mechanism*. J Biol Chem **279:** 1768-1776

YOSHIMURA A, OHKUBO T, KIGUCHI T, JENKINS NA, GILBERT DJ, COPELAND NG, HARA T, MIYAJIMA A (1995) *A novel cytokine-inducible gene CIS encodes an SH2-containing protein that binds to tyrosine-phosphorylated interleukin 3 and erythropoietin receptors*. EMBO J **14:** 2816-2826

YOSHIURA S, OHTSUKA T, TAKENAKA Y, NAGAHARA H, YOSHIKAWA K, KAGEYAMA R (2007) *Ultradian oscillations of Stat, Smad, and Hes1 expression in response to serum*. Proc Natl Acad Sci USA **104:** 11292-11297

YU D, ELLIS HM, LEE E-C, JENKINS NA, COPELAND NG, COURT DL (2000) *An efficient recombination system for chromosome engineering in Escherichia coli*. Proc Natl Acad Sci USA **97:** 5978-5983

ZANDI E, ROTHWARF DM, DELHASE M, HAYAKAWA M, KARIN M (1997) *The IkappaB kinase complex (IKK) contains two kinase subunits, IKKalpha and IKKbeta, necessary for IkappaB phosphorylation and NF-kappaB activation*. Cell **91:** 243-252

ZHANG T, KEE WH, SEOW KT, FUNG W, XINMIN C (2000) *The Coiled-Coil Domain of STAT3 is essential for its SH2 domain-mediated receptor binding and subsequent activation induced by Epidermal Growth Factor and Interleukin-6*. Mol Cell Biol **20:** 7132-7139

ZHONG M, HENRIKSEN MA, TAKEUCHI K, SCHAEFER O, LIU B, HOEVE JT, REN Z, MAO X, CHEN X, SHUAI K, DARNELL JE (2005) *Implications of an antiparallel dimeric structure of nonphosphorylated STAT1 for the activation–inactivation cycle*. Proc Natl Acad Sci USA **102:** 3966-3971

ZOHLNHOFER D, GRAEVE L, ROSE-JOHN S, SCHOOLTINK H, DITTRICH E, HEINRICH PC (1992) *The hepatic interleukin-6 receptor. Down-regulation of the interleukin-6 binding subunit (gp80) by its ligand*. FEBS Lett **306:** 219-222